An Investigation of the Structure-Function Relationship in Human Cervical Tissue

by

Kristin M. Myers

B.S., University of Michigan (2002)
S.M., Massachusetts Institute of Technology (2005)

Submitted to the Department of Mechanical Engineering
in partial fulfillment of the requirements for the degree of

Doctor of Philosophy

at the

MASSACHUSETTS INSTITUTE OF TECHNOLOGY

February 2008

Signature of Author .....
Department of Mechanical Engineering
25 January 2008

Certified by .....
Simona Socrate
d'Arbeloff Assistant Professor of Mechanical Engineering
Thesis Supervisor

Accepted by .....
Lallit Anand
Professor of Mechanical Engineering
Chairman, Department Committee on Graduate Students

An Investigation of the Structure-Function Relationship in Human Cervical Tissue

by

Kristin M. Myers

Submitted to the Department of Mechanical Engineering
on 25 January 2008, in partial fulfillment of the
requirements for the degree of
Doctor of Philosophy

Abstract

The cervix plays a crucial role in maintaining a healthy pregnancy, acting as a mechanical barrier to hold the fetus inside the uterus during gestation. Altered biochemical and mechanical properties of the cervical tissue are suspected to play an important role in spontaneous preterm birth. Slight changes in the biochemical properties are known to cause softening of the cervical tissue thus weakening the structure. Premature softening of the cervical tissue is associated with spontaneous preterm birth and the clinical condition known as cervical insufficiency. "Cervical insufficiency" is clinically defined as a history of spontaneous preterm birth associated with a painless contraction-free delivery. Diagnosing cervical insufficiency remains elusive in the medical community because the etiology of this disease is unknown. Therefore, there is a need to establish a better understanding of this disease to aid in the identification and management of patients. This doctoral study explores the relationship between the biochemical and mechanical properties of human cervical tissue. The structure-function relationship is investigated by measuring the stress-response of the tissue in various modes of deformation and assaying the tissue for biochemical content. To generate material properties which reflect the tissue's biochemical content, micro-structurally based constitutive relationships are fit to the experimental data from mechanical tests. Values of the constitutive model parameters corresponding to the best fit to the material response in all modes of deformation represent the "mechanical properties" of the sample. Mechanical properties and the structural properties of the collagen and proteoglycans of each sample are compared, and it was found that the mechanical and biochemical properties vary for women with different obstetric backgrounds. Pregnant tissue is softer than nonpregnant tissue, and nonpregnant tissue from women with previous vaginal deliveries is softer than nonpregnant tissue from women with no previous vaginal deliveries. These changes in mechanical characteristics correspond to a shift in biochemical content with the softer tissue having a higher collagen solubility and an altered glycosaminoglycan content. An improved knowledge of the structure-function relationship is an important first step in understanding how the microstructure of the extracellular matrix (ECM) relates to its macroscopic mechanical response. In addition, the identification of key biochemical regulators of mechanical properties can constitute the basis for pharmacological intervention to correct pathological abnormalities in tissue response.

Thesis Supervisor: Simona Socrate
Title: d'Arbeloff Assistant Professor of Mechanical Engineering

Acknowledgements

I want to especially thank my thesis advisor Professor Simona Socrate. I want to thank my committee: Dr. Michael House, Professor Roger Kamm, and Dr. Ed Chien. I also want to thank everybody who has welcomed me into their lab for teaching and instruction: Robert Kokenyesi, Dr. Phyllis Leppert, Han-Hwa Hung, Dr. Huiling Ji, Vit Long, and Professor Alan Grodzinsky. I want to acknowledge my fellow graduate students who have contributed and collaborated with me on this work. These students include: Dimitrios Tzeranis who processed the Second Harmonic Generation images, Petr Jordan who developed the Matlab model fitting tool, Sebastien Febvay who formulated the groundwork for the testing protocols, and especially my dear friend Anastassia Paskaleva who developed the 3-dimensional material model for cervical tissue. I want to end with thanking my family and officemates: Petch Jearanaisilawong, Bruce Wu, Timothy Johnson, Thibault Prevost, and my dear friend Asha Balakrishnan. Without their love and support, this doctoral work would have not been possible.

Contents

List of Figures

List of Tables

Chapter 1

Introduction and Literature Review

This doctorate work is a presentation of my graduate research which includes the foundation presented in my Master's thesis, *The Mechanical and Biochemical Properties of Human Cervical Tissue* [90]. This Ph.D. thesis extensively covers the clinical, experimental and theoretical aspects of the structure-function relationships in the uterine cervix in the pregnant and non-pregnant state. The motivation for this work is to uncover the etiology of the pre-term labor condition known as "Cervical Insufficiency" (CI).

1.1 The Uterine Cervix

1.1.1 Non-pregnant

The cervix is a dense fibrous organ located at the lower end of the uterus. Figure 1-1 illustrates the location of the cervix in the female pelvic region during the non-pregnant state. The cervix is approximately cylindrical in shape, and is generally 3cm long and 2.5cm in diameter. These dimensions vary considerably between women depending on age, number of previous births, and the menstrual cycle [11]. The end of the cervix which is attached to the lower uterine segment is referred to as the internal os, and the end protruding into the vaginal canal is referred to as the external os. The cervix is made of dense connective tissue as opposed to the mainly muscular uterus. In the non-pregnant state the cervix acts as a barrier to infection, and during pregnancy it takes on a mechanical role to retain the fetus inside the uterus.

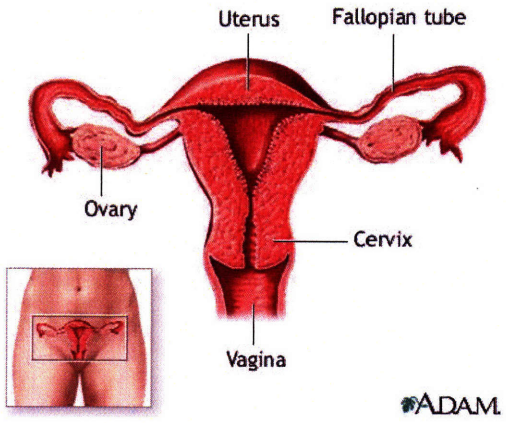

Figure 1-1: The location of the uterine cervix in the non-pregnant state. (modified from www.adams.com)

1.1.2 Pregnant

During pregnancy, the cervix is a mechanical barrier that holds the fetus inside the uterus. It has a dual function in that it remains firm until the fetus reaches term around 38 weeks. Then, at time of delivery, the cervical tissue dramatically softens and dilates to allow the baby passage. Figure 1-2 illustrates the location of the cervix in the female pelvic region during pregnancy. This figure also illustrates the different tissue layers comprising the cervix. The core is a dense connective tissue region called the stroma. The stroma is responsible for the mechanical strength of the organ. Surrounding the stroma are the fascia and the mucosa. The mucosa lines the inner canal while the fascia surrounds the outside of the cervix. The mucosa lines the inner canal. Its load bearing capabilities are likely minimal because it is invaginated with cervical glands. The endopelvic fascia surrounds the outside of the cervix and holds the cervix in its pelvic location.

A successful delivery of the fetus require coordinated actions of the uterus and the cervix. The uterus is mainly composed of muscle, and at time of delivery uterine contractions pull on the cervix. The cervix is composed of connective tissue, and at time of delivery it must dramatically soften to dilate. The process of cervical softening is called maturation, and it begins with a biochemical cascade of events triggered by hormonal change. The exact biochemical events leading up to cervical dilation remain unclear in the literature to this date. It is unknown if

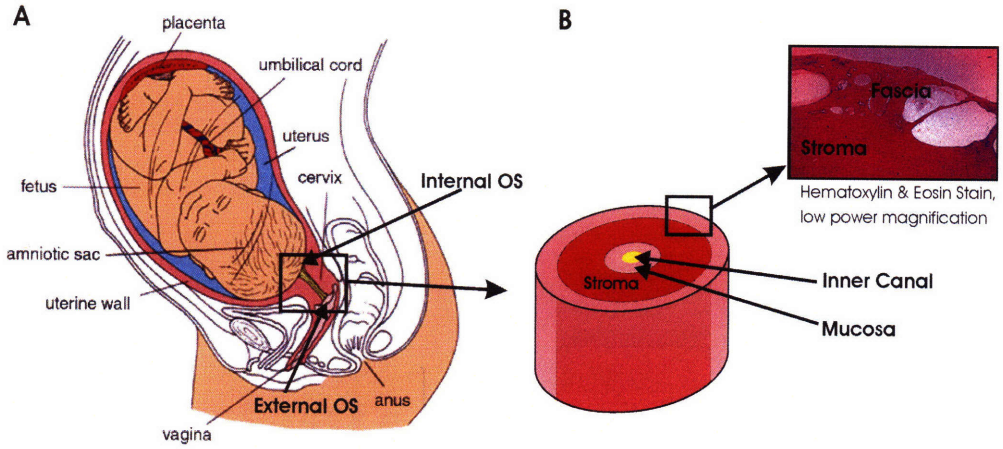

Figure 1-2: A) The anatomical location of the cervix in relation to the female pelvic region. The internal OS of the cervix is adjacent to the uterus, and the external OS protrudes into the vaginal canal (modified from www.adam.com). B) An idealized schematic of the stroma, fascia, and mucosa layers of the cervix. The collagen dense stroma region is surrounded by two regions of soft cellular material, the mucosa lining the inner canal and the fascia surrounding the outside.

the cervix gradually softens during the second and third trimester with a dramatic ripening occurring at time of delivery [100], or if the cervix remains firm until time of delivery. The literature review presented in Section 1.3 discusses the biochemical composition of the pregnant and non-pregnant cervix, and it outlines the current research concerning the cervical maturation process.

1.2 Cervix Pathology: Case of Cervical Insufficiency

The premature softening of the cervical tissue associated with spontaneous preterm birth is clinically known as Cervical Insufficiency (CI). Pre-term delivery is typically defined as birth before 37 weeks gestational age, and CI is clinically defined as a history of spontaneous preterm birth associated with a painless contraction-free delivery typically during mid second trimester to early third trimester. CI is an asymptomatic condition in which the patient can be unaware of the condition until unstoppable labor begins.

Despite increases in prenatal care the rate of pre-term birth has increased in the past years. In the United States, the rate of pre-term birth has increased to 12.5% in 2006, a 27% increase

since 1981 [12]. Preterm birth is one of the leading causes of morbidity and mortality in newborn infants, and cervical insufficiency is estimated to cause approximately 15% of pre-term birth. Regardless of the low occurrence of pre-term birth associated with CI, this condition is of substantial medical relevance because it is associated with extremely premature deliveries. The survival rate of the baby is directly dependent on its gestational age. Survival increases from 5% for babies born at 23 weeks to more than 95% by week 32 [111][102]. Therefore, deliveries associated with CI typically result in newborn death or severe neurological abnormalities. The impact of cervical insufficiency remain unknown because criteria for a conclusive diagnosis are still controversial.

Diagnosing CI remains elusive in the medical community because the etiology of this disease is not fully understood. Altered biochemical and mechanical properties of the cervical tissue are suspected to play an important role in spontaneous preterm birth. Currently, it is known that slight changes in the biochemical properties are known to cause softening of the cervical tissue thus weakening the structure [33][78][101][91]. However, it is not known how the mechanical properties of cervical tissue play a role in pre-term deliveries because there is no objective tool to measure cervical tissue strength in the clinical setting. This doctoral thesis sets out to investigate the mechanical properties of cervical tissue, and to link material parameters to the microstructural content of the connective tissue of the cervix.

1.2.1 Risk Factors

CI is different from other causes of pre-term labor such as pre-term ruptured membranes, bleeding, and intraamniotic infection in that its degree of severity is a continuous variable spanning a wide range of conditions [58]. The severity of cervical insufficiency is dependent on a combination of congenital, anatomical, obstetric, and biochemical factors. In an attempt to develop an early diagnostic tool researchers have suggested that cervical insufficiency may be identified from a combination of these factors.

Known obstetric history risk factors associated with CI are [47]:

- History of previous pre-term birth before 28 weeks
- Cervical injury from previous late surgical termination of pregnancy

Risk Factor	Test Cutoff	Odds Ratio for < 32 weeks	Odds Ratio for < 35 weeks
Fetal Fibronectin Level	≥50ng/ml	32.7	9.1
Short Cervix	< 25mm	5.8	5.5
Previous Spontaneous Pre-term Birth	Positive	4.5	4.3.

Table 1.1: Risk Factors for spontaneous preterm delivery before 32 and 35 weeks gestation assessed by the Preterm Prediction Study (Goldenberg et al.)

- Cervical injury from obstetrical cervical lacerations
- Cervical injury from extensive conization procedures
- High fetal fibronectin level during pregnancy

One of the major risk factors for pre-term birth is a history of previous pre-term birth. The risk of future pre-term birth increases as the number of previous pre-term birth increases. The subsequent risk also increases with decreasing gestational age of the prior birth. For example, there is a 10-fold increase in having a subsequent pre-term birth if the previous pre-term birth was less than 28 weeks gestation, and there is a 22-fold increase in pre-term birth for those women who had a previous pre-term birth between 23 and 28 weeks of gestation [47].

A recent report by Goldenberg et al. in 2003 outlined several risk factors associated with pre-term birth. The report reached conclusions based on the The Pre-term Prediction Study conducted by the Maternal Fetal Medicine Network between 1993 and 1996 [47]. The study surveyed risk factors for pre-term birth in over 3,000 women at 10 centers. The monitored risk factors include obstetric history as well as clinical findings of the current pregnancy. Results of the Pre-term Prediction Study indicate that the three most important risk factors associated with cervical insufficiency are cervical/vaginal fetal fibronectin concentration during current pregnancy, history of pre-term birth, and short cervical length. Table 1.1 outlines these risk factors and their associated odds ratios. The odds ratio is the odds in favor of the condition for the experimental group divided by odds in favor of the condition for the control group. Fetal fibronectin had the highest odds ratio. The relative risk of pre-term birth doubles with increasing values of fetal fibronectin from 20-40ng/ml to 60-90ng/ml [47].

1.2.2 Genetic Factors

A very recent study published in 2007 suggests that CI may stem from a genetic condition which predisposes patients to a connective tissue disorder. The study was conducted by Warren et al. [114], and reveals that polymorphisms in the COL1A1 and the TFG-β genes are more prevalent in patients with CI. The COL1A1 and the TFG-β genes have been well studied in the connective tissue literature, and specific polymorphisms in these genes have been found to cause abnormalities in connective tissue and the extracellular matrix (i.e. fibroid formation[15], osteoporosis [49][15], and hypertension[15]).

The Warren study conducted DNA testing from blood samples of women with and without CI. The results show that 27.2% of the women with CI had a first-degree relative who also suffered from CI and that 0% of the control group had a relative with the condition. Further, there was a statistically significant difference between the test and control groups with an increase in the polymorphisms in the COL1A1 and TFG-β genes for the CI group. This genetic evidence supports the hypothesis that CI could be caused by a connective tissue disorder that is governed by genetic factors [114]. More studies will be needed to further test this hypothesis.

1.2.3 Clinical Presentation and Diagnosing CI

Diagnosis of CI is difficult. If the patient does not have a history of spontaneous preterm birth, diagnosis of CI relies on nonspecific clinical parameters associated with the patient's current pregnancy. Further, CI is often diagnosed too late to stop progression to pre-term delivery. The clinical findings that are most often associated with cervical insufficiency are:

- Cervical funneling
- Membrane prolapse
- Excessive uterine volume
- Abnormal anatomical factors (i.e. short cervical length)

Cervical funneling is characterized by a T, Y, V, U pattern of progressive cervical deformation which can be observed by ultrasound and Magnetic Resonance Imaging [32]. Figure 1-3

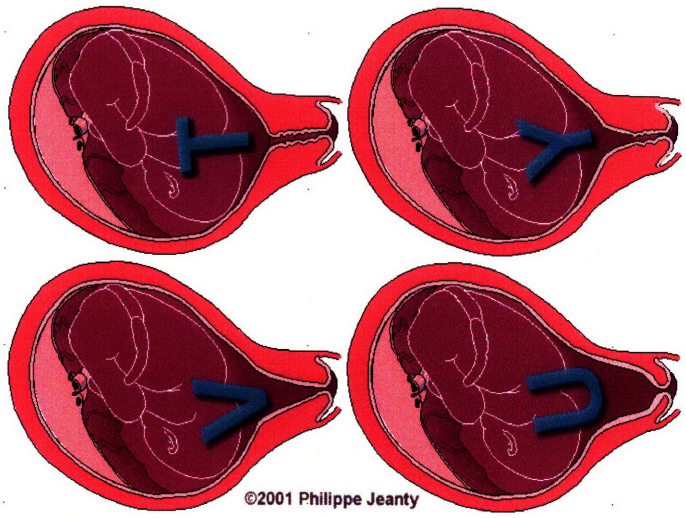

Figure 1-3: T,Y,V, and U cervical dilation pattern during cervical funneling.

Figure 1-4: Membrane prolapse into vaginal canal.

is a diagram of the cervical funneling pattern. Membrane prolapse is characterized by "hour-glassing" of the fetal membrane into the vaginal canal. "Hourglassing" refers to the shape of the fetal membrane as it slips into the inner cervical canal and bulges into the vaginal canal. Figure 1-4 shows bulging membranes observed during vaginal examination in a patient with cervical insufficiency. Typically, the progression of labor is difficult to stop with the onset of funneling and prolapse.

The most common anatomic abnormality associated with CI is a short cervix. The length of the cervix is measured during a transvaginal ultrasound. Two cohort studies by Iams et al. and Guzman et al. found a correlation between cervical canal length and cervical insufficiency. These research groups performed studies on women with previous pre-term births and women

with normal previous pregnancies. Iams et al. [58] conducted an early cross-sectional study of women with previous pre-term birth before 26 weeks, pre-term birth at 27 to 32 weeks, pre-term birth at 33 to 35 weeks, and women with normal obstetric history. This study identified a direct correlation between the gestational age of the previous pre-term delivery and cervical length such that earlier deliveries were typically associated with shorter cervical length. Guzman et al. [50] conducted a retrospective cohort study on women with normal and abnormal obstetric histories. The study investigated the cervical lengths of the women's current pregnancy between 15 and 20 weeks and between 21 and 24 weeks gestation. Guzman et al. concluded that the gestational age of the prior delivery could be directly correlated to the length of the cervical canal during the current pregnancy.

Guzman et al. [51] also investigated if a different set of anatomical factors (funnel width and length, cervical length, percent funneling and cervical index) were better predictors for pre-term labor. A cohort of 496 high risk patients were evaluated between 15 and 24 weeks gestations and followed to the end of pregnancy. Investigators found that each parameter did equally well in predicting the outcome of pre-term birth. They recommended that cervical length was a good predictor of spontaneous pre-term births because it was the easiest to measure with reasonably low error. Based on the results of this study, Guzman et al. recommended bed rest and possible cerclage for women with cervical lengths between 2.0cm and 1.6cm and cerclage placement for cervical length below 1.6cm. Further, they cautioned that cervical length as a predictor is strongly influenced by obstetric risk factors such as prior spontaneous pre-term birth. The investigators cited high sensitivity, specificity and negative predictive value for the cervical length diagnostic test. However, the positive predictive values were extremely low. The positive predictive value is the probability that the women will develop the condition given positive test result. Because of this statistical discrepancy and the difficulty in measuring congenital factors, this diagnosis criterion is still controversial.

1.2.4 Prevention and Treatment

Preventive measures for preterm birth associated with cervical insufficiency are bed rest and cerclage. They are prescribed according to the severity of the individual patient's condition. The most prescribed measures are bed rest and cerclage. Bed rest is a non-surgical solution

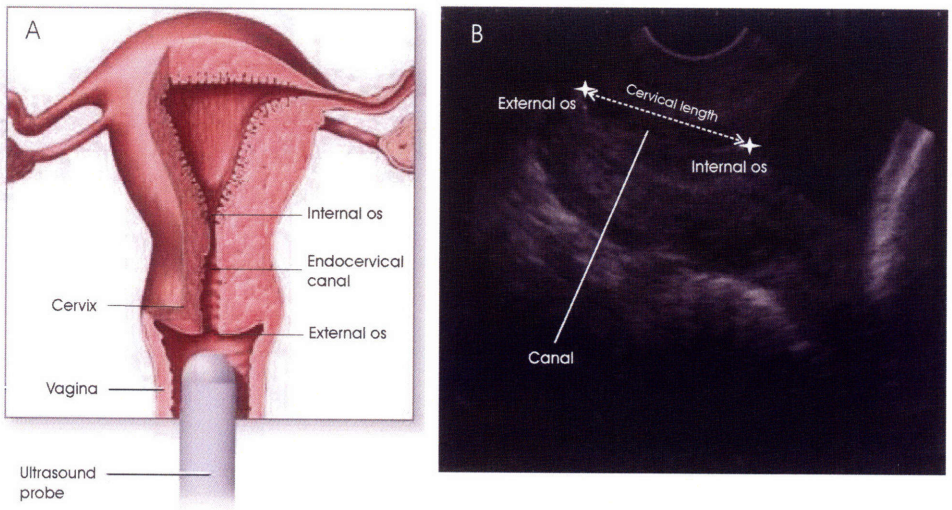

Figure 1-5: A) Illustration of the ultrasound probe location in the vagina. B) Image of the cervix and the defination of the cervical length measured on the image.

to relieve gravity and to prevent further cervical funneling. In extreme situations the patient is inclined at a negative angle. A more invasive treatment option is to surgically place a transvaginal or transabdominal cerclage. Cerclage is a suture stitch used to tie the cervix closed.

Transvaginal cerclage is used for women with a history of cervical insufficiency (preventive cerclage) or women with a current presentation of cervical insufficiency. A cerclage is not placed in patients with active labor, cervical anomalies, intrauterine infection or premature rupture of membranes (PROM). Preventive cerclage is typically placed at 13-14 weeks gestation, and is performed vaginally. See Figure 1-6 for an illustration of a transvaginal cerclage. The two types of transvaginal cerclage are the McDonald and Shirodkar Procedure. The McDonald Procedure uses a 5mm thick non-dissolvable suture material which is weaved through the cervix and tied off. The Shirodkar is similar to the MacDonald procedure. However, in the Shirodkar procedure, the vaginal epithelium is dissected off the cervical stroma so that the suture can be placed closer to the uterus. This procedure can be used with a short cervix, however it is more difficult to place and more difficult to remove. The success rates for both procedures are not significantly different. McDonald procedure success rate is 63-89%, and the Shirodkar procedure success rate is 75-85% [16].

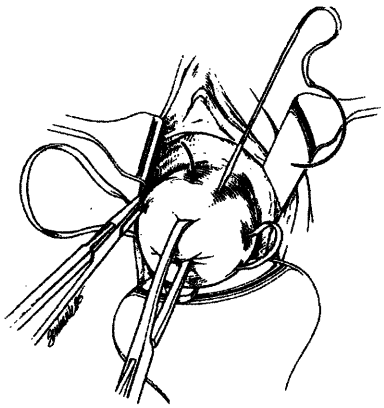

Figure 1-6: Surgical procedure for transvaginal cerclage.

Transabdominal cerclage is used for women with previous failed transvaginal cerclage and for women whose cervix is too short for vaginal cerclage. As illustrated in Figure 1-7, the cervix is accessed through the abdomen and it is sewn closed at the internal OS. This stitch is higher than the transvaginal stitches and it requires cesarean section delivery. This method has a reported higher success rate of 82-100% [86]. However, it requires major abdominal surgery with complications including hemorrhage, infection, fetal loss, and PROM.

The effectiveness of the cerclage procedure is unclear because diagnostic criteria for cervical insufficiency are still controversial, and identifying high risk patients is extremely difficult [104][42]. Three observational studies [13][52][54] and two randomized trials [1][106] assess cerclage procedures. Results from these individual studies reach conflicting conclusions. Two of the observational studies, Heath et al. [52] and Hibbard et al. [54] found pre-term birth before 34 weeks was statistically lower in the cerclage group. On the other hand, the third observational study, Berghella et al. [13], found no statistical difference between the cerclage and control groups.

Althuisius et al. and Rust et al. conducted prospective randomization studies to assess the effectiveness of cerclage procedures and reached opposite conclusions. Althuisius et al. [1] claimed that cerclage is an effective treatment for women at risk of cervical insufficiency. The group defined high risk patients as women with previous pre-term delivery before 34 weeks of gestation, previous pre-term rupture of membranes before 32 weeks of gestation, history of cold

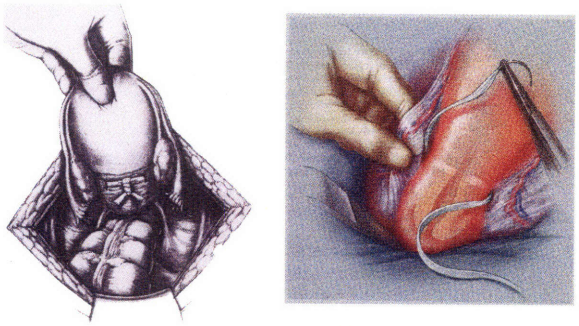

Figure 1-7: Surgical procedure for transabdominal cerclage.

knife conization, diethylstilbestrol exposure, uterine anomaly, or cervical length below 2.5cm before 27 weeks of gestation. The high risk patients were randomized into two groups: the cerclage and the bed rest groups. The cerclage group received a single purse-string suture and prescribed bed rest. The bed rest group received bed rest only. The cerclage group had significantly lower pre-term delivery before 34 weeks and significantly lower compound neonatal morbidity (neonatal morbidity is admission to the neonatal intensive care unit or neonatal death) [1].

On the other hand, Rust et al. [106] concluded that there is no benefit to cerclage therapy. Their study randomized 135 patients into two groups, a cerclage group and a no-cerclage group. Women included in the study were between 16 and 24 weeks gestation and showed the following signs of cervical insufficiency: a short cervix below 25mm, internal os dilation, or membrane prolapse into the cervical canal at least 25% of the cervical length [106].

The difference in study design may contribute to the conflicting results between Rust et al. and Althuisius et al. The two groups used different criteria of inclusion for their randomized trials. Rust et al. included women with prolapsing membranes, but Althuisius et al. did not include women with prolapsing membranes. Further, Althuisius et al. only had 35 women in their study while Rust et al. included 113 patients. More recently, Jorgensen et al. [63] conducted an individual patient data meta-analysis across nine different cerclage studies in the literature to assess the effectiveness of the cerclage for singleton pregnancies and multiple

gestations. This study standardized the definitions and outcomes used in each study to be able to compare and combine results. By combining the results from the nine studies, Jorgensen et al. found that cerclage may reduce the risk of neonatal loss or death. However, this result was not statistically significant at the 5% level. The group concludes that further studies need to be conducted to assess if cerclage is beneficial for singleton pregnancies. For multiple gestations, Jorgensen et al. claims that there is statistically significant evidence that cerclage increases the risk of pre-term loss [63]. These conflicting results highlight the need to improve our understanding of the mechanisms leading to cervical insufficiency.

1.3 Biochemical Characteristics of Cervical Tissue

The uterine cervix is a dense fibrous organ with its biochemical properties and microstructure determining its strength and integrity. The microstructure of the cervical stroma is composed of a dense, hydrated, and highly cross-linked collagen network embedded in a viscous proteoglycan groundsubstance. These biochemical components exist on varying length scales from the nanometer to the millimeter, and act together in a cooperative nature to give the cervix tensile and compressive strength. It is established in the literature that a shift in the microstructural components of the stroma are responsible for cervical maturation during pregnancy. However, the process of cervical ripening and softening is still not completely understood with varying biochemical data [105] and maturation theories [100] in the literature.

This section reviews the biochemical literature relating to pregnant, non-pregnant and insufficient cervix. The components of the extracellular matrix (ECM) of the non-pregnant cervix are fully described with a detailed explanation of how each biochemical component changes in concentration during cervical maturation. Further, collagen and proteoglycan structure and function are thoroughly discussed in the context of cervical strength in the pregnant and non-pregnant state.

1.3.1 Extracellular Matrix Components of Cervical Tissue

Cervical tissue is primarily composed of a dense insoluble extracellular matrix (ECM). The ECM supports cervical cells, mainly fibroblasts and smooth muscle cells. The cellular compo-

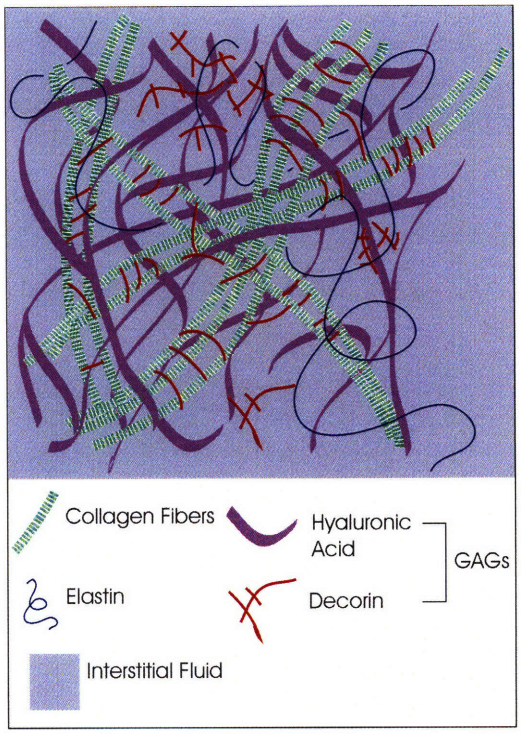

Figure 1-8: A schematic representation of the extracellular matrix of human cervical tissue. The ECM is composed of a three-dimensional collagen fibril network containing type I and III fibrils. Surrounding the collagen network are proteoglycans, glycosaminoglycans, elastin and interstitial fluid.

nent is typically around 20% per volume with 10-15% of the total cervix volume being smooth muscle cells[80]. The ECM provides strength and rigidity to resist mechanical loading, and provides a scaffold for cell attachment and migration. The biochemical constituents of the ECM are tissue and function specific. The constituents of cervical ECM include a three dimensional collagen network embedded in a highly viscous proteoglycan groundsubstance which is interlaced with the protein elastin. The collagen network contains highly crosslinked type I and III fibrils, and the groundsubstance is composed of interstitial fluid, proteoglycans (PGs) and glycosaminoglycans (GAGs). The glycosaminoglycans are present either in the form of proteoglycans such as dermatan sulfate in decorin, or they are embedded in the matrix without a core protein as in the case of hyaluronic acid. Figure 1-8 represents the biochemical constituents of the cervical ECM. See Table 1.2 (from [40]) below for the percentage of each constituent [71].

Water	80%				
Dry tissue	20%				
	Collagen		GAGs		Elastin
	~70% [80]		~0.2% ([112], [99])		~2% [81]
	Type I	Type III	Dermatan sulfate	Heparan sulfate	Hyaluronic acid
	~70%	~30%	76%	13%	11%
	([70], [60])		[112]		

Table 1.2: Main constituents of human cervical tissue in non-pregnant women

Cervical maturation is independent of uterine activities, and is associated with cervical tissue remodelling. Leppert and Garfield et al. have summarized cervical conditioning as an inflammatory cascade of events which is triggered by hormonal changes [76][45]. This process includes:

- Release of proinflammatory cytokines
- Migration of white blood cells to the cervical tissue
- Release and activation of degradative enzymes such as matrix metalloproteinases
- Increase in collagen and glycoprotein turnover and synthesis
- Disruption of collagen network superstructure
- Change in decorin and collagen ratio
- Increase in hyaluronic acid concentration
- Increase in interfibrillar fluid

Studies on both human and animal models have examined cervical softening at different stages of pregnancy. Shimizu et al. [108] analyzed human biopsy samples for glycosaminoglycan content and its related biochemical alterations at different gestation periods. Kokenyesi and Woessner [73] studied dermatan sulfate levels related to mechanical creep properties of rat cervix at different gestational age. Danforth and Ekman [33] investigated the collagen solubility of human biopsy specimens in a variety of solvents to measure the strength of collagen cross-linking. The Danforth study also measured hydration and collagen concentration levels for

non-pregnant and at term human cervical specimens. Substantial differences in methods and protocols to test and prepare cervical tissue result in large discrepancies in the results of these studies. Therefore, conflicting mechanical and biochemical data exist in the literature.

1.3.2 Water Content

Studies on nonpregnant and postpartum human cervical tissue [33][108][101] have found that there is an increase in water content during cervical maturation. Danforth et al. [33] measured the hydration levels in human postpartum and nonpregnant cervix. This study found a slight increase from 74.4% to 78.4% in water content from the nonpregnant to the postpartum cervix. Shimizu et al. [108] also found that water content in human cervix was higher in postpartum than in nonpregnant tissue. The water content was 78.1%, 79.7%, and 83.6% for proliferative phase nonpregnant, secretory phase nonpregnant, and postpartum cervix, respectively. Rechberger et al. [101] found that the water content is 81.1% for nonpregnant tissue and 85.5% for multipara postpartum tissue.

1.3.3 Collagen

Collagen Synthesis and Structure

Collagen is the most abundant protein in humans and exists in at least 20 different forms. Different forms appear in various organs and tissues depending on their function. The extracellular matrix of load-bearing soft tissue contains a high percentage of fibril collagen with strong tensile strength. The fibril collagen types are mainly type I, II, and III, and they are insoluble in solvents which disrupt ionic interactions and hydrogen bonding [113]. In the cervix, collagen accounts for 85% of dry mass with 70% type I and 30% type III fibrils [38].

Figure 1-9 illustrates the path for collagen fibril and fiber formation. This diagram is specifically for Type I collagen. Type II and III have similar fibril structures. Collagen molecules are first synthesized in the fibroblast rough ER and Golgi Complex. The cell secretes collagen as long procollagen molecules with additional amino acid chains at the N and C terminus. These additional amino acid chains are called the propeptides and believed to be responsible for proper formation of the helical structural. Extracellularly, the propeptides are cleaved

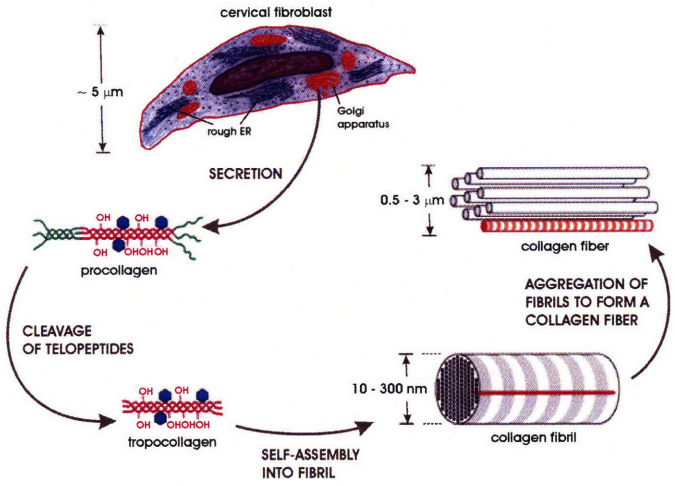

Figure 1-9: Collagen molecules are formed and modifided in a sequence of events which occur in the rough ER, Golgi complex, and the extracellular space. Collagen molecules self aggregate into collagen fibrils which further aggreate to form collagen fibers. (Adapted from Alberts et al, Molecular Biology of the Cell, 3rd ed., Garland Publishing 1994) [40].

through an enzymatic reaction and the collagen molecule becomes tropocollagen which is the basic building block of the collagen fiber[36].

The tropocollagen is approximately 300nm long and 1.5nm thin. It is composed of three coiled peptide chains, two $\alpha 1$ and one $\alpha 2$ chains. The peptide chains have a repeating triplet amino acid sequence of Gly-X-Y. This triplet forms a chain of 1050 amino acids where every third amino acid is glycine. The X and Y can be any amino acid, but most often they are proline and hydroxyproline. The three peptide chains form a right handed helix with three amino acids per turn. The space between the peptide chains are only small enough to fit one side chain of glycine. This center location is the site of a strong hydrogen bond between the glycine side chain and a residue from a neighboring amino acid on another chain. This intramolecular bond and the well-packed triple helical structure give the tropocollagen molecule its strong tensile properties.

The tropocollagen self assembles laterally to form the collagen fibril. The tropocollagen pack together in a side-by-side array where every row is displaced by approximately 67nm. Because of this displacement the collagen fibers appear banded in electron micrographs. See Figure 1-10 for fiber and fibril representations. The fibril assembly is driven by spontaneous

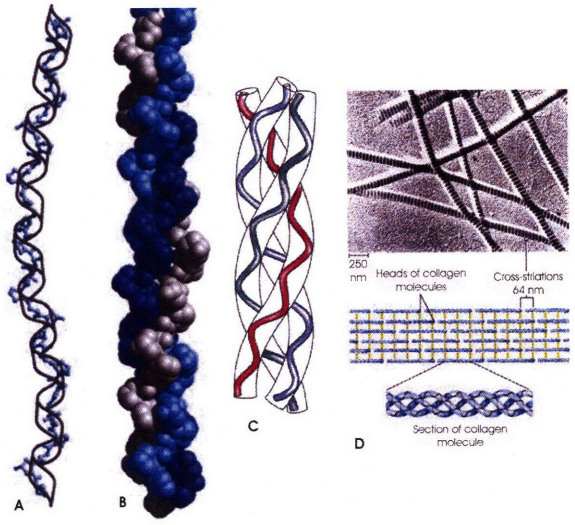

Figure 1-10: A, B, and C are interpretations of the basic tropocollagen molecule. D illustrates the staggered array of the collagen molecule into the fibril formation [40].

associations with adjacent collagen molecules and hydrophobic interactions. The fibril assembly is stabilized by covalent cross-links between adjacent tropocollagen molecules. The cross-links are located specifically between the N and C terminus of neighboring molecules, and are formed by an enzymatic reactions located on the lysine and histidine side chains. Up to four side chains can be crosslinked [113] [36].

Once the collagen molecules assemble into fibrils, the fibrils can aggregate into larger "rope-like" fibers. This aggregation of fibrils is tissue and function specific. For example, tendon fibrils are in a parallel bundles optimized to support uniaxial tensile forces. The collagen in skin forms sheets of fibrils which are layered at many angles to withstand biaxial forces [46]. The collagen of articular cartilage can be organized in a three-dimensional anisotropic matrix to support compression forces [17].

The collagen fibrils of the extracellular matrix are intramolecularly and intermolecularly crosslinked. The intramolecular cross-links are the strong hydrogen bonds between peptide chains of the tropocollagen triple helix. The intermolecular cross-links are the stable covalent cross-links between adjacent collagen molecules of the fibril. These cross-links occur at the non-helical N and C terminus of adjacent tropocollagen molecules (See Figure 1-11) [36][113].

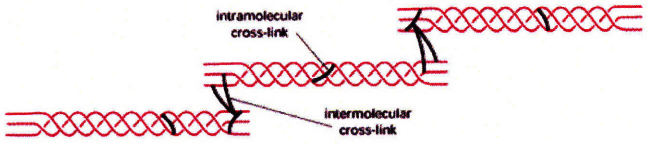

Figure 1-11: Intramolecular links are hydrogen bonds between peptide chains. Intermolecular links are convalent links between collagen molecules. These crosslinks form at the N and C terminus of the molecule [113]

In addition to these strong covalent bonds there are weaker non-covalent crosslink interactions between fibrils which help to maintain the integrity of the structure. Many of the these non-covalent cross-links are associated with the fibril entanglement of the collagen network [18].

Collagen Orientation in the Human Cervix

MRI [116] and X-ray [4] studies have shown that the collagen structure has a preferred orientation to resist cervical effacement and dilation. Both studies revealed that the cervix has three seamless zones of structured collagen in the stroma: the innermost and outermost rings of stroma contain collagen fibers preferentially aligned in the longitudinal direction, and the middle layer contains collagen fibers preferentially aligned in the circumferential direction (See Figure 1-12 for a schematic diagram of the zones of preferentially aligned collagen in the cervical stroma).

An early study by Aspden et al. [4] determined the collagen organization for 8 non-pregnant human cervix using an X-ray diffraction technique. The study found that nonpregnant human cervix contained three zones of organized collagen as pictured in Figure 1-12. (The same study found similar organization in rat cervix). The collagen fibrils transition smoothly between the different zones to avoid any discontinuities. The innermost and outermost zones of collagen fibrils range from 3-5mm in the radial dimension and the middle zone ranges from 5-12mm. These ranges represent the variability between the patients.

The most recent study to investigate the collagen organization in non-pregnant human cervix is from Weiss et al. [116]. This study conducted ex vivo measurements on five specimens from premenopausal women using three-dimensional magnetic resonance (MR) diffusion tensor imaging (DTI). Similar to the early Aspden data, this study also concluded that the

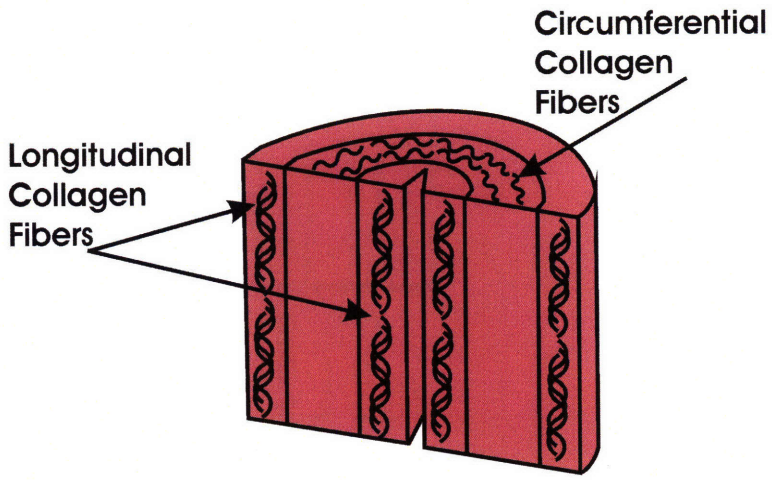

Figure 1-12: A schematic representation of the cervical stroma (the fascia and mucosa have been removed) and the three seamless zones of preferentially aligned collagen fibers. X-ray and MRI data on human cervical tissue indicate that the middle layer of stroma contains collagen fibers preferentially aligned in the circumferential direction and the outer and inner layers contain collagen fibers preferentially aligned in the longitudinal direction [116][4]. (Figure adapted from [4]).

human cervix contains three zones of structured collagen; Inner and outermost zones contain longitudinal fibers and the middle zone contains circumferential fibers. During pregnancy, this collagen orientation changes with maturation. Early studies by Danforth [33][118][19] have reported changes in the collagen network during maturation where the network breaks down and becomes disorganized (discussed below in more detail).

Collagen Content: Pregnant vs. Nonpregnant Tissue

It is disputed in the literature on whether collagen is lost during cervical softening at term, or if the concentration decreases due to an increase in other biochemical contents. Leppert discusses this discrepancy in [77], and asserts that the collagen content does not decrease during gestation or at term. Instead, the collagen concentration decreases because there is an increase in other ECM components, mainly water, at term. Leppert reports an increase in collagen synthesis during pregnancy and an even larger increase in the water content and other cervical proteins. Early studies by Maillot and Zimmermann [82] and Kleissl et al. [70] also confirm that the collagen content when measured per tissue dry weight does not change between pregnant and

nonpregnant tissue specimens.

A number of studies, however, have concluded that there is a decrease in the collagen concentration during cervical ripening [33][45]. In both studies it is unclear if the collagen concentration was measured with respects to the wet weight or the dry weight of the tissue. Again, it is unclear if the actual collagen content decreased, or if the collagen content remained the same while other biochemical components increased during the softening process. While the collagen concentration in pregnant and nonpregnant tissue is debated in the literature, it is clear among researchers that the collagen network is disrupted during cervical maturation. The next Section discusses the collagen network remodelling process during gestation and maturation.

Collagen Network Remodelling and Degradation During Pregnancy

Many studies suggest that the remodelling and degradation of the collagen network play a large role in cervical softening [82][107][70][33][118][19]. In a normal nonpregnant cervix, the collagen fibers are in a tight, organized bundled network. Aspden et al. [5] found that at term cervical tissue has altered collagen fiber length, alignment, and organization. The collagen fibers become smaller and the collagen network becomes loose and disorganized. The authors claim that the collagen fibers need a critical length of 20μm to maintain tensile strength [5] suggesting that the alteration of collagen fibers plays a role in cervical softening.

The reorganization of the collagen network during cervical softening is facilitated by an inflammatory process which breaks down insoluble collagens. In coordination with this process, there is an increase in collagen synthesis by the cervical fibroblasts [77][82]. In late pregnancy, the collagen synthesis rate increases and fibroblasts produce altered soluble collagen molecules [77]. With the breakdown of the insoluble collagen and the increase in the soluble collagen, the collagen network is over-turned and the tissue softens. The alteration of the collagen network is evident when comparing the morphology of pregnant (or postpartum) tissue to the morphology of the nonpregnant tissue (See discussion in Section 1.4) Further, the collagen network alteration is evident when testing the tissue's solubility in different extraction solvents. The tissue will become more soluble in late pregnancy when compared to the nonpregnant or early pregnancy state. Studies measuring cervical tissue solubility in the nonpregnant and pregnant state are discussed below, and studies on patients with previously diagnosed CI are

presented in Section 1.3.3.

Inflammatory Process Sennstrom et al. [107] argued that there is a distinct inflammatory process that increases the collagenase activity during cervical ripening to cause collagen degradation. The study measured increased levels of metalloproteinases (MMP), a collagenase group, in human postpartum cervical samples as compared to nonpregnant cervical samples. Specifically, the levels of MMP-8 for postpartum women was 7300ng/mg wet weight and 86ng/mg wet weight for nonpregnant women. Immunohistochemical stains of nonpregnant and postpartum samples confirm increased activity of MMP-8 in the stromal cells of postpartum cervix. Another study by Nagase [92] suggests that cervical dilation is associated with the breakdown of collagen fibrils. This study concludes that increased levels of MMPs are associated with cervical softening and maturation.

Collagen Extractability (Solubility): Normal Tissue Results from extractability experiments (the measure of tissue solubility in an extraction solvent) on human and rat cervical tissue give evidence that the collagen network becomes disrupted during pregnancy [33][82][70][59][101][48]. During cervical maturation there is an increase in the content of soluble collagen, and there is a breakdown of intact collagen crosslinks. When the tissue is experimentally exposed to a given solvent, only the strong cross-links will remain intact. The weaker cross-links will be disrupted, and a fraction of the collagen will become soluble. A measure of the soluble collagen gives a measure of the tissue's "extractability" and gives an indication of the strength of the collagen network. Many studies have explored the solubility of cervical collagen in different solvents and have concluded that tissue solubility increases during cervical maturation.

Danforth et al. [33] extracted human cervical tissue in a succession of water, saline, guanidine hydrochloride, and urea solutions. The study compared non-pregnant with postpartum cervical tissue. A large percentage of the collagen in the postpartum cervical samples were solubilized in the extractions: 84% of the original collagen of the postpartum cervical tissue was extracted in the first water extraction. In the end, only 24% of the collagen in the postpartum specimens remained insoluble as compared to 67% of the collagen in the non-pregnant cervix.

Maillot et al. [82], Kleissl et al. [70], Ito et al. [59], Rechberger [101], and Granström et al. [48] also measured the extractability of human cervical tissue. Despite variations in the

extraction protocols for each study, all groups concluded that postpartum (or pregnant) tissue had a higher solubility when compared to nonpregnant tissue.

Maillot and Zimmermann [82] extracted human cervical tissue in 0.175M acetic acid at 48 hours followed by a serial extraction in 8M urea for 24 hours at 25°C and for another 24 hours at 40°C. The group took tissue specimens from 48 women: 15 nonpregnant, 5 pregnant in the first and second trimester, 19 in the late third trimester, 10 at term, and 8 postpartum. The study found a significant increase in tissue solubility in the acetic acid for the pregnant tissue at term when compared to the nonpregnant tissue. When comparing the nonpregnant tissue with tissue specimens from the early and late pregnancy group, there was only a slight change in tissue solubility. The largest increase in tissue solubility occurred during labor. There was a significant change in tissue solubility between partially dilated patients and fully dilated patients. These results suggest that the collagen network drastically changes during the short period of active labor while it remains intact during the full gestation of the pregnancy.

Kleissl et al. [70] extracted human cervical tissue in 0.125M acetic acid and Ito et al. [59] extracted human cervical tissue in 0.5M acetic acid. Both groups found increased tissue solubility for postpartum tissue when compared to the nonpregnant controls. Granström et al. [48] measured the solubility of human cervical tissue in patients with protracted labor and patients with normal labor. This study extracted tissue samples 0.5M acetic acid with 1mg/ml pepsin, and found that women with protracted labor had a lower tissue solubility when compared to women with normal labor. Again the results from these studies suggest that a correlation exists between the strength of collagen crosslinks and different stages of pregnancy and cervical maturation.

Kokenyesi and Woessner [73] extracted rat cervix in 4M guanidine-hydrochloric acid solvent containing protease inhibitor. They extracted the tissue for 24 hours and separated out the resulting supernatant to analyze for collagen content. The solubility of collagen in 4M guanidine-HCl was 8 times higher at time of delivery than in the nonpregnant state. The collagen fibers were 8 times more soluble in the pregnant state because the fibers were loose and not well organized. Kokenyesi and Woessner state that this particular extraction procedure does not disrupt the covalent collagen bonds, and only disrupts the weak nonconvalent bonds (i.e. ionic and van der Waals' forces).

Collagen Solubility and Genetic Studies: Patients with CI

It has been suspected that CI is caused by a connective tissue disease which compromises the collagen network [114]. However, not many studies have been performed on human cervical tissue taken from patients with diagnosed CI. Not much is known about the underlying mechanisms and biochemical change of cervices that have failed during pregnancy. Further, it is not known if the mechanisms weakening the collagen structure in the insufficient cervix are the same mechanisms associated with cervical ripening at the time of delivery in the healthy cervix. Three studies which focus on tissue specimens taken from CI patients have found that CI may be related to weaker collagen crosslinking [101][97] or a genetic defect affecting the collagen network [114].

Rechberger et al. [101] and Petersen et al. [97] investigated the solubility of collagen in nonpregnant cervical tissue from women with previous cervical insufficiency and women with normal obstetric history. Rechberger et al. [101] solubilized human cervical tissue from patients with CI and compared the results with nonpregnant and normal postpartum tissue. The study extracted the tissue in 0.5M acetic acid containing 1mg/ml pepsin. The results indicate that the CI tissue had a higher extractability when compared to the nonpregnant tissue where 87.6% of the CI tissue was solubilized and 66.8% of the normal tissue was solubilized. The solubility of the CI tissue (from patients in their second trimester) was comparable to the solubility of the postpartum tissue which was 91.1% soluble. These results indicate that there is a connective tissue change in women with CI, and this change is similar to the collagen network changes that happen during cervical maturation.

Similar to Rechberger et al., Petersen et al. extracted biopsy specimens in 0.5M acetic acid containing 1mg/ml pepsin and measured the collagen (hydroxyproline) content in the extract. The study found higher amounts of hydroxyproline in the extracts from women with previous cervical insufficiency. The extractability was 80.2% for women with previous cervical insufficiency as compared to an extractability of 49.5% for normal parous women. The increased tissue solubility for both the insufficient and postpartum cervix suggests that the collagen network in these tissues have been compromised or disrupted.

A very recent study published in 2007 by Warren et al. [114] found genetic evidence linking CI patients to a genetic defect that is known to cause connective tissue disorders. Polymor-

phisms in the COL1A1 and the TFG-β genes were found in a statistically significant pool of patients having previously diagnosed CI. These same polymorphisms have been previously connected to abnormalities in other connective tissues (i.e. [49][15]). The results of the Warren study are discussed in Section 1.2.2.

1.3.4 Proteoglycans and Glycosaminoglycans

Structure

Proteoglycans are glycoproteins consisting of a core protein to which at least one glycosaminoglycan chain is covalently attached [113]. They are typically identified by their glycosaminoglycan side chain. Glycosaminoglycans may also exist without the core protein as in the case of hyaluronic acid. Glycosaminoglycans are linear polymers of repeating disaccharides. Disaccharides are two linked monosaccharides which are simple sugars. The simplest GAG structure is hyaluronic acid which consists of alternating polymers of the monosaccharides N-Acetylglucosamine and glucuronic acid. Chondroitin-4 Sulfate has repeats of glucuronic acid and N-Acetylgalactosamine and is sulfated on the 4th carbon. Chondroitin-6 Sulfate is analogous to Chrondroitin-4 Sulfate but it is sulfated on the 6th carbon. Dermatan sulfate is similar to Chondroitin-4 sulfate except its repeats of L-Iduronate and N-Acetylgalactosamine [113]. Figure 1-13 illustrates the disaccharide units of common glycosaminoglycans. Each of these units is repeated to create the polymer chain of the glycosaminoglycan.

Hyaluronic acid (HA) does not link to a core protein and exists as a glycosaminoglycan in the extracellular matrix. In solution, hyaluronic acid has a randomly kinked coil structure that can entangle and form stiff networks [117]. When hydrated, pure HA can swell to one thousand times its dry weight, forming a highly viscous gel. During cervical softening hyaluronic acid concentration increases. This increase causes the tissue to imbibe water and disrupts the collagen network by increasing the spacing between fibrils.

The main proteoglycan in cervical tissue is decorin, a dermatan sulfate proteoglycan. It belongs to a family of PGs called Small Leucine Rich Proteoglycans (SLRPs) which include biglycan, fibromodulin, lumican, epiphycan, and keratocan. The common feature of this family is their three domain structure. The amino-terminal domain is the attachment site for the negatively charged glycosaminoglycan. The core protein domain contains eight to ten

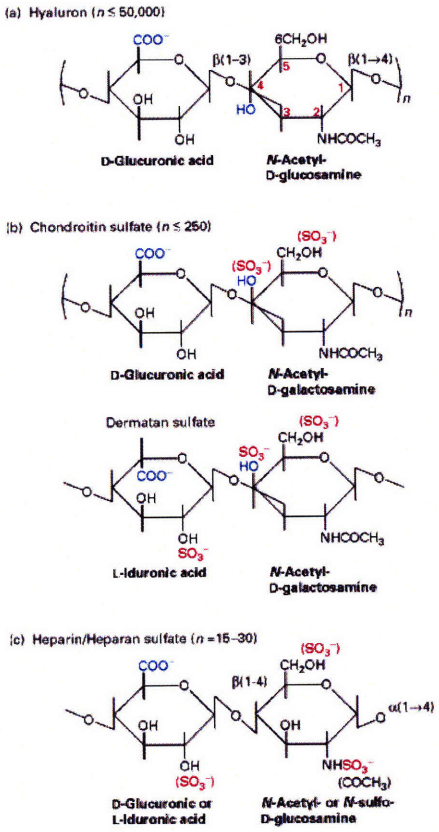

Figure 1-13: Glycosaminoglycans are composed of repeating dissacharides units. "n" represents the number of repeats of each unit [40].

Tissue	Hyaluronic Acid	Chondroitin Sulfate	Dermatan Sulfate	Heparan Sulfate	Acidic GP
Non-pregnant Proliferative	1.09 (11.6)	0.87 (9.3)	6.18 (66.0)	0.45 (4.8)	0.77 (8.2)
Non-pregnant Secretory	0.90 (10.1)	0.62 (7.0)	6.29 (70.5)	0.52 (5.8)	0.59 (6.6)
Post Partum	2.72 (17.7)	2.34 (15.2)	5.18 (33.7)	2.18 (14.2)	2.95 (19.2)

Table 1.3: Glycosaminoglycan count for human cervix from Shimuzu et al. study. Numbers are expressed in mg of GAG (in terms of hexosamine)/g dry tissue

leucine repeats. This core protein domain has a specific amino acid sequence located between repeats 4 and 6 that bind specifically to fibril types of collagen. The end domain contains two cysteine residues and its function is unknown [35]. The small leucine rich PG family is involved with regulating cell proliferation, differentiation, adhesion and migration [55].

Proteoglycans and structural glycosaminoglycans are embedded within the collagen network of the extracellular matrix. Their main function is to generate high osmotic pressure, maintaining tissue hydration and allowing the tissue to sustain compressive forces, and to regulate collagen fibril formation and spacing.

Glycosaminoglycan Concentrations During Pregnancy

An early biochemical study on human cervix was conducted by Shimizu et al. [108]. Biopsy specimens were taken from proliferative and secretory phase nonpregnant patients and from postpartum patients. Glycosaminoglycans were measured before and after specific enzymatic digestions of Streptomyces hyaluronidase, chondroitinase AC-II and chondroitinase ABC. The hyaluronic acid, chondroitin sulfate, heparan sulfate and acidic glycosaminoglycan content was higher in the postpartum cervix as opposed to the nonpregnant cervix. Only the dermatan sulfate content was significantly lower in the postpartum cervical specimen than in the nonpregnant specimen [108]. See Table 1.3 for glycoprotein measurements.

A study conducted by Rath et al. [99] reports an increase in total glycosaminoglycans during pregnancy, but a large decrease in dermatan sulfate at time of parturition. Biopsy specimens were taken from 87 pregnant and nonpregnant women. Samples from the pregnant cases were

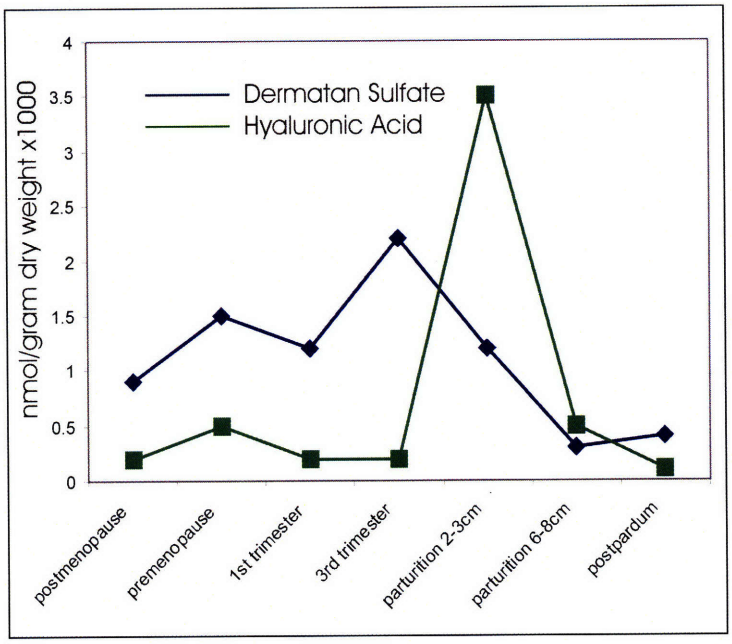

Figure 1-14: The dermatan sulfate levels in human cervix decrease significantly at parturition. The hyaluronic acid concentration increases significantly at time of parurition and falls again by time of post pardum. Graph adapted from Rath [99][40]

taken at different stages of pregnancy: first trimester, third trimester, parturition at cervical dilation of 2-3cm, and parturition at cervical dilation of 6-8cm. Samples were defatted with acetone and digested with papain overnight. Samples were analyzed using high-performance liquid chromatography (HPLC) for glycosaminoglycan content. It was found that the changes in proteoglycan content happens rapidly with the onset of labor. The large decrease in dermatan sulfate is thought to destabilize the collagen fibers thus allowing the cervix to dilate and ripen. The results for dermatan sulfate and hyaluronic acid concentration are in Figure 1-14.

Hyaluronic acid (HA) has an affinity for water molecules, thus an increase in HA concentration causes an increase in hydration for soft tissues. Maradny et al. [83] studied the HA concentration and its effects on pregnant and non-pregnant rabbit cervix. The increase in water content in the cervical tissue caused the collagen bundles to fragment and separate. The interfibrillar spaces increased and the network became less organized and less dense [83]. The study concludes that HA is responsible for increased tissue hydration, stimulation of collagenase,

and ultimately control of cervical ripening. HA was injected into pregnant and non-pregnant rabbit cervix and in both cases HA induced cervical ripening and caused a large increase in water content.

1.3.5 Elastin

Elastic fibers are another major component of the extracellular matrix, which complex structure contains elastin, microfibrillar proteins, and lysyl oxidase. The major protein of mature elastic fibers is elastin, characterized by a high degree of reversible extensibility and capability of sustaining large deformation with the application of small forces [10]. Elastin provides the elastic fibers with the characteristic properties of elastic recoil.

The cervical stroma has a small composition of mature and cross-linked elastin ranging between 0.9% and 2.4% of dry tissue weight, which does not change during pregnancy [80]. In the uterus, at parturition, the elastin increases to 800% over its normal level and decreases rapidly after the delivery [80]. The uterine elastin contributes significantly to the restoration of the extended organ by means of elastic recoil [80]. In contrast to the stiff collagen fibrils of the cervix, the elastic tissues in the uterus are soft and extensible [80].

The thin elastic fibers in the nonpregnant cervix form a loose network structure composed of membranes and fibrils interconnected to give a fishnet-like appearance, which runs parallel to and between the layers of the collagen fibers. Late in pregnancy, the elastin fibers have a slightly increased diameter and demonstrate very little organization. Immediately postpartum certain dissociation and branching of the fibers has been observed. The elastic membranes in the uterus have a sponge-like appearance and are freely stretchable in any direction. Such a structure provides support for the growing fetus without exerting any excess pressure.

The precise biomechanical properties of the elastin have not been fully characterized. It is believed that elastin has rubberlike characteristics and therefore can be modeled as a network or cross-linked and randomly oriented chains to which the theory for rubberlike materials can be applied. According to the rubber theory such a network is in a state of maximum disorder or entropy, and extension of the material aligns the elastic fibers in the direction of the applied deformation, thus reducing the number of possible configurations for the fibers and decreasing the entropy of the system. The two configurations are depicted in figure 1-15, where 1-15.A

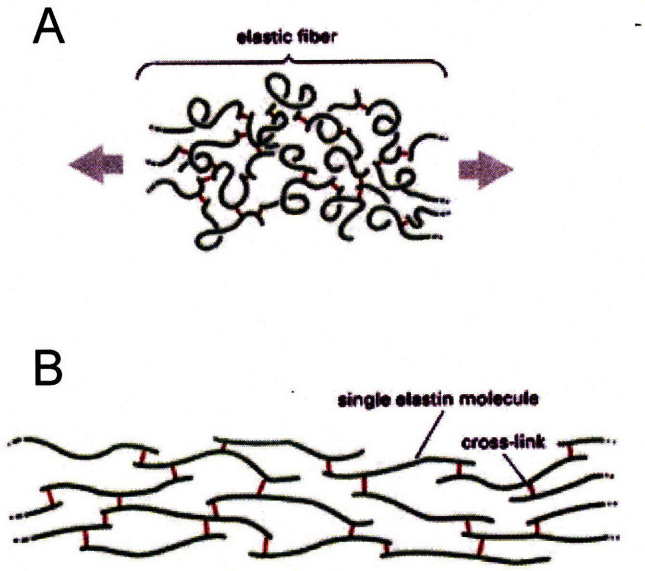

Figure 1-15: The elastic fiber network. (A) The loose network of cross-linked elastin fibrils (B) Uniaxial extension of the elastic fibers.

shows the unstretched elastic fiber network and 1-15.B shows the aligned network under uniaxial extension. Upon release, the elastic fibrils spontaneously return to their initial random configuration in order to restore the original entropy level. Because of their mechanical behavior it is believed that the elastic fibers play a major role after parturition, when by means of elastic recoil they facilitate the recovery of the distended organ of the uterus [80], [77]. Leppert argues that decreased levels of elastin in the cervical stroma of women with cervical insufficiency provide evidence for the role of this protein in pregnancy [77]. In their work Bank et al. [7] report an estimated Young's modulus of $0.3\text{x}10^6$ Pa for elastin, while the corresponding value for collagen is $0.1\text{x}10^9$ Pa for collagen fibrils [81]. Danforth reports that elastic fibers appear to constitute but a fraction of 1% of the total fibrous tissue in the human cervix [34].

1.3.6 Glycosaminoglycan and Collagen Functional Interdependence

Proteoglycans (PGs) and collagen fibers interact to maintain a balance of internal forces in the tissue and to regulate the mechanical function of the extracellular matrix. PGs induce a high osmotic pressure to imbibe interstitial water. The collagen fibers have tensile strength

to counteract this swelling tendency and to limit the increase in tissue volume. The PGs also specifically bind to collagen fibrils to enhance collagen cross-linking and to regulate collagen fibril spacing. These interactions are an example of how biochemical content influence the mechanical integrity of soft tissue. Many investigators have studied the interplay between proteoglycans and collagen. Danielson et al. [35] mechanically tested skin of Decorin-null mice. Maroudas et al. [8] experimentally measured the osmotic pressure and tensile force in articular cartilage. Broome et al. [17] mechanically tested articular cartilage before and after proteoglycan degradation. All of these investigations noted abnormal mechanical properties when the balance between collagen and glycoproteins was disrupted.

Hydrostatic Stress Balance in Hydrated Tissue

Hydrated soft tissue maintains its shape and mechanical integrity through a balance of swelling and tensile forces. The fixed charge density associated with proteoglycans tends to imbibe fluid, and the tensile forces in the collagen network oppose the swelling tendency and limit the increase in volume. The contributing factors to the tissue swelling pressure are the Donnan osmotic interactions, the affinity between the matrix and solvent, and the thermal motion of matrix macromolecules. The Donnan electrostatic forces include the repulsive forces between charged proteoglycans and the large counterions concentration that must be present in the tissue to maintain electroneutrality. The Donnan forces decrease with increased swelling, increased bath saline concentration and decreased fixed charge density. If one component of this force balance is altered then the mechanical response of the tissue may be compromised [37].

Maroudas et al. [8] measured the collagen tensile force in articular cartilage by applying known external osmotic pressure to in-vitro human cartilage samples and measuring the resulting hydration. The external osmotic pressure was applied with calibrated baths of Polyethylene glycol (PEG) solutions, and the osmotic pressure of the proteoglycans was governed by the fixed charge density which was established by the proteoglycan concentration. The three forces considered in the Maroudas experiment were the hydrostatic stress (tensile) from the collagen network P_C, the applied isotropic pressure from the PEG bath π_{PEG}, and the osmotic pressure from the proteoglycans π_{PG}. The tensile force of the collagen network P_C and the applied isotropic osmotic pressure of the bath π_{PEG} tended to force water out of the sample.

The osmotic pressure π_{PG} from the proteoglycans tended to imbibe water. The balance of forces was given by Equation 1.1.

$$P_C + \pi_{PEG} = \pi_{PG} \tag{1.1}$$

Maroudas et al. measured P_C for different cartilage samples as a function of hydration. The samples included normal and trypsin-treated cartilage and one osteoarthritic joint. Cartilage specimens were equilibrated overnight in 0.15M NaCl. The specimen were then placed in a dialysis bag, re-equilibrated in calibrated PEG solutions, and immediately weighed to determine its hydration. The resulting osmotic pressure, π_{PG}, was then calculated from an empirical relationship between hydration, fixed charged density and osmotic pressure of a solution of isolated proteoglycans at the same concentration. The main assumption of this approach was that the osmotic pressure produced by the PGs in the tissue was equal to the osmotic pressure of isolated PGs at the same concentration. With the applied pressure π_{PEG} known, and the π_{PG} calculated from this empirical relationship, the tensile force in the collagen, P_C, could be calculated from equation 1.1. This procedure was repeated for different PEG solutions at different hydration levels.

Figure 1-16 Graph A gives an example of the balance of forces in normal adult cartilage. The collagen tensile force P_C versus hydration levels for the normal and trypsin treated cartilage samples were very similar. However, Graph B illustrates that the collagen tensile force P_C versus hydration curve for the osteoarthritic patient was much lower than the normal and trypsin treated specimens. The stiffness of the collagen network controls the level of hydration in-vivo and gave the tissue dimensional stability. The osteoarthritic samples were thought to have a weaker collagen network and therefore were unable to maintain high PG concentrations and resist mechanical loading.

In similar experiments Broom and Poole [17] enzymatically digested proteoglycans from articular cartilage and measured the compressive strength in normal and PG-free specimens. These experiments had different objectives from the studies of Maroudas et al.; Broom and Poole investigated the effects of PGs on the tissue's compressive strength, while the Maroudas study investigated the tensile strength of the collagen fibrils in osteoarthritic patients. Broom and Poole obtained articular cartilage from cows and tested three specimens from a single

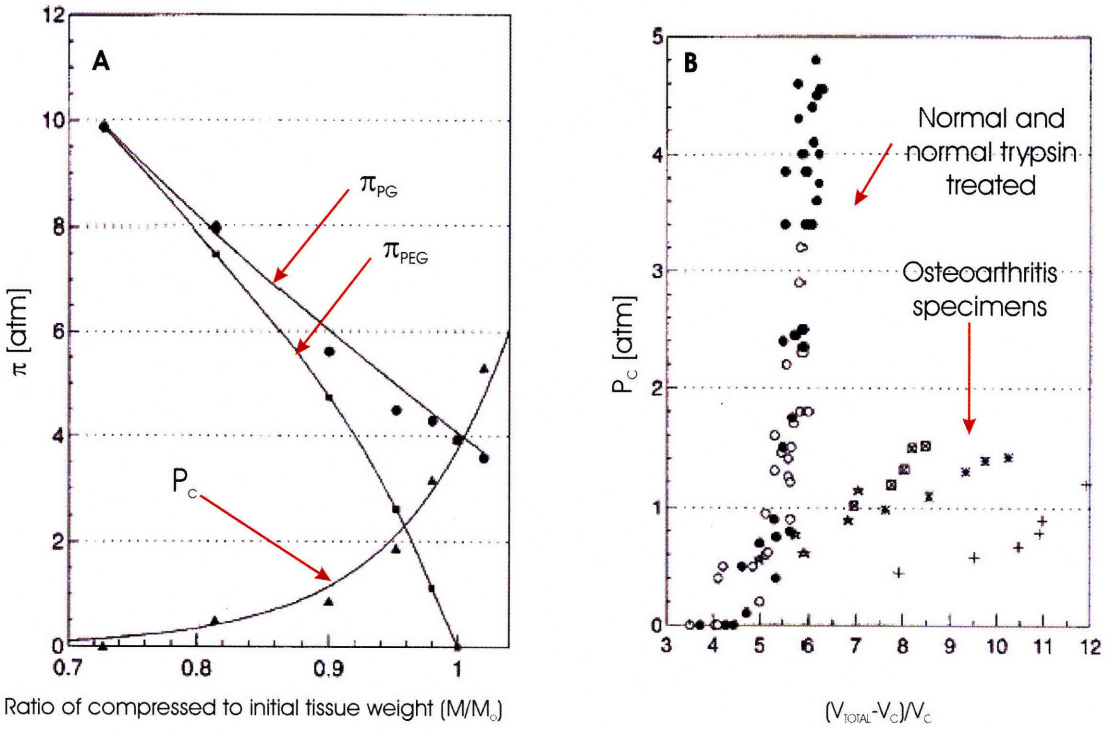

Figure 1-16: A) The forces in hydrated soft tissue in the Mardous et al. experiment are balanced between the tensile force of the collagen fibril P_c, the isotropic compressive force of the PEG solution π_{PEG}, and the osmotic pressure of the proteoglycans π_{PG}. The difference between the π_{PG} and π_{PEG} gives the force in the collagen fibril P_C. B) The collagen stiffness was considerably lower for the osteoathritus patients when compared to the normal adult cartilage samples and cartilage samples that have been treated with trypsin to rid the proteoglycans. Both graphs are adapted from Maroudas et al. [8]

slice. The three specimens were incubated in three different buffer solutions: bovine testicular hyaluronidase, acetate, and Ringer's solution. The acetate and Ringer's served as the control, and hyaluronic acid was degraded and removed from the specimens subjected to hyaluronidase. Twelve specimens were tested and in each case the hyaluronidase specimens had consistently weaker compressive strengths compared to the controls. The degraded specimens lost most of their compressive strength within one hour of incubation. Without hyaluronic acid, the collagen network became an unsupported fibrous structure and under compressive loads the collagen fibrils buckled and compacted. The control specimens in the acetate solution had a slight decrease in compressive strength when compared to the Ringer specimens, and the Ringer specimen maintained their compressive integrity during the length of all the tests.

The softening mechanisms responsible for osteoarthritic in articular cartilage is a combination of weak collagen fibrils as reported by Maroudas et al. [8] and a lower concentration of hyaluronic acid and other GAGs as reported by Broom and Poole [17]. The weak collagen fibrils allow the tissue to swell. The lack of GAGs inhibits the water binding ability of the extracellular matrix which decreases the compressive strength of the tissue. It is not fully known if these mechanisms also play a part in cervical softening or cervical insufficiency. The proteoglycans could arguably play a different role in cartilage and in cervical tissue, as the proteoglycans in cartilage have a much larger molecular weight.

Decorin-Collagen Interaction

Decorin is the main PG in healthy nonpregnant cervical tissue, representing 70% weight of all PGs. Decorin is structured to carry out specific roles in collagen network formation. Decorin binds collagen fibrils and maintains proper fibril spacing in the extracellular matrix. One collagen triple helix rod binds to the inner concave surface of the U-shape decorin. The glycosaminoglycan side chain aligns perpendicular to the collagen fibril to give correct spacing between fibrils which gives the collagen its staggered appearance. The side chain also prevents lateral fusion of collagen fibrils Figure 1-17 illustrates the relationship between decorin and a collagen fibril [115]. Keene et al. [65] confirmed that the decorin glycoprotein folds into an arch-shaped structure. This study measured the dimensions of purified decorin with rotary shadowing electron microscopy. The overall dimension were on the order of 7nm between the

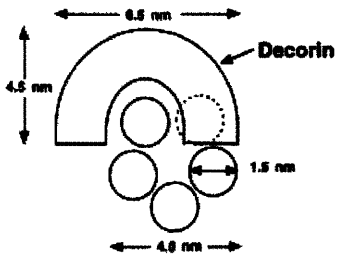

Figure 1-17: The arch-shaped decorin interacts with an individual collagen fibril. One triple helix of the fibril fits within the arch of decorin, and another triple helix interacts with the arm of decorin. Illustration from [115]

two arms and 5nm between the base of the arch and the apex.

Danielson et al. [35] investigated the relationship between decorin and collagen fibrillogenesis by comparing the collagen of wild mice and decorin-free, knock-out mice. The knock-out mice, compared with the wild mice controls, had extremely thin and frail skin. Immunohistochemistry results of the knock-out mice's collagen matrix showed extreme lateral fusion and non-uniform cross-sectional profiles of collagen fibers. Collagen fibril diameters of knock-out mice ranged from 40 to 260nm whereas the collagen fibril diameters from the wild mice ranged from 40 to 180nm. Figure 1-18 shows the irregular cross-sectional profiles of collagen fibrils in the decorin-null mice. Because of the decorin deficiency, smaller fibrils fused to larger fibrils creating irregular profiles. This irregular collagen fibrils created a weak morphology and reduced the tensile strength of the skin. Figure 1-19 is the graph of the load displacement curves for the decorin-null and wild type mice. The breaking point for the wild type mice was five times higher than the one for the decorin-knockout litter. In conclusion, the Danielson team explains:

> *The evidence favoring protein-protein interaction as the major function of SLRPs is persuasive. For example, decorin binds non-covalently to the surface of the fibrillar collagen, primarily type I, and retards the rate and degree of collagen fibrillogenesis in-vitro. This specific interaction is mediated by the protein core, whereas the glycosaminoglycan chain of decorin extends laterally from adjacent collagen fibrils, thereby maintaining interfibrillar spacing. This lateral orientation has also been*

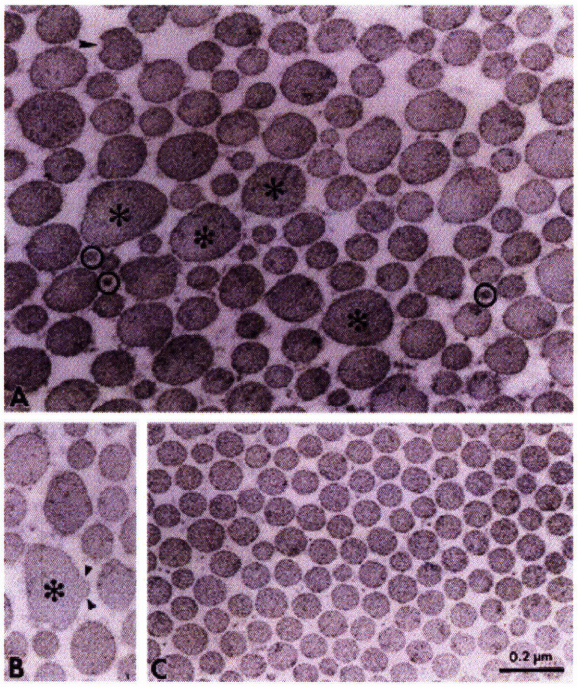

Figure 1-18: A and B represent transmission electron micrographs of the dermal collagen from the decorin-null mice. C represents collagen from wild type mice. The decorin-null mice have irregular fiber diameters while the wild type mice have compact and regularly spaced fibrils [35].

> *demonstrated in collagen fibrils reconstituted in vitro in the presence of decorin. Thus, coordinated expression of decorin and associated collagens may regulate an orderly matrix assembly*[35].

An excess of decorin, or its associated GAG dermatan sulfate, might also result in impaired tissue properties. The studies of Kokenyesi and Woessner [73] suggest that an increase in the ratio of dermatan sulfate to collagen can be responsible for cervical softening. An excess of dermatan sulfate will bind and coat a newly synthesized collagen fibril thus not allowing it to bind to other fibrils.

To investigate this hypothesis, Kokenyesi and Woessner used a rat model and measured the mechanical and biochemical properties of the cervix at different stages of pregnancy. They measured the circumference, rate of creep, and extensibility of the cervix. For the same

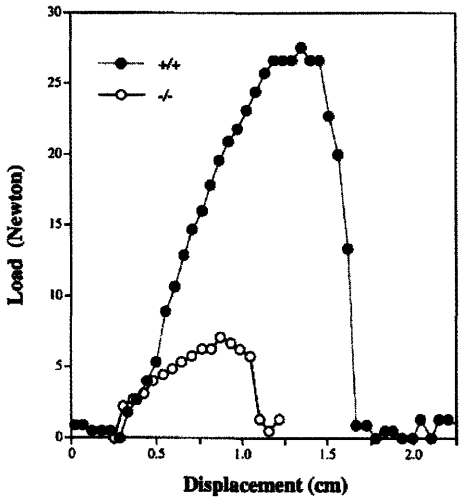

Figure 1-19: The tensile strength of the skin from the decorin-null (-/-) mice is considerably reduced. Dumbell shaped bar specimens were made with a central cross-section 1cm^2 The tensile specimens were pulled at a constant strain rate of 1mm/s to failure. Graph from Danielson et al. [35]

specimens, they also measured collagen and proteoglycan concentration and the extractability of collagen in 4M guanidine-HCl. The cervical circumference was found to best correlate to cervical dilation behavior at term and postpartum. Further, cervical circumference had a strong positive correlation with the dermatan sulfate to collagen ratio. As the dermatan sulfate to collagen ratio increased the cervical circumference increased. This relation was true for both softening trends at term and stiffening trends postpartum.

Another finding in the Kokenyesi and Woessner study was that the total collagen content did not change significantly through pregnancy. Consequently as the total weight of the cervix increases significantly through the gestational period, the concentration of collagen per wet weight reduces significantly during pregnancy, then rises again slightly at postpartum. This finding disputes the belief that an increased enzymatic and collagenase activity causes cervical softening. Because the collagen concentration does not recover fully postpartum to match the observed recovered mechanical integrity, other mechanisms must be present to stiffen the tissue. Kokenyesi and Woessner postulate that the main contribution to the recovery of tissue stiffness is the significant decrease in dermatan sulfate in the 4 hours postpartum. This decrease in dermatan sulfate allows the collagen network to organize again to regain its strength.

In a similar study, Leppert and Kokenyesi [79] investigated the decorin to collagen ratio in rat gestation. They obtained cervices from pregnant rats at 5, 11, 18, and 21 days gestation. A sensitive immunohistochemical technique was used to identify the amount and location of decorin in the rat cervix. The proposed hypothesis was that: *"... decorin expression increased progressively throughout pregnancy and is consistent with the hypothesis that an excess of decorin near term is capable of initiating a decorin-collagen interaction that lead to collagen fibril disruption and decreased cervical tensile strength."* Increased decorin staining was observed with increasing gestational age. In early pregnancy, decorin was first located in the deep stroma around the stromal fibroblasts. As pregnancy continued, decorin was increasingly observed in the subepithelial stroma and in, lesser amounts, in the deep stroma. In late pregnancy, the decorin was present homogeneously throughout the cervical tissue. At this stage in late pregnancy the collagen fibers were disorganized and formed a loose network.

1.3.7 Thrombospondin 2 Deficiency

More recent work by Kokenyesi et al. [72] investigated the role of thrombospondin 2, an extracellular matrix glycoprotein, in cervical softening. The lack of thrombospondin 2 has been associated with abnormal collagen fibril morphology in skin and tendon. Kokenyesi measured the mechanical and biochemical properties of mice cervix in a thrombospondin 2 knock out line and a wild type line. Mechanical measurements included creep tests where two pins in the inner canal were pulled apart by a 50g weight. The distance between the pins were recorded with time to measure the circumference of the inner canal. Measurements were taken at a non-pregnant state, 10, 14, and 18 days gestation. Clear evidence was found that the TSP2 knockout mice cervical tissue had altered biomechanical properties when compared to the control wild type mice.

1.4 Morphology and Histology of the Human Cervix

Determining the ECM architecture of human cervical tissue is crucial for relating mechanical properties to its biochemical content. Different microscopy techniques are available to image soft collagenous tissues on the different biologically relevant length scales. Traditional mi-

croscopy of the ECM involves staining thin sections (~10μm) of tissue for specific proteins, i.e. Masson's Trichrome stain for collagen, and then imagining the stained sections under a light microscope. To measure network birefringence (tissue organization), picrosirius red stained tissue sections can be viewed under a polarized light. Another more recent method for imagining structural proteins is Second Harmonic Generation (SHG) imagining. In contrast to the polarized light method, SHG does not require staining of the tissue which reduces tissue damage and imaging artifacts [31].

Below is an outline and discussion of the literature relating to microscopy techniques used to image cervical tissue. This Section reviews studies relating to cervical tissue and cervical maturation in human and rat tissue. To date, there are no published results for polarized light or Second Harmonic Generation images for human cervical tissue. However, this doctoral work presents a morphology study of human cervical tissue in Section 4.2.5.

1.4.1 Hematoxylin and Eosin Stain

Figure 1-20 is a Hematoxylin and Eosin stain of a transverse section of a nonpregnant human cervix. The lower magnification image shows the entire width of the cervix. At this magnification, the different tissue layers can be clearly distinguished - the collagen dense stroma, the glandular mucosa, and the cellular fascia. In the stroma, the collagen fibers appear to be preferentially aligned in the circumferential direction, and in the mucosa the cervical glands branch into the perimeter of the inner canal. Inspecting the tissue at a higher magnification, the stroma region appears dense with collagen fibers while the mucosa contains interspersing cervical glands. These cervical glands belong to the mucus-secreting epithelium that line the inner canal, which act as a barrier for the cervical stroma [110].

1.4.2 Polarized Light

Collagen organization can be visualized and measured using picrosirius red staining and polarized light microscopy. This method requires thin sections of tissue ($\sim$10μm) stained with Sirius red and a polarized light filter attached to a light microscope. Sirius red is a linear polar molecular which acts as a color dye and fluorescent probe for collagen. When attached to collagen, the Sirius red will enhance the birefringence of the fibrils [31]. Polarized light

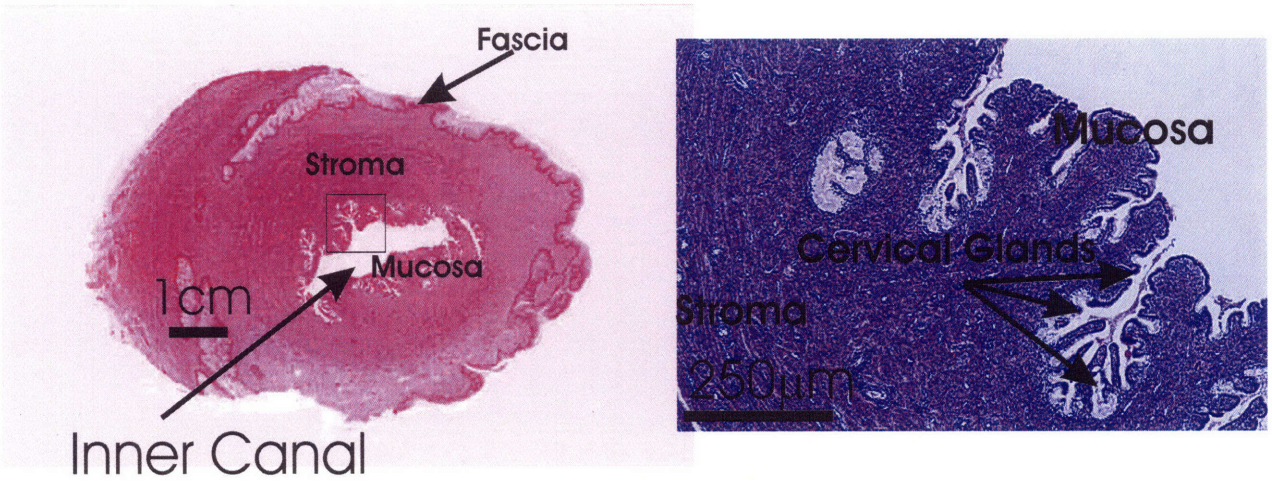

Figure 1-20: Hematoxylin and Eosin Stains of a transverse section of human cervical tissue. (adapted from bu.edu/histology)

allows the microscope to selectively image the fluorescent molecules that have absorption transition dipoles that are parallel to the exciting light [53]. When the stained sections are viewed through a polarizer, the contrast and brightness of the image will be proportional to the amount of organized collagen.

Currently, there are no published polarized light images of human cervical tissue. This doctoral work presents a polarized light study of pregnant and nonpregnant human cervical tissue in Section 4.2.5. However, there are two animal model studies investigating the collagen network of cervical tissue under polarized light. Yu et al. [118] studied cervical ripening in normal timed-pregnant rats. The study found that nonpregnant tissue and tissue from early pregnancy (1-10 days of gestation) consisted of a well-packed collagen network. The cervices were noted to be firm and rigid with a regular arrangement of tightly packed collagen molecules. These cervices had a homogeneous birefringence with collagen bundled into long fibers. In contrast, the pregnant tissue from days 18-21 of gestation had a discontinuous birefringence with fibers that appeared to be disarrayed and disoriented.

In a similar study, Clark et al. [27] imaged the cervical tissue of timed-pregnant rats that have been administered Mifepristone, a progesterone receptor antagonist. Decreased levels of the hormone progesterone are believed to facilitate cervical ripening. As in the Yu et al. study,

Clark et al. also measured a decrease in the collagen birefringence when comparing pregnant rat tissue to nonpregnant tissue. Additionally, the group found a significant decrease in the area of the organized collagen when comparing the Mifepristone treated rats to the control rats on day 16 of pregnancy. These results were accompanied by cervical creep tensile tests which showed that the creep rate increased in the second half of pregnancy for the tissue controls, and cervical tensile strength decreased for the Mifepristone treated rats when compared to the controls on day 15 of gestation. This evidence suggests that the disruption of the collagen network plays a role in cervical softening and that administering Mifepristone can aid in the cervical softening process.

1.4.3 Second Harmonic Generation

Second Harmonic Generation (SHG) is a nonlinear optical process that sums the second harmonic fields radiated by a medium that lacks a center of symmetry. SHG produces a high contrast image in relation to the intrinsic structure of the medium (i.e. an anisotropic crystal or polar collagen fibril). For a detailed review of SHG theory the reader is referred to a review by Millard et al. [88] and a review by Mohler et al. [89]. Historically, SHG microscopy began with the imaging of crystalline quartz in 1962 [69]. The first demonstration of SHG for collagenous tissues was in the late 1980s with the imaging of rat tail tendon [43] at a 50μm resolution.

Since the late 1980s, Second Harmonic Generation microscopy has been found to image structural proteins at high resolution and high contrast [89][31][75]. The high resolution and contrast enable quantitative measurements of ECM protein organization at the molecular level. In contrast to the polarized light imaging technique, SHG is not an absorptive process and does not require staining of the tissue. Instead, SHG relies on the intrinsic anisotropy of the collagen molecules to produce the contrast of the image therefore enabling molecular level features to be measured. Further, SHG imaging has the ability to image in 3-dimensions with the reduction of out-of-plane photobleaching and phototoxicity, and SHG imaging has the ability to measure intact tissue up to $\sim$500μm thickness. These qualities give an advantage over the traditional staining histology of soft tissue, and offer molecular level details that are typically lost in the traditional preparation process [88].

Typical examples of connective tissue imaged by SHG are muscle [89], human endometrium [31], liver [31], and skin [75]. Recent SHG studies on biological tissue have focused on using SHG as a tool for distinguishing different collagen types and finding aberrant collagen in diseased tissue. A study by Kim et al. [67] demonstrated a difference in SHG signal for collagenous tissue samples that have been thermally denatured, enzymatically digested, and glyco-oxidatively damaged. The study found that the SHG signal decreased when the collagen was damaged or denatured. This trend was found for a number of different tissues including tendon and cartilage. Cox et al. [31] imaged human endometrium and cirrhotic liver tissue using SHG. The study found that SHG was useful for clearly imaging the circumferential collagen fibers surrounding the mucus glands in the endometrium and the fibrillar collagen around cells responsible for the diseased liver. Cox et al. claims that these detailed collagen fibril images could only be generated by SHG, and that subtle changes in the collagen structure could be deduced from the second harmonic signal. In a similar study, LaComb et al. [75] imaged normal and diseased skin samples using SHG. The goal of this study was to develop a diagnostic tool using SHG to detect diseased tissue. The group was able to relate SHG image intensities and signal directionality to the observed morphology of normal and diseased skin. This ongoing research is a promising technology for using SHG as a diagnostic tool to identify tissue pathology. More studies will be needed to confirm the correlation between SHG signal intensity and collagen structure.

1.5 Previous Mechanical Tests on Human Cervical Tissue

Previous studies have shown that cervical tissue properties vary with biochemical content [101][112], obstetric history [91][101][119][68][2], anatomical site [29], and direction of loading [96]. It is known that mechanical changes happen during pregnancy with dramatic softening occurring at time of delivery [101]. Rechberger et al. tested biopsy specimens from non-pregnant and postpartum patients. Rechberger et al. also conducted a study on patients diagnosed with cervical insufficiency and tested specimens from pregnant patients during their second trimester. The study found a decrease in mechanical strength in the postpartum and cervical insufficiency tissue. The study also discovered that the reduction in mechanical strength was associated with

an increase in collagen extractability, reduction in sulfated glycosaminoglycans, and increase in hydration [101]. In another study, Petersen measured the mechanical tensile instantaneous stiffness of non-pregnant hysterectomy specimens. The Petersen study found that the mechanical properties were dependent on the direction of loading, where tissue cut in the longitudinal direction had a higher creep rate when compared to tissue cut in the circumferential direction [96].

Studies of the mechanical properties of the cervix during pregnancy were conducted by Conrad et al. and Cabrol et al. Cabrol et al. developed an in-vivo device to measure cervical distensibility in pregnant and non-pregnant patients. The study found that there was a progressive increase in cervical distensibility during pregnancy as indicated by data at 22 weeks and at full term (40 weeks), with a decrease in distensibility postpartum [22]. An earlier study conducted by Conrad et al. [29] found that non-pregnant hysterectomy specimens were significantly stiffer than pregnant hysterectomy specimens. Also, the non-linear stiffening behavior observed in the non-pregnant cervix was absent in the pregnant cervix, which continued to elongate under constant load. Lastly, Conrad et al. found that mechanical strength varied longitudinally and radially in the cervix. Specimens from different locations were tested in tension, and it was found that the site of maximum resistance was at the inner os located in the stroma immediately adjacent to the inner canal [29].

Evaluation of non-pregnant specimens using in-vivo balloon and dilators to measure cervical resistance have shown that testing the cervix in a non-pregnant state can be an indicator of cervical insufficiency in subsequent pregnancies [119]. Zlatnik et al. measured the cervical resistance on non-pregnant patients with a history of early delivery. The study found that cervical resistance was lower for patients who had early deliveries associated with cervical insufficiency [119]. In a similar study, Anthony et al. measured in-vivo cervical resistance in non-pregnant patients with normal obstetric history and patients with a history of previous spontaneous pre-term birth. The study found that women with a history of cervical insufficiency had a lower cervical resistance when compared to normal women [2]. Further studies by Kiwi et al. have also confirmed that women with history of preterm birth have a lower cervical elastance (resistance) in the non-pregnant state compared to normal patients. The Kiwi study also confirmed a large variance of mechanical properties between individual patients [68].

A study by Mazza et al. used a mechanical aspirator to test uterine cervix in-vivo. Measurements were made in-vivo on eight menopausal patients. Four of the specimens were subsequently tested ex-vivo. There was no significant difference in stiffness between the in-vivo and ex-vivo measurements. However, there was a difference between the measured time-dependent properties. The main limitation of this in-vivo tool is that the relative displacement range, 1-3mm, may be too small to test the load-bearing stroma [87].

These previous mechanical studies on human cervical tissue form a basis for investigating cervical tissue by establishing the following:

1. Mechanical properties are dependent on biochemical content [101].
2. Mechanical properties are dependent on specimen orientation and anatomical location [96].
3. Mechanical properties tested in the non-pregnant state can be a good indicator of cervical insufficiency in subsequent pregnancies [119][2].
4. Mechanical properties do not vary from in-vivo measurements when compared to in-vitro measurements [87].

However, because of the complex geometry, the poorly defined boundary conditions, and the limited range of loading histories considered, the results of these previous studies can only be interpreted in a qualitative framework. The concept of stiffness and strength are loosely defined. For example, the Kiwi study introduced a stiffness measurement 'elastance' which relates to a specific testing geometry and loading history [68]. While there is agreement in the literature that softening of cervical tissue is associated with both normal cervical maturation and with abnormal pathological conditions associated with cervical insufficiency, the non-linear, time-dependent, anisotropic properties of the tissue cannot be obtained from these limited studies.

Most recently, Myers et al. conducted compression tests on non-pregnant and cesarean hysterectomy specimens. The obstetric cases studied are listed in Table 1 [91]. Ramp-relaxation and load-unload compression tests were performed on cervical stroma samples where true stress versus axial nominal strain was measured and compared. It was found that the qualitative features of the stress curve are similar between specimens with different obstetric histories.

However, the amplitudes of stress are significantly different when comparing pregnant and non-pregnant specimens. It was also found that women with previous vaginal deliveries had a more compliant stroma when compared to women who had never had a vaginal delivery. More importantly, this study established reliable and repeatable protocols to test cervical tissue in compression, and methodically measured the stress and strain relationships for patients with different obstetric backgrounds. This study, however, did not account for tissue anisotropy.

1.6 Review of Existing Models for Human Cervical Tissue

The paucity of data on the mechanical behavior of the human cervical tissue renders its constitutive characterization an extremely challenging task. To date, there are only two known such models which attempt at constitutive modeling of the stroma and relating the changes in the mechanical properties of the uterine cervix with the altered biochemical composition of the stroma during pregnancy. In a considerably simplified model assuming linear behavior of the underlying load bearing components, small strains and neglecting volume changes, Aspden [5] treats the stroma of the cervix as a fiber-reinforced composite material. Despite the simplicity of the proposed model, it suffices to enlighten the inherent features of the theory in order to provide an insight into the mechanical behavior of the cervix. A more sophisticated model proposed by Febvay et al. [41], [40] captures specific aspects of the biomechanical response of the cervix accounting for the contributions of the individual constituents as well as their complex interaction. This model was thoroughly presented in chapter 4 of this thesis. Here we will briefly introduce the model proposed by Aspden.

Aspden [5] considers the stroma of the human cervix as a composite material in which the collagen fibers are embedded into a gel-like structure of GAGs. In his theory the linear superposition of the strengths of the individual components of the stroma gives the tensile strength of the entire composite. Aspden calculated the breaking stress of the cervical tissue $\boldsymbol{\sigma}_{breaking}$ as a weighted sum of the breaking stress of the collagen fibers $\boldsymbol{\sigma}_{fibers}$ and the breaking stress of the ground substance $\boldsymbol{\sigma}_{GAG}$ given by

$$\boldsymbol{\sigma}_{breaking,total} = \beta \boldsymbol{\sigma}_{fibers} + (1-\beta)\boldsymbol{\sigma}_{GAG}, \tag{1.2}$$

where β is the volume fraction of the collagen in the intact fully hydrated tissue. The cellular volume is neglected in the above relation. As the breaking stress of the GAGs is much smaller in comparison with the breaking stress of the collagen fibers the second term in 1.2 is negligible.

β is referred to as the degree of reinforcement and has been shown to fall at parturition to approximately half the value in the non-pregnant stroma of rats therefore reducing the tensile strength as calculated in 1.2. Accounting for the fiber orientation of the collagen in the cervical stroma Aspden introduces a new parameter η which is called the efficiency of reinforcement. The efficiency of reinforcement η is a function of the angle between the fibers and the applied stress φ and was defined as

$$\eta = \cos^4 \varphi. \tag{1.3}$$

Therefore η varies between 1 for perfectly aligned fibers with maximum efficiency and 0 for fibers aligned perpendicularly to the direction of the applied load. For randomly organized fibers $\eta = 0.2$ which signifies low efficiency, which is nevertheless uniform in every direction. Accounting for the efficiency, 1.2 modifies to

$$\boldsymbol{\sigma}_{breaking,total} = \beta\eta\boldsymbol{\sigma}_{fibers} + (1-\beta)\boldsymbol{\sigma}_{GAG}. \tag{1.4}$$

Assuming the same relationship between the Young's moduli of the individual constituents, the Young's modulus of the substrate E_{total} is given by a weighted sum of the Young's moduli of the collagen fibers E_{fibers} and the ground substance E_{GAG}, and is given by

$$E_{total} = \beta\eta E_{fibers} + (1-\beta)E_{GAG}. \tag{1.5}$$

Poisson effects are neglected in the above simplified expression. The strains involved are assumed to be small and the behavior of the fibers and the ground substance are assumed to be linear.

A previous study by the same investigator uses X-ray diffraction to measure the collagen fibril orientation in the non-pregnant cervices of humans and mice, based on which an orientation distribution function describing the probability of finding a fibril at a given angle to a chosen reference axis is derived. The result of the same study showed that in the non-pregnant state

the collagen fibril organization is associated with an efficiency of 0.6 both along and around the cervix, which dropped down to 0.2 at delivery. This result signifies the fact that at parturition the collagen organization is more random and therefore the effective strength and stiffness of the stroma decreases by a factor of 3 from the non-pregnant to the pregnant state at term.

The collagen organization accounts partially for the variation of the stiffness and the strength of the stroma during pregnancy. Additionally, Aspden investigated the effectiveness of the stress transfer between the strong fibers and the weak ground substance. A critical length l_c of the collagen fiber is defined as

$$l_c = \frac{r\sigma_{fibers}}{\tau}, \tag{1.6}$$

where σ_{fibers} is the breaking stress of the collagen fibers, τ is the shear stress exerted on a fiber by the ground substance, and r is the radius of the fibre. Equation 1.6 signifies that an individual fiber can only be stressed maximally if its length exceeds the critical length l_c, since a length shorter than the critical length renders the fiber ineffective in reinforcing the surrounding ground substance of glycosaminoglycans. The shear stress exerted from the ground substance to the collagen fibers depends on the specific glycosaminoglycans in the stroma. Changes in the ground substance composition at term may alter the shear strength of the stroma and therefore affect the critical length A comparison between the different shear strengths exerted by specific GAG present in the cervical stroma renders the relation $\tau_{\text{dermatan sulfate}} > \tau_{\text{hyaluronic acid}} > \tau_{\text{keratan sulfate}}$. Aspden reports a marked change in the relative amounts of these GAGs, which leads to decrease in the shear stress exerted on the collagen fibers therefore yielding an increase in the critical length. Assuming that the collagen fibril length remains the same throughout pregnancy the increase in l_c renders most of the collagen fibers shorter than l_c, therefore reducing the effectiveness of the reinforcing they provide.

Another aspect of the mechanical behavior of the cervical stroma considered by Aspden is the water content of the stroma. At term, the water content of the human cervical stroma is increased by 5%. The amount of water in the tissue affects the concentration of the separate species in the stroma and therefore affecting the possibility for molecular rearrangement. This molecular reconfiguration governs the creep properties of viscoelastic materials and the cervical stroma as such, affecting the Young's modulus in 1.5 which becomes effectively a function of time, $E_{total}(t)$. Increased water content at parturition would increase the freedom for molecular

rearrangement in the stroma, therefore increasing the creep properties and reducing the stiffness of the cervix.

Aspden also suggests that elastin, a highly extensible rubberlike protein with almost constant weight throughout the gestation, may be component of the stroma providing a restoring stress postpartum and facilitating recovery of the strength and stiffness of the stroma.

1.7 Conclusion

Cervical stroma is an extremely biologically active material during pregnancy, and its mechanical integrity is paramount for a healthy gestation. From the obstetrics literature, it can be concluded that the etiology of "Cervical Insufficiency" remains elusive in the medical community. The diagnostic tools available for clinicians are scarce due to the multiple clinical factors associated with preterm labor and CI. It is hypothesized that the mechanical integrity and the biochemical composition of the cervix play a major role in determining the outcome of pregnancy. However, not much is known about the mechanical properties of cervical tissue or how these properties relate to its biochemical microstructure. The mechanics literature relating to cervical tissue is limited to a few studies on human tissue and a few studies calculating stress and strain relationships. With the rate of preterm birth on the rise in the United States and elsewhere, there is an immediate need to uncover the structure-function relationship of human cervix and to properly characterize and measure the mechanical and biochemical properties of the cervical stroma.

This doctoral study aims to characterize the structure-function relationships in human cervical tissue. The following study is organized into four remaining chapters. Chapters 2 and 3 present mechanical investigations, Chapter 4 details the biochemical analysis, and Chapter 5 discusses continuing research topics and conclusions. Chapter 2 presents the methodology, results, and discussion for a preliminary study that develops the initial mechanical testing and tissue handling protocols for cervical tissue. The basis for this preliminary work is presented in my Master's thesis [90] and the journal publication *The Mechanical and Biochemical Properties of Human Cervical Tissue* [91]. Chapter 3 is an extension of the mechanical study of the tissue and represents the most up-to-date experimental protocols. It evolves the initial

mechanical testing protocols, from Chapter 2, to include the characterization of the anisotropic mechanical properties of the cervical stroma. This study measures the stress response for cubical specimens tested along anatomically relevant orthogonal directions, and it derives a microstructurally inspired 1-dimensional material model to fit the data. The resulting best-fit material parameters are correlated to the different obstetric cases of the tissue. A manuscript of this work has been accepted to the ASME Journal of Biomechanical Engineering. Chapter 4 presents methodology and results related to the biochemical analysis for human cervical tissue (refer to my Master's thesis [90] for specific protocol development). Chapter 5 concludes this doctoral work with a brief investigation of the 3-dimensional anisotropic material behavior of the tissue. A 3-dimensional material model developed by Paskaleva [94] is used to fit a set of mechanical data from the anisotropy study in Chapter 3. This material fit is discussed in terms of the observed morphology and measured fiber direction of the tissue specimen. The results of this doctoral work confirm that there is a strong correlation between the mechanical properties of the tissue and its biochemical architecture. Further, this correlation is a function of the obstetric history of the patient with both the material parameters and the measured biochemical variables being a function of the patient's pregnancy history.

Chapter 2

A Preliminary Mechanical Study of Human Cervical Tissue

This chapter presents the initial studies of the mechanical properties of cervical samples from human hysterectomy specimens. This chapter comprehensively covers the development of the tissue harvesting and specimen preparation protocol, and it details the first completed study of the compression and tension behavior of cylindrical compression specimens and ring tension specimens. This study was the first important step towards obtaining appropriate testing protocols for human cervical tissue. The main challenges of these initial studies were to develop: tissue handling protocols, cutting methods to obtain feasible specimen geometry, and appropriate loading protocols to avoid the transient effects of tissue swelling.

Three clinical cases were investigated: non-pregnant hysterectomy patients with previous vaginal deliveries, non-pregnant hysterectomy patients with no previous vaginal deliveries, and pregnant hysterectomy patients at time of cesarean section (See Table 2.1 for Obstetric Cases). Tissue samples were tested in confined compression, unconfined compression, and tension. Results from the mechanical tests indicate that cervical stroma has a non-linear, time-dependent stress response with varying degrees of conditioning and hysteresis depending on its obstetric background. It was found that the non-pregnant tissue was significantly stiffer than the pregnant tissue in both tension and compression.

Obstetric History	Abbreviation
Non-Pregnant: No Previous Vaginal Deliveries	NPND
Non-Pregnant: Previous Vaginal Deliveries	NPPD
Pregnant: Taken at time of Cesarean Section	PCS

Table 2.1: Three obsetric cases studied.

2.1 Methods

2.1.1 Tissue harvesting and specimen preparation

Hysterectomy specimens from pre-menopausal women with benign gynecological conditions were obtained from the Tufts - New England Medical Center. Two cervices were obtained from cesarean hysterectomy patients. Both patients underwent cesarean hysterectomy because of suspected placenta accreta and did not labor. Non-pregnant cervices were categorized according to parity and labeled NPND for women with no previous vaginal deliveries and NPPD for women with previous vaginal deliveries. The pregnant specimens were labeled PCS. Please refer to Table 1 for abbreviation definitions and to Table 2.2 for specific patient obstetric history. Approval from the Institutional Review Board was obtained from both Tufts - New England Medical Center and MIT prior to initiating the study.

The uterus and cervix were excised from the patients and placed on ice. A custom designed stainless steel sectioning tool (Fig. 2-1) was used to obtain from each cervix four 4mm parallel disks perpendicular to the inner canal. Each cervical slice was labeled to distinguish position relative to the internal and external os (Fig. 2-1). Note that 2cm of cervix closest to the external os was not tested because this portion was reserved for pathological examination. The cervical tissue slices were stored flat at -80°C (Fig. 2-2). Preliminary tests performed on fresh and previously frozen tissue from the same cervical slice [40] confirmed that freezing does not alter mechanical properties, a result consistent with similar findings for cartilage (see, e.g., [66]). Prior to testing, each 4mm slice was thawed for approximately 3 minutes in phosphate buffered

Patient	Age	G	P	Hysterectomy Indication	Obstetric History	Labor?	Endometrial Pathology
NPND Patient 1	37	0	0	Fibroid Uterus		No	Proliferative
NPND Patient 2	38	4	4	DUB	C/Sx4	No	Secretory
NPND Patient 3	43	4	3	Fibroid Uterus	C/Sx3	Dilated to 4cm in 1st pregnancy.Did not labor in 2nd &3rd pregnancies.	Secretory
NPND Patient 4	37	0	0	Fibroid Uterus		No	Proliferative
NPND Patient 5	35	0	0	Fibroid Uterus		No	Secretory
NPPD Patient 1	53	2	2	Fibroid Uterus	NSVDx2	Yes	Proliferative
NPPD Patient 2	43	2	2	DUB	NSVDx2	Yes	Dysynchronous
NPPD Patient 3	46	1	1	Fibroid Uterus	NSVDx1	Yes	Proliferative
PCS Patient 1	33	4	2	34 weeks Suspected Placenta Increta	C/Sx 2	No, C/S performed prior to labor	Increta Confirmed
PCS Patient 2	32	5	5	37 weeks Suspected Placenta Accreta	C/Sx 5	No, C/S performed prior to labor	Accreta Confirmed

Table 2.2: Patient Specific Obstetric History (G = Gravida, P = Para, DUB = Dysfunctional Uterine Bleeding, NSVD = Normal Spontaneous Vaginal Delivery, C/S = Cesarean Section)

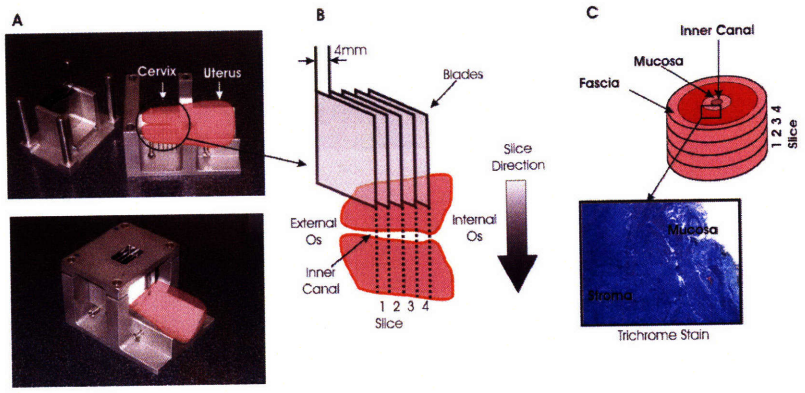

Figure 2-1: Specimen preparation. A) Stainless steel sectioning tool. B) Cervical slice labeling convention and blade orientation. C) Cervical tissue. The mucosa is the soft cellular layer lining the cervical canal. The stroma is the firm fibrous inner core

saline (PBS) at an ionic concentration of 0.15M.

Mechanical and biochemical specimens were cut exclusively from the cervical stroma. The location of the cervical stroma in relation to the cervical mucosa and fascia is illustrated in Fig 2-1. For compressive mechanical tests, cylindrical specimens were cut with an 8mm biopsy punch at the same radial location for each slice, with the cylinder axis parallel to the inner canal. Care was taken in labeling the samples according to their anatomical site as data in the literature [30] indicate some variation in mechanical properties with longitudinal position along the axis of the cervix, and radial distance from the cervical canal. For tension mechanical experiments, two concentric circular blades were used to obtain from each slice a singular ring of stroma of, approximately, 6mm to 8mm inner diameter and 16 to 18mm outer diameter. For biochemical specimens, approximately 20mg of tissue adjacent to the location of the mechanical specimens were excised from the stroma.

Each cervical slice yielded compression specimens (1 to 3 specimens, depending on the visual homogeneity of individual slices) or a single tension specimen, as well as several biochemical specimens. The mechanical specimens were weighed and equilibrated overnight in PBS at 4°C, and the biochemical specimens were stored at -80°C until time of pulverization.

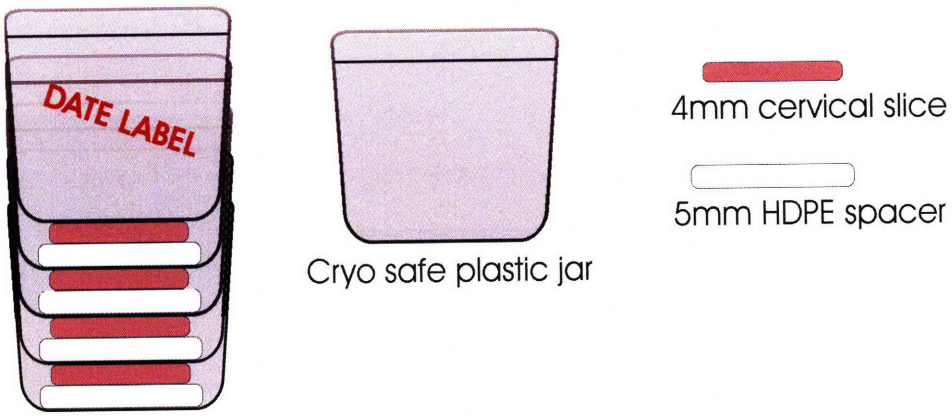

Figure 2-2: Plastic device used to store cervical slices.

2.1.2 Mechanical Testing

All tests were conducted on a universal material testing machine (Zwick Z2.5 TS1S, Ulm, Germany) with the specimens immersed in a PBS bath in custom-designed acrylic fixtures (Fig. 2-3B). A 20N load cell was used to collect compression data, and a 500N load cell was used to collect tension data. Video extensometer data was collected with a Qimaging Retiga 1300 CCD camera equipped with a 200mm f4 Nikon lens. Strain data was obtained with Digital Image Correlation (DIC) techniques using the Correlated Solutions VIC-2D (version 4.4.0) software.

Measurement variability is inherent in the Zwick load cell and video extensometer analysis. The resolution of the 20N Zwick load cell is $\pm$0.001N (~0.01kPa for an 8mm diameter specimen), and the resolution of the 500N Zwick load cell is $\pm$0.025N (~1.0kPa for a typical ring geometry). The tolerance of the lateral stretch measurements is a function of the resolution and contrast quality of the video extensometer image. A full discussion of error calculations for the video extensometer can be found in Parson [93]. For our unconfined compression tests an estimate of error was obtained by performing a lateral stretch analysis multiple times for the same image data. The variation in strain due to noise in the video extensometer analysis was found to be within $\pm$ 1% for testing conditions typical of the unconfined compression configuration. For the ring tension tests, a preliminary image-analysis experiment was conducted using rigid body motion to calibrate the strain error for a particular speckle pattern and camera resolution. For

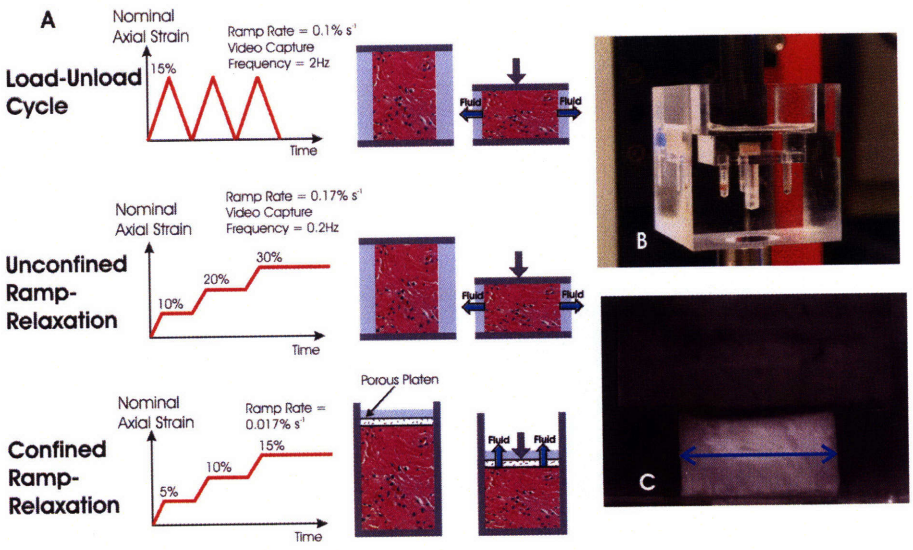

Figure 2-3: Compression test protocol. (A) Imposed deformation history for each testing mode. (B) Cervical specimen in compression fixture. (C) Cervical specimen in unconfined compression. Radial stretch history is recorded by a video extensometer.

the resolution and speckle pattern used in the tension experiments, the strain error was found to be within $\pm$ 0.1%.

All mechanical specimens were equilibrated overnight in PBS at 4°C, weighed, and measured prior to testing. A discussion of the motivation and implications for this equilibration procedure, which alters the hydration level of the tissue, is presented in Section 2.3.1.

Each compression specimen was subjected to three different testing modes: load-unload cycle; unconfined ramp-relaxation; and confined ramp-relaxation. A preload of 0.005N (corresponding to a compressive stress of 100 Pa) was imposed on each sample prior to testing in order to accurately determine the sample thickness and, for the confined compression tests, improve confinement. Fig. 2-3A illustrates the imposed deformation histories for the three tests. The compression testing protocol for each specimen consisted of the following sequence of tests: (1) load-unload cycle, (2) unconfined ramp-relaxation, (3) load-unload cycle, (4) confined ramp-relaxation. Each specimen was first loaded in unconfined compression to 15% axial-engineering strain and unloaded to 0% strain at a constant engineering strain rate of 0.1% s^{-1}. This load-unload cycle was repeated three times. After re-equilibration in an unloaded state for at least

thirty minutes in PBS at 4°C, the specimen was subsequently subjected to an unconfined ramp-relaxation test to axial-engineering strain levels of 10%, 20%, and 30% with a ramp strain rate of 0.17% s^{-1}. Each strain level was held for 30 minutes to measure the relaxation response of the tissue. After re-equilibration in an unloaded state for at least thirty minutes in PBS at 4°C, the load-unload cycle test was repeated. The measured response was compared to the response recorded in the first load-unload test to verify that the specimen had not undergone any damage or degradation altering its mechanical response. The specimen was then allowed to re-equilibrate for 30 minutes in PBS. After equilibration, the specimen was placed in an 8mm impermeable rigid well and subjected to a confined ramp-relaxation test to axial strain levels of 5%, 10%, and 15% with a ramp strain rate of 0.017% s^{-1}. Each strain level was held for 30 minutes to measure the relaxation response of the tissue. The history of radial stretch for the unconfined compression tests (both load-unload cycles and ramp-relaxation) was recorded using the video extensometer. The video capture frequencies for the load-unload cycle and the ramp-relaxation test were 2Hz and 0.2Hz respectively. Figure 2-3C shows a typical video image for an unconfined compression test.

For tensile tests, prior to loading an airbrush pattern was applied to the ring-shaped tension specimens using India ink. A representative speckle pattern density is illustrated in Fig. 2-4A. The speckled cervical rings were extended along a diameter using 5mm wide woven Kevlar strips, which were looped around the specimen and gripped in tensile jaws (Fig.2-4). This testing configuration was selected to reduce stress concentration in the gripped region of the specimen, while adding negligible axial compliance to the grip assembly. Specimen and grip assembly were immersed in a PBS bath in an acrylic fixture (Fig. 2-4B). The inner diameter of the cervical ring was elongated at a rate of 0.05mm s^{-1}. Multiple tension-loading cycles were imposed on each specimen, with 30 minutes of equilibration time between each cycle. Images of the deforming specimen were recorded at a frequency of 10Hz. The 2-d strain field was calculated for the two central regions of the specimen as indicated in Figure 3A using the Correlated Solutions Vic 2-D DIC software [93]. Axial and lateral stretch histories were then averaged for these mostly-uniform regions of deformation. Based on lateral stretch history and initial specimen dimensions, a (true) axial stress history for the central region of the specimen was estimated.

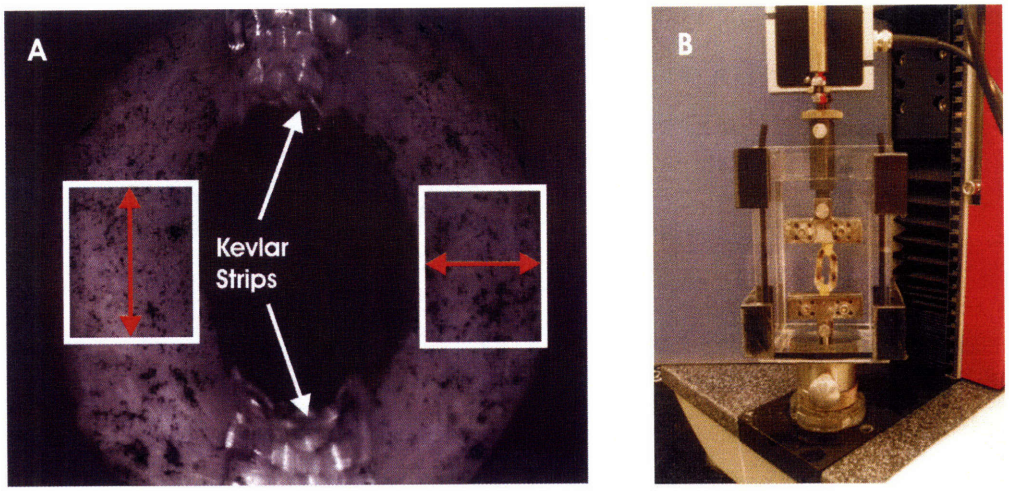

Figure 2-4: Tension test configuration. (A) Representative speckle pattern for cervical tension specimens. Axial and lateral stretch histories are recorded for the boxed regions indicated in the figure, where the deformation is sufficiently homogeneous, and the stress state more closely approaches uniaxial tension. (B) Experimental fixture for cervical tension test. Two strips of woven Kevlar are looped around the specimen and gripped in tensile jaws.

2.2 Results

Mechanical and biochemical properties were measured for the NPPD, NPND, and PCS (Refer to Table 2.1 for abbreviation definitions) clinical cases and averaged according to this classification. N_c represents the number of cervices and N_s represents the total number of specimens tested for each clinical case.

The appearance and the texture of cervical tissue were visibly different for the three clinical cases. The pregnant tissue was noticeably softer and the collagen network appeared to be loosely connected, in agreement with observations reported in the literature [77]. The non-pregnant tissue appeared fibrous, with a densely connected collagen network, especially for the NPND clinical cases.

Compression tests were performed, on cylindrical specimens, and Fig. 2-5 shows the averaged stress responses of the tissue to the load-unload compression cycles for the three clinical cases. The averaged peak stresses in Fig. 2-5 reflect an order of magnitude difference between the averaged responses for the NPND and PCS cases, and a substantial difference between the NPND and NPPD responses. Standard variations in peak stress (at 15% axial strain) for the

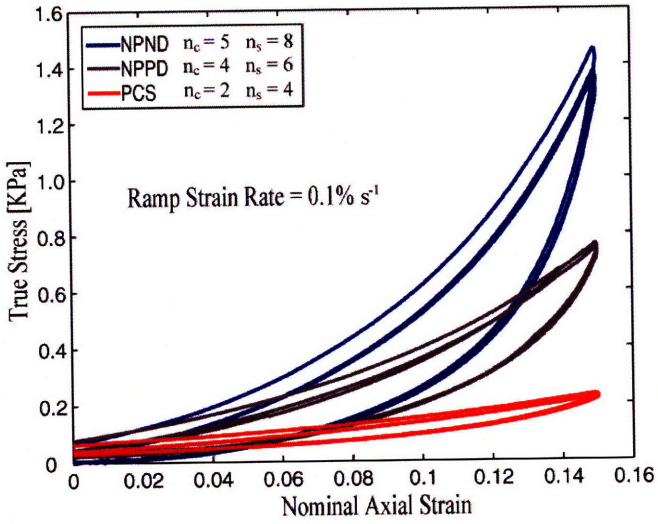

Figure 2-5: Cervical stroma response to uniaxial compression cycles. Experimental curves were averaged for each obstetric case.

Obstetric History	N_c	N_s	Standard variation in peak stress [kPa]
NPND	5	7	±1.2
NPPD	3	9	±0.4
PCS	2	3	±0.1

Table 2.3: Standard variation in peak stress kPa

three obstetric histories are reported in Table 2.3.

For constant strain rate load-unload cycles, the material displays a nonlinear response, with marked hysteresis. The first loading cycle is consistently associated with a stiffer response and more substantial hysteresis. The response in subsequent loading ramps becomes more compliant while the unloading response is not substantially altered between cycles. This softening behavior with subsequent deformation cycles has been observed in other classes of soft tissues and it is often referred to as "conditioning".

Figure 2-6 shows the averaged stress responses of the tissue to the ramp-relaxation tests in unconfined and confined compression for the three clinical cases. Standard variations in peak stresses and equilibrium stresses are reported in Table 2.4 and 2.5. There is a trend towards significantly decreased amplitude in the stress response of pregnant tissue when compared to non-pregnant tissue (p=0.1, Student's t-test) and in NPPD tissue when compared to NPND

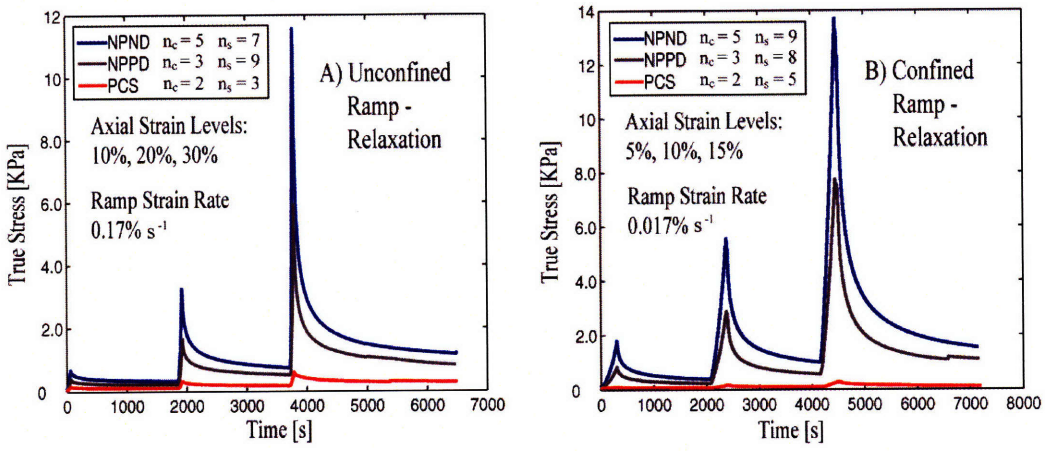

Figure 2-6: Cervical stroma response to ramp-relaxation (A) unconfined compression, and (B) confined compression. Expereimtnal curves were averaged for each obstetric case.

Obstetric Case	N_c	N_s	10% Peak (kPa)	20% Peak (kPa)	30% Peak (kPa)	10% Equilibrium (kPa)	20% Equilibrium (kPa)	30% Equilibrium (kPa)
NPND	5	7	0.66±0.46	3.3±3.2	12±14	0.31±0.24	0.72±0.53	1.2±0.78
NPPD	3	9	0.39±0.38	1.6±2.3	6.0±9.6	0.21±0.17	0.50±0.39	0.82±0.76
PCS	2	3	0.15±0.12	0.30±0.24	0.56±0.64	0.10±0.06	0.17±0.15	0.28±0.23

Table 2.4: Three obsetric cases studied.

tissue (p=0.1, Student's t-test). These findings are consistent with the clinical observation that pregnant tissue is softer than non-pregnant tissue, and women with previous deliveries tend to have a softer cervix when compared to women who have not delivered vaginally.

Averaged transverse stretch histories for the three clinical cases in unconfined ramp-relaxation tests are reported in Fig. 2-7. The results indicate that the specimens undergo a substantial volume change in unconfined compression tests. Error bars are not indicated in the figure to avoid cluttering, but typical variations among specimens were of order ±0.03. This large variation in transverse stretch measurements was probably due to tissue anisotropy and specimen orientation inconsistencies: the loading direction is "anatomically" consistent for all specimens (longitudinal in the cervix, i.e., parallel to the direction of the inner canal, see Fig. 2-1). However the orientation of each specimen with respect to radial and circumferential direction in the cervix was not recorded or marked on each specimen, and transverse direction for which the

Obstetric Case	N_c	N_s	10% Peak (kPa)	20% Peak (kPa)	30% Peak (kPa)	10% Equilibrium (kPa)	20% Equilibrium (kPa)	30% Equilibrium (kPa)
NPND	5	9	1.8±3.7	5.6±9.4	14±17	0.38±0.57	0.99±1.1	1.5±1.4
NPPD	3	8	0.82±2.0	2.9±5.7	7.8±13	0.23±0.40	0.55±0.78	1.1±1.2
PCS	2	5	0.12±0.07	0.17±0.10	0.28±0.18	0.07±0.07	0.10±0.08	0.12±0.08

Table 2.5: Three obsetric cases studied.

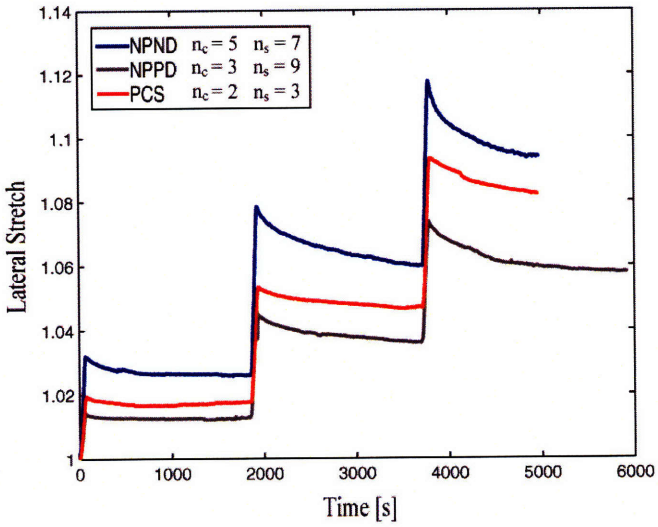

Figure 2-7: Radial transverse stretch of specimens subjected to ramp-relaxation unconfined compression. Experimental curves were averaged for each obstetric case.

stretch was recorded was not anatomically consistent among specimens.

Figures 2-8 and 2-9 show the results for preliminary tension experiments conducted on cervical specimens with different obstetric backgrounds and different anatomical locations. Figure 2-8 shows results from three specimens taken from cervices with different obstetric backgrounds. Figure 2-9 shows results from two specimens taken from the same pregnant cervix, where the specimens were taken from different anatomical sites. Results are presented in terms of averaged true stress vs. averaged axial stretch in the central regions of the specimens, as discussed in Section 2. Fig 2-8 shows that pregnant tissue is found to be orders of magnitude more compliant than non-pregnant tissue. This result confirms trends identified in the compression tests. Further, Fig. 2-8 indicates no significant difference in the stress-stretch response for the two

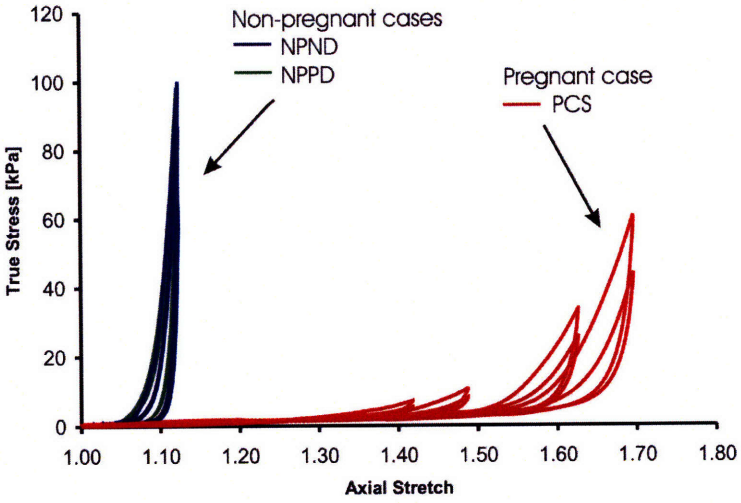

Figure 2-8: Cervical stroma response in tension for three specimens from three patients with different obstetric backgrounds. Between each cycle, the unloaded specimen was equilibrated for 30 minutes in PBS.

non-pregnant cases. Figure 2-9 shows that the stress response of cervical tissue is dependent on anatomical site. The specimen taken closer to the external os has a stiffer stress response when compared to the specimen taken closer to the internal os. This result is consistent with clinically observed progression in cervical ripening.

The tensile response of the tissue is extremely non-linear, with a degree of hysteresis which increases with the level of applied deformation. Similarly to the findings for compressive axial deformation, the response of non-pregnant cervical tissue experienced a degree of conditioning during the first loading cycle, and then stabilized in subsequent cycles. Conversely, the pregnant tissue continued to elongate with each loading cycle.

2.3 Discussion

This study had two complementary objectives: first, the establishment of a stringent experimental protocol to collect data on the biochemical composition and mechanical properties of cervical tissue under different loading modes; second, a preliminary investigation of normal ranges of variation in tissue properties for non-pregnant and pregnant patients. Here we discuss

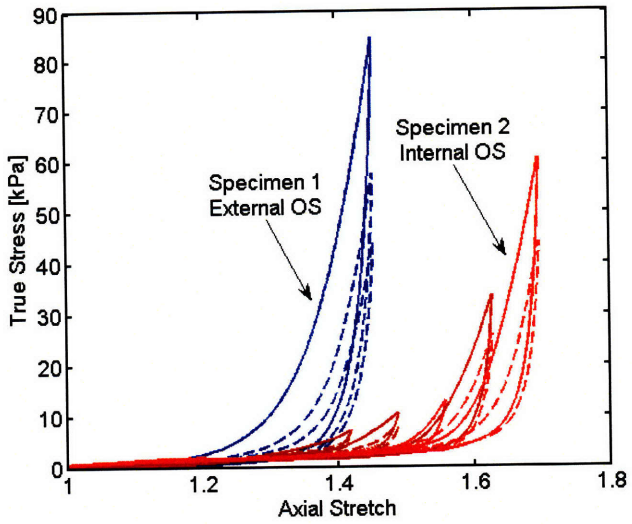

Figure 2-9: Cervical stroma response in tension for two specimens from a single pregnant cervix. Specimen 1 was taken close to the external OS, and specimen 2 was taken close to the internal OS. Between each cycle, the unloaded specimen was equilibrated for 30 minutes in PBS.

the motivation and implications of our testing protocols, discuss the experimental results, explain the sources of variability in the experimental findings, and suggest changes to the current experimental protocol for future studies.

2.3.1 Discussion of the Testing Protocol

The motivation behind the selected modes of deformation, strain levels, and strain rates arises from physiological considerations, ranges of operation of testing equipment, and mechanical modeling concerns. This extensive experimental characterization of the mechanical tissue response was necessary to guide the development of an appropriate constitutive model for cervical stroma [40]. The experimental protocol was designed so as to provide sufficient data to uniquely determine the constitutive material parameters that describe the mechanical behavior of each cervical specimen [40]. The advantage of testing each cervical specimen in both confined and unconfined compression is that these combined protocols provide sufficient data to characterize the three-dimensional, poroelastic and viscoelastic nature of the tissue response [37][21][25]. Confined compression tests impose larger volume changes, and the experimental response is

typically interpreted in a poroelastic framework to provide estimates for the (strain-dependent) hydraulic permeability of the tissue [6]. Unconfined compression tests typically result in larger levels of shear deformation. The three-dimensional behavior of the tissue is captured by the lateral stretch measurements taken by the video extensometer.

The rational for testing samples along the longitudinal direction in compression tests, and testing samples along the circumferential direction in tensile tests arises from physiological considerations [4][29] and from preliminary results of Finite Element Analyses (FEA) of the loading conditions in pregnant patients [56]. Gravity, intrauterine pressure, and the weight of the fetus impose a complex three-dimensional stress state on the cervix where the weight of the fetus gives rise to compression loads in the longitudinal direction and the resistance to cervical dilation gives rise to tensile loads in the circumferential direction [4][56].

Strain levels and strain rates were selected on the basis of preliminary experimental investigations [40]. Strain levels were selected to meet the criteria that they should not cause damage to the specimens, but should be high enough to capture the non-linearity of the tissue response. Physiologically, the strain rates experienced in-vivo by the tissue under time-varying loading conditions (gravity, uterine contractions, etc.) will vary widely among patients. Strain rates for the load-unload cycles and for the ramp loading in relaxation tests reflect the short loading times characteristic of physiological conditions such as uterine contractions and temporary increases in intraabdominal pressure (e.g., from coughing). The relaxation transient is meant to capture longer term (and equilibrium) tissue response. The strain rate for the tension tests protocol is similar to the rate adopted in the tension tests by Conrad et al. [29]. Also, strain rates were selected so as to meet the following criteria: (1) the load did not exceed the limit of the load cell; (2) the tissue samples were not damaged during loading; (3) inertial effects could be neglected; and (4) the time-dependent nature of the tissue response (hysteresis, relaxation) could be captured. The characteristic relaxation times in confined compression experiments are dominated by the effects of fluid diffusion and are higher than the characteristic relaxation times in unconfined compression. To avoid overloading the specimen and load cell, lower strain levels and strain rates were selected for confined compression tests.

We found that, to obtain repeatable results, a number of precautions were necessary. First, to prevent tissue degradation, the cervical slices were stored at -80°C at time of excision until

time of experiments. Second, to eliminate transient effects associated with swelling, mechanical specimens were equilibrated overnight in PBS at 4°C prior to testing.

The hydration levels of the stroma significantly affect its mechanical response. As mechanical specimens are excised from the surrounding tissue, constraints from the interconnected collagen network are relaxed. Freezing the tissue can also result in partial loss of hydration. When the excised tissue is placed in saline at physiological concentration, the specimen swells to reach a new equilibrium state at a higher hydration level. Typical swelling curves for compression specimens are shown in Fig.2-10 where the wet weights of two specimens are plotted as a function of the hydration time in PBS. These curves display a rapid rise in hydration level, immediately following the placement of the specimen in saline, with exponentially decreasing hydration rates over time. Typical characteristic time constants for this hydration transient ($\sim$5hr) are comparable with testing time intervals. If a specimen is not allowed to properly equilibrate prior to testing, the testing results will be confounded by the superposition of effects due to the hydration process.

Fig.2-11 demonstrates the significant influence of hydration levels on the measured mechanical properties. Two compression samples were excised from the same cervical slice and tested after short hydration intervals (1.5 and 3hrs). The sample that was allowed to hydrate for a longer interval displayed a stiffer response. The same specimens were then placed in saline, equilibrated overnight and retested. A noticeably stiffer response was obtained for the fully equilibrated specimens. Interestingly, the sample that had originally appeared stiffer proved to be the more compliant of the two when equilibrated. It could be argued that the adopted equilibration protocol alters the tissue properties from their in-vivo state. However, the purpose of this investigation was not to obtain absolute values of tissue properties, but rather to identify overall qualitative features of the tissue response and to investigate relative variations in properties between specimens from patients with different obstetric histories. The equilibration protocol is evenly applied to all samples, and the increased hydration level only affects the amplitude of the stress response and not the qualitative feature of the curves. For the purpose of this investigation, the effects of the equilibration step are therefore inconsequential. In future studies, we propose to use a stronger ionic bath, both in the equilibration and in the mechanical testing procedures, to limit the swelling of the tissue and reach equilibrium hydration levels

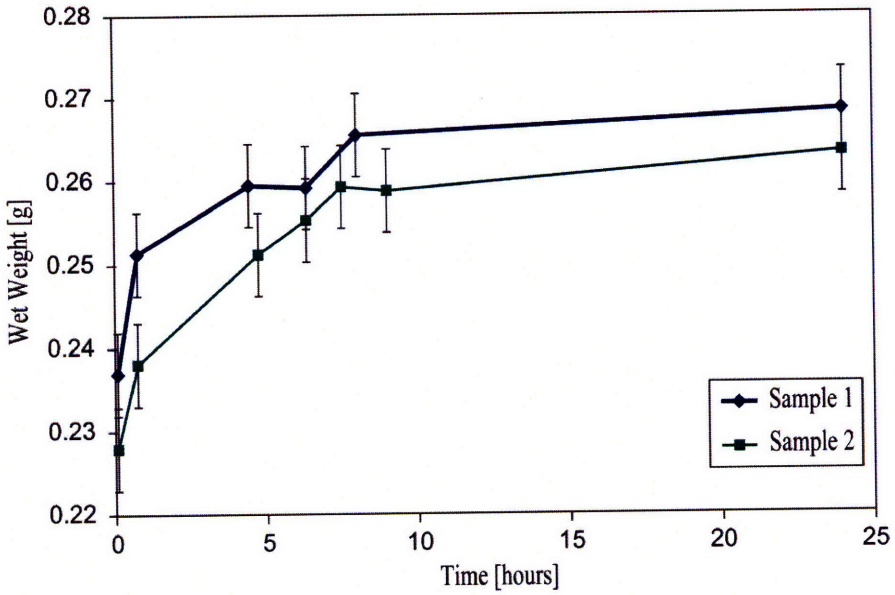

Figure 2-10: Swelling curve from two compression specimens obtained from the same cervical slice.

comparable to the in-vivo levels.

2.3.2 Discussion of Results

Many observations about the characteristics of the material response can be used to guide the development of an appropriate constitutive model for the mechanical behavior of cervical stroma. The stress-strain behavior is noticeably nonlinear both in tension and compression, with a much stiffer response when the tissue is loaded in tension: in nonpregnant tissue, for strain levels of approximately 10% , there are two orders of magnitude between the corresponding stress levels in tension (~100 kPa) and compression (~1 kPa). The non-linearity of the stress-strain behavior is also reflected in the relationship between peak stresses and strains for the ramp-relaxation results in confined and unconfined compression. Conversely, for both unconfined and confined compression tests, and for all three clinical cases, the increase in equilibrium stresses with axial strain was nearly linear. While the peak stress levels for the non-pregnant specimens were an order of magnitude higher than the equilibrium levels, the peak stress levels for the preg-

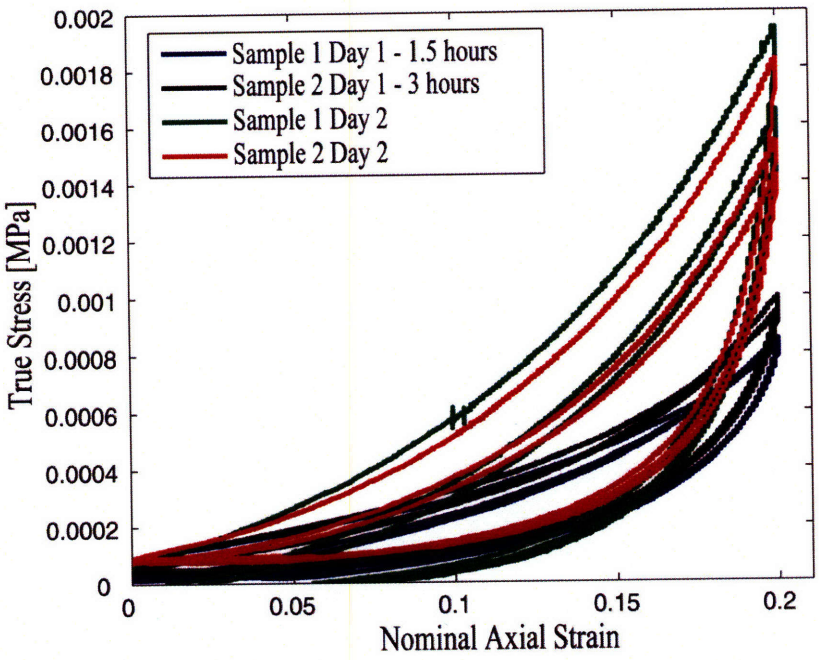

Figure 2-11: Uniaxial load-unload compression cycle response for different equilibration times. The two specimens were obtained from the same cervical slice.

nant specimens were not substantially higher than the equilibrium levels. Since fluid diffusion controls the transient peak response, this result is consistent with qualitative observations of the tissue morphology: much higher hydraulic permeability coefficients are probably associated with the loosely connected pregnant tissue.

The data suggests that the relaxation behavior is associated with at least two separate mechanisms. The first mechanism occurs in a very short time interval (~10s) with substantial relaxation immediately following the loading ramp. After this sharp stress drop, the stress continues to decrease at much lower rate, suggesting the presence of a second relaxation mechanism with a much larger characteristic decay time. A relaxed state is only partially attained at the end of the 30-minute relaxation interval. Also, relaxation times are slightly reduced for the unconfined compression cases, possibly due to differences associated with the transient diffusion of interstitial fluid. This difference arises because the surface of the unconfined specimens in contact with the bathing solution is nearly doubled. Furthermore, the confined compression configuration imposes a volumetric strain on the tissue equal to the axial strain, while in the unconfined compression configuration the specimen is free to expand radially (friction effects between specimen and compression platens are negligible). In the unconfined compression configuration the volumetric strains (and thus interstitial fluid outflow) are therefore controlled by the balance between the bulk and shear stiffness of the specimen.

Although the unconfined compression test subjects the specimens to two-fold levels of axial strain, and a ten-fold ramp strain rate, as compared to the confined compression tests, the recorded peak stresses and equilibrium stresses are comparable for the two testing modes.

2.3.3 Variability in Mechanical Measurements

In agreement with the findings of Conrad et al. [29], we noted some degree of variability in stroma properties for samples excised from the same cervix but at different anatomical site. On average, the maximum variability for samples taken from the same cervix was ± 0.2kPa for equilibrium and ± 2.4kPa for peak stress at 30% axial strain in unconfined compression. In general, there is a larger variability in tissue properties between patients (even patients with the same obstetric history) than between specimens from the same cervix. The standard variation in the stress levels reported in Tables 3, 4 and 5 is due to the combined effects of variability

among different patients and different cervical anatomical sites.

Preliminary histological studies were performed on stained stroma samples from human cervices obtained from hysterectomy specimens [40]. We were not able to identify a substantial degree of anisotropy in the arrangement of the collagen bundles; therefore, effects of specimen orientation were not expected to be significant, and during unconfined compression experiments no particular care was taken to align the transverse direction consistently among specimens. In other words, it was unknown if the lateral stretch measured from the video extensometer was associated with the circumferential, radial or any intermediate direction within the cervix. A large variability was noted in the lateral stretch measurements. If the tissue is anisotropic, then the lateral stretch will be dependent on tissue orientation and the variability in the findings can be easily explained.

2.4 Conclusion

This study represents a first important step towards the attainment of an improved understanding of the complex mechanical behavior of cervical tissue. The protocols developed here represent the first attempt to fully characterize the three-dimensional stress and strain behavior of the cervical stroma. The results of this preliminary study indicate that cervical tissue is nonlinear and time-dependent with softening and hysteresis evident in the load-unload behavior. Further, it was established that the stress response in tension and compression vary depending on the obstetric history of the patient with pregnant tissue being orders of magnitude softer than nonpregnant tissue.

The variability in the experimental data suggested that improvements to the mechanical testing protocol were needed. Section 1.3.3 of this doctoral work discusses the structure and organization of the collagen network of the cervical stroma. It is known that cervical stroma contains zones of preferentially aligned collagen fibrils, and that these aligned collagen fibrils contribute to tissue anisotropy. Modifications to both the tension and compression testing protocols were made to account for this anisotropy. Modifications were also made to the tension protocol to improve the tissue specimen shape and to improve the video strain measurements. The improved protocols and results are presented in the next Chapter.

Chapter 3

Anisotropy Study

This chapter details the results of a more refined study of the mechanical properties of human cervical tissue, which investigated anisotropy effects by cutting tissue sample along relevant anatomical direction and measuring mechanical responses, in uniaxial loading, along three orthogonal axes. Cervical tissue samples from hysterectomy and cesarean hysterectomy patients were tested in unconfined compression and tension using a load-unload, ramp-relaxation deformation protocol (Fig. 3-2). Tissue specimens were marked to indicate anatomical position and orientation, and the patient's obstetric history is noted. A 1-dimensional, nonlinear viscoelastic mechanical model was used to fit the experimental stress/strain response of each specimen in each testing direction to obtain a corresponding set of model parameters. The model parameters represented a quantitative measure of the material properties and were used to investigate the effects of anatomical position, anatomical orientation, and obstetric history on material response.

The results from the mechanical tests, presented below, suggest that non-pregnant cervical tissue is anisotropic with a mechanical response depending on the direction of loading. We hypothesize that this anisotropy is a result of collagen orientation in the stroma region in correlation with previously discovered regions of preferential collagen alignment [4][116]. This study is the first line of evidence to support this hypothesis with further evidence being gathered with a parallel histological study of the tested specimens.

Patient	Age	G	P	Hysterectomy Indication	Obstetric History	Labor?	Endometrial Pathology
NPND Patient 1	31	0	0	Chronic Pelvic Pain	No Preg.	No	Adenomyosis, Inactive endometrium
NPND Patient 2	35	0	0	Fibroid Uterus	No Preg.	No	Secretory
NPND Patient 3	47	1	1	DUB	Prior C/S	Cervix dilated to 3cm before C/S	Proliferative
NPPD Patient 1	47	2	2	DUB, Chronic Pelvic Pain	NSVDx2	Yes	Proliferative
NPPD Patient 2	47	1	1	Fibroid Uterus	NSVDx1	Yes	Proliferative
NPPD Patient 3	39	4	4	DUB	NSVDx4	Yes	Proliferative
PCS Patient 1	32			30 weeks Suspected Placenta Accreta	Prior C/S	No	Accreta confirmed
PCS Patient 2	28			35 weeks Suspected Placenta Percreta	Prior C/S	No	Percreta confirmed

Table 3.1: Patient Specific Obstetric History (G = Gravida, P = Para, DUB = Dysfunctional Uterine Bleeding, NSVD = Normal Spontaneous Vaginal Delivery, C/S = Cesarean Section)

3.1 Methods

Hysterectomy specimens from pre-menopausal women with benign gynecological conditions were obtained from the Tufts - New England Medical Center. Each cervical specimen was categorized according to the obstetric history of the patient. The three categories are listed in Table 2.1, and are the same categories investigated in Myers et al. [91]. Approval from the Institutional Review Board was obtained from both Tufts - New England Medical Center and MIT. Table 3.1 lists the specimens used in this study and the patients' specific obstetric history.

The uterus and cervix were excised from the patients and placed on ice. Four 4mm parallel slices were immediately cut from the cervix perpendicular to the inner canal and stored flat at -80°C (according to [91]). One day prior to testing, cube specimens (~$125mm^3$) were cut

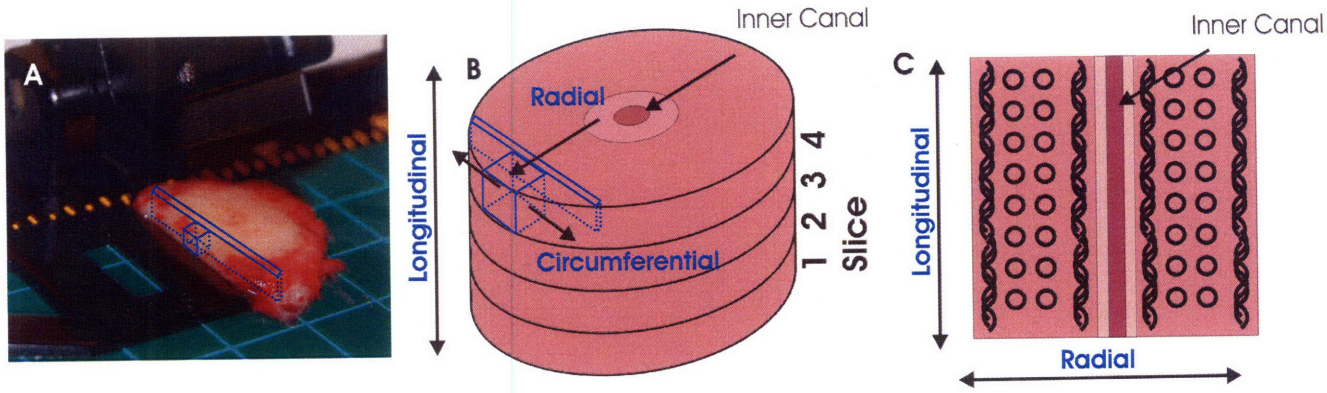

Figure 3-1: A) Specimen preparation of compression cubes and tension strips. B) Anatomical directions of the cervix. Multiple samples are cut along the radial direction to capture different fiber orientations. Cervical samples are only excised from the stroma region. C) Directions of "preferential" collagen fiber orientation [5, 6]. Circles indicate fibers in the circumferential direction (out of plane).

from partially thawed stroma regions of a single slice and marked according to anatomical orientation and radial position (Fig. 3-1). Thin tension strips (~2mm thick, ~10mm gage length) were cut adjacent to the cubes with the axial (loading) direction aligned with the circumferential direction. Tension specimens were cut so that sufficient tissue was available to be securely constrained in the tension grips while the specimen gauge length would consist primarily of stroma aligned in the circumferential direction. Compression cubes and tension strips were then equilibrated overnight in phosphate buffered saline (PBS) at 4°C one day prior to testing.

3.1.1 Mechanical Tests

All mechanical tests were conducted on a universal material testing machine (Zwick Z2.5/TS1S, Ulm, Germany) equipped with a 20 N load cell . All specimens were bathed in PBS fluid bath during testing. The transverse specimen deformation was captured with a video extensometer (Qimaging Retiga 1300 CCD camera, 200mm f/4 Nikon lens). Images were taken at 1Hz, and a right-angle prism captured the orthogonal plane of deformation. Lateral and axial stretch data was obtained with Digital Image Correlations (DIC) techniques using the Correlated Solutions VIC-2D (version 4.4.0) software [91][93]. Typical errors in strain measures obtained with this

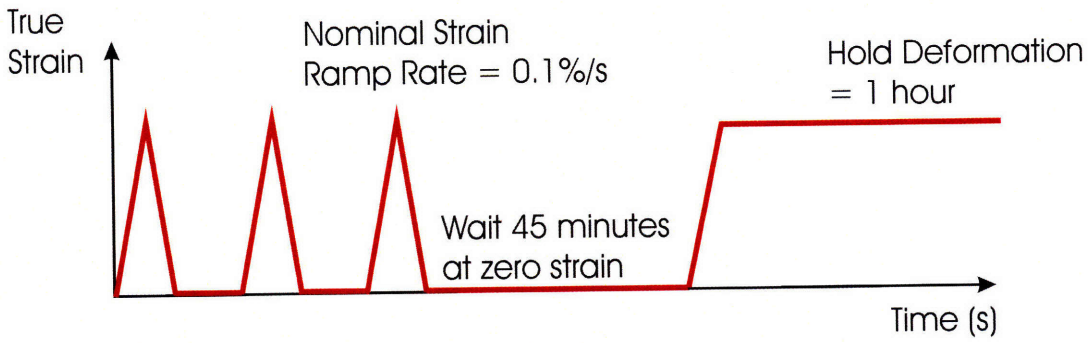

Figure 3-2: Load-unload, ramp-relaxation deformation protocol. Compression and tension specimens were loaded to different levels of true strain.

technique are of order 5%.

Compression

After overnight equilibration in PBS, each compression specimen was subjected to the uniaxial load-unload, ramp-relaxation deformation protocol (Fig. 3-2) in the longitudinal and circumferential directions. First, the compression specimen was loaded uniaxially in the circumferential direction to approximately 45% true compressive strain using the load-unload, ramp-relaxation protocol, then it was allowed to re-equilibrate for 45 minutes (unloaded) in PBS at 4°C . After re-equilibration, the specimen was loaded uniaxially in the longitudinal direction to approximately 45% true compressive strain using the load-unload, ramp-relaxation protocol. Three-dimensional deformation was captured using the video extensometer and a right-angle prism (Fig. 3-3).

Tension

After overnight equilibration in PBS, tension strips were air brushed with India ink and then secured into stainless steel tension grips using sand paper and ethyl cyanoacrylate. Once secured in the tension grips and placed in the fluid bath, the tissue was loaded to 15% true strain following the load-unload, ramp-relaxation deformation protocol and then allowed to equilibrate for at least 45 minutes without removing the tissue from the tension grips. After equilibration

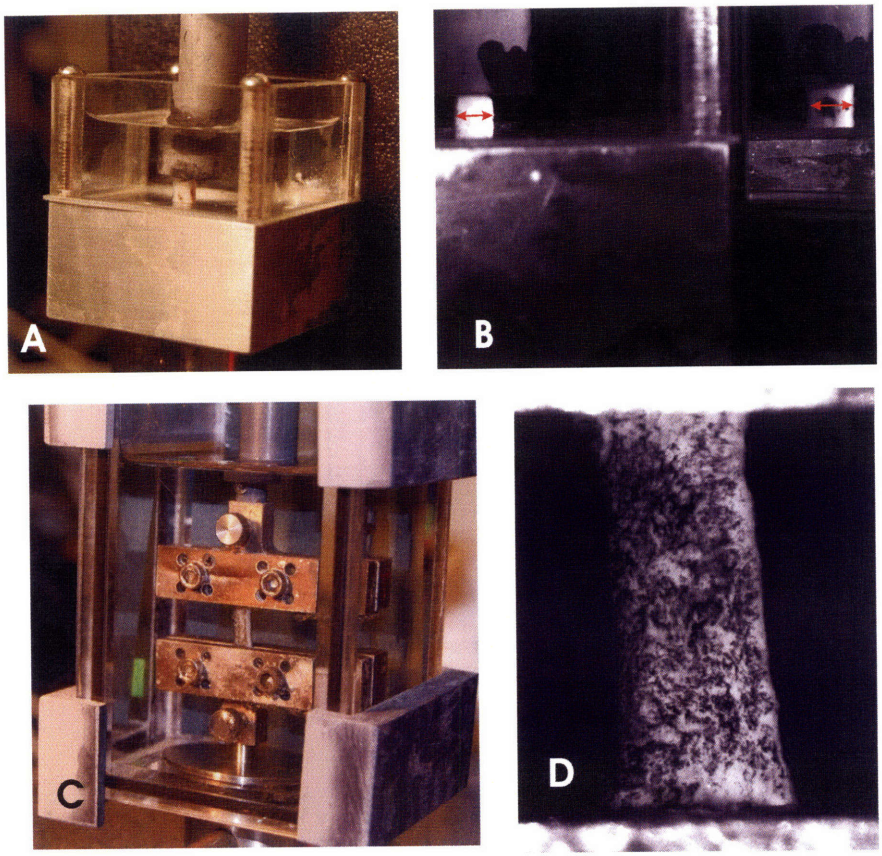

Figure 3-3: A) Compression specimen in loading fixture. B) Video extensometer view of the compression test. The right specimen image is the right-angle prism view. The red arrows indicate the direction transverse to the loading axis. C) Tension specimen in the loading fixture. D) Video extensometer view of the tension specimen.

the tissue was loaded to a higher level strain using the load-unload, ramp-relaxation deformation protocol and then allowed to equilibrate for at least 45 minutes. These steps were repeated for increasing levels of true strain. Axial and lateral displacement fields were captured using the video extensometer (Fig. 3-3). The specimen displacement fields were analyzed to confirm that the specimens did not slip from the tension grips.

3.1.2 One-dimensional Rheological Model

The mechanical response of each cervical tissue specimen depends on the obstetric history of the patient, the anatomical location of the specimen, and the relative orientation of the loading direction relative to the preferential alignment of the collagen network. The tissue response, both in tension and compression, is highly nonlinear and time dependent [91]. In order to quantitatively compare the responses of different specimens, one approach would be to consider phenomenological parameters, such as tangent or secant moduli for the loading and unloading responses, equilibrium moduli from the relaxation tests, ratios of moduli in sequential cycles of loading, and so forth. These arbitrary parameters, each capturing the superposed contributions of different mechanisms of resistance to deformation, do not provide significant insight into the underlying connections between mechanical response and tissue architecture and composition. A more promising approach to elucidate these relationships is to express differences in mechanical response in terms of differences between the values of fitting parameters for a nonlinear rheological model.

A simple 1-D model can be employed to capture the stress-strain response of the tissue in tension or compression because all tests were conducted in the same (uniaxial) mode of deformation. As detailed in the previous section, we collected compression properties of the tissue by testing cubical specimens along the circumferential and longitudinal directions, and tension properties along the circumferential direction by testing tissue strips cut adjacent to the compression specimens. Differences between compressive and tensile responses of the tissue, as well as differences between the compressive responses along orthogonal loading directions, arise from three-dimensional effects of the deformation of the underlying anisotropic collagen network [95]. Within the simplified 1-D modeling framework employed in this study, three different sets of parameters will be needed to fit the corresponding experimental stress-strain data . This

shortcoming is balanced by the ease and flexibility of a 1-D modeling tool, which allowed us to explore a wide range of different rheological configurations and constitutive relationships for the viscous and elastic elements and to determine an appropriate non-linear time-dependent constitutive framework for the uniaxial tissue response. Our goal was to identify a minimal set of viscoelastic components that could capture the essential features of the material behavior, and a corresponding set of model parameters representing the "mechanical properties" of the tissue samples in tension or compression. The rheological model schematically represented in Fig.3-4 was found to meet these objectives, with a corresponding minimal set of seven model parameters [E, α, f_v, S_o, n, η, E_{back}], as further discussed in the Constitutive Model Development section below. The governing differential equations for the 1-D constitutive model can be numerically integrated over a prescribed strain history to provide model predictions of uniaxial tissue response for a given set of model parameters. By fitting model predictions to experimental nominal stress-strain data for each tested specimens, a set of "best fit" material parameters [E, α, f_v, S_o, n, η, E_{back}] was obtained to "quantify" the results of each tension and compression test.

The numerical integration of the governing equations, as well as the optimization search for the best-fit model parameters (simplex method) were performed using a Matlab (Mathworks, Natick, MA) script [62]. The normalized error in the least squares fit was prescribed not to exceed a tolerance of 0.1%. For each compression specimen, two separate model fits were performed and two sets of parameters were obtained to match compression test results along the longitudinal and circumferential directions. For each tension specimen, the tissue response was only measured along the circumferential direction, so a single set of parameters was obtained.

3.2 Constitutive Model Development

Model development was guided by the microstructure of the tissue, where biochemical components and corresponding mechanisms of deformation resistance are conceptually associated with model elements. In a minimalist interpretation of the mechanical roles of tissue components, we can state that the tissue consists of a fibrous collagen network embedded in a viscous groundsubstance, where hydrated proteoglycans provide bulk resistance as well as weak sec-

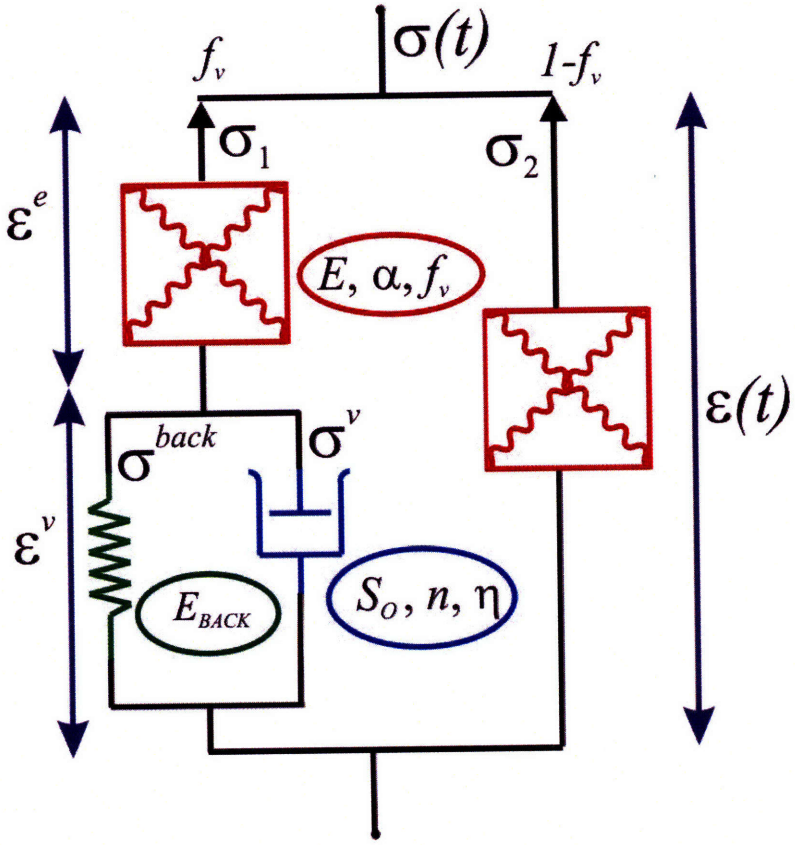

Figure 3-4: The 1-dimensional rheological mechanical model for cervical tissue. Material parameters are circled.

ondary links between collagen fibrils/fibers. If a collagenous tissue is instantaneously subjected to an imposed deformation, all the collagen crosslinks (weak bonds, strong bonds and physical entanglements) are temporarily "frozen", since relative molecular sliding and rearrangements can only be accomplished through viscous mechanisms and require time. Under these conditions, collagenous tissues display a stiff, nonlinear response, where an initial compliant toe region, corresponding to the uncrimping and unbending of collagen fibers between crosslinks, is followed by a sudden upturn of the tissue stiffness when the fibers have lost their "slack" and approach their limit of extensibility. This instantaneous (elastic) behavior is well captured by an exponential relationship [44] in the form

$$\sigma = \frac{E}{\alpha}\left(\exp\left[\alpha\varepsilon^{e}\right] - 1\right) \tag{3.1}$$

where the stiffening stress response with elastic strain, ε^{e},is captured through two model parameters [E, α]. The small-strain modulus, E, captures the initial stiffness of the collagen network and is postulated to increase with collagen density and mean fiber diameter. The parameter α is inversely related to the instantaneous extensibility of the collagen network, and is postulated to increase with crosslink density. Materials with densely interconnected collagen networks will be less extensible (larger α) than materials with a loosely connected network.

Under the effects of an imposed deformation, the stress in the tissue will activate viscous mechanisms and, with time, lead to a reconfiguration and relaxation of the collagen network. The rheological model in Fig. 3-4 reflects the notion that, in general, only a fraction (f_v) of the entire collagen network can relieve its stress through viscous relaxation. The stress response of the tissue is therefore decomposed in a contribution from the viscoelastic left branch, σ_1, and a contribution from the purely elastic right branch, σ_2:

$$\sigma(t) = \sigma_1(t) + \sigma_2(t) = f_v\frac{E}{\alpha}\left(\exp\left[\alpha\varepsilon^{e}\right] - 1\right) + (1 - f_v)\frac{E}{\alpha}\left(\exp\left[\alpha\varepsilon\right] - 1\right) \tag{3.2}$$

This constitutive relationship combines the responses of the nonlinear elastic elements in the two branches of Fig. 6, which are therefore associated with the three model parameters [E, α, f_v].

The viscous flow in the tissue is accommodated by processes with a range of energy barriers.

Collagen reorganization and realignment entail scission of secondary bonds and reptation of the collagen fibrils/fibers through physical entanglements. Increasing levels of stress will enable additional slipping mechanisms to become active. This notion gives rise to a nonlinear viscous constitutive relationship in which the viscous strain rate increases nonlinearly with the driving stress, σ^v:

$$\dot{\varepsilon}^v(t) = \dot{\varepsilon}_o \left(\frac{\sigma^v(t)}{S_o} \right)^n \tag{3.3}$$

In this relationship $\dot{\varepsilon}_o$, $=1\text{s}^{-1}$ is a constant introduced for dimensional consistency, while S_o and n are model parameters. A physical interpretation of the constitutive parameters, [S_O, n], can be obtained by considering the dependence of viscous strain rate on the driving (viscous) stress. The viscous strength, S_O, represents the viscous stress necessary to drive viscous strain at a rate of 100% per second ($\dot{\varepsilon}_o$). The stress exponent, n, represents the stress sensitivity of the viscous mechanisms. For n =1 the model behaves as a linear Newtonian material (with viscosity $S_O/\dot{\varepsilon}_o$). For larger values of n, the model captures the effects of superposing stress-activated mechanisms on viscous flow, and the viscous rate dramatically increases for stresses exceeding S_O. Since this constitutive relationship attempts to capture the viscous resistance of the ground substance to collagen reorientation, we postulate that the [S_O, n] parameters will be primarily controlled by the characteristics of the proteoglycan component of the tissue and by the collagen/proteoglycan interactions. We found that this simple form of the constitutive relationship for viscous flow was not sufficient to account for the experimental behavior of the tissue. As viscous strain accumulates in the tissue, and the collagen network exhausts all possible avenues of reorganization to accommodate the imposed deformation, the viscous strain rate (under constant driving stress) tends to decrease. This is a well known effect in macromolecular solids [23,24] where this effect is ascribed to the physics of reptation of elastically inactive macromolecules. Following [24], we express the dependence of strain rate on accumulated viscous deformation through a single additional model parameter, η:

$$\dot{\varepsilon}^v(t) = \dot{\varepsilon}_o \frac{\eta}{|\varepsilon^v| + \eta} \left(\frac{\sigma^v(t)}{S_o} \right)^n \tag{3.4}$$

Note that for ε_v=0 the form (3) of the constitutive relationship is recovered, and, at constant driving stress, the viscous strain rate diminishes with increasing levels of accumulated viscous

strain. Typical values of the parameter η are in the range [0.0001 to 0.01], where larger values of η provide the ability to accommodate larger levels of viscous strain through collagen reptation and realignment, and can be therefore associated with loosely crosslinked collagen networks. In the rheological model in Fig. 3-4, this constitutive relationship is taken to represent the response of the dashpot element in the left branch, which is therefore associated with the three model parameters [S_o, n, η].

Finally, the left branch of the rheological model includes an elastic "backstress" element in parallel with the viscous dashpot. This element captures the "elastic memory" of the tissue, which is observed to recover its initial configuration upon unloading. As the collagen network disentangles, reptates, and realigns under the effects of the viscous driving stress, strong covalent bonds between collagen fibers become the limiting factor for continued viscous flow. For simplicity, we associate a linear response to the dependence of the elastic backstress on the extent of viscous deformation through a single elastic modulus E_{back}:

$$\sigma^{back} = E_{back}\varepsilon^{v}(t) \tag{3.5}$$

The driving stress for viscous flow is then obtained as the difference between the applied stress and the network backstress:

$$\sigma^{v}(t) = \sigma_1(t) - \sigma^{back}(t) \tag{3.6}$$

The two tissue components represented by the left and right branch of the rheological model in Fig. 6 are taken to deform in an affine manner, so that compatibility arguments yield the final relationship needed to complete the constitutive formulation of the 1D model:

$$\varepsilon(t) = \varepsilon_2(t) = \varepsilon_1(t) = \varepsilon^{e}(t) + \varepsilon^{v}(t) \tag{3.7}$$

As a final note on the physical interpretation of the proposed 1D rheological model, we should mention an observation concerning the contributions of shear and bulk resistance to the uniaxial response of the tissue. In uniaxial deformation, these two contributions play an equally important role. Arguably, the shear component of the tissue response is dominated by the collagen network contribution. However, the bulk response is given by a combination of

contributions from the collagen network and from the proteoglycan ground substance, which resists decreases in volume through osmotic pressure effects. It is therefore important to recognize that the elastic moduli [E and E_{back}] in the 1D model will reflect structural and compositional characteristics not only of the collagen network, but also of the proteoglycan component of the ground substance.

3.3 Results

3.3.1 Mechanical Stress Response in Compression - NPND

Figure 3-5 illustrates typical experimental responses for uniaxial load-unload compression tests, where true axial stress and lateral stretch are plotted as a function of the imposed levels of true axial strain. Following the protocol in Fig. 3-2, each curve comprises three successive load-unload cycles. Figure 3-5 illustrates the responses of two tissue samples excised on the same cervical slice from a nonpregnant patient who had one previous cesarean section and no previous vaginal deliveries (NPND Patient 3). The stress-strain response is nonlinear, with substantial hysteresis. The first loading ramp is typically stiffer than the subsequent cycles, and this "conditioning" response can be re-attained by allowing the tissue to equilibrate between tests [91]. Both the stress response and the transverse stretch response display some degree of anisotropy. Sample 1 of Fig. 7 was excised from the middle radial region of the cervix. Previous morphological studies [116][4] indicate that the collagen fibers in this region are preferentially aligned in the circumferential direction. For Sample 1, the peak axial stresses recorded by compressing the specimen in the longitudinal direction were higher than the peak axial stresses recorded by compressing the specimen in the circumferential direction. In addition, by considering the transverse (lateral) stretch data, it can be seen that the circumferential direction displayed the highest resistance to transverse stretching.

Sample 2 of Fig. 3-5 was excised from the outer radial region where the collagen fibers are reported [116][4] to be preferentially aligned in the longitudinal direction. For this sample the trends concerning the directionality of the tissue response were reversed: for Sample 2 the peak axial stresses were higher for the compression test in the circumferential direction, and the longitudinal direction displayed the highest resistance to elongation, as indicated by the

lateral stretch data.

Figure 3-6 illustrates typical stress-time and lateral stretch-axial strain responses in ramp-relaxation tests, collected for the same two specimens. Peak stresses and lateral stretches at the end of the loading ramps reflect a directionality dependence of material properties in good agreement with the trends established by the load-unload tests. However, following the stress relaxation transient, the equilibrium stresses measured for a single sample were typically the same for both loading directions. These trends for peak stresses and lateral stretches were confirmed in samples from a second NPND patient with no previous pregnancies (NPND Patient 3). Again two samples from the same cervical slice were tested using the above compression protocol. The mechanical data suggests that the tissue is anisotropic with evidence that collagen orientation influences the material response.

.

3.3.2 Mechanical Stress Response in Compression - NPPD

Figure 3-7 illustrates the uniaxial compression responses in load-unload tests for two samples taken from the same cervical slice of a non-pregnant patient with 1 previous vaginal delivery (NPPD Patient 2). Results from these tests indicate that the mechanical properties of this cervix are also anisotropic. Sample 1 was taken from a region where the collagen fibers are suspected to be preferentially aligned in the circumferential direction, and Sample 2 was taken from a region where the collagen fibers are suspected to be preferentially aligned in the longitudinal direction. Similar to the results for the NPND cervix in Fig. 3-5, Sample 1 exhibited a higher stress response when compressed along the longitudinal direction, and Sample 2 had a higher stress response when compressed along the circumferential direction. Also, the highest resistance to lateral stretch was in the circumferential direction for Sample 1 and in the longitudinal direction for Sample 2. Again, these results suggest that the tissue is anisotropic and that the differences in collagen alignment, previously identified in [116][4], influence the mechanical response of the specimen.

Figure 3-8 illustrates the ramp-relaxation stress response for the two NPPD samples. Similar to the findings for the NPND cervix, the peak stresses vary with loading directions for a single sample. However, the measured equilibrium stresses for a single sample were the same for both

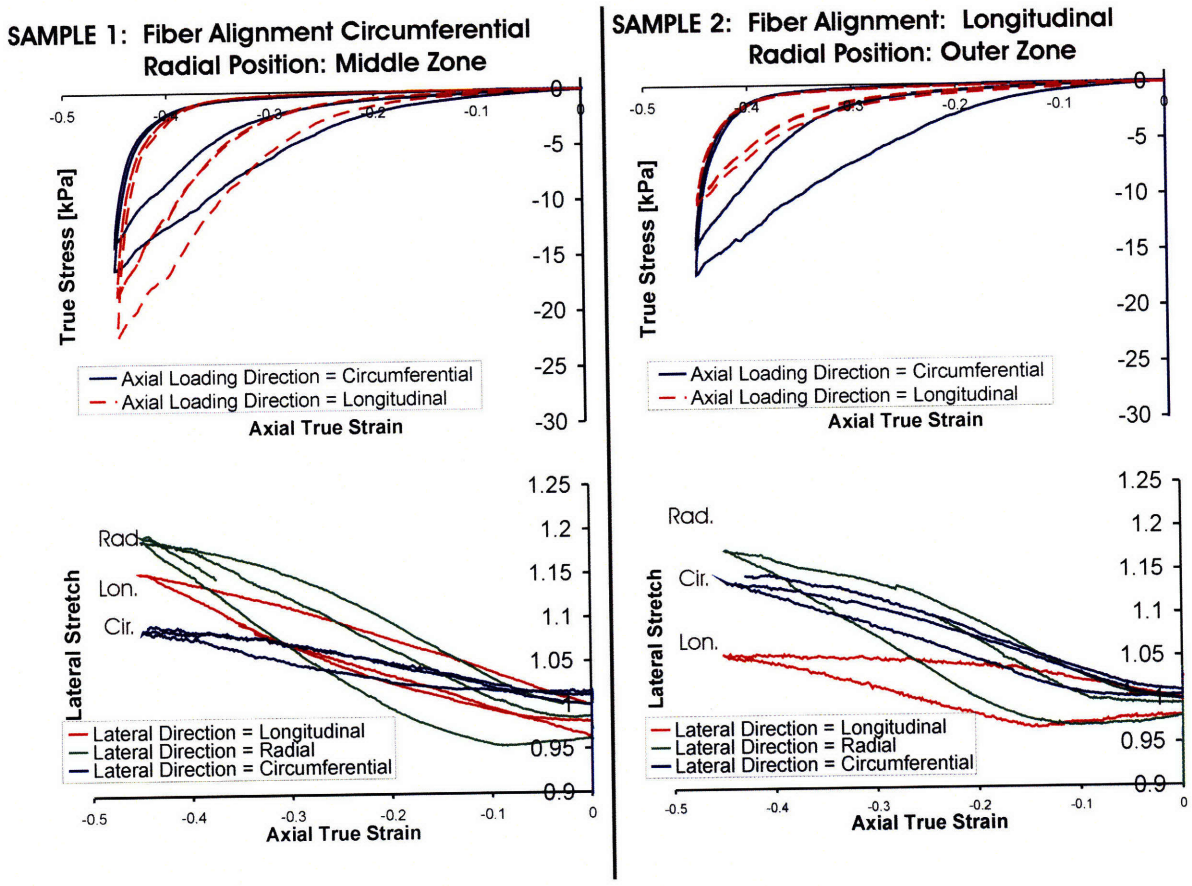

Figure 3-5: True stress and lateral stretch response for two specimens from the same non-pregnant cervical slice (NPND Patient 3) for the load-unload tests. Each specimen was excised from different radial locations on the slice, and each specimen was tested along two different directions of uniaxial compression. Sample 1, data presented on the left, was excised from the middle stroma region, and Sample 2, data presented on the right, was excised from the outer stroma region. By investigating the stress and stretch response for a single sample, a difference in peak stress and stretch is recorded between the different loading directions. Further, by comparing Sample 1 and Sample 2, differences in the stress and stretch responses can be ascribed to differences in the direction of preferential collagen alignment. (The lateral stretch for the radial direction represents the average from the longitudinal and circumferential tests).

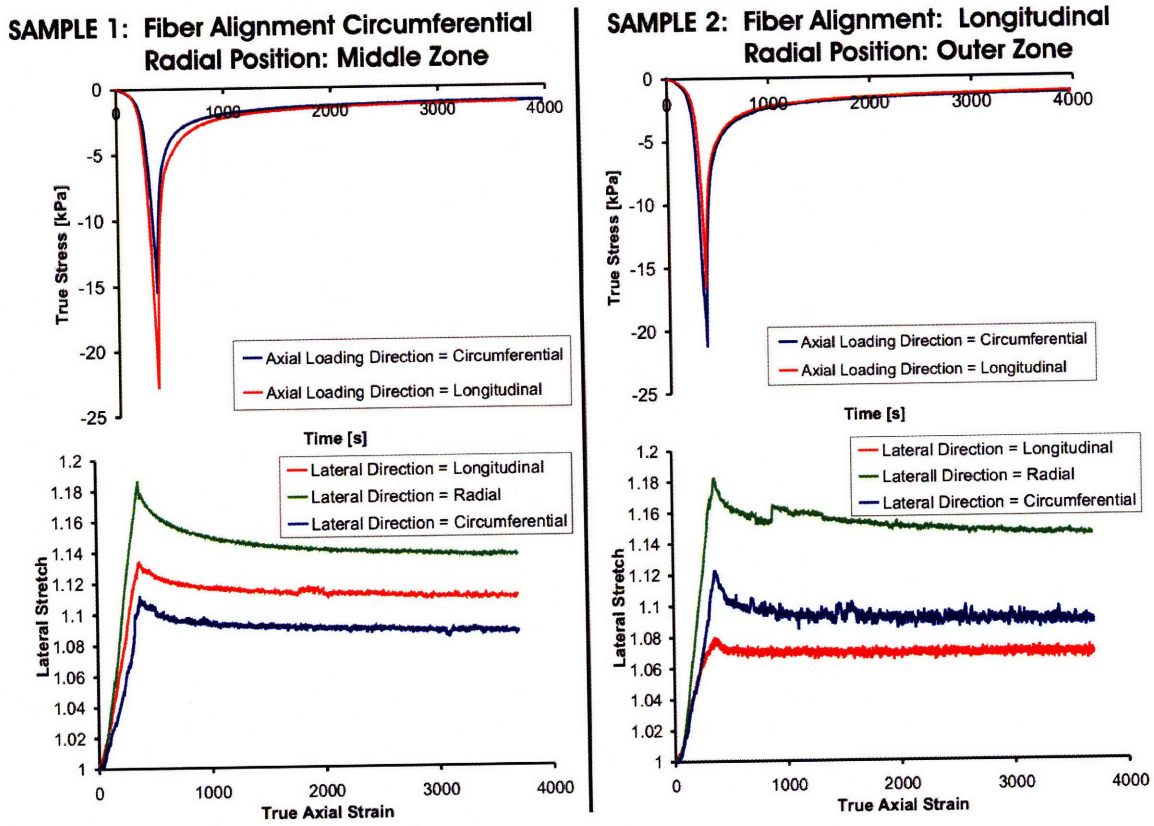

Figure 3-6: True stress and lateral stretch response for the ramp-relaxation tests for the same two specimens presented in Fig. 3-5 (NPND Patient 3). Each specimen was excised from different radial locations on the slice, and each specimen was tested along two different directions of uniaxial compression. The peak stresses and stretches are different when comparing the different loading directions for a single sample. However, the equilibrium stresses are the same when comparing loading directions. (The lateral stretch for the radial direction represents the average from the longitudinal and circumferential tests).

loading directions.

Consistent trends for the true stress, true axial strain, and lateral stretch were found in a second NPPD cervix from a patient with 2 previous vaginal deliveries (NPPD Patient 1). Again, two tissue samples from the same cervical slice were tested using the compression protocol, and the stress response was anisotropic with higher peak stresses for loading directions that were perpendicular to the inferred directions of preferential alignment for the collagen fibers.

We encountered only one case for which the response measured in the inferred circumferential and longitudinal directions were not found to strongly differ. This tissue specimen was obtained from a patient with 4 previous vaginal deliveries (NPPD Patient 3). The cervical canal for this patient was not a circular cylinder, but rather a distorted slot, and the degree of axisymmetry of the cervical slices was rather poor. Again, two tissue specimens were tested from the same cervical slice. The samples were taken from different radial locations and subjected to the same compression loading protocol. Both samples had similar responses (peak axial stresses and lateral stretches) along the inferred longitudinal and circumferential directions. It is arguable that, for this case, precise anatomical directions were difficult to determine, so that the specimen orientation was not properly characterized.

3.3.3 Mechanical Stress Response in Compression - PCS

Figure 3-9 and Fig. 3-10 illustrate the uniaxial compression responses in the load-unload and ramp-relaxation tests, respectively, for tissue specimens obtained from a pregnant patient at the time of Cesarean section (PCS Patient 2). The stress responses for the PCS specimens were noticeably more compliant when compared to the non-pregnant specimens, with amplitudes of the stress responses reduced by an order of magnitude. In addition, some degree of softening ("damage") was noticed for PCS specimens after the first cycle of compression tests. The presence of "damage" mechanisms was inferred based on the inability of the tissue sample to recover their original configuration (dimensions and stress-strain response) after re-equilibration. Softening effects are exemplified by the stress response of Sample 1 in Fig. 3-9. For this specimen, two successive complete tests (following the protocol in Fig. 3-2) were performed along the same (circumferential) direction, followed by a third test along the longitudinal direction. A re-equilibration period of 45 minutes was introduced between tests. Data in Fig. 3-9 indicate

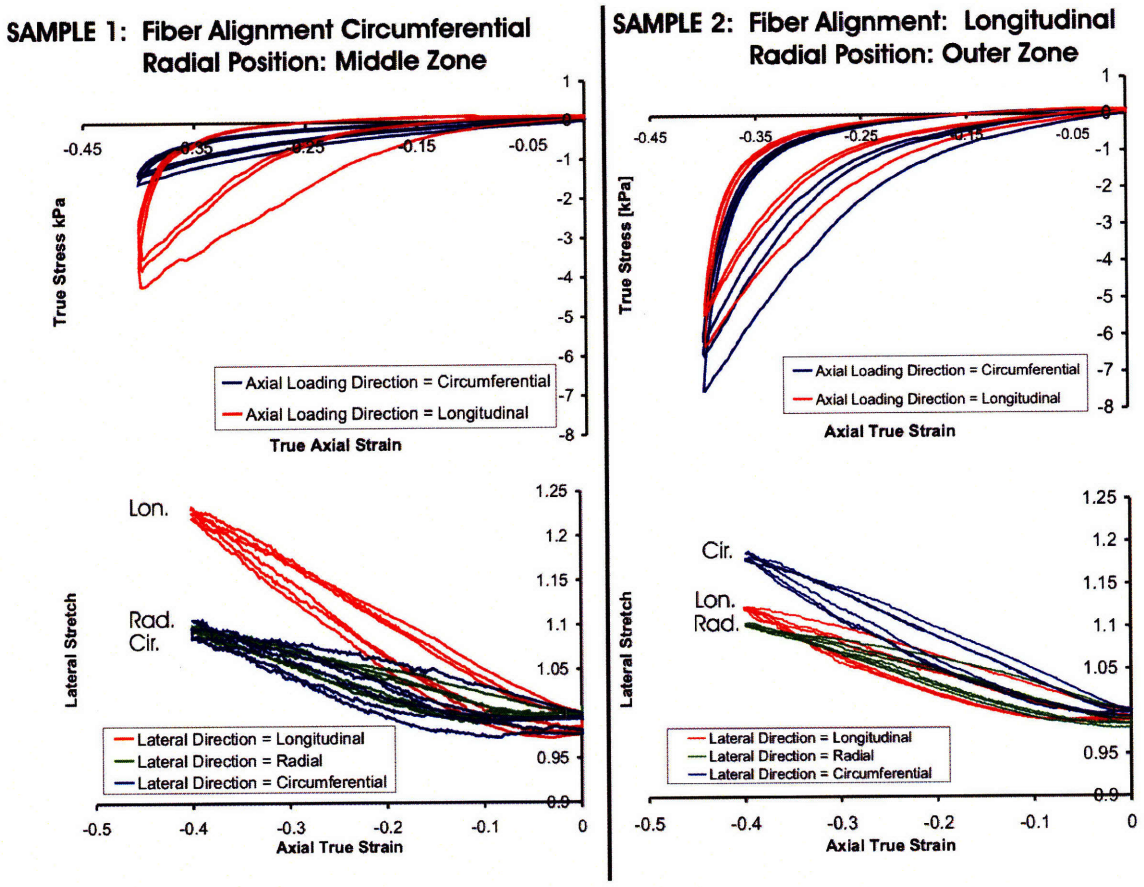

Figure 3-7: True stress and lateral stretch response for two specimens from the same non-pregnant cervical slice (NPPD Patient 2) for the load-unload tests. Each specimen was excised from different radial locations on the slice, and each was tested along two different directions of uniaxial compression. The same anisotropic trends measured for the NPND specimens in Fig. 3-5 are also measured for these two specimens. (The lateral stretch for the radial direction represents the average from the longitudinal and circumferential tests).

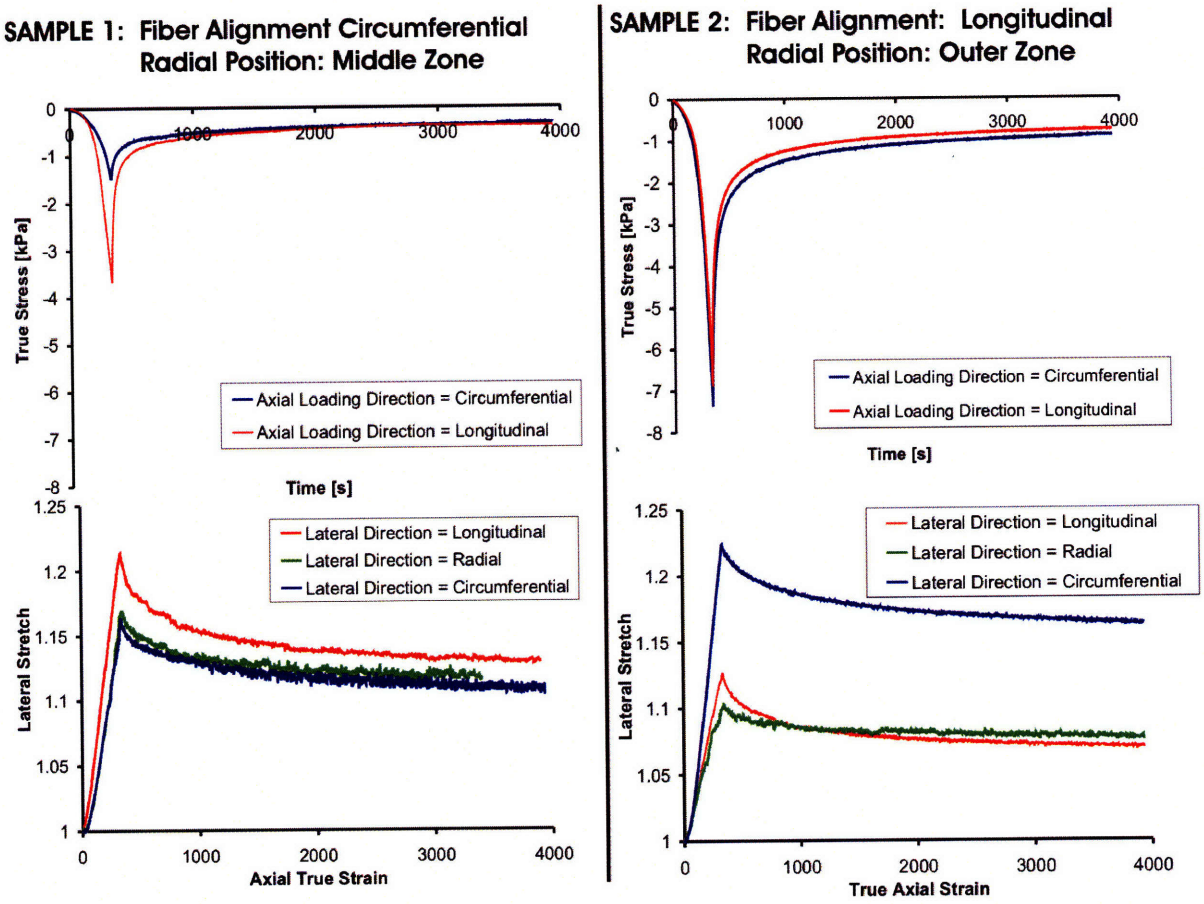

Figure 3-8: True stress and lateral stretch response for the ramp-relaxation tests for the same two specimens presented in Fig. 3-7 (NPPD Patient 2). Each specimen was excised from different radial locations on the slice, and each was tested along different directions of uniaxial compression. The peak stresses and stretches are different when comparing the different loading directions for a single sample. However, the equilibrium stresses are the same when comparing loading directions. (The lateral stretch for the radial direction represents the average from the longitudinal and circumferential tests).

some degree of softening from the 1st to the 2nd response, proving that (unlike non-pregnant tissue) pregnant tissue does not completely recover between tests. These findings introduce some difficulty in interpreting results of subsequent tests performed along different anatomical direction for pregnant tissue, where directionality effects can be partially confounded by softening effects.

3.3.4 Mechanical Stress Response in Tension – All Obstetric Cases

Figure 3-11 depicts the stress and lateral stretch response at multiple levels of true strain for a non-pregnant cervical strip taken from a patient with no previous pregnancies (NPND Patient 1). Note that, following the protocol in Fig. 3-2, each load-unload cycle (Fig. 3-11a) is followed by a ramp-relaxation test conducted to the same axial strain amplitude (Fig. 3-11b) Therefore, the softening behavior between loading cycles (Fig. 3-11a) is magnified by the effects of the intermediate ramp-relaxation tests conducted after each cycle. Images from the video extensometer confirmed that the specimen did not slip out of the tensile grips. In tension, the stress response for non-pregnant cervical tissue is non-linear with a characteristic shallow toe region for small strains and a sharp upturn towards a peak stress for increasing levels of strain. There is evidence of softening between multiple tests with a more compliant stress response for subsequent loading. Further, there is evidence of hysteresis in the load-unload cycles where differences between loading and unloading responses indicate a substantial contribution from dissipative mechanisms of resistance to deformation. Similar characteristics for the stress response were also found in NPPD cervical samples as shown in Fig. 3-12.

Figure 3-13 depicts the stress and lateral stretch response for a PCS cervix for multiple tension tests (PCS Patient 2). The stress response had characteristics similar to the non-pregnant case, with non-linear behavior, and evidence of softening and hysteresis. However, the response for the PCS cervix was more compliant, with the tissue reaching higher levels of stretch before displaying a sharp upturn in the stress. Typically, non-pregnant tissue could only reach approximately 35% true strain before the tissue began to significantly stiffen, slip from the grips, or tear. The pregnant tissue was able to reach true strain levels up to 75% without tearing or slipping from the grips. Further, the small strain regime for the pregnant tissue was nearly elastic with minimal hysteresis and non-linearity (see inset of Fig. 3-13). With strain

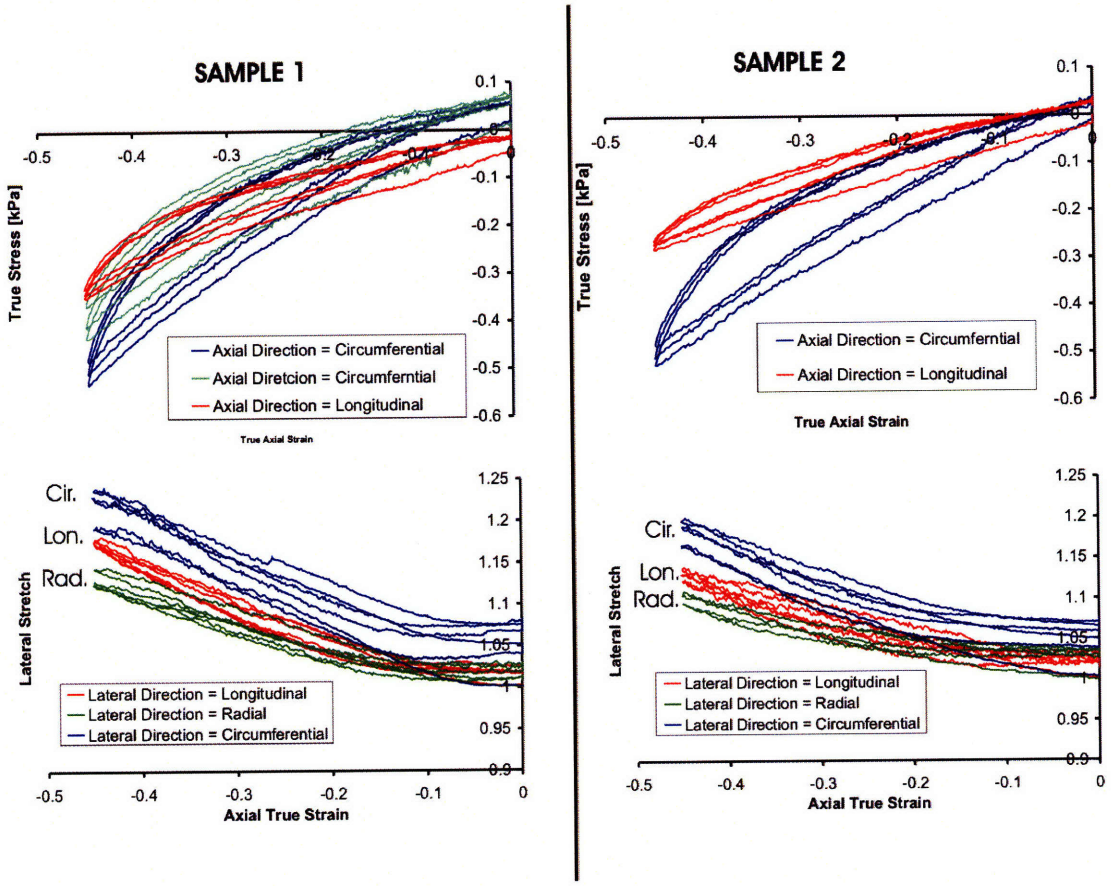

Figure 3-9: True stress and lateral stretch response for two specimens from the same pregnant cervical slice (PCS Patient 2) for the load-unload tests. Each specimen was excised from different radial locations on the slice, and each specimen was tested along two different directions of uniaxial compression. It was evident that the pregnant tissue underwent some "damage" during each testing step and was unable to completely recover its "virgin" conditions by re-equilibration between tests. For example, Sample 1 was tested twice in the circumferential direction, and the amplitude of the stress response for the second circumferential test was smaller than the amplitude of the stress response for the initial circumferential test. Therefore, sequential testing along different directions is not a reliable approach to determine anisotropy effects in pregnant tissue.

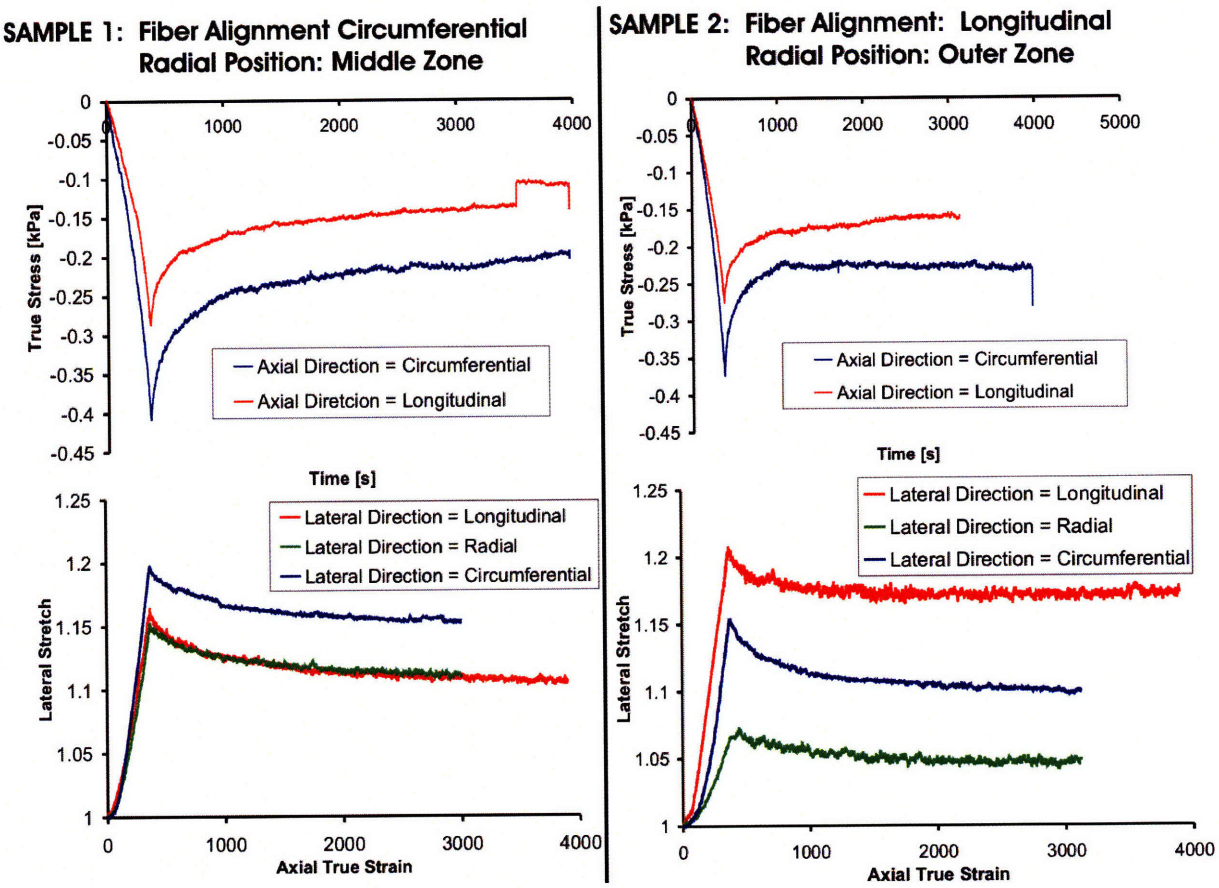

Figure 3-10: True stress and lateral stretch response for the ramp-relaxation tests for the same two specimens presented in Fig. 3-9 (PCS Patient 2). Each specimen was excised from different radial locations on the slice, and each was tested along different directions of uniaxial compression. (The lateral stretch for the radial direction represents the average from the longitudinal and circumferential tests).

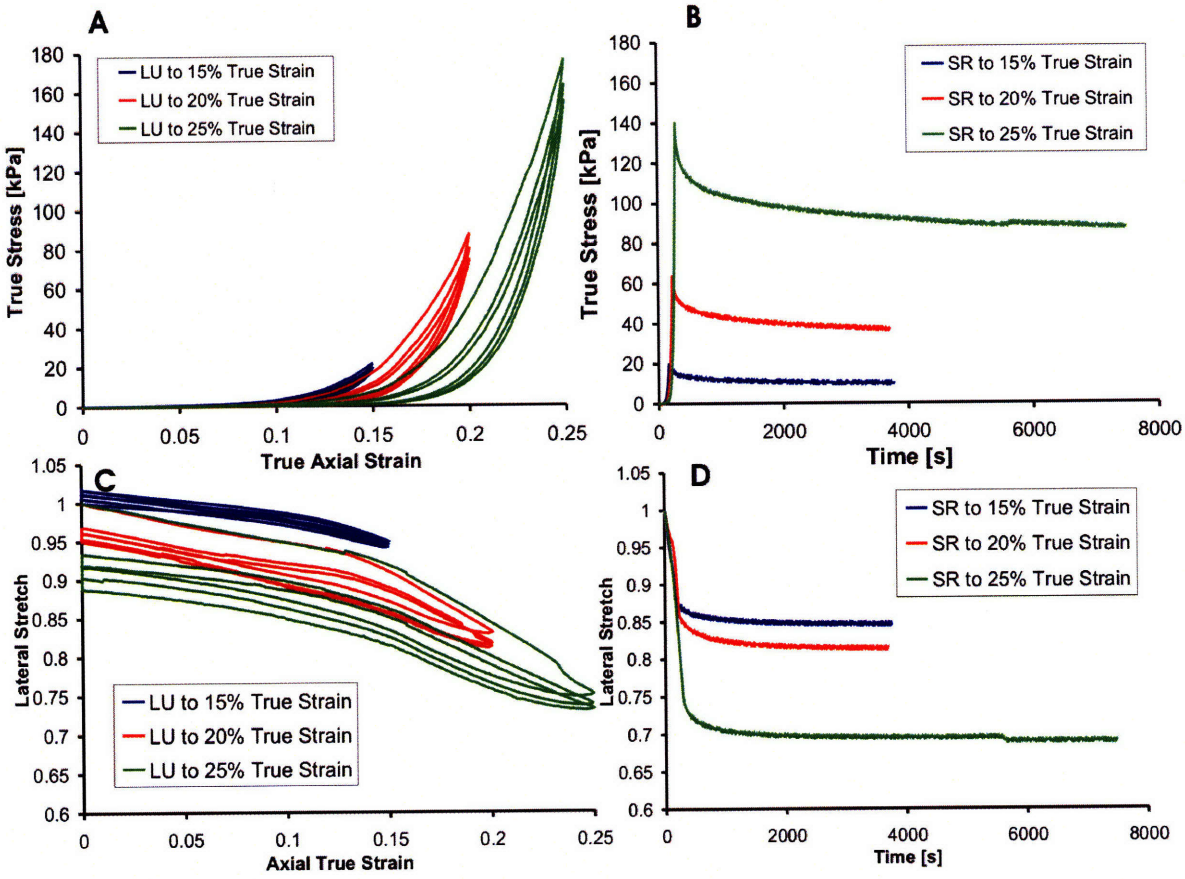

Figure 3-11: The true stress and lateral stretch response for a single tension strip from NPND Patient 1. A) True stress response for the load-unload tests. Note that three load unload cycles are followed by a stress-relaxation test at each strain level. Therefore, when plotting the load-unload stress-strain cycles on the same axes the softening effects between cycles are magnified. B) True stress response for the ramp-relaxation tests. C) Lateral Stretch response for the load-unload tests. D) Lateral Stretch response for the ramp-relaxation tests

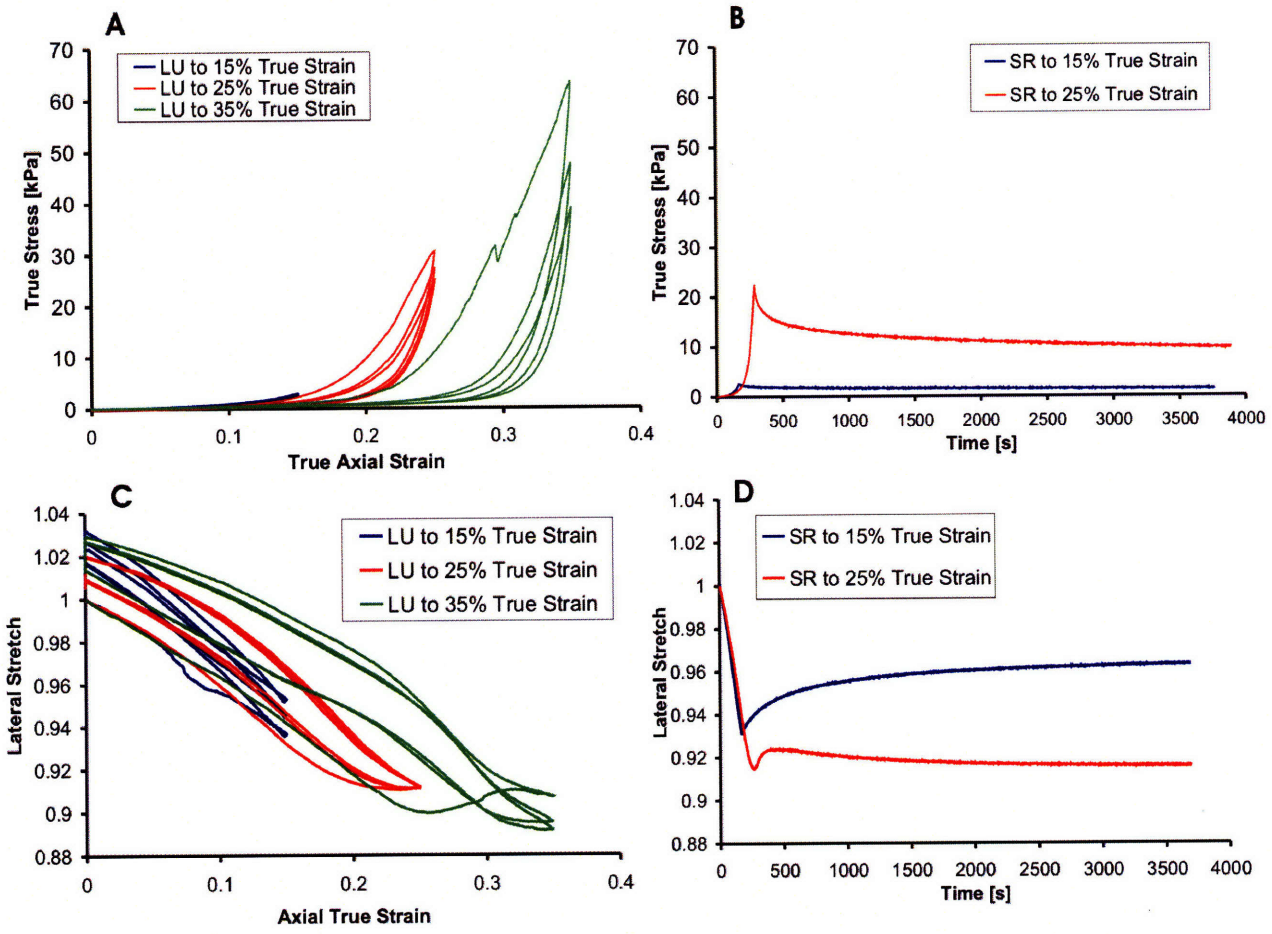

Figure 3-12: The true stress response for a single tension strip from NPPD Patient 3. The specimen slipped from the grips during the 35% true strain load-unload test therefore the ramp-relaxation test was omitted. A) True stress response for the load-unload tests. B) True stress response for the ramp-relaxation tests. C) Lateral Stretch response for the load-unload tests. D) Lateral Stretch response for the ramp-relaxation tests

levels above 35% the stress response became more non-linear with hysteresis loops occurring during the load-unload cycles. Finally, softening effects in subsequent cycles are considerably magnified for pregnant tissue samples, with substantial residual elongation which cannot be recovered by re-equilibration.

The large strain response for human cervical tissue is non-symmetric in tension and compression. This asymmetry is typical for collagenous materials (as well documented by extensive studies on cartilage, see, e.g., [24]). Figure 3-14 depicts the uniaxial tension and compression behavior for a non-pregnant patient in the circumferential direction. The data represents the stress response from a compression cube and tension strip taken from the same cervical slice. The large strain response in tension is much stiffer when compared to compression. However, for the small strain regime, the slopes of the stress/strain plot match well for tension and compression (see inset of Fig. 3-14).

3.3.5 Model Fit to Compression and Tension Data

The proposed 1-D rheological model was successful at capturing the essential features of the uniaxial time-strain-stress response of the cervical tissue, including the nonlinearity, softening, hysteresis, and relaxation behavior. A minimal set of material parameters [E, α, f_v, S_o, n, η, E_{back}] were sufficient to characterize the response of each compression and tension sample.

The best fit model prediction for Sample 1 of the compression data presented in Fig. 3-7 is plotted in Fig. 3-15 (NPPD Patient 2). This specimen was excised from the middle stroma region where the collagen fibers were suspected to be preferentially aligned in the circumferential direction. The model successfully captures the compression response in both the longitudinal and circumferential loading directions using two sets of material parameters. For this specimen, the best-fit material parameters along the circumferential direction were [E=101.2Pa, α=25.3, f_v=1, S_o=8.7kPa, n=1.4, η=0.00044, E_{back}=2.8kPa] and along the longitudinal direction were [E=119.7Pa, α=34.9, f_v=1, S_o=9.7kPa, n=1.3, η=0.00026, E_{back}=2.4kPa]. Note that one set of best-fit material parameters for each loading direction is able to capture both the load-unload and ramp-relaxation stress behavior. Typically, significant differences were found for the best-fit material parameters α and η when comparing the stress responses for the two loading directions on a single sample. As shown in Fig. 3-15, the amplitude of the stress response

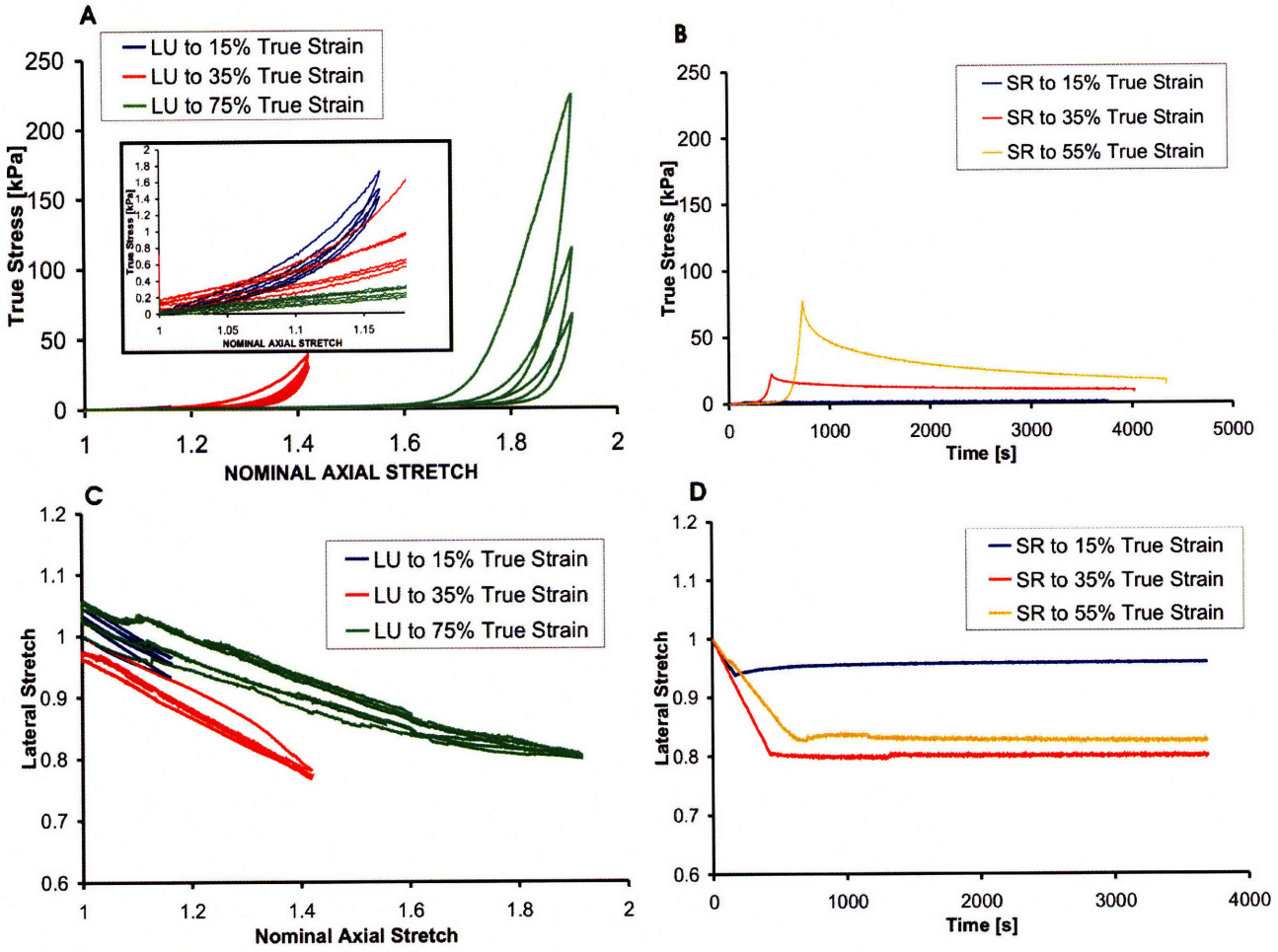

Figure 3-13: The true stress response for a single tension strip from PCS Patient 1. A) True stress response for the load-unload tests. There was an error in data acquisition for the intermediate load-unload test conducted to 55% true strain, therefore these data have been omitted from the graph. Further, the inset of the load-unload graph illustrates the small strain regime response of the pregnant tissue. B) True stress response for the ramp-relaxation tests, The specimen slipped from the grips in the stress-relaxation test conducted to an a true strain of 75%, therefore these data has been omitted from the graph. C) Lateral Stretch response for the load-unload tests. D) Lateral Stretch response for the ramp-relaxation tests

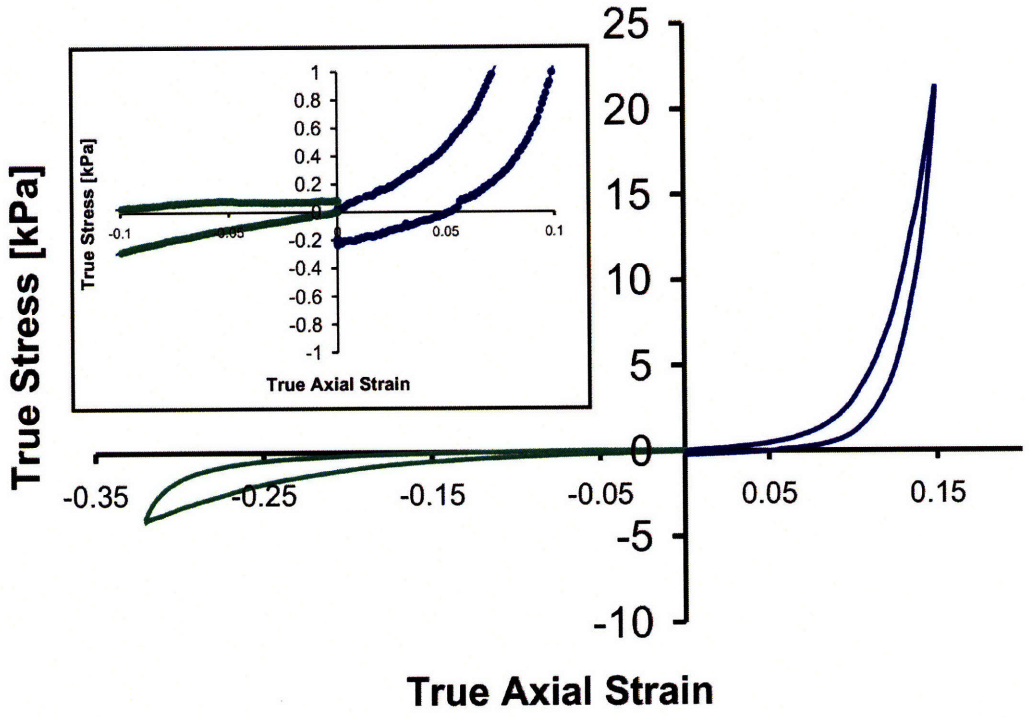

Figure 3-14: Tension and compression data along the circumferential direction for two specimens taken from a single cervical slice from NPND Patient 1. In the large strain regime, the tension-compression stress response is asymmetric. However, in the small strain regime, the uniaxial loading stiffness matches well match well (see inset).

in the circumferential direction was lower than the amplitude of the stress response in the longitudinal direction. The higher stress amplitude in the model fit to the longitudinal test is primarily obtained by decreasing the value of the material parameter η and increasing the value of the material parameter α. The best-fit values of parameters E, S_o, n, and E_{back} were found to be similar when comparing the model fit for two loading directions on the same sample. This trend was found for 6 additional specimens obtained from the non-pregnant patients.

A summary of the compressive material properties for the different obstetric cases is given in Table 3.2 and Figure 3-16, where n_C is the number of cervices tested and n_S is the number of specimens tested for each obstetric case. The values in Table 3.2 were averaged over all testing directions for specimens tested for each obstetric case, and the standard deviation represents the error within each obstetric case. Significant trends were noted for the material parameters α, S_o,η, and E_{back} as a function of obstetric history. On average, the material parameters α, S_o, and E_{back} decreased for pregnant specimens when comparing them to non-pregnant specimens, as well as for NPPD specimens when comparing them to NPND cases. For these material parameters, the difference between pregnant and non-pregnant specimens was statistically significant (Student t-test, $p<0.05$), and the difference between the two classes of non-pregnant cases tended towards statistical significance (Student t-test, $p=0.2$). In addition, there was a statistically significant difference for the material parameter η between pregnant and non-pregnant patients with η being significantly higher for pregnant patients (Student t-test, $p<0.05$). When comparing the non-pregnant cases, η was not significantly higher for the NPPD cases when compared to the NPND cases. With an increase in sample size, the power of the study can be increased and these trends confirmed. There were no significant differences for the best-fit material parameters E and n when comparing different obstetric cases.

A typical best-fit model prediction for a set of uniaxial tension data from NPPD Patient 2 is presented in Fig. 3-17. The 1-D rheological model was able to capture the stress response accurately for the load-unload and ramp-relaxation tests up to 15% true strain for the set of material parameters: [E=3887, Pa, α=35.5, f_v=0.91, S_o=31.2kPa, n=1.9, η=0.00026, E_{back}=56.3kPa]. A summary of tensile material properties for the different obstetric cases are in Table 3.3. The values presented in Table 3.3 and Figure 3-18 are averaged over all specimens for the specific obstetric cases where n_C is the number of cervices tested and n_S is the number of specimens

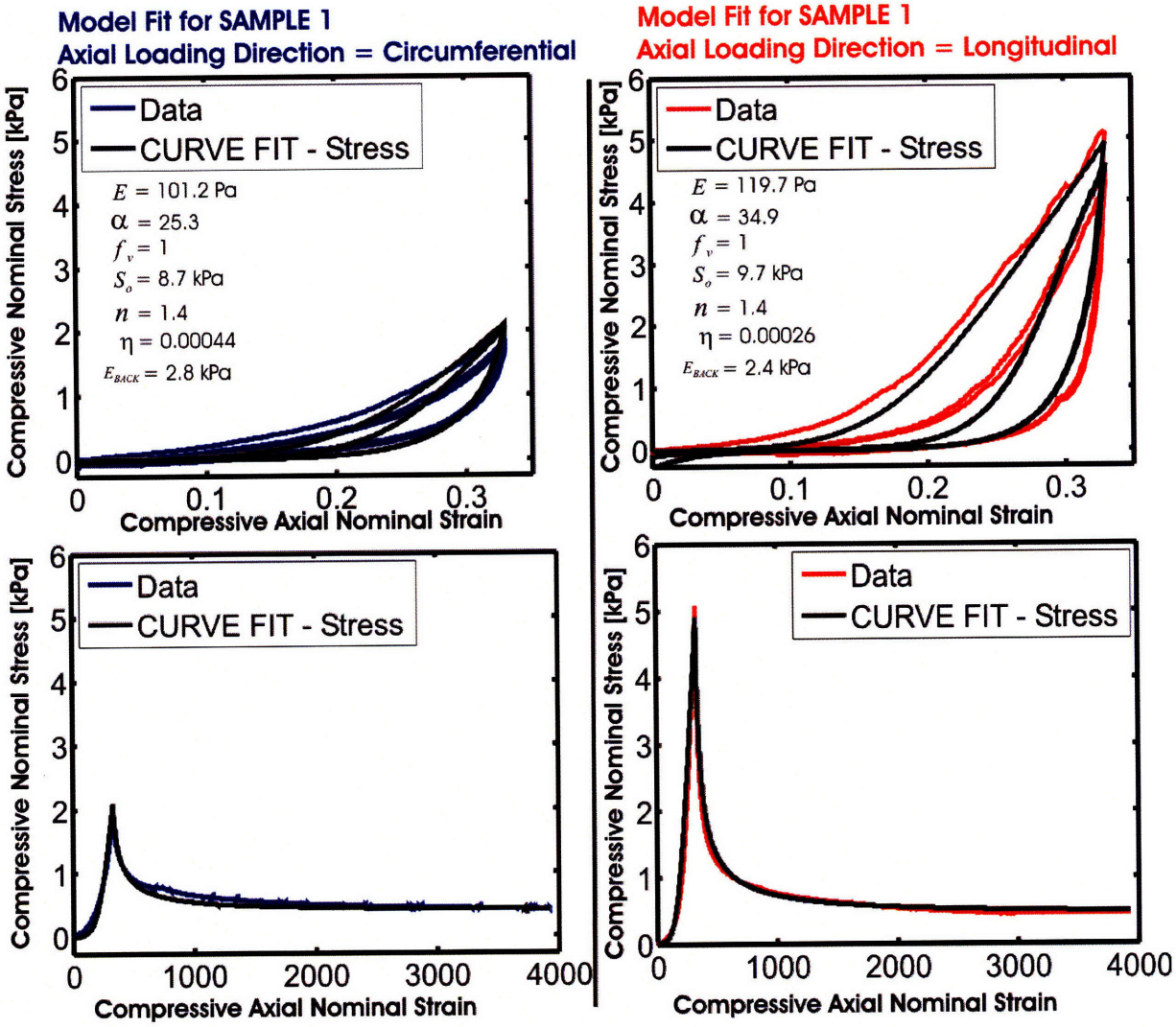

Figure 3-15: Model fit for Sample 1 in Figure 3-7 (NPPD Patient 2). The model captures stress behavior well along both directions of axial loading. One set of best-fit material parameters for each loading direction is able to capture both the load-unload and ramp-relaxation stress behavior. Sample 1 was excised from the middle stroma region and believed to have collagen fibers preferentially aligned in the circumferential direction. Differences between best-fit material parameters indicate that the tissue is anisotropic. The differences in parameters [α and η] are the most critical in modifying model predictions to fit the stress responses along the two loading directions.

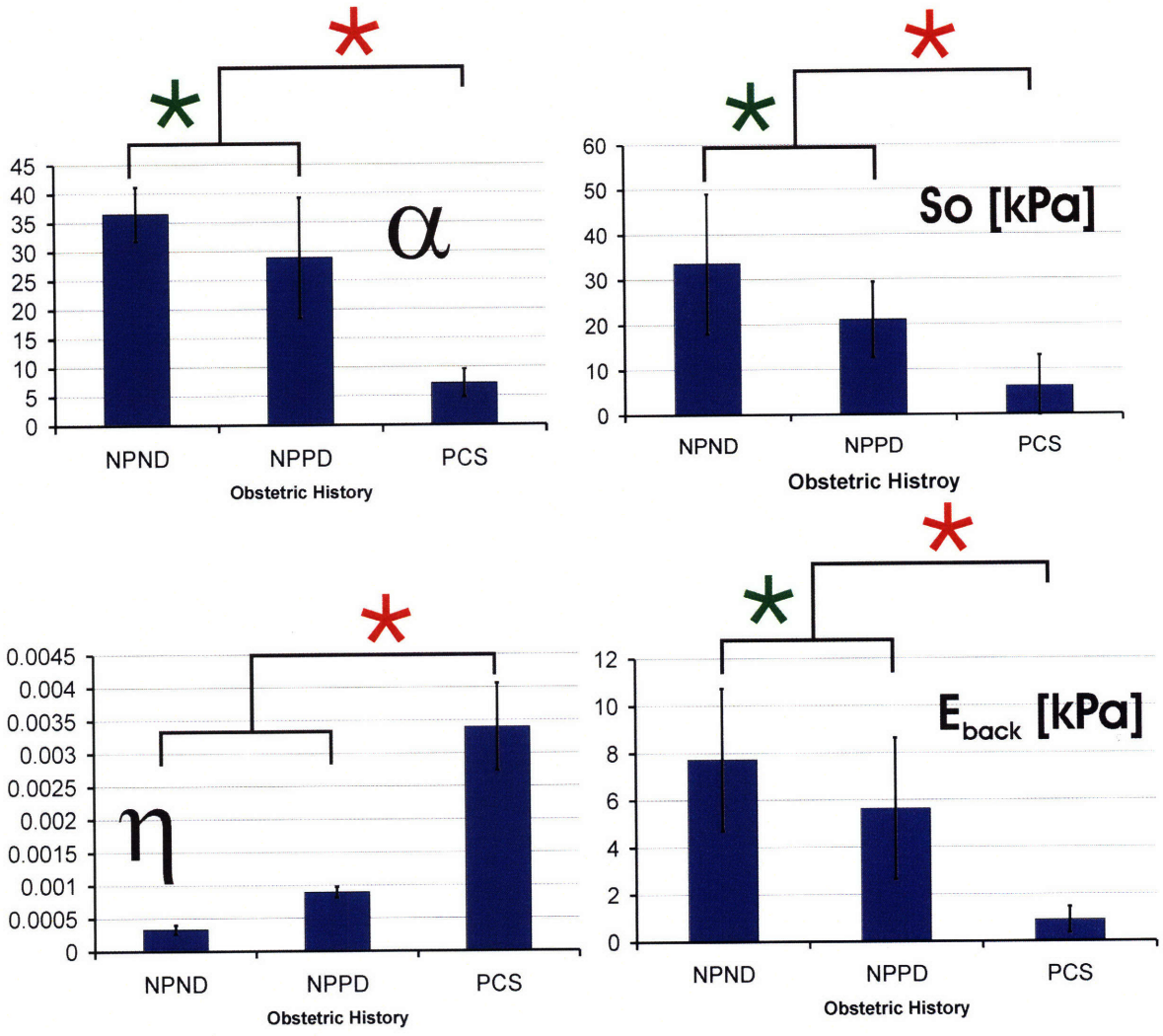

Figure 3-16: In compression, significant trends were noted for the material parameters α, S_o, η and E_{back} as a function of obstetric history. The red star indicates a statistically significant difference with a p<0.05 for a Student's t-test, and a green star indicates a trend towards a statistically significant difference with p=0.2.

Obstetric History	E [Pa]	α	f_v	S_o [kPa]	n	η	E_{back} [kPa]
NPND	207.82	36.52	1	33.53	1.19	0.00033	7.72
n_c=2, n_s=3	min: 33.4	min:31.8		min: 4.2	min: 1	min:0.00001	min: 5.0
	max:478.6	max: 43.7		max: 45.9	max:1.3	max:0.0006	max: 11.7
NPPD	213.61	28.92	1	21.06	1.23	0.000896	5.64
n_c=3, n_s=11	min:44.0	min: 6.8		min:2.5	min: 1	min:0.00002	min: 0.9
	max:941.0	max: 42.1		max:120.2	max:1.7	max: 0.01	max: 9.1
PCS	421.51	7.23	1	6.23	1.70	0.00340	0.90
n_c=2, n_s=4	min: 317.8	min:4.7		min:0.03	min:1.2	min:0.00007	min:0.05
	max:510.5	max:9.0		max: 16.1	max:2.0	max: 0.007	max: 1.4

Table 3.2: Average best-fit material parameters for different obstetric cases in compression

Obstetric History	E [Pa]	α	f_v	S_o [kPa]	n	η	E_{back} [kPa]
NPND	2.11	47.63	0.9	68.3	1.44	0.000066	85.32
n_c=2, n_s=2	min:1.9	min:45.6	min:0.88	min:12.2	min:1.2	min:0.00002	min:22.1
	max:2.4	max:49.6	max:0.93	max:124.4	max:1.7	max:0.0001	max:148.5
NPPD	5.53	33.65	0.96	57.68	2.13	0.000080	434.48
n_c=3, n_s=4	min:3.9	min:10.1	min:0.94	min:6.0	min:1.9	min:0.00001	min:17.7
	max:7.2	max:46.1	max:1	max:122.6	max:2.4	max:0.00026	max:854.8
PCS	2.65	11.17	1	18.82	1.39	0.000669	16.77
n_c=2, n_s=2	min:1.9	min:3.4		min:14.4	min:1.1	min:0.00001	min:16.5
	max:3.4	max:19.0		max:23.2	max:1.7	max:0.00132	max:17.0

Table 3.3: Average best-fit material parameters for different obstetric cases in tension

tested for each obstetric case. Significant differences were noted for the material parameters α and η, when comparing obstetric cases in tension. Best-fit values for α are significantly lower for the pregnant specimens when compared to the nonpregnant specimens (Student t-test, $p<0.05$), and best-fit values for η tended towards being significantly lower for the pregnant specimens when compared to the non-pregnant specimens (Student t-test, $p=0.08$). There was no statistically significant difference between the two non-pregnant cases.

3.4 Discussion

This study represents a first step towards a complete characterization of the anisotropic nature of the mechanical response of human cervical tissue. Evidence from MRI tensor diffusion measurements and X-ray imaging techniques clearly show a degree of alignment of the collagen

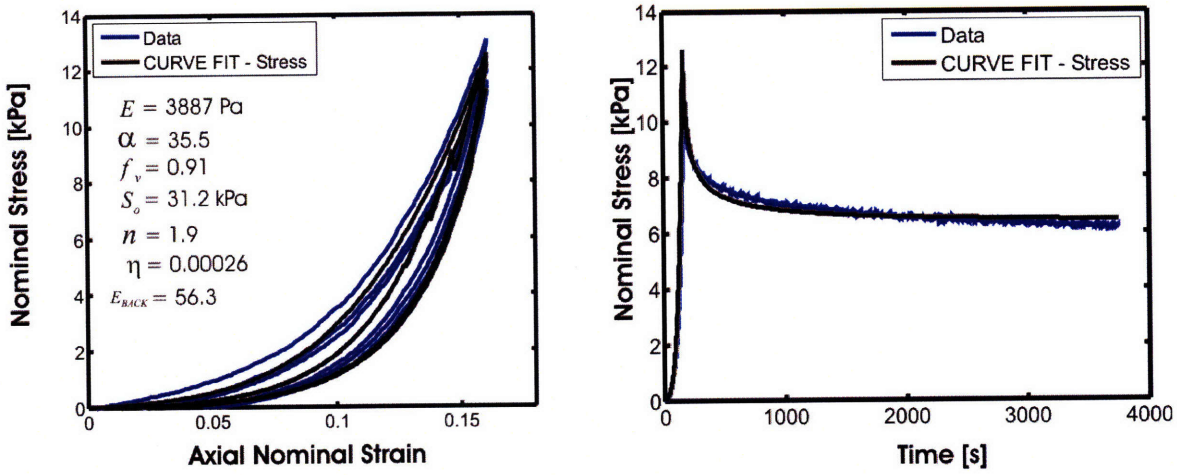

Figure 3-17: Model fit for a non-pregnant tension specimen (NPPD Patient 2). The model captures the stress behavior well in tension. One set of best-fit material parameters is able to capture both the load-unload and ramp-relaxation stress behavior.

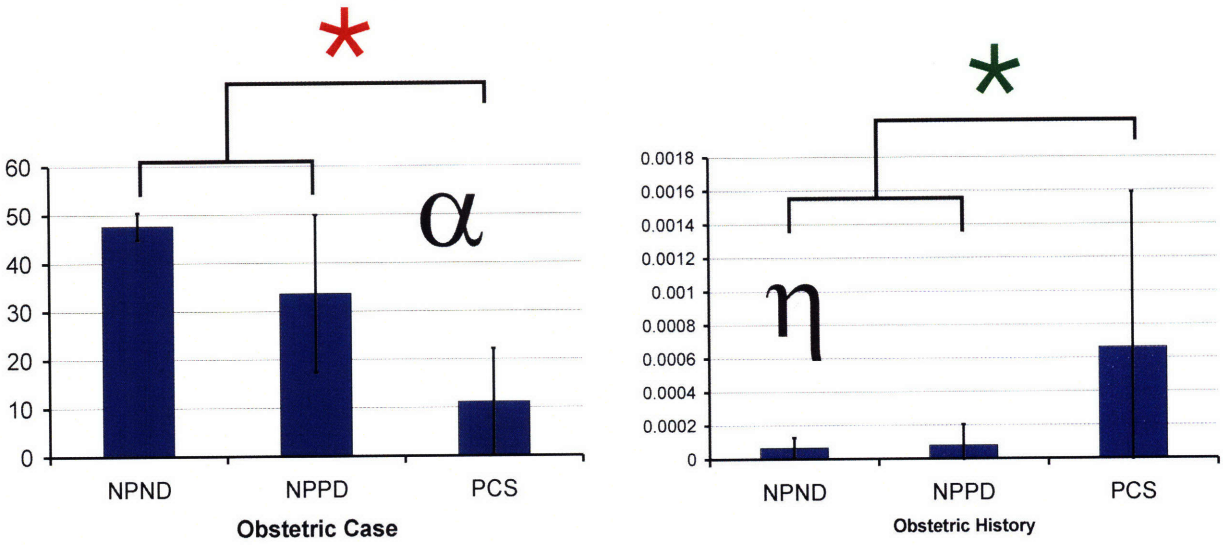

Figure 3-18: In tension, significant trends were noted for the material parameters α and η as a function of obstetric history. The red star indicates a statistically significant difference with a $p<0.05$ for a Student's t-test, and a green star indicates a trend towards a statistically significant difference with $p=0.08$.

network, with collagen fibers oriented preferentially in the circumferential or longitudinal direction depending on radial distance from the cervical canal [116][4]. As noted in other collagenous connective tissues, such as cartilage, the mechanical response of cervical tissue is controlled by a complex interplay between the (network/tensile) response of the collagen and the (volumetric/compressive) response of the hydrated "ground substance". Under uniaxial (unconfined) compression, the axial stress is determined by the balance between the hydrostatic (osmotic) pressure in the ground substance, resisting changes in volume, and the constraint of the collagen network, resisting the lateral stretches needed to minimize volume changes. For axial loading directions orthogonal to the direction of preferential collagen alignment, the effectiveness of the collagen network in constraining lateral stretches results in a stiffer axial stress response. This argument provides an interpretation of the mechanical findings in agreement with the indications of the morphological studies: for samples with collagen fibers aligned preferentially in the longitudinal directions, compression tests along the circumferential direction yield the largest stress amplitudes, and vice versa.

Results of this study are in good agreement with preliminary findings on the dependence of mechanical properties on obstetric history 3-15. However, while in the previous study only qualitative comparisons could be drawn between specimens, in this study we were able to rely on a simple modeling tool to associate a set of model parameters to each time-strain-stress specimen response. The statistical trends in parameter values established by this study can be considered in light of their proposed mechanistic/morphological interpretation. Increased levels of collagen crosslinking in non-pregnant tissue (particularly for NPND tissue) [91] are consistent with the increased values of the collagen locking parameter α and decreased values of the reptation strain parameter η. The pregnant tissue is also associated with significantly lower values for the parameters [E_{back}, S_o] which can be conceptually associated with the strength of the secondary bonds between the collagen network and the hydrated ground substance. It is interesting to note that the non-linear equilibrium contribution of the right branch of the model in Fig. 3-4 was only necessary to fit the data for non-pregnant specimens in tension, where the imposed axial stretch directly constrains the collagen network elongation and cannot be entirely accommodated by collagen realignment.

The one-dimensional rheological model overall does a good job of capturing the time-

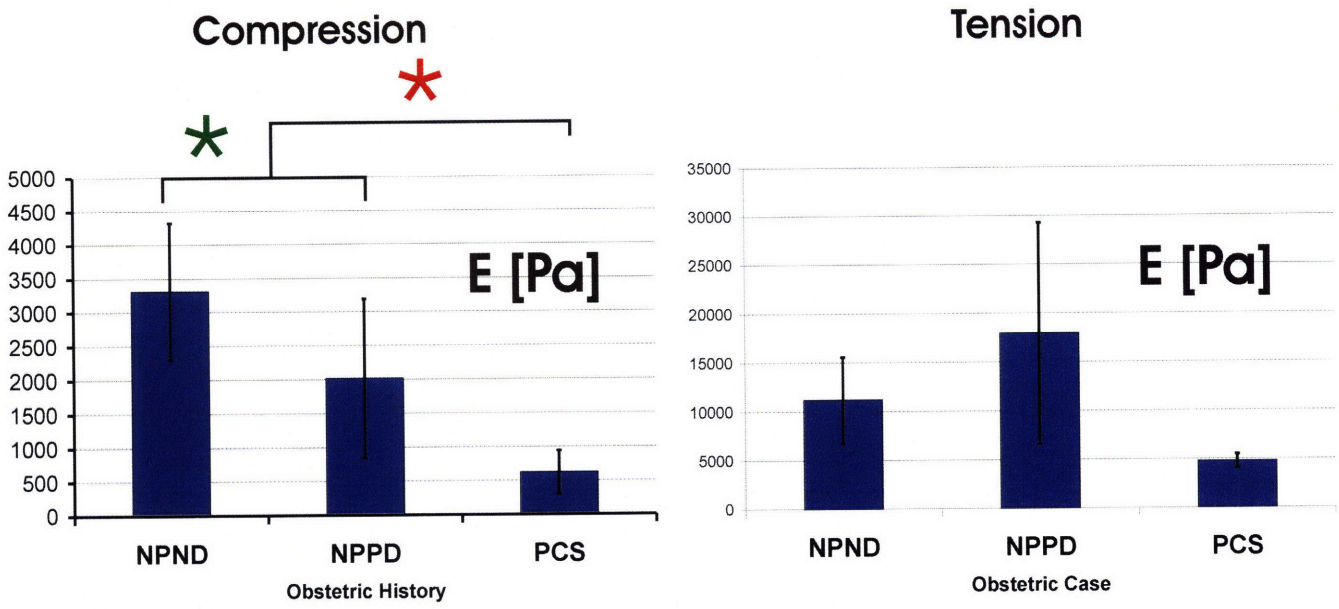

Figure 3-19: The hand-fit measurements of the initial parameter E for the different obstetric cases. The red star indicates a statistically significant difference with a $p<0.05$ for a Student's t-test, and a green star indicates a trend towards a statistically significant difference with $p=0.1$.

dependence of the stress response for the cervical tissue. However, a shortfall of the model is its inability to capture the initial slope of the stress response for both tension and compression. By comparing the model response with the data, the model parameter E underestimates the initial slope of the data. Therefore, hand-fit measurements of the initial slope up to a nominal strain of 5% were taken from the mechanical data. The average hand-fit initial slope for the different obstetric cases in compression and tension are reported in Figure 3-19. For compression, there was a statistically significant difference between the nonpregnant and pregnant tissue (Student's t-test, $p<0.05$) with a lower initial modulus for pregnant tissue. There was a trend towards a statistically significant difference when comparing the two nonpregnant cases (Student's t-test, $p=0.1$) with a lower initial modulus for NPPD tissue. Because of the large error in the tension test, no statistically significant differences were calculated.

As a final note on the statistical interpretation of data in Tables 3.2 and 3.3, we should mention that there is typically a substantial variability in tissue properties between patients (even patients with the same obstetric history) and also some degree of variability between

specimens from the same cervix 3-15. As highlighted by the results of this study, even the same specimens can exhibit different responses when loaded along different anatomical directions. The standard variations in the material properties reported in Tables 3.2 and 3.3 result from the combined effects of variability among patients within the same obstetric group, the differences in samples from different cervical anatomical sites, and the differences in stress responses for different loading directions 3-15. Regardless of the combined effects of these statistical variables, a significant difference in material parameters was established between the different obstetric cases based on the number of cervices tested.

3.5 Conclusion

During gestation, the cervix and the uterus are subjected to time-varying physiological loading and undergo large deformations. Complex three-dimensional stress states develop in the cervical stroma encompassing regions characterized by predominantly tensile stresses and regions in which compressive stresses dominate [57]. It is therefore necessary to characterize cervical tissue properties through comprehensive testing protocols. This study establishes appropriate mechanical testing protocols to investigate the response of human cervical tissue in uniaxial tension and compression along relevant anatomical directions. The tissue behavior exhibits non-linearity and time dependence, with pronounced differences between tensile and compressive responses. The time dependent response of tissue samples in each direction of uniaxial loading was captured with a 1-dimensional rheological model. Model development was guided by the microstructure of the tissue, where biochemical components and corresponding mechanisms of deformation resistance are conceptually associated with model elements. Even in its extreme simplicity, this modeling effort accomplishes two important goals: (1) it provides guidelines to select an appropriate time-dependent rheological framework for more advanced 3-dimensional modeling efforts [94], and (2) it provides sets of best-fit model parameters to quantitatively describe the complex response of each tissue specimen. Using these material parameters, mechanical properties can be compared between samples from patients with different obstetric backgrounds, between samples from different anatomical sites, and between the different loading directions for a single specimen. Trends in best-fit values for each obstetric

history were found to be in good agreement with the proposed mechanistic interpretation of model parameters. The results of this study represent a formidable foundation to identify an appropriate 3-dimensional anisotropic constitutive framework for cervical tissue.

A parallel biochemical, histological and morphological study is presented in Chapter 4 and Chapter 5. The biochemical content of the tissue is compared between the three obstetric cases investigated in the mechanical studies of Chapter 2 and Chapter 3 (refer to Table 2.1 for case definitions).

Chapter 4

Biochemical Analysis and Morphology of the Human Cervix

Human cervical tissue was analyzed for its biochemical content and morphology using standard biochemical assays and microscopy techniques. Small tissue samples (~20mg wet wt.) were pulverized and subjected to biochemical assays, and larger tissue samples (~25mm^3) were sectioned for microscopic analysis. Biochemical assays included measuring hydration, collagen concentration per tissue dry weight, collagen solubility, total sulfated glycosaminoglycan concentration per tissue dry weight, and individual disaccharide concentration per tissue dry weight. The biochemical measurements were compared between the different obstetric cases (refer to Table 2.1), and the results were quantitatively correlated to the mechanical properties measured for the different obstetric cases (refer to Tables 3.2 and 3.3 in Chapter 3). In addition to the biochemical measurements, the ECM architecture was visualized using the following microscopy and staining techniques: polarized light microscopy, Masson's Trichrome stain, and Second Harmonic Generation imaging Previous studies have shown that cervical stroma contains zones of preferentially aligned collagen fibers and that this collagen structure evolves with cervical maturation. Therefore, it is crucial to investigate the histology and morphology of the tissue samples in this study and to conceptually link biochemical content and architecture to the measured trends in the mechanical behavior.

4.1 Methods

4.1.1 Tissue Harvest

Hysterectomy specimens from pre-menopausal women with benign gynecological conditions were obtained from the Tufts - New England Medical Center. The uterus and cervix were excised from the patients and placed on ice. A custom designed stainless steel sectioning tool (Fig. 2-1) was used to obtain from each cervix four 4mm parallel disks perpendicular to the inner canal. Each cervical slice was labeled to distinguish position relative to the internal and external os (Fig. 2-1) and labeled according to obstetric history (Table 2.1). The 4mm slice was thawed for approximately 3 minutes in phosphate buffered saline (PBS) at an ionic concentration of 0.15M to facilitate cutting. For biochemical specimens, approximately 20mg of wet tissue was excised adjacent to the mechanical specimens and stored at -80°C until time of pulverization. For morphology specimens, tissue cubes approximately $25mm^3$ were excised from the stroma region and placed in Optimum Cutting Temperature (OCT) embedding fluid and stored at -80°C.

4.1.2 Homogenization

Cervical tissue was homogenized and pulverized before all biochemical assays. To pulverize the tissue, approximately 20mg of wet tissue was wrapped in aluminum foil and flash frozen in liquid nitrogen. A biopulverizer chamber (Figure 4-1) was also pre-cooled in liquid nitrogen for approximately ten minutes. The frozen tissue was then crushed within the pre-cooled chamber using a hammer. The flattened tissue was then placed into pre-weighed 1.5mL eppendorf centrifuge tubes. The tubes were re-weighed to calculate the tissue wet tissue weight. The samples were stored at -80°C until time of biochemical assay. Care was taken not to let the tissue thaw before assay.

4.1.3 Hydration

The tissue hydration was calculated from the wet and dry weights of the cervical tissue. Sample weights were taken in pre-weighed 1.5mL eppendorf tubes on a micro balance. Wet weight was measured after pulverization, and dry weight was measured after 24 hours of freeze drying.

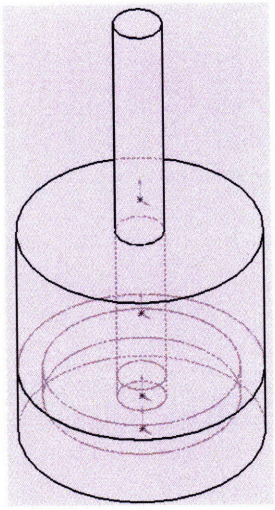

Figure 4-1: The biopulverizer chamber to homogenize cervical tissue

Hydration was calculated using Equation 4.1.

$$hydration = \frac{\text{wet weight - dry weight}}{\text{wet weight}} \tag{4.1}$$

4.1.4 Proteoglycans and Glycosaminoglycans

Sulfated Glycosaminoglycan - Dimethylmethylene Blue (DMB) Assay

Sulfated glycosaminoglycans (GAGs) content was measured using a standard DMB (Dimethylmethylene Blue) assay [39] with chondroitin-6-sulfate (Sigma-Aldrich) as the standard. Approximately 20mg of wet cervical tissue was pulverized and then freeze-dried overnight. The dry tissue was then incubated overnight in 1mL of 0.1mg/ml solution of proteinase K (Roche Applied Science). After incubation, the tissue was assayed for sulfated GAGs using a 1,9-Dimethylmethylene blue dye (Polyscience INC). A spectrophotometer measured the absorbency of the samples at a wavelength of 520nm. A calibration curve was derived from the chondroitin-6 sulfate standards (e.g. Figure 4-2). All calibration curves were a 2nd order polynomial fit to the standard data points. The GAG concentration in terms of the tissue dry weight was calculated by Equation 4.2.

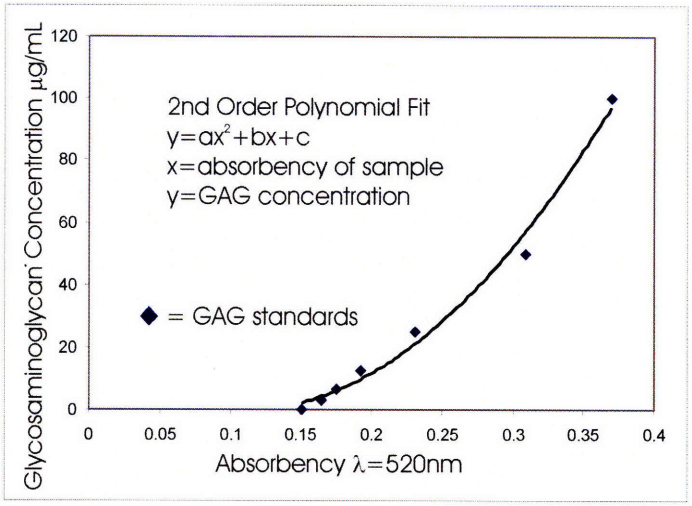

Figure 4-2: A 2nd order polymomial used to fit the standard data points.

$$\text{Gag concentration} = \frac{\text{GAG concentration measured [mg/ml]}}{\text{dry weight concentration loaded into well [mg/ml]}} \tag{4.2}$$

Fluorophore-assisted carbohydrate electrophoresis (FACE)

The individual disaccharides of the glycosaminoglycan chains of the cervical tissue were measured using the (FACE) protocol developed by Calabro, Plaas, and co-workers [23][98]. The protocol was adjusted to accommodate cervical tissue by including a serial enzymatic digestion of the tissue with Chondroitinase ABC and Hyaluronidase (Seikagaku Co.). Tubes of disaccharide standards (Sigma Aldrich) were prepared with 5μg of: chondroitin disaccharide Δdi-0S, chondroitin disaccharide Δdi-2S, chondroitin disaccharide Δdi-4S, chondroitin disaccharide Δdi-6S, and hyaluronic acid disaccharide Δdi-HA. All standards were prepared by reconstituting each salt in double distilled water at a concentration of 1mg/ml, and then 5μl of each standard was aliquot into a single tube and stored at -80°C.

Cervical tissue was pulverized according to the homogenization technique in Section 4.1.2, and then approximately 20mg of wet tissue was freeze dried overnight. The dry tissue was then incubated overnight at 60°C in 1mL of 0.1mg/ml solution of proteinase K (Roche Applied

Science). The digests were boiled for five minutes to inactivate the proteinase K, and then cooled to room temperature. Then the samples were centrifuged to recover the supernatants while the undigested tissue was discarded. The supernatants were then run through a Microcon 3 filter (Millipore) in a centrifuge (45 minutes, 9,500g at room temperature). The GAGs were collected by turning the filters over and spinning them down in a centrifuge (3 minutes, 1000g). 5μg of GAG from each sample was placed in a separate tube and freeze dried overnight. The dried GAGs were then digested overnight at 37°C with Chondroitinase ABC (Seikagaku Co.) in an ammonium acetate buffer at pH 7 (making sure all solids were dissolved in the enzyme solution). After incubation, the samples were cooled and then recovered in ice-cold ethanol for two hours and freeze dried. The dried contents were then digested overnight at 37°C with Hyaluronidase (Seikagaku Co.) in an ammonium acetate buffer at pH 7 (making sure all solids were dissolved in the enzyme solution). After incubation, the samples were cooled and then recovered in ice-cold ethanol for two hours and freeze dried. The freeze dried digests and disaccharide standards were fluorotagged overnight at 37°C by reductive amination with 2-aminoacridone (Sigma Aldrich). The tagged specimens were stored at -80°C for up to 3 months until the day of running the gel. Once the specimens were ready to run, 30μl of 25% glycerol was added to each specimen tube (adding glycerol before the day of test will cause turbidity.) 10μl of each sample was loaded into separate lanes of a pre-made Glyco MONO Face gel (Glyco Inc.), and the samples were run at a constant voltage of 400V for 1 hour and 20 minutes.

After the electrophoresis run, the gel was imaged using an ultraviolet light in a BioRad imaging station (Molecular Imager ChemiDoc XRS). The gel image was saved and analyzed using the BioRad Quantity 1 Software. The intensity of the sample bands were measured and compared to the standard lanes using the volume tool.

4.1.5 Collagen Concentration - Hydroxyproline Assay

Collagen content was measured following a standard hydroxyproline assay referenced in Woessner [64] and Stegemann and Stalder [109]. The hydroxyproline content was obtained using a colorimetric procedure, and was converted into collagen content using a mass ratio of collagen to hydroxyproline of 7.46:1. Collagen content was normalized by tissue dry weight.

This hydroxyproline protocol was a variation of a procedure used for articular cartilage. Cervical tissue samples were pulverized and then freeze dried for 24 hours. Dry samples were transferred to preweighed 11mL Pyrex tubes and weighed for tissue dry weight. After weighing, 1mL of 6M HCl was added to the sample tube and vortexed. The Pyrex test tubes were sealed with rubber Teflon caps and heated at 115°C overnight for hydrolyzation. After hydrolyzation, the samples were titrated to pH 7. Deionized water was used to bring each of the sample tubes to the same volume (11mL). Sample concentration before the assay dilution was calculated by Equation 4.3.

$$\text{sample concentration before dilution} = \frac{\text{dry weight (mg)}}{\text{11mL}} \tag{4.3}$$

Hydroxyproline (Sigma-Aldrich) standards of known concentrations were assayed along with the tissue samples. The samples and standards were mixed with Chloramine T for 20 minutes and p-Dimethylaminobenzaldehyde (pDAB) for 30 minutes at 60°C. After these reactions, the absorbancy of the samples and standards were read with a spectrophotometer microassay at wavelength of 560nm.

A linear regression line for the measured absorbancy versus known hydroxyproline concentration was used as a calibration curve for the samples. Figure 4-3 plots a typical calibration curve. The collagen concentration per dry weight of tissue was calculated by dividing the measured collagen concentration by the sample concentration loaded into the well. Equation 4.4 calculates the collagen concentration per dry weight of cervical tissue.

$$\frac{\text{collagen concentration}}{\text{dry weight of cervical tissue}} = \frac{\text{collagen concentration measured in microwell } (\frac{mg}{mL})}{0.1 \cdot \frac{\text{dry weight } (mg)}{11(mL)}} \tag{4.4}$$

4.1.6 Collagen Extractability (Solubility)

Collagen solubility was measured by extracting approximately 20mg of wet pulverized tissue in 0.5M acetic acid containing 1mg/mL of pepsin (150μL/mg wet tissue) for 3 days at 4°C. The sample was centrifuged at 15,000g for 1 hour and the supernatant and tissue pellet were stored at -80°C. The hydroxyproline content was measured in the tissue pellet and the supernatant. The extractability is defined as the fraction of hydroxyproline in the supernatant compared to

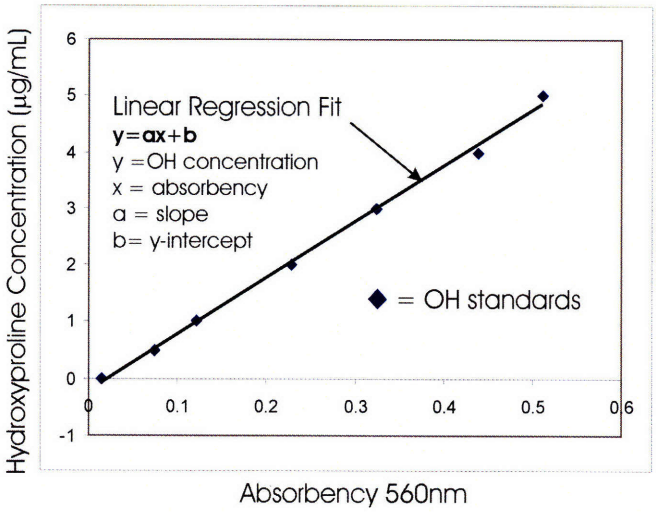

Figure 4-3: The calibration curve for the known hydroxyproline (OH) standards is a linear regression fit of the standard's data points. The above graph is an example of data points collected from the standard concentrations.

the total amount of hydroxyproline.

4.1.7 Morphology - Collagen Architecture

Masson's Trichrome Stain and Light Microscopy

Tissue stroma sections were taken from patients with different obstetric backgrounds and categorized according to Table 2.1. Tissue blocks were cut from partially frozen cervical slices and placed in Optimum Cutting Temperature (OCT) embedding liquid. Tissue blocks were stored at -80°C until time of cryosectioning Tissue blocks were sectioned into 10μm thick slices onto microscope slides using a freezing microtome, and then stored at -80°C until time of fixation. Tissue slides were fixed, stained and imaged at the Women and Infants Hospital of Rhode Island and Tufts New England Medical Center pathology labs. For a complete staining protocol refer to the text by Conn [28].

Sirius Red Stain and Polarized Light Microscopy

Tissue stroma sections were taken from patients with different obstetric backgrounds and categorized according to Table 2.1. Tissue blocks were cut from partially frozen cervical slices and

placed in OCT embedding liquid. Tissue blocks were stored at -80°C until time of cryosectioning Tissue blocks were sectioned into 8μm thick slices onto microscope slides. (For this study, the anatomical direction was not marked).

The microscope slides were stained with 0.1% Sirius Red F3BA in saturated picric acid, as described in Clark et al. [27]. Digital images were captured with a camera connected to a microscope at X200 magnification (Olympus MagnaFirge: Optronics Goleta, CA). Multiple random images were taken of each specimen at the same camera settings. The area of the field above a fixed, common background grey threshold value was calculated for each image and then divided by the total area. The percentage of the field above the background threshold is the measured amount of organized collagen in the tissue, or the birefringence of the tissue. The measurements were compared between the different obstetric cases and reported below in Section 4.2.

Second Harmonic Generation

Tissue stroma sections were taken from patients with different obstetric backgrounds and categorized according to Table 2.1. Tissue blocks were cut from partially frozen cervical slices and placed in OCT embedding liquid. Tissue blocks were stored at -80°C until time of cryosectioning (Note: If the tissue block was mechanically tested, the tissue specimen was equilibrated overnight in PBS and subjected to the appropriate mechanical testing protocol before placing specimen in OCT.) Tissue blocks were cryosectioned into 50μm and 30μm thick slices onto microscope slides. The tissue slides were then stored at -80°C until time of imaging. Care was taken to mark the anatomical direction and location of each specimen. No staining or fixation was used before imaging the specimens.

Tissue slides were processed by a fellow graduate student Dimitrios Tzeranis from Professor Peter So's lab at MIT. The reader is referred to a paper by Buehler et al. [20] for the optical microscopy set-up in the So lab.

Obstetric History	n_c	n_s	Hydration
NPND	6	46	74.9±7%
NPPD	11	106	75.9±8%
PCS	4	18	81.0±5%

Table 4.1: Hydration measured in human cervical tissue for the different obstetric cases.

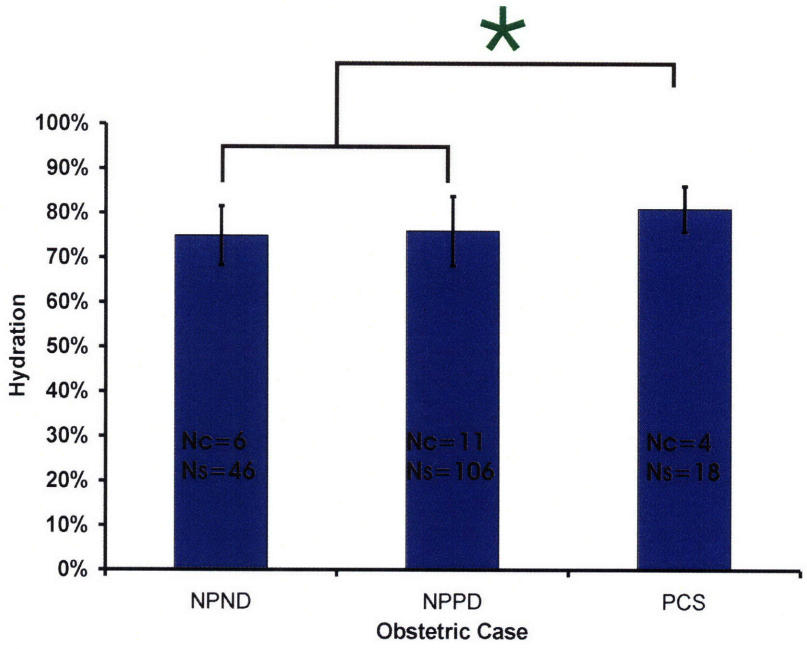

Figure 4-4: Hydration measured in human cervical tissue for the different obstetric cases. There is a trend towards a statistically significant difference between pregnant and nonpregnant tissue, Student's t-test p=0.09. (Nc = number of cervices tested and Ns = number of samples tested).

4.2 Results

4.2.1 Hydration

Figure 4-4 and Table 4.1 report the hydration levels for human cervical tissue for the different obstetric cases. There was a trend towards a significant difference between the nonpregnant and pregnant cases (Student's t-test, p=0.09). There was no difference in hydration level when comparing the two non-pregnant cases. These results match well with previously reported levels of hydration [33][108][101] where increased hydration is reported for pregnant tissue.

Obstetric History	n_c	n_s	Sulfated GAG Content [mg/mg dry wt.]
NPND	5	23	1.62±0.56%
NPPD	9	29	1.52±0.98%
PCS	3	6	2.55±0.85%

Table 4.2: Total Sulfated GAG measured in human cervical tissue for the different obstetric cases.

4.2.2 Proteoglycans and Glycosaminoglycans (GAGs)

Total Sulfated GAGs

Figure 4-5 and Table 4.2 report the total glycosaminoglycan content for human cervical tissue measured for the different obstetric cases. There is a statistically significant difference between the nonpregnant and pregnant tissue with an increase in the total glycosaminoglycan levels for the pregnant tissue (Student's t-test, $p<0.05$). There is no significant difference when comparing the two non-pregnant cases.

These results match well with previous reports in the literature for overall GAG content. Danforth [33] measured an increase in the GAG for postpartum tissue when comparing to nonpregnant tissue. Further, Rath et al. [99] and Shimuzu et al. [108] measured an overall increase in the sulfated GAG content for postpartum tissue when compared to non-pregnant tissue. However, both research groups found a decrease in the dermatan sulfate content for postpartum tissue.

Disaccharides

Figure 4-6 is a typical FACE result for pregnant and nonpregnant human cervical tissue. The two end lanes of the gel represent the disaccharide standards, and the middle lanes are the experimental samples. The following disaccharides were detected in human cervical tissue: chondroitin disaccharide Δdi-0S, chondroitin disaccharide Δdi-4S, chondroitin disaccharide Δdi-6S, and hyaluronic acid disaccharide Δdi-HA. Figure 4-7 and Table 4.4 report the measured amount of the different disaccharides detected in human cervical tissue for the different obstetric cases, and Table 4.3 indicates the number of samples and the number of different cervices tested. There was no significant difference in the amount of the different disaccharides when comparing

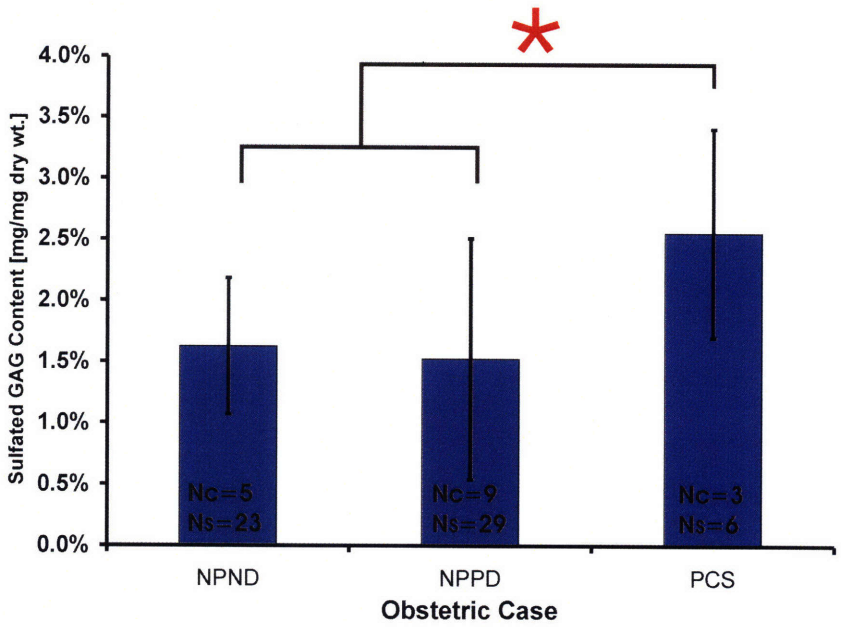

Figure 4-5: Total Sulfated GAG measured in human cervical tissue for the different obstetric cases. There is a statistically significant difference between pregnant and nonpregnant tissue, Student's t-test, $p<0.05$. (Nc = number of cervices tested and Ns = number of samples tested).

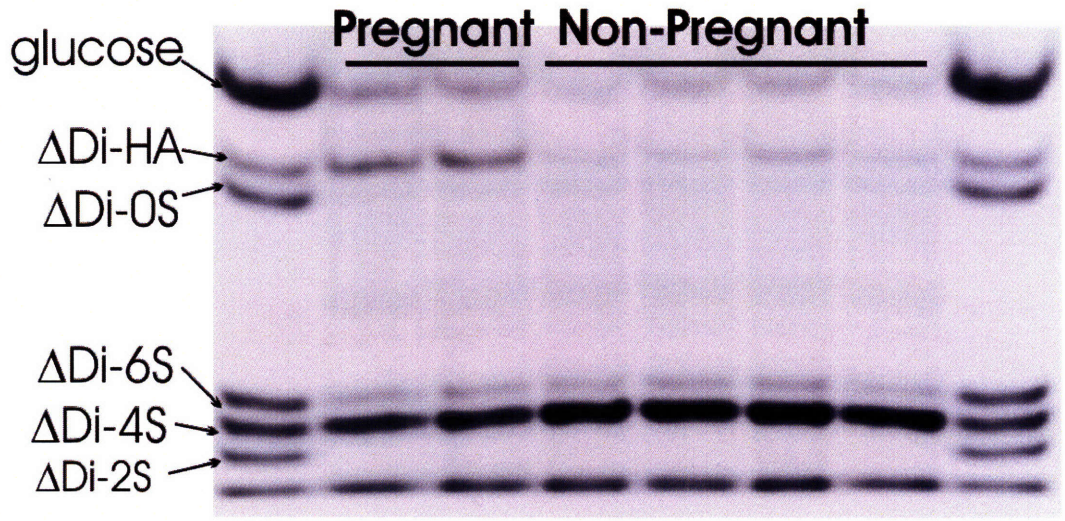

Figure 4-6: A typical FACE result for pregnant and nonpregnant human cervical tissue. The first and last lanes are the disaccharide standards.

Obstetric History	n_c	n_s
NPND	2	4
NPPD	3	9
PCS	3	11

Table 4.3: The number of FACE samples. Nc = number of cervices and Ns = number of samples

the two nonpregnant cases. There was a statistically significant difference for the Δdi-6S and the Δdi-HA disaccharides when comparing pregnant and nonpregnant tissue. There was a significant increase in the measured amounts of Δdi-6S and Δdi-HA for pregnant tissue (Student's t-test, $p<0.05$). It should be noted that, on average, there was a decrease in the amount of Δdi-4S for the pregnant tissue when compared to the nonpregnant tissue.

The amount of the different disaccharides are comparable to values measured for pregnant and nonpregnant rat. The measured disaccharide content in rat tissue is listed in Table 4.5. This unpublished data was compiled by my collaborator Dr. Huiling Ji from Brown Women and Infants Hospital.

Obstetric History	Δdi-0S [mg/mg GAG]	Δdi-4S [mg/mg GAG]	Δdi-6S [mg/mg GAG]	Δdi-HA [mg/mg GAG]
NPND	0.033±0.006	0.187±0.039	0.042±0.009	0.032±0.006
NPPD	0.039±0.005	0.216±0.021	0.056±0.008	0.050±0.019
PCS	0.037±0.004	0.168±0.044	0.065±0.009	0.096±0.020

Table 4.4: The disaccharide content in human cervical tissue.

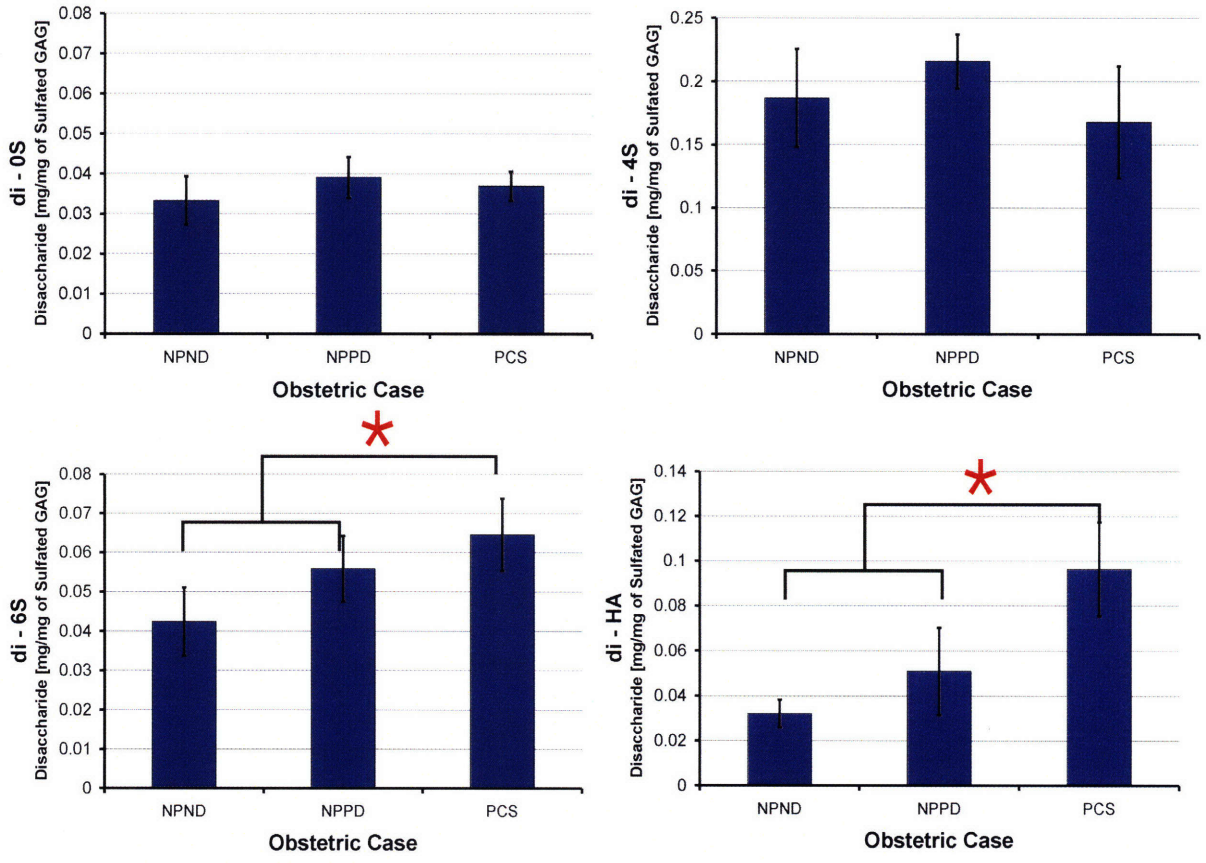

Figure 4-7: Disaccharide content in human cervical tissue. There is a statistically significant increase for the di-6S and di-HA disaccharides in the pregnant tissue when compared to nonpregnant tissue (Student's t-test, $p<0.05$).

	Δdi-0S [mg/mg GAG]	Δdi-4S [mg/mg GAG]	Δdi-6S [mg/mg GAG]	Δdi-HA [mg/mg GAG]	chain length [# of disaccharides]
Nonpregnant	0.028	0.245	0.041	0.025	21.5
Pregnant Day 20	0.034	0.192	0.044	0.050	11.5

Table 4.5: The disaccharide content for pregnant and nonpregnant rat tissue. Data collected by Dr. Huiling Ji from Brown University Women and Infants Hospital of Rhode Island.

Obstetric History	n_c	n_s	**Collagen Content [mg/mg dry wt.]**
NPND	4	28	70.8±8.5%
NPPD	8	22	77.3±9.1%
PCS	2	8	77.6±9.8%

Table 4.6: Collagen content measured in human cervical tissue for the different obstetric cases.

4.2.3 Collagen

Figure 4-8 and Table 4.6 report the collagen concentration (measured per dry weight of tissue) for human cervical tissue measured for the different obstetric cases. There is no statistically significant difference between the obstetric cases. This trend is consistent with reports from Leppert et al. [77] and Malliot et al. [82] stating that the collagen content does not change with cervical maturation (refer to the collagen content discussion in Section 1.3.3)

4.2.4 Collagen Extractability

Figure 4-9 and Table 4.7 report the collagen solubility (extractability) for human cervical tissue measured for the different obstetric cases. There is a statistically significant difference between nonpregnant and pregnant tissue (Student's t-test, $p<0.05$) with the pregnant tissue having a significantly higher solubility when compared to the average of the nonpregnant cases. Further, there is a trend towards a statistically significant difference when comparing the two nonpregnant cases (Student's t-test, $p=0.13$) with the NPPD tissue having a higher solubility when compared to the NPND tissue.

These trends agree with previous reports in the literature of the collagen solubility of human cervical tissue. See discussion in Section 1.3.3.

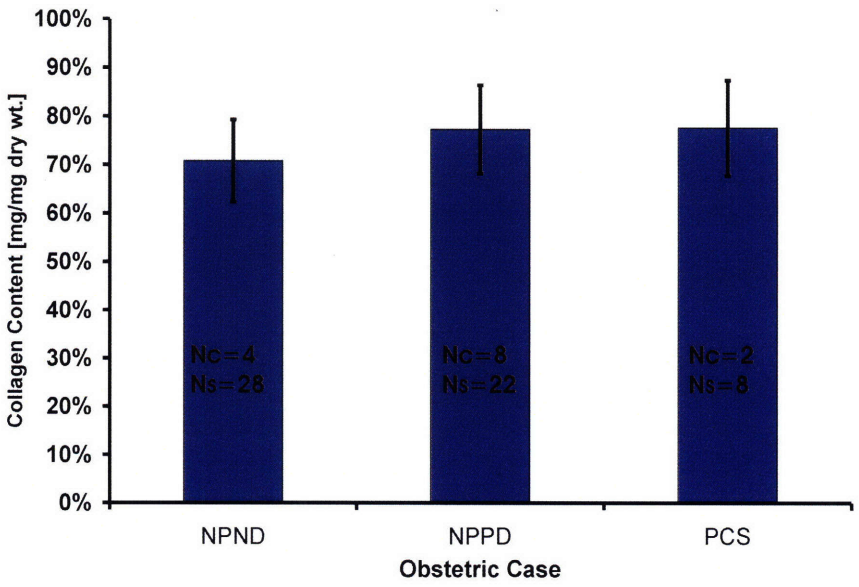

Figure 4-8: Collagen content measured in human cervical tissue for the different obstetric cases. There is no statistical difference between the obstetric cases. (Nc = number of cervices tested and Ns = number of samples tested).

Obstetric History	n_c	n_s	**Soluble Collagen [mg soluble OH/mg total OH]**
NPND	3	9	31.8±7.0%
NPPD	7	18	40.5±11.1%
PCS	3	8	80.7±10.5%

Table 4.7: Collagen solubility measured in human cervical tissue for the different obstetric cases.

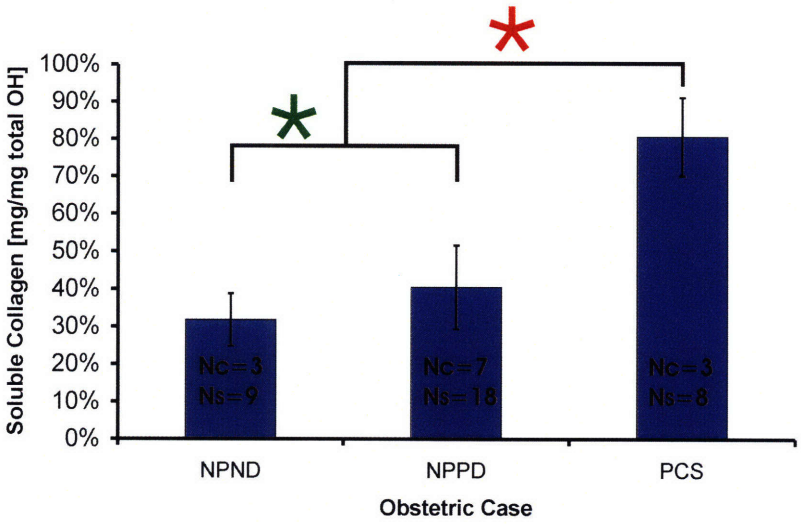

Figure 4-9: Collagen solubility measured in human cervical tissue for the different obstetric cases. There is a statistical significant difference between pregnant and nonpregnant tissue (Student's t-test, $p<0.05$), and there is a trend towards a statistically significant difference when comparing the two nonpregnant cases (Student's t-test, $p=0.13$). (Nc = number of cervices tested and Ns = number of samples tested).

4.2.5 Morphology - Collagen Architecture

Cervical tissue sections were stained and imaged using different histology techniques to discern the extracellular matrix architecture for the different obstetric cases. By investigating the results from the different techniques, the biochemical components of the tissue were visualized and measured. The results of this study match well with previous findings that the collagen-rich stroma region dominates the middle layer of the cervix, and the mainly cellular mucosa and fascia occupy the outer and inner perimeters of the organ. Newer techniques used in this study, mainly Second Harmonic Generation Imaging, reveal for the first time the molecular details of the collagen network of the nonpregnant and pregnant tissue. By comparing SHG images with traditional images, it can be seen that the muscle cells are dispersed throughout the stroma with collagen fibers roping around them in a preferential direction. Further, these collagen fibers are noticed to go through qualitative change during pregnancy with fibers appearing diffuse and more randomly aligned in the pregnant tissue. The following sections present the results of the currently histology study of human cervical tissue.

Hematoxylin and Eosin Stain

Figure 4-10 is an Hematoxylin and Eosin stain of a nonpregnant cervical tissue sample. This sample was processed at the New England Medical Center Pathology lab. This stain clearly visualizes the cervical fibroblasts that are interspersed in the cervical stroma. The cells appear as block dots and are on the order of 10μm. They are evenly distributed throughout the collage-rich stroma region, with the collagen stained in pink in the image.

Masson's Trichrome Stain

Figures 4-11 and 4-12 are a series of trichrome stained images of nonpregnant human cervical tissue at different magnifications. The Masson's trichrome protocol stained the collagen fibers intense blue, mucus was stained blue, intercellular fibers were stained vermilion red, cytoplasm was stained vermilion red, and nuclei were stained black [28]. Figure 4-11 contains images from the smallest magnification, and Figure 4-12 contains images from the largest magnification. These samples were processed at the New England Medical Center Pathology lab. The samples were taken from a nonpregnant patient, and the tissue was sectioned directly after excision from

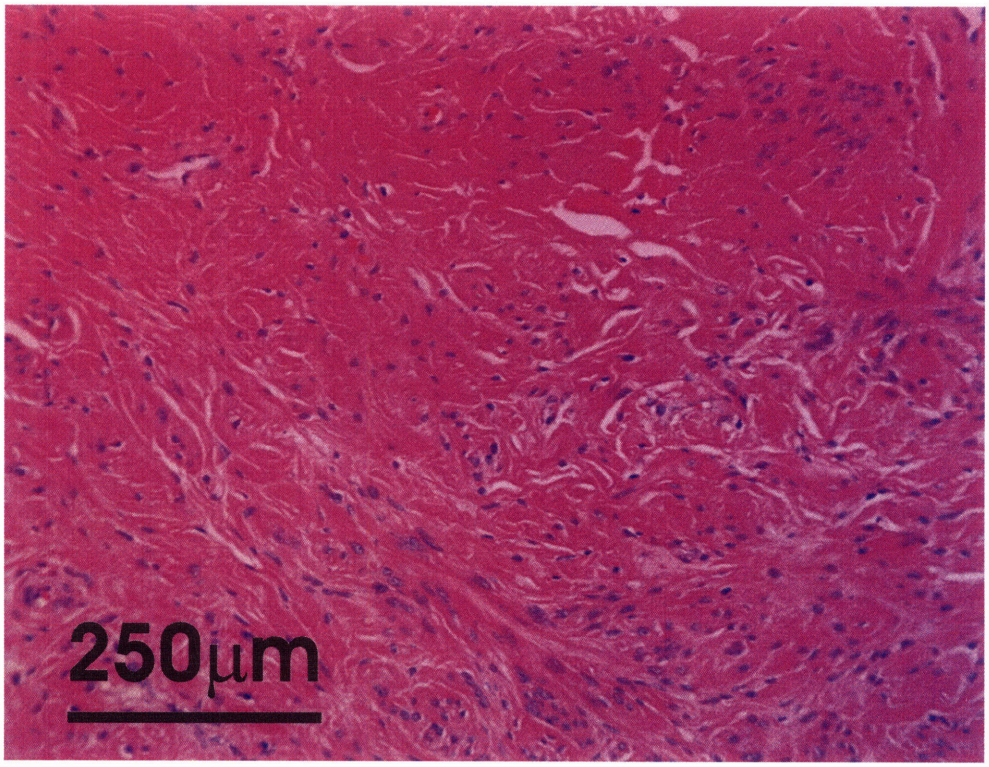

Figure 4-10: A hematoxylin and eosin stain of nonpregnant human cervical tissue.

the organ. Therefore, no swelling artifacts from mechanical testing are present in the images below.

Figure 4-11A is a low magnification image that captures both the stroma and the mucosa. The mucosa region is located on the edge of the sample with cervical (mucus) glands branching into the tissue (refer to arrows in Figure 4-11A). The stroma region is the inner region of intense blue stained collagen. This region contains the highly cross-linked collagen network which is responsible for the mechanical integrity of the cervix. Figure 4-11B is a magnification of A, and offers a closer inspection of the collagen dense stroma region. At this magnification, the smooth muscle cells, stained in red, and the collagen fibers traversing around them are visible.

Figure 4-12 reveals magnified views of the smooth muscle cells and the collagen fibers of the stroma region. From these images, the smooth muscle cells are measured to be on the order of 100μm which is consistent with the literature. The muscle cells are nested within the collagen network, and at the higher magnifications the collagen fibers can be seen to follow the perimeter of the cells. The boundary between cells and collagen fibers are unclear from these trichrome stains because in this histology protocol the blue stain did not specifically stain only the collagen. Therefore, it is difficult to distinguish the preferential alignment of the collage fibers. Additional histology techniques specific to collagen will be needed to discern the collagen network orientation.

Figure 4-13 contains trichrome images from a section of tissue containing a cluster of blood vessels. The inset magnification indicates a region of blood vessels that are bundled together. By comparing the images, it can be seen that the blood vessels typically cluster together in specific regions of the stroma. The vessels range in size from 100μm to 500μm, which tend to be bigger than the smooth muscle cells. These vessel clusters cause inhomogeneities in the cervical stroma. The implication of these disruptions in the collagen network on the mechanical response of the tissue is dicussed in Section 5.1.1 *3-Dimensional Material Model Development.*

Polarized Light Studies

Three human cervical tissue samples stained with Sirius red were imaged under a polarized light, and the tissue slides were measured for birefringence (organized collagen content). Figure 4-14 is a representative image taken from a NPND patient with no previous pregnancies (NPND

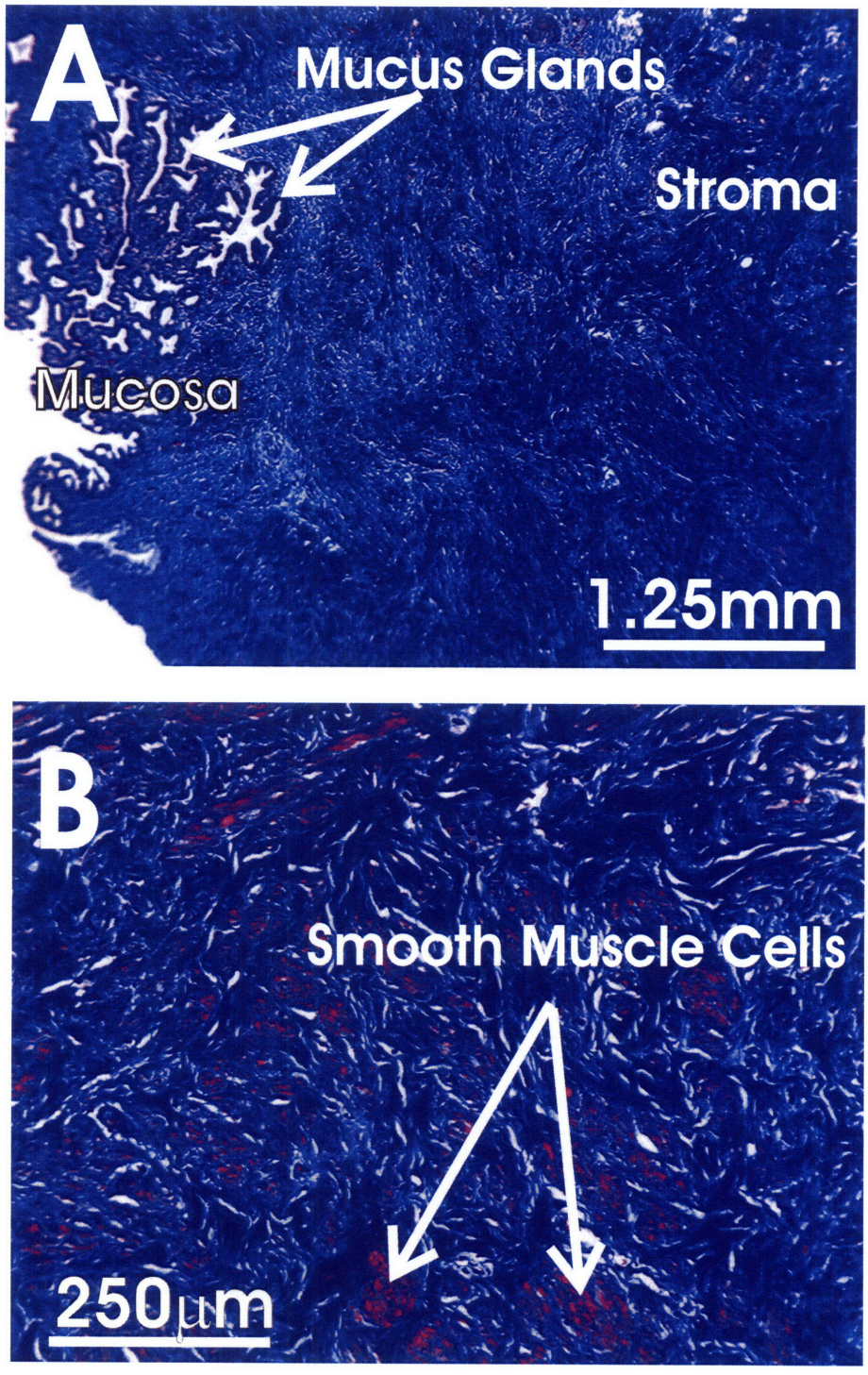

Figure 4-11: Trichrome images of nonpregnant human cervical tissue. A) A low magnification of the mucosa and stroma regions. B) A higher magnification image detailing the collagen-rich stroma region. Smooth muscle cells are represented in red, and are evely distributed throughout the stroma.

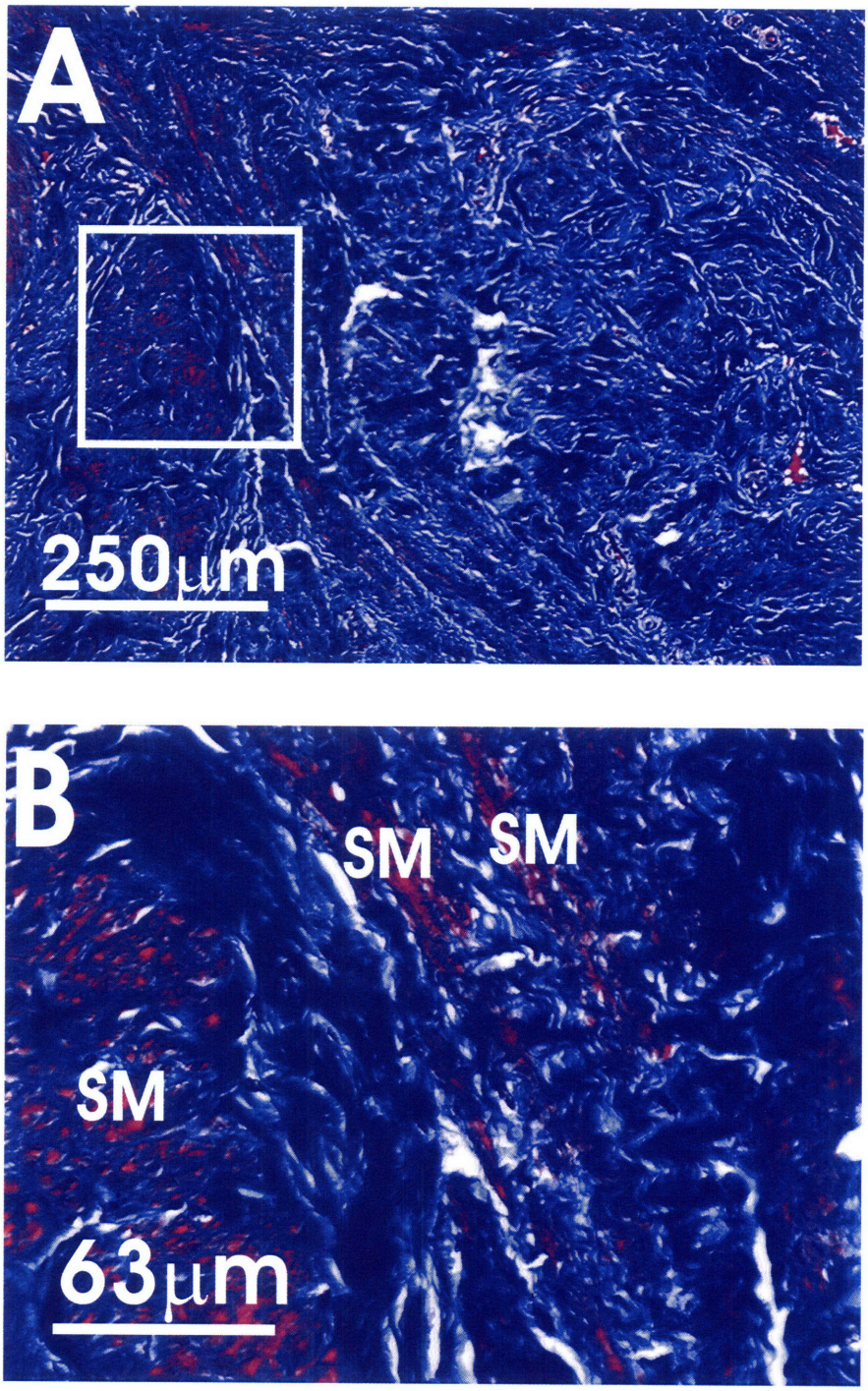

Figure 4-12: Trichrome images of nonpregnant human cervical tissue. A) Detail of the stroma region. B) A higher magnification view (an inset of A) detailing the smooth muscle cells in the stoma. SM = smooth muscle cell

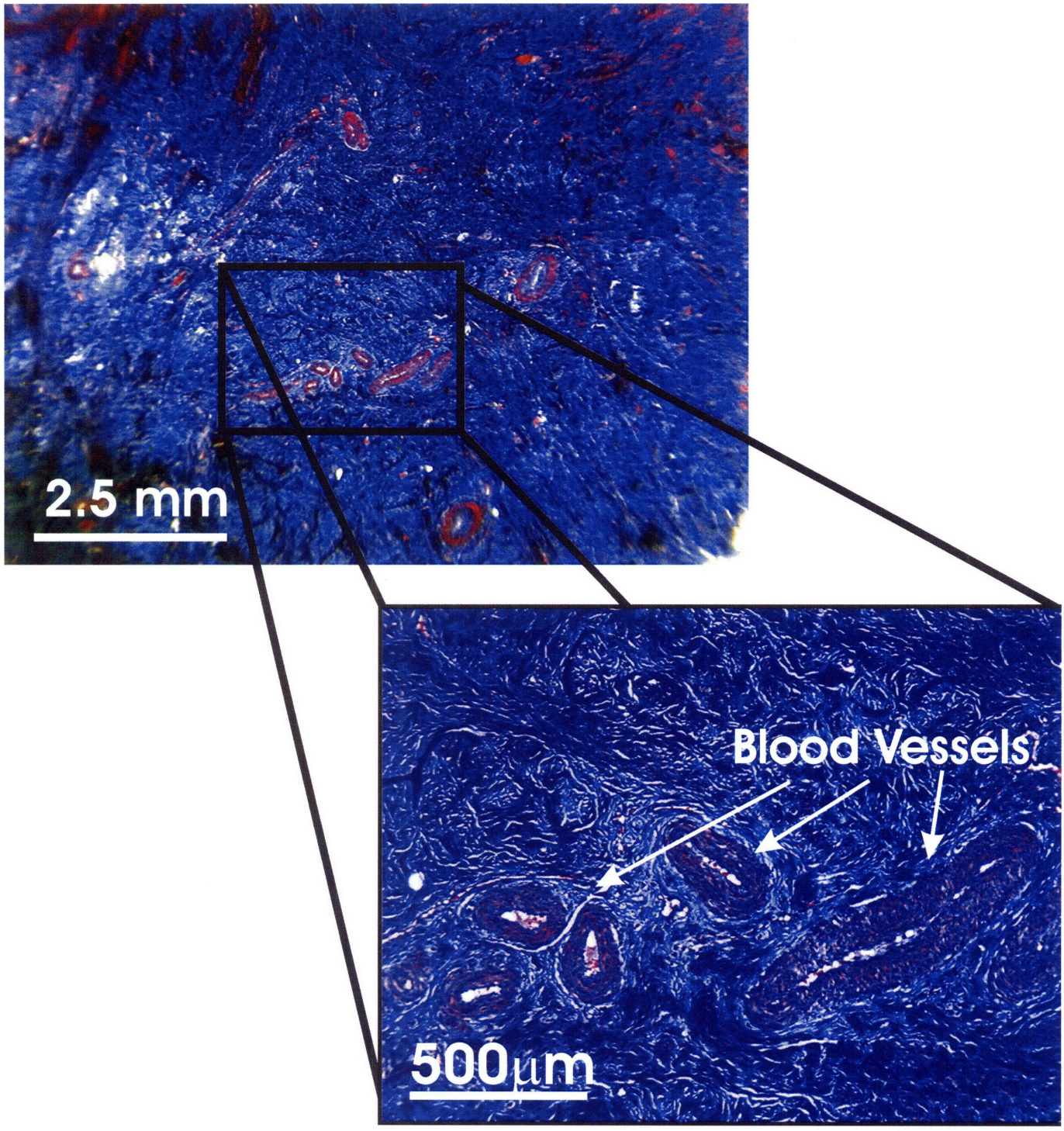

Figure 4-13: Trichrome images of nonpregnant human cervical tissue. Blood vessels cluster together throughout the stroma.

Specimen	Percentage of Measured Organized Collagen
NPND - Figure 4-14	56.7±7%
NPND - Figure 4-15	67.8±7%
PCS - Figure 4-16	32.6±4%

Table 4.8: Amount of organized collagen in three different cervical samples

Patient 4 from Table 2.2). Figure 4-15 is an image taken from a NPND patient with 3 previous cesarean sections (NPND Patient 3 from Table 2.2). Figure 4-16 is an image taken from a PCS patient with 5 previous cesarean sections (PCS Patient 2 from Table 2.2). These tissue samples were sectioned directly after thawing from storage. Therefore, there are no swelling or mechanical testing artifacts in the images.

Each tissue sample was imaged at x200 in 8 random locations, and for each location the percentage of the area occupied by organized collagen was recorded. The average of the 8 measurements for a single sample was calculated and are listed in Table 4.8 for the three different specimens. The error tolerance represents the variability of the birefringence measurement within a single tissue sample.

Qualitatively, the two nonpregnant specimens have comparable polarized light images with the collagen bundles clearly dominant in the bright field. This collagen is highly organized and oriented in bundled ropes. When comparing the pregnant image with the nonpregnant images, the collagen becomes more diffuse and sparse with an increased interfiber distance. The bright field in the pregnant image is reduced indicating that the collagen fibers have lost their organized structure and directionality. Quantitatively, the results in Table 4.8 report the measured amount of organized collagen for the different obstetric cases. These results indicate that nonpregnant tissue has a higher birefringence when compared to pregnant tissue. These results confirm trends in the literature that the organized collagen network breaks-up during cervical maturation.

Second Harmonic Generation

Second Harmonic Generation images were taken of nonpregnant and pregnant tissue specimens. Each specimen was marked for anatomical direction and location. Specimens were imaged on

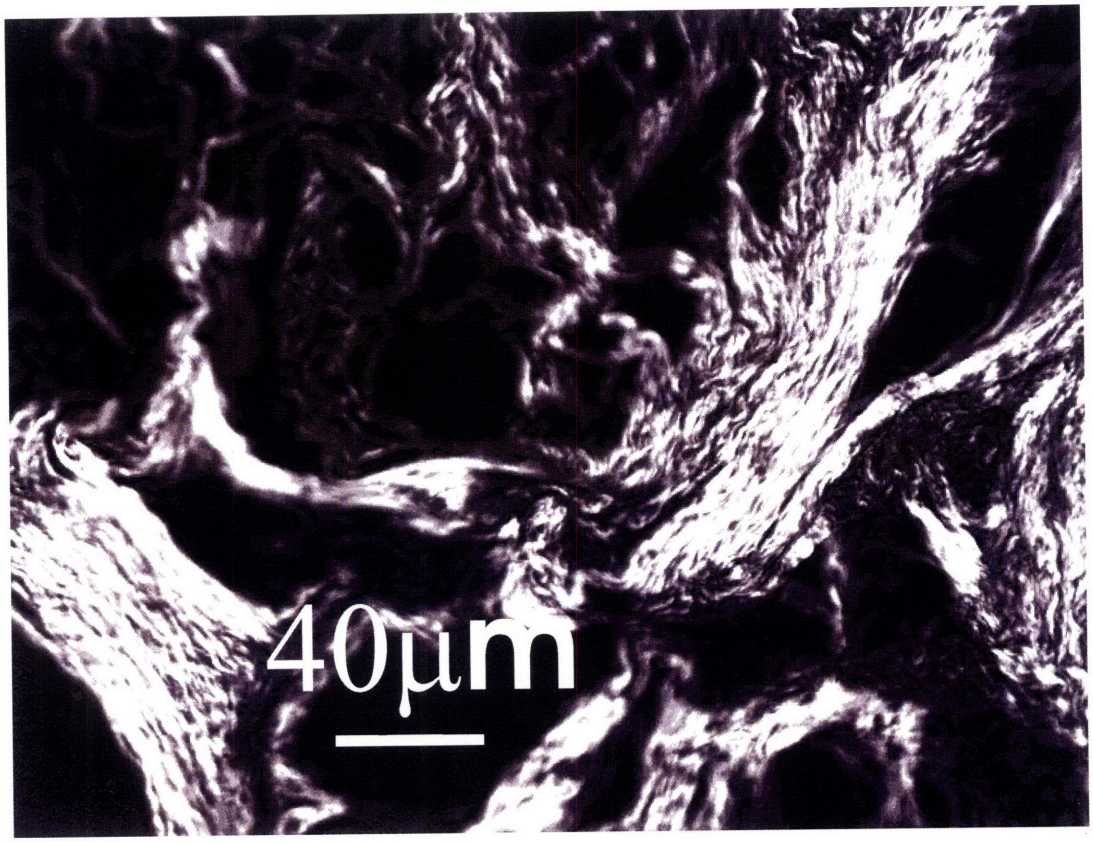

Figure 4-14: A representative polarized light image taken from NPND patient 4 (refer to Table 2.2). This patient had no previous pregnancies.

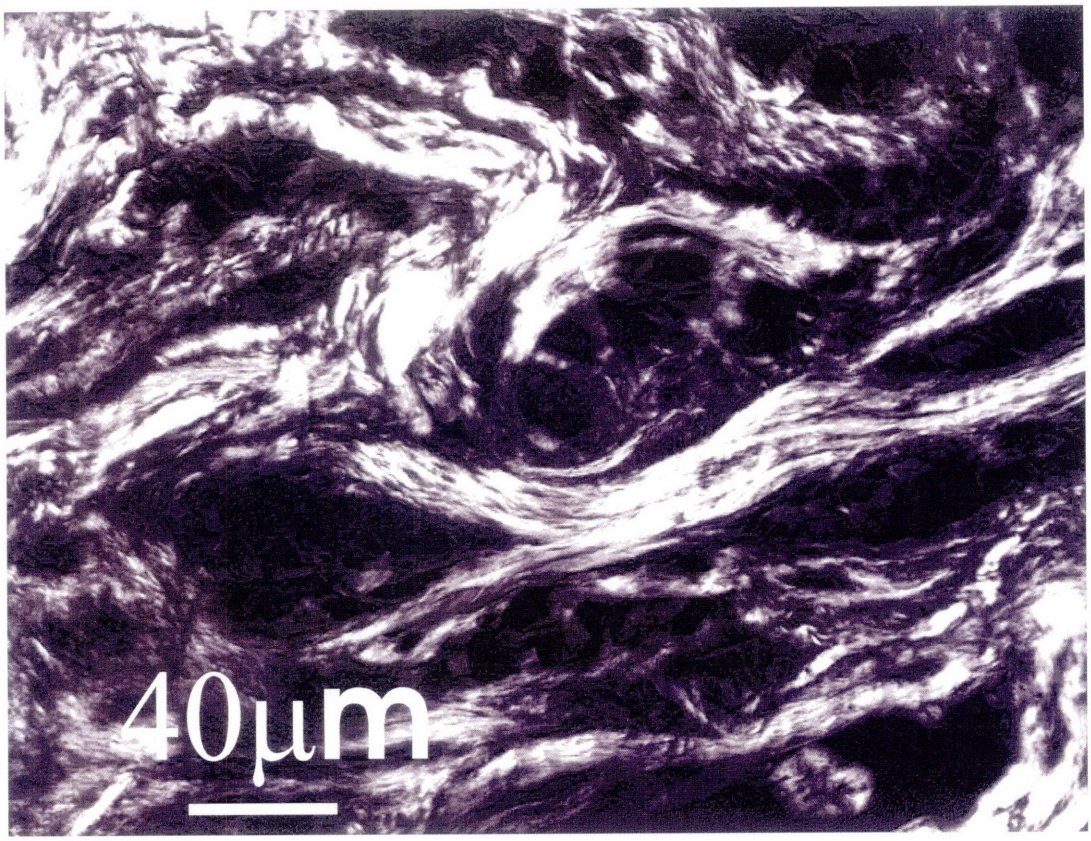

Figure 4-15: A representative polarized light image taken from NPND patient 3 (refer to Table 2.2). This patient had 3 previous cesearan sections.

Figure 4-16: A representative polarized light image of a pregnant tissue sample taken from PCS patient 3 (refer to Table 2.2). This patient had 5 previous cesearan sections.

two orthogonal planes to discern the preferential alignment of the collagen network. Figure 4-17 is an SHG image for a nonpregnant tissue specimen, and Figure 4-18 is an SHG image for a pregnant tissue specimen. The plane of the image is perpendicular to the anatomical longitudinal axis of the cervix, with the radial and circumferential directions marked accordingly on the figures. The nonpregnant specimen was from NPND patient 3 and the pregnant specimen was from PCS patient 2 (refer to Table 3.1). The nonpregnant sample was mechanically tested before imagining, and swelling artifacts exist because the mechanical specimen was equilibrated overnight in PBS before mechanical tests. The "holes" in this figure are on the order of 250μm which is typically bigger than the average smooth muscle cell. The pregnant sample was not tested mechanically therefore there are no swelling effects in this image

SHG imaging captures the intrinsic qualities of collagen fibers and fibrils of the ECM by processing the second harmonic signal of the collagen molecule. This signal is unique to the collagen fiber, therefore, specific molecular details of the collagen protein can be visualized. By investigating the nonpregnant image on the larger scale (Figure 4-17), the collagen fibers can be seen to rope around spaces which contain smooth muscle cells. The large collagen fibers traverse around the cells with a specific preferential alignment in the circumferential direction. Upon closer inspection at a smaller scale, the collagen fibers are seen in their characteristic wavy and kinked configuration. The fibers consist of smaller fibrils bundled together into tightly aligned ropes, and the fibrils have their characteristic bands with a period of $\sim$67nm.

Figure 4-18 shows the SHG results for the pregnant tissue sample. Qualitatively, there are many differences in the collagen network for the pregnant tissue when compared to the nonpregnant tissue. At the larger scale, the collagen network is seen with the same smooth muscle cell holes, but the collagen fibers do not have a preferential alignment. Further, the second harmonic signal is much weaker. This low contrast of the second harmonic signal suggests a qualitative change to the collagen fibrils. By investigating the pregnant tissue at a smaller scale, the collagen fibrils are diffuse and appear disorganized. The difference in the second harmonic signal between the pregnant and nonpregnant tissue sample gives a first line of evidence to suggest that cervical maturation involves the alteration of the collagen network. The molecular level detail of these images also suggest that this alteration could occur on the molecular of fiber length scale. Correlating second harmonic signals to collagen structure is

still an active area of research. More studies are needed to confirm the correlation between SHG signal intensity and collagen structure.

4.3 Conclusion

The biochemical content of human cervical stroma consists of a crosslinked collagen network embedded in a viscous proteoglycan groundsubstance. Shifts in the concentration and organization of these components play a large role in the cervical softening process during pregnancy. The biochemical results presented in this Chapter matched well with previous studies in the literature for both nonpregnant and pregnant tissue. There was a statistically significant increase in the collagen solubility, total sulfated glycosaminoglycan, Δdi-6S disaccharide, and Δdi-HA disaccharide measured for the pregnant tissue when compared to the nonpregnant tissue. Biochemical trends were also noted when comparing the two nonpregnant cases. Further, for the first time, the disaccharide content of the human cervix was measured using the FACE technique where results matched well with studies conducted on timed-pregnant rats.

This biochemical study was a necessary step to eluciate the structure-function relationships in cervical tissue. The biochemical results complemented the mechanical characterization of the tissue by indentifying changes in the collagen and proteoglycan networks for the different obstetric cases which can help to interpret the corresponding changes in mechanical properties. For example, the increase in collagen solubility corresponded to the increase in the stiffening parameter α presented in Chapter 3 suggesting that the biochemical architecture influences the mechanical properties of the tissue. In conclusion, this biochemical study inspired the development of the microstructurally-based, 3-dimensional material model presented in the next Chapter. A full discussion of the model develop and recommendations for a regression analysis of material parameters and biochemical content is given in the following Chapter.

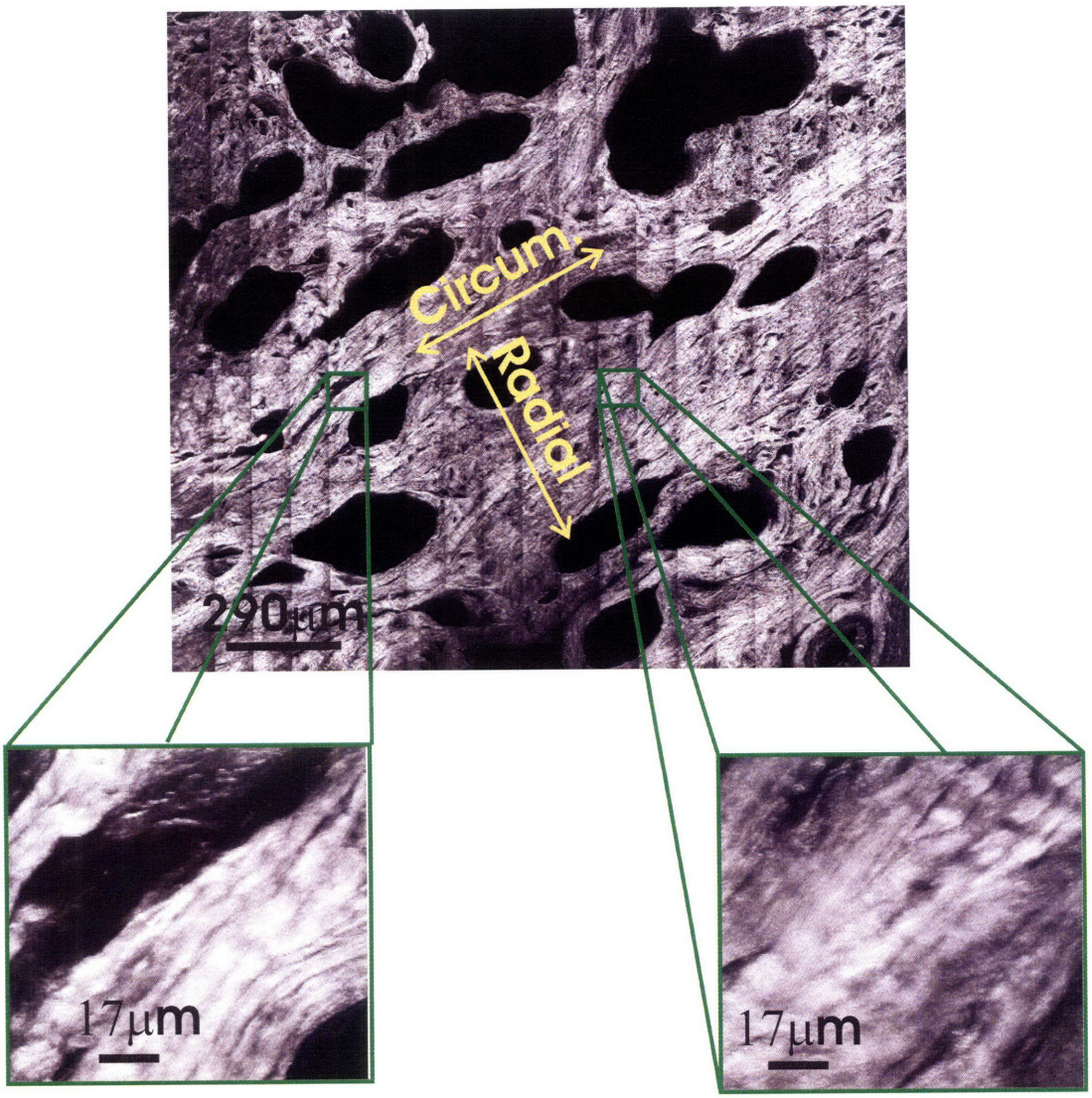

Figure 4-17: A second harmonic image of nonpregnant cervical tissue. The plane of this image is perpendicular to the longitudinal direction of the cervix. This specimen was taken from NPND patient 3 (refer to Table 3.1) This image details the dense connective tissue of the stroma region. Note, this specimen was equilibrated overnight in PBS before sectioning. Images taken by Dimitrios Tzeranis from the So Lab - Bioinstrumentation Engineering Analysis and Microscopy at MIT.

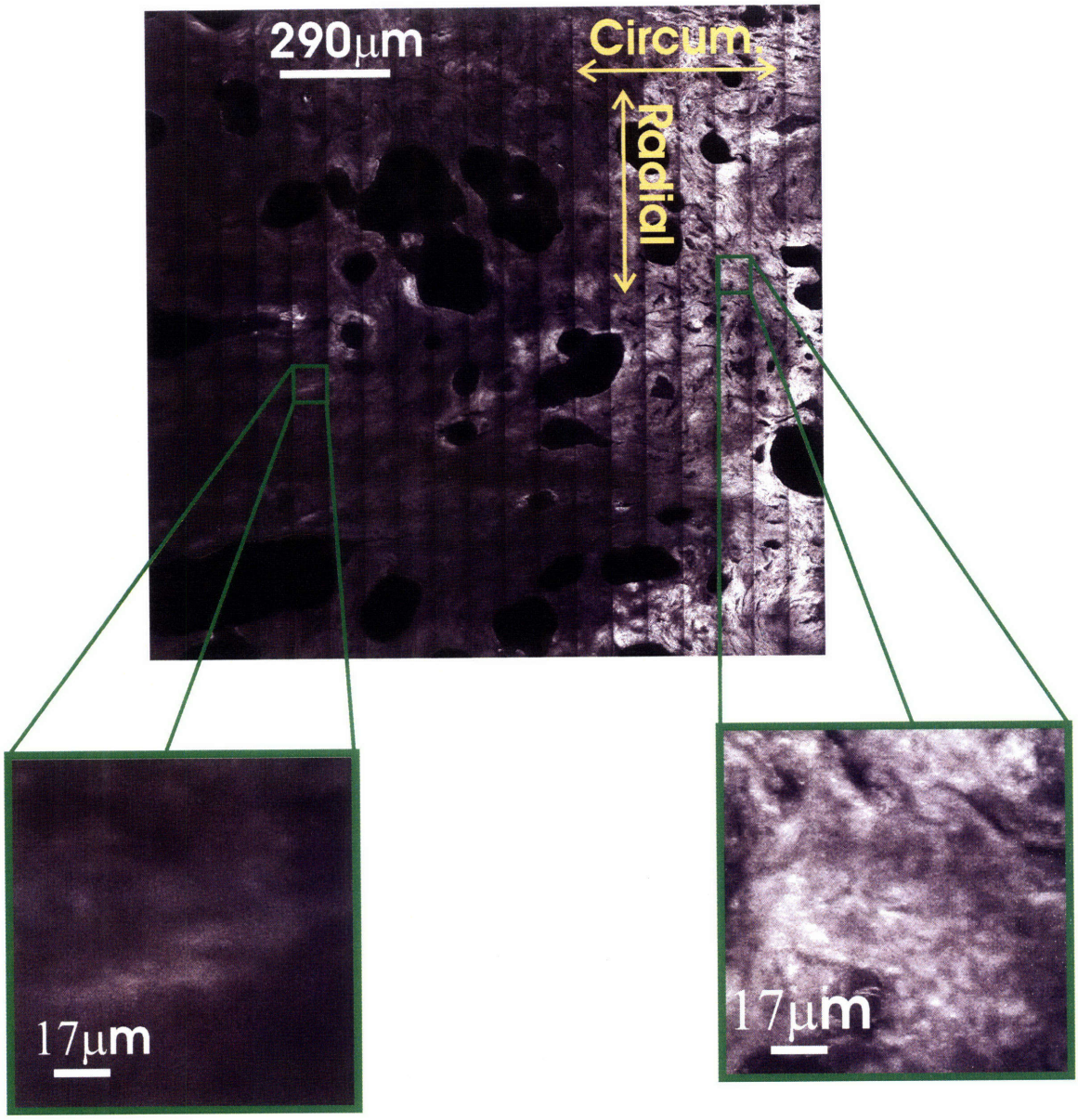

Figure 4-18: A second harmonic image of pregnant cervical tissue. The plane of this image is perpendicular to the longitudinal direction of the cervix. This specimen was taken from PCS patient 2 (refer to Table 3.1). Images taken by Dimitrios Tzeranis from the So Lab - Bioinstrumentation Engineering Analysis and Microscopy at MIT.

Chapter 5

Future Work and Conclusions

The protocols and results presented in this doctoral work characterize the mechanical and biochemical characteristics of human cervical tissue for three different obstetric cases. For the first time, a complete set of mechanical and biochemical data exist to appropriately guide the development of a micro-structurally based, three-dimensional material model. The mechanical data characterize the full three-dimensional anisotropic material behavior of cervical stroma in compression and tension, and the biochemical data characterize the extracellular matrix components of the tissue with specific detail concerning the collagen and glycosaminoglycan network. With this structure-function foundation, continuing research efforts should include fitting a 3-dimensional anisotropic constitutive relationship to the anisotropic mechanical data, testing additional samples to increase the statistical power of the study, and conducting a regression analysis to derive mathematical relationships between measured material properties and biochemical content. This doctoral thesis will conclude with an investigation into the 3-dimensional anisotropic material properties of cervical tissue and give recommendations for future work.

Efforts can now be continued with the development and verification of the 3-dimensional anisotropic model for human cervical tissue derived in the doctoral work of Anastassia Paskaleva [94]. The anisotropic mechanical data collected in Chapter 3 include relationships between stress, strain, and volume change of multiple tissue specimens (additional data can be found in Appendix B). With the results presented in this thesis, the anisotropic model can be fit and verified for a wide range of material behaivor that exist in the patient population. In addition

to these relationships, the histology collected from the Second Harmonic Generation imaging give insight to the preferred direction of the collagen network. Section 5.1 presents a brief study that utilizes the micro-structurally relevant constitutive model developed in Paskaleva's Ph.D. thesis and the morphology information from the SHG data. The model is fit to the anisotropic stress and volume response measured for a NPPD patient, and the directionality of the fibers are quantified for this specific specimen. The measured directionality of the collagen fibers are noted and compared to the best-fit material parameters. A review of the constitutive relationships and results for this model fit are presented in the following sections.

5.1 3-Dimensional Anisotropic Constitutive Model for Human Cervical Tissue

A 3-dimensional hyper-, visco-, and poro-elastic constitutive model was concurrently developed by a fellow Ph.D. student Anastassia Paskaleva who graduated from our lab in September 2007. Her derivation of a material model for cervical tissue is presented in her Ph.D. thesis [94], and the reader is referred to this work for the complete mathematical derivation of the constitutive model and its implementation into a finite element framework. The following section gives a brief review of this model, and an example of a model fit to a complete set of mechanical data for a NPPD patient.

The development of the constitutive relationships were guided by the results of the mechanical experiments from this doctoral work. A 3-dimensional isotropic model was initially developed to fit the results of the preliminary study presented in Chapter 2. Once a good fit was found for the cylindrical compression stroma specimens, an isotropic fit was attempted for both tension and compression data. The isotropic model did not capture both the tension and compression data with a single set of material parameters. This discrepancy and the knowledge that the stroma contains zones of preferentially aligned collagen motivated the development of a 3-dimensional anisotropic model. Further, insight into the anisotropic behavior of cervical stroma was realized with the modification of the mechanical testing protocols to include cubical specimens that were tested along anatomically relevant axes.

5.1.1 3-Dimensional Material Model Development

The constitutive model for human cervical tissue presented in Paskaleva's doctoral work [94] treats the tissue as a composite material comprised of a wavy-kinked collagen fibril network embedded in a hydrated viscous groundsubstance of proteoglycans and glycosaminoglycans with a volume-restoring elastin network. The rheological model relates the shear and bulk deformation of the stroma to the major biochemical constituents of the tissue and attempts to capture the anisotropic, time-dependent, and hyper-elastic nature of the stress response. To accomplish this task, model development was guided by the measured stress-response of the stroma to different modes of deformation and the stroma's biochemical architecture.

The tissue is discretized into two different compartments where the collagen network dominates Compartment 1 while Compartment 2 is a collagen-free region with free swelling cellular and glycosaminoglycan components. The model is derived by individually assigning constitutive relationships for the biochemical compartments, and the resulting macroscopic stress in the cervical stroma is a combination of these contributions:

$$\tilde{\boldsymbol{\sigma}} = \frac{1}{J}(f_1^0 J_1 \boldsymbol{\sigma}_1 + f_2^0 J_2 \boldsymbol{\sigma}_2) + \boldsymbol{\sigma}^h_{elastin} + \mathbf{\Delta P}_{Darcy} \tag{5.1}$$

where J is the total volumetric stretch, $J_1$and J_2 are the volumetric stretch for the different compartments, f_1^0 and f_2^0 are the initial volume fractions, $\boldsymbol{\sigma}^h_{elastin}$ is the stress response for the volume-restoring elastin network, and $\mathbf{\Delta P}_{Darcy}$ is the fluid pressure of the diffusing interstitial fluid of the porous tissue.

The reader is referred to Chapter 5 of Paskaleva's thesis [94] for the full discussion on how the constitutive relationships were cast for each biochemical component. A short discussion is presented here on how the model elements were inspired by the collagen and proteoglycan network of the cervical stroma. The resulting material parameters and rheological representation of the constitutive model are in Table 5.1 and Figure 5-1.

Splitting the Waters: Biochemical Compartments

To accurately account for the biochemical components and to account for the non-linearities of the stress-response, the cervical stroma is idealized to be composed of individual biochemical

Parameter	Unit	Description
f_2^0		*Initial Free GAG volume fraction*
μ_0	Pa	*Initial collagen modulus*
λ_L		*Collagen locking stretch*
$\mathbf{K}_{FG}$	Pa	*Bulk modulus free GAG*
$\mathbf{K}_{BG}$	Pa	*Bulk modulus bound GAG*
$\mathbf{K}_{elastin}$	Pa	*Bulk modulus elastin*
$\frac{\dot{\varepsilon}_v^0}{\sigma^{0^m}}$		*Lumped flow parameter*
m		*Flow sensitivity*
a^2		*Structural parameter*
b^2		*Structural parameter*
c^2		*Structural parameter*

Table 5.1: Material parameters for the cervical stroma. The structural parameters are included to account for anisotropy

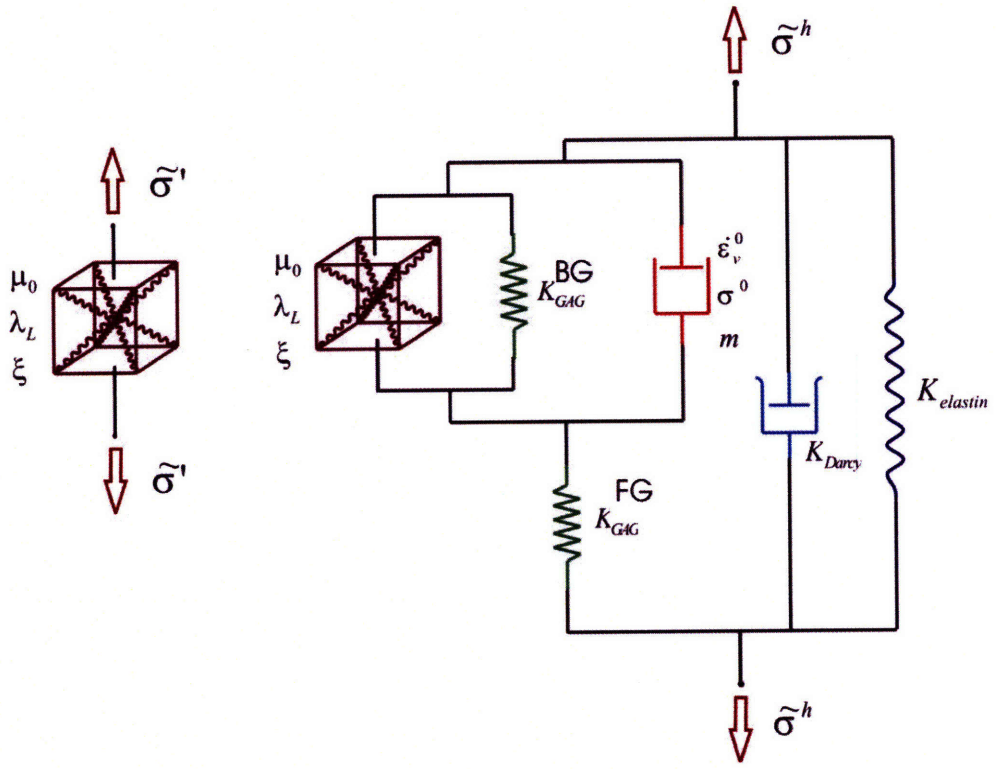

Figure 5-1: Rheological model for the macroscopic response of the stroma of the cervix. A) The deviatoric stress response. The model only accounts for the shear response of the collagen network in the deviatoric stress response. B) The volumetric resposne. The volumetric response was modelled as a combination of the two ECM compartments, the elastin network, the fluid pressure, and the transient fluid exchange between ECM compartments.

compartments. The idea of splitting the interstitial fluid into different compartments arises from the cartilage research of Maroudas and co-workers [9][85]. Paskaleva applied this idea to modeling the cervical stroma, and idealized the tissue into a Free GAG (FG) and Bound GAG (BG) compartment. The BG compartment was dominated by the crosslinked collagen network while the FG compartment was free to swell without the constraints of the collagen network. At the time of model development, the FG compartment was hypothesized to be a region of swollen glycosaminoglycans (hence the name Free GAG). In light of recent histology images of the cervical stroma (refer to Section 4.2.5), the stroma was confirmed to contain regions dominated by the collagen and regions that are free to swell. However, in addition to Free GAGs, the regions not dominated by collagen also contained other stroma components, namely smooth muscle cells and blood vessels. In the discussion that follows, Paskaleva model is fully reviewed using the terminology presented in her thesis work. At the end of this section, recommendations for appropriate correlations of the biochemical structure to model elements will be dicussed.

It is well known that the ECM of articular cartilage and cervical stroma share a number of similarities in the structure of their ECM and mechanical behavior. Both tissues are comprised of a network of highly negatively charged ground substance intertwined with the kinked structure of the collagen. The GAGs present in the cartilage, mainly aggrecan, are bigger than the ones present in the cervical stroma. The small GAGs of the cervical tissue, such as the decorin, organize the collagen bundles and are essentially a part of the collagen structure. In the work of Maroudas [84], two compartments occupied by different constituents of the ECM are presented: an interfibrillar water compartment occupied by collagen fibrils which excludes the PGs and an extrafibrillar water compartment of fluid and PGs with highly negatively charged groups. The water amount in the intrafibrillar and the extrafibrillar compartment varies with the type of tissue and is governed by the concentration of charged PGs in the particular type of stroma. The space occupied by the extrafibrillar water comprised by a PG-water gel is compared to a porous mesh of very thin solid PGs filled with liquid. The authors argue that the swelling tendency of the tissue due to the osmotic pressure of PGs depends on the PGs' content in the extrafibrillar space and the collagen fiber organization. This reasoning is used to justify the higher hydration levels (swelling tendency) of excised specimens immersed in physiological

saline in which the collagen fiber organization is disrupted due to the excision of the tissue from the surrounding organ.

For cervical tissue, the Paskaleva model split the waters through the separation of the PGs. Paskaleva separates the PGs of the cervical stroma into two disparate categories, namely Bound Water PGs (BG) and Free Water PGs (FG). The two PGs occupy two different compartments of the tissue (represented schematically in Figure 5-2):

- Compartment 1: Occupied by collagen bundles and the Bound Water PGs and GAGs (BG). This compartment is dominated by the balance between the osmotic swelling of the negatively charged PGs and the tensile forces of the collagen network.

- Compartment 2: Occupied entirely by Free Water PGs and GAGs (FG). This compartment is governed only by the bulk resistance of the FG with no contributions from the collagen network. This compartment is partially an artifact of cutting the mechanical testing specimens from the surrounding stroma. When the specimens are cut from the stroma, collagen fibrils are severed and the network is compromised locally. This region of disrupted collagen has reduced tensile resistance, therefore allowing increased levels of swelling. In addition to the swelling caused by the release of residual stress, the stroma is also hypothesized to contain hetergeneous pockets of disruptions in the collagen network. These regions would include clusters of blood vessels and smooth muscle cells that were evident in the histology of tissue sections (Figure 4-13) and small cysts.

GAG Response

The main contribution of the GAG network considered by the model is the resistance to volumetric deformation. The two GAG compartments were constitutively prescribed a simple logarithmic characterization relating the volumetric stretch of each compartment to its hydrostatic stress through two material parameters K_{FG} and K_{BG}. Both compartments share the same overal isochoric deformation, however the two compartments accommodate the total volumetric stretch $\widetilde{J}$ in different proportions:

$$J_1 \neq J_2 \neq \widetilde{J}. \tag{5.2}$$

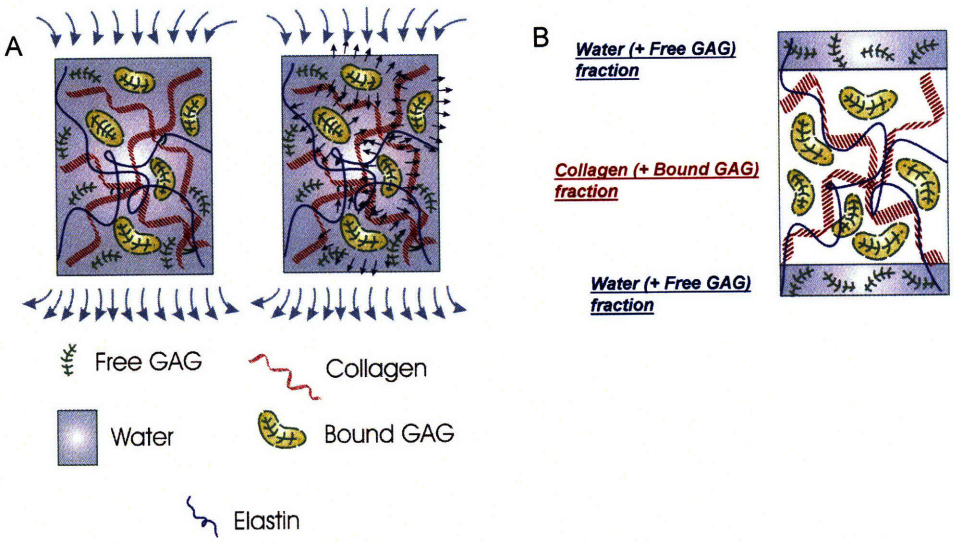

Figure 5-2: Idealized representation of the cervical stroma ECM. A) Components of the idealized stroma B) Diffrent water comparents. (Figure from Paskaleva [94])

The resistance to volumetric deformation of compartment 1 is described through the volumetric stretch of this compartment J_1 such as

$$\boldsymbol{\sigma}^h_{BG} = \mathbf{K}_{BG}\ln(J_2), \tag{5.3}$$

and the resistance to volumetric deformation of compartment 2 is described through the volumetric stretch of this compartment J_2 such as

$$\boldsymbol{\sigma}^h_{FG} = \mathbf{K}_{FG}\ln(J_2) \tag{5.4}$$

The initial values of the Jacobians for these compartments were $J_1^0 = J_2^0 = 1$.

Collagen Network

The collagen network of the cervical stroma is composed of kinked collagen fibers connected by chemical cross-links. The structure of the collagen opposes the osmotic swelling of the GAGs by providing resistance in tension. The integrity of the network comes from the strength of

the individual fibers and the network-like structure of the chemical cross-links. To account for this structure, the collagen network was modeled similar to the network models of polymeric materials where the cervical stroma response comprises both a deviatoric and a hydrostatic component.

When subjected to a certain level of deformation the collagen fibrils stretch and align with the direction of the applied load [103], [26], mimicking the behavior of a polymer network subjected to external loads. The basic characteristic of the stress-strain behavior of the collagen network can be well captured by statistical mechanics treatment of rubber-elasticity. The force-stretch behavior of a molecular chain differs from the kinked fibril in the physical origin of their behavior. The force-stretch behavior of a molecular chain is entropic in origin and is a result from the change in the configurational entropy of the chain. On the other hand, the physical origin of the force-stretch behavior of a fibril arises from the change of the internal energy of the fibril due to unbending. Despite these differences, the force-stretch behaviors of these two structures are quite similar. As a result, the individual collagen fibrils were characterized by Langevin chain statistics proposed by Kuhn and Gruen [74]. For an isotropic treatment, the individual fibrils were arranged in an 8-chain representative element according to Arruda and Boyce [3] (refer to the left cube in Figure 5-3).

To account for the tissue anisotropy due to the preferential alignment of the collagen network, Paskaleva incoporated the Bischoff-Arruda [14] orthotropic unit cell to replace the isotropic Arruda-Bocye 8-chain representation (refer to the right cube in Figure 5-3). In 2002 Bischoff et al. proposed a microstructurally based orthotropic hyperelastic constitutive law for a general case class of polymer and polymerlike materials, which exhibit hyperelastic orthotropic mechanical behavior. Due to the similarities of the force-stretch behavior of the polymer and the collagen network, the basic characteristics of the stress-strain behavior of the collagen network can be well captured with classical rubber-elasticity constitutive models.

The fixed orientation of the orthotropic unit cell is specified by the orthogonal principal material axes $\mathbf{a}$, $\mathbf{b}$, and $\mathbf{c}$ (presented in green in figure 5-3). This orientation is rotated relative to a reference coordinate system $\mathbf{X}_1$, $\mathbf{X}_2$, $\mathbf{X}_3$. The normalized dimensions of the unit cell are a, b, and c, respectively, along the axes $\mathbf{a}$, $\mathbf{b}$, and $\mathbf{c}$. The fixed orientation of the unit cell together with the unit cell dimensions give rise to the orthotropy of the mechanical response of

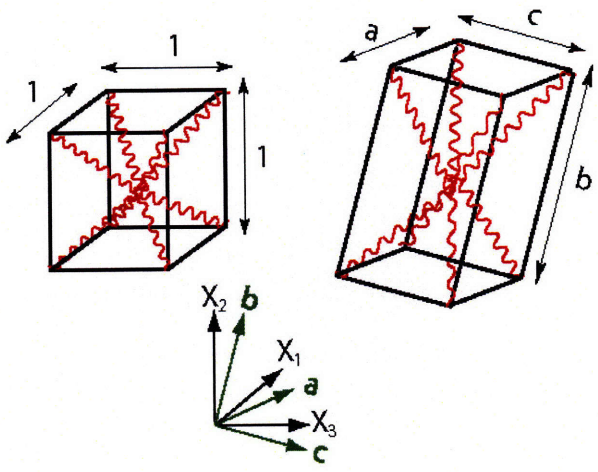

Figure 5-3: Eight-chain models. Left: Three dimensional isotropic unit cell proposed by Arruda and Boyce [3]; right: Three-dimensional orthotropic unit cell proposed by Bischoff and Arruda [14].

a network with preferred fiber orientation.

The representation of the stress state in the collagen network relies on 5 material parameters in the model for the collagen, which needed to be fit to the experimental data:

· μ_0 is the initial collagen modulus.

· λ_L is the limiting stretch for the collagen fibril.

· a^2 is a structural parameter to account for fiber bias in the longitudinal direction.

· b^2 is a structural parameter to account for fiber bias in the circumferential diretion.

· c^2 is a structural parameter to account for fiber bias in the radial direction.

The model fits in this thesis work were done such that the **a**, **b**, and **c** axes were aligned with the mechanical testing directions. The principal directions **a**, **b**, and **c** corresponded to the anatomical directions of the cervix. The normalization condition is enforced by imposing $a^2 + b^2 + c^2 = 3$, and isotropy was recovered when a, b, and c were equal to unity.

Transient Tissue Response

The entire time-varying response of the tissue is modelled by considering the time-dependent volume change of the collagen network. Changes in volume give rise to changes in fibril stretch, which also affects the deviatoric collagen network response. The time-varying response of the

collagen network is influeced by the exchange of waters between the two ECM compartments described in Section 5.1.1. The flow of fluid between the compartments is driven by the imbalance of the hydrostatic stresses of the two compartments, $\boldsymbol{\sigma}^h_{FG}$ and $(\boldsymbol{\sigma}^h_{BG} + \boldsymbol{\sigma}^h_c)$. This imbalance is the intercompartmental (IC) pressure given by

$$\boldsymbol{\sigma}^h_{IC} = \boldsymbol{\sigma}^h_{FG} - (\boldsymbol{\sigma}^h_{BG} + \boldsymbol{\sigma}^h_c) \tag{5.5}$$

and is the driving force for fluid flow between the bound GAGs and the free GAGs compartments.

The evolution of the volumetric Jacobian of the collagen compartment is given by

$$\dot{J}_1 = \dot{\varepsilon}_v J_1, \tag{5.6}$$

where $\dot{\varepsilon}^v$ is the volumetric flow rate. In order to fully characterize the intercompartmental flow the rate of change of the volumetric strain $\dot{\varepsilon}^v$ needs to be constitutively prescribed.

The flow equation for the intercompartmental flow is given by:

$$\dot{\varepsilon}_v = \dot{\varepsilon}^0_v \left(\frac{\boldsymbol{\sigma}^h_{IC}}{\boldsymbol{\sigma}^0} \right)^m . \tag{5.7}$$

In the above equation $\dot{\varepsilon}^0_v$ is the rate of change of the volumetric strain corresponding to an intercompartmental pressure $\boldsymbol{\sigma}^h_{IC} = \boldsymbol{\sigma}^0$, $\boldsymbol{\sigma}^0$can be considered as a flow strength and m is a flow rate sensitivity parameter.

The limit of $m \longrightarrow 1$ recovers linear flow behavior and in this case the flow equation reduces to a linear dependence for the flow between the compartments:

$$\dot{\varepsilon}_v = \left(\frac{\dot{\varepsilon}^0_v}{\boldsymbol{\sigma}^0} \right) \boldsymbol{\sigma}^h_{IC} , \tag{5.8}$$

where $\frac{\dot{\varepsilon}^0_v}{\boldsymbol{\sigma}^0}$ is a lumped material parameter to be fitted to experimental data.

Elastin

The elastin in the elastic fibers is characterized by a high degree of reversible extensibility. The elastin has the capability of sustaining large deformation with the application of small forces and can be viewed as the "elastic memory of the tissue". Under the action of a macroscopic deformation gradient $\mathbf{F}$ the elastin provides a contribution to the stress, which was implemented as a simple linear relationship between the hydrostatic stress and the macroscopic volumetric deformation. Such a description of the stress state of the elastin depends on a single constitutive parameter, namely the bulk modulus $\mathbf{K}_{elastin}$ of the elastin in the stroma and is given by

$$\boldsymbol{\sigma}^{h}_{elastin} = \mathbf{K}_{elastin}(\tilde{J} - 1)\mathbf{I}. \tag{5.9}$$

The shear response of the elastin is negligible as compared with the collagen. Its contribution is regarded as a part of the collagen deviatoric response.

5.1.2 3-Dimensional Model Fit: Nonpregnant Cervical Tissue

The anisotropic constitutive model from Paskaleva was fit to tension and compression stress-responses measured from stroma specimens taken from a single cervical slice from NPPD patient 3 (refer to Table 3.1 for patient history). The mechanical data was collected according to the protocol in Section 3.1.1. The compressive stress-response was measured for a cubical specimen tested uni-axially along the circumferential and longitudinal directions. The tensile stress-repsonse was measured on an adjacent tissue sample, and was tested in the circumferential direction only. The model was fit to both compression responses and to the tensile response up to 15% true strain. The compression specimen utilized for this model fit was also analyzed for fiber direction using Second Harmonic Generation Imaging (see results in Section 5.1.3).

The best-fit material parameters found for the tension and compression responses are in Table 5.2. Figures 5-4 and 5-5 illustrate the model fit for the load-unload cycles, and Figures 5-6, 5-7, and 5-8 illustrate the model predictions for the ramp-relaxation deformation protocol. Model fits were guided by material parameters explored previously by Paskeleva [94], and adjusted accordingly to capture the time-dependence and anisotropy of the stress and volume response.

Overall the 3-dimensional model derived by Paskaleva captures the anisotropic behavior of the tissue well with one set of material parameters being able to characterize the compressive (in two orthogonal directions) and tensile (in the circumferential direction) load-unload responses. The structural parameters were adjusted to give fiber preference to the longitudinal direction to capture the larger peak stresses in the circumferential loading direction. By investigating Figure 5-4, it can be seen that the model predicts the peak values of the experimental tests well with the one set of best-fit parameters. Also, the volume behavior is captureed very well for the longitudinal testing direction and reasonably well for the circumferential testing directions for tension and compression (refer to Figure 5-5).

A shortfall of the model, or perhaps the testing protocol, was capturing the initial slope of the stress response in compression. The model over-predicted the initial modulus of the compression responses because larger initial slopes were used to accomodate the tensile response. There could be many reasons for the slight discontinuity of the initial slopes between the tension and compression data. Experimental conditions may not accurately capture the small strain response due to the imperfections in geometry and alignment of the biological specimens. Much care was taken to assure even testing specimens, however, overnight equilibriation of the tissue may cause inhetergeneous swelling.

Figures 5-6, 5-7, and 5-8 illustrate the experimental stress-relaxation response and model fit using the best-fit parameters in Table 5.2. The model was sucessful at capturing the volume response in the circumferential testing direction (refer to Figure 5-6). Overall, though, the model fit to the stress-relaxation data was poor in comparison to the load-unload results. Adjustments to the bulk moduli of the GAG network will need to be investigated to allow for smaller equilibrium stresses. Further, additional model elements may be needed to capture the swelling tendencies of the specimens during testing. Experimental evidence suggests that the mechanical testing specimen may swell during testing. Currently, there is no mechanism in the model to account for this behavior.

5.1.3 Tissue Anisotropy

Second harmonic images of two orthogonal planes of the cubical specimen from the model fit presented in the previous section were analyzed for fiber directions. The molecular level

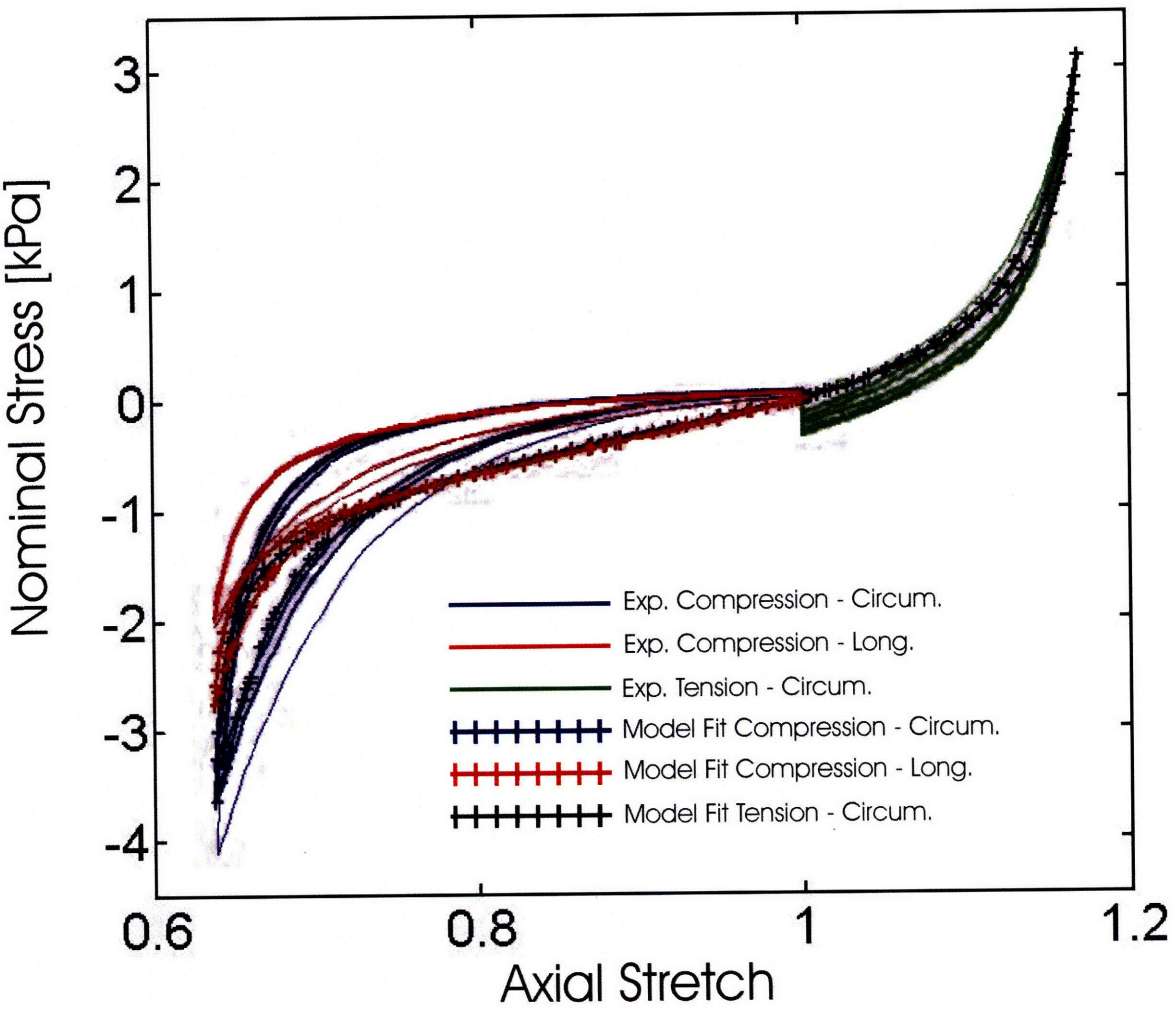

Figure 5-4: Model fit for the tension and compression data from a single cervical slice from NPPD Patient 3 (refer to Table 3.1 for patient history). Dashed lines indicate model fits.

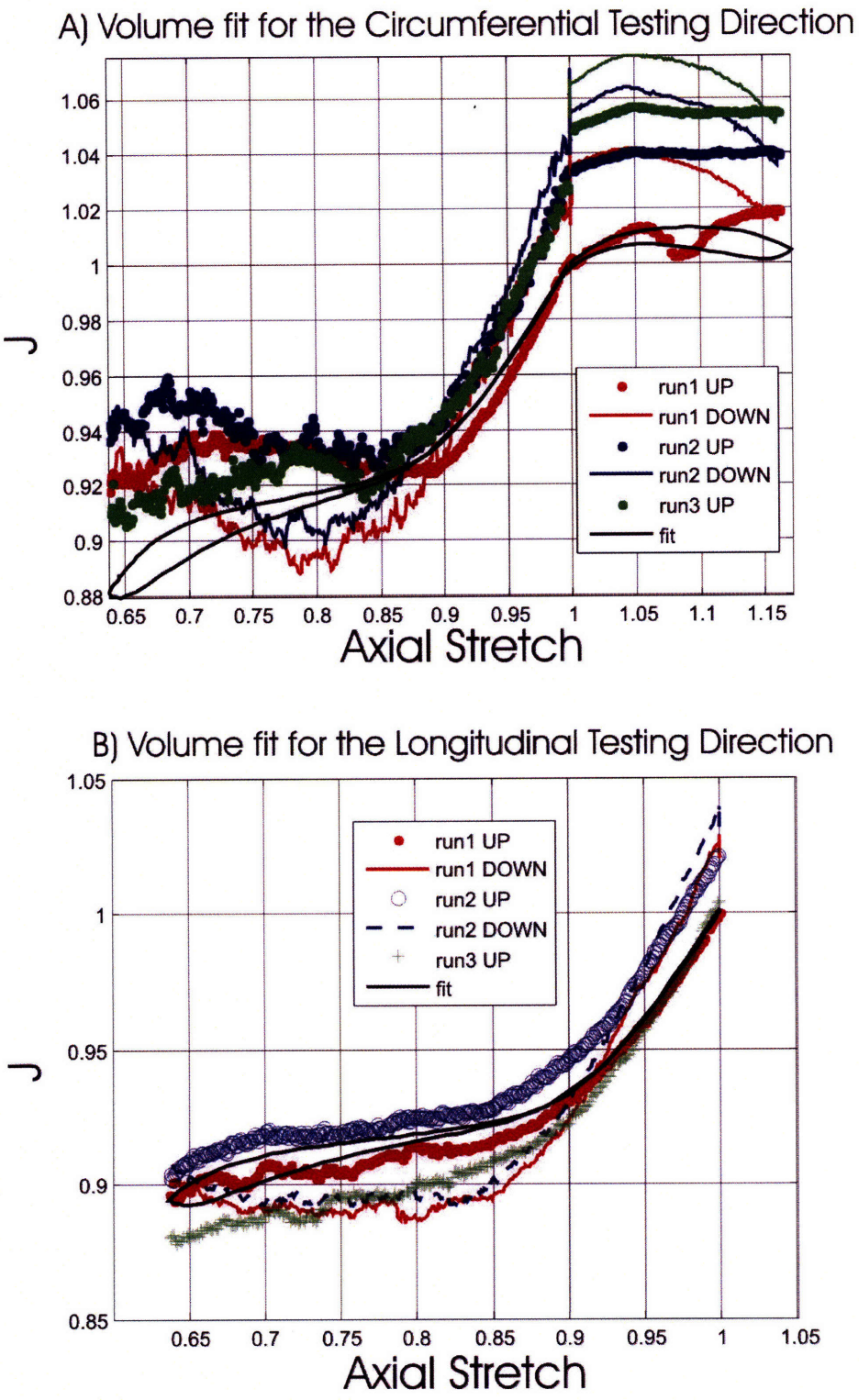

Figure 5-5: Model fit to the volumetric response for the tension and compression specimens of NPPD Patient 3. A) Model fit for the compression and tension test in the circumferential testing direction. B) Model fit for the compression test in the longitudinal direction.

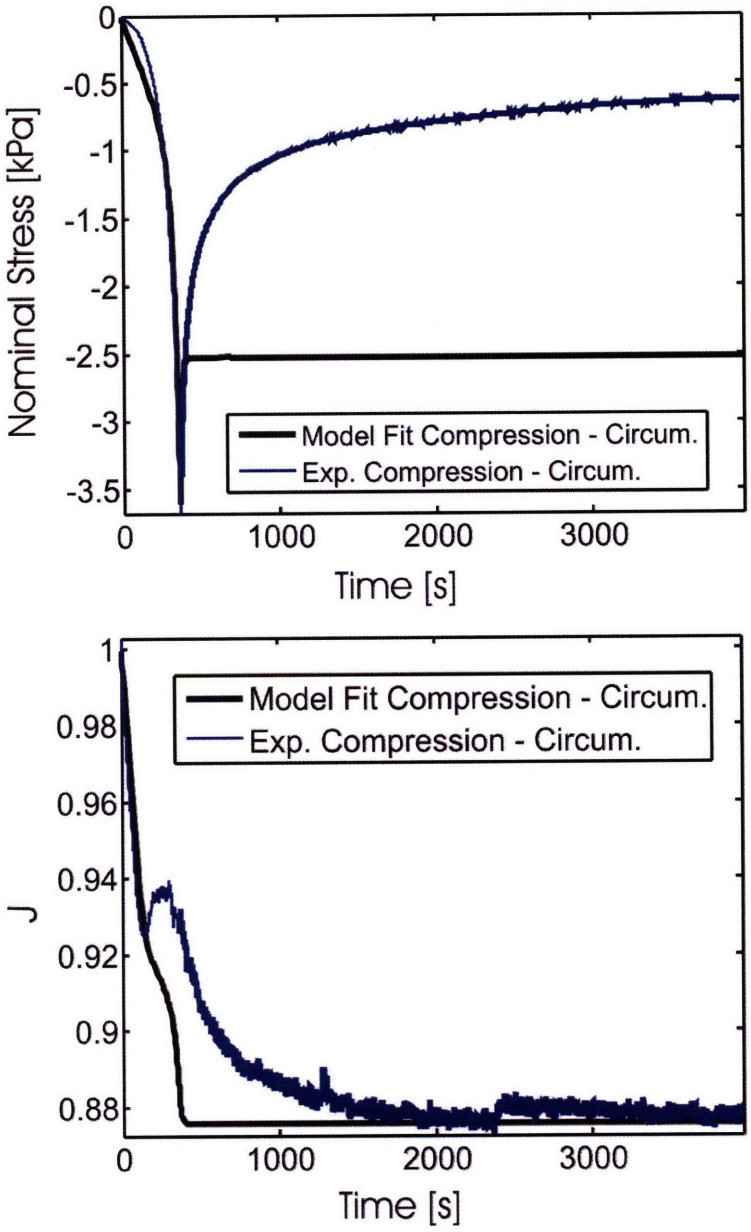

Figure 5-6: The stress relaxation model fit for the compressive stress and volumetric responses in the circumferential testing direction. The model does not capture the stress relaxation of the stress, however it does a good job modelling the time-varying volumetric response.

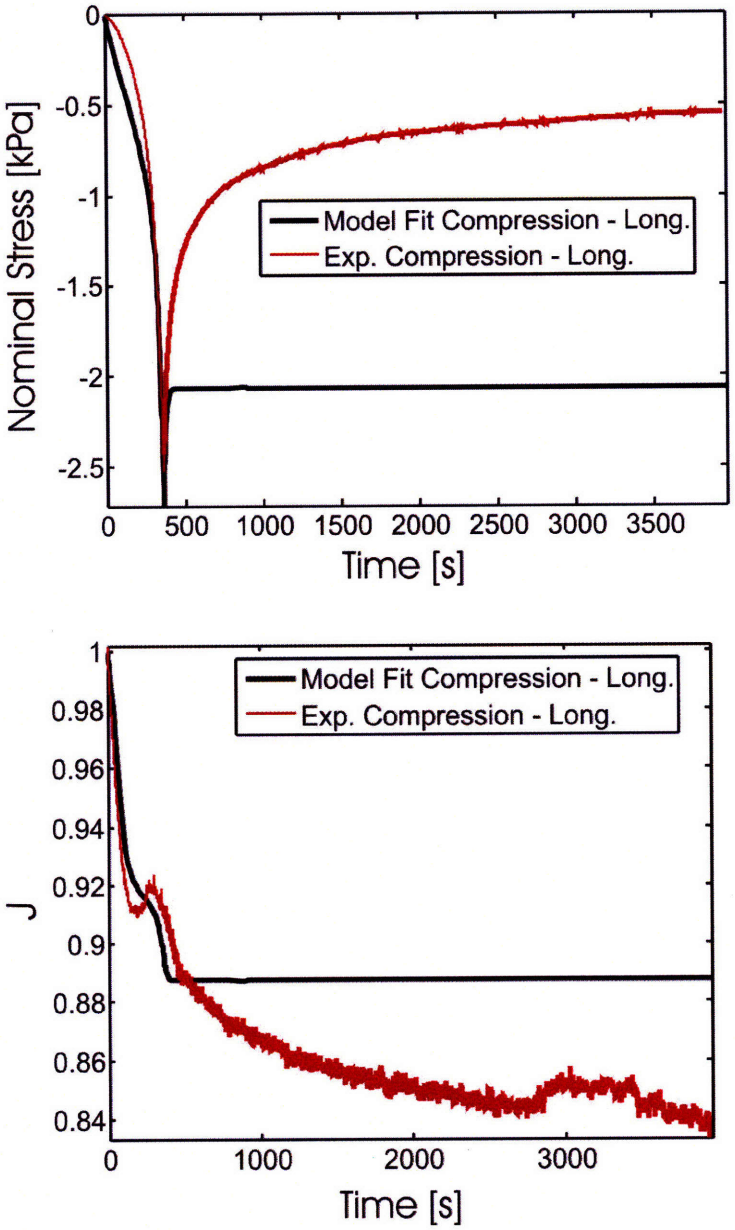

Figure 5-7: The stress relaxation model fit for the compressive stress and volumetric responses in the longitudinal direction. The model does not capture the stress relaxation of the stress, and it does not capture the time-varying volumetric response in this testing direction.

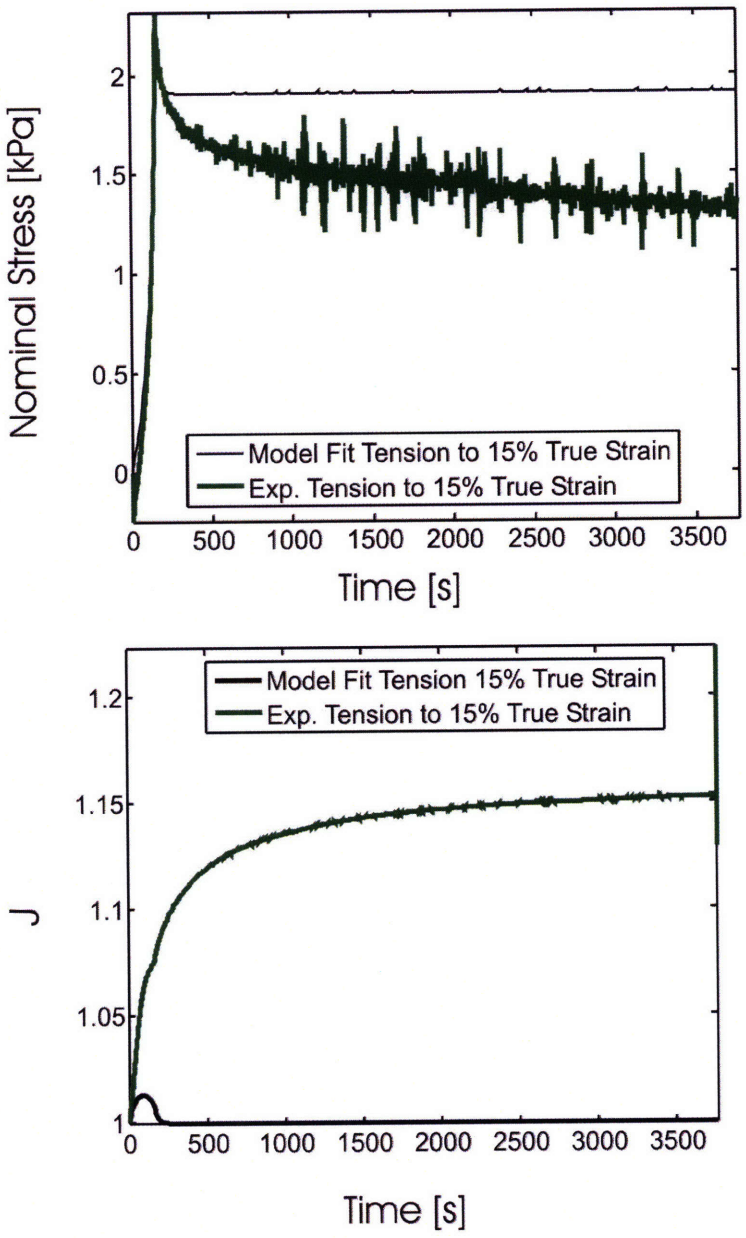

Figure 5-8: The stress relaxation model fit for the tensile stress and volumetric responses in the circumferential direction. The model does not capture the stress relaxation of the stress, and it does not capture the time-varying volumetric response in this testing direction.

Parameter	Unit	Description	Value
f_2^0		*Initial Free GAG volume fraction*	0.09
μ_0	Pa	*Initial collagen modulus*	40
λ_L		*Collagen locking stretch*	1.011
$\mathbf{K}_{FG}$	Pa	*Bulk modulus free GAG*	20
$\mathbf{K}_{BG}$	Pa	*Bulk modulus bound GAG*	60e3
$\mathbf{K}_{elastin}$	Pa	*Bulk modulus elastin*	1000
$\frac{\dot{\varepsilon}_v^0}{\sigma^{0m}}$		*Lumped flow parameter*	$3.5e-7$
m		*Flow sensitivity*	1
a^2		*Structural parameter*	1.236
b^2		*Structural parameter*	1.164
c^2		*Structural parameter*	0.60

Table 5.2: Anisotropic material parameters for the healthy cervical stroma. Stress-response measured for NPPD Patient 3 (refer to Table patientspecificobhistory2 for patient information)

details available in the SHG images allow for the quantification of fiber directions. Figure 5-10 represents the SHG analysis for the specimen looking down the longitudinal axis, and Figure 5-11 represents the SHG analysis for the same specimen looking down the circumferential "testing" direction. Note, the circumferential "testing" direction does not match the true circumferential direction of the cubical specimen. The specimen was cut from a region of the stroma were it was difficult to align the cutting blade with the true circumferential direction. Therefore, the specimen was tested along axes that were skewed from the true anatomical directions.

This misalignment is evident when constructing the directionality ellipse for the specimen in the two orthogonal directions. To quantitatively analyze the direction of the collagen fibers, the SHG images were processed using a Matlab algorithm which calculates the angle of orientation of the individual collagen fibers. This processing was done and developed by Dimitrios Tzeranis from the So Bioinstrumentation Lab at MIT. In short, the algorithm used a numerical differentiation scheme to calculate the derivatives of the image intensity along the x and y axis. The derivatives from individual 15x15 pixel windows formed a "structure tensor" in which the the eigenvectors and eigenvalues represented the orientation of the fiber signal and its significance, respectively. For more information on this algorithm the reader is referred to Chapter 13 in the text by Jäuhn [61].

Figures 5-10B and 5-11B represent the results of the SHG analysis of the fiber direction for the two orthogonal planes, and Figure 5-9 is the color legend for the direction angle. A

histogram and a rose plot of these results are in C and D where the percentage of fibers at a certain angle from the x-axis is represented at the different angle intervals. It is evident from Figure 5-10 that the preferential fiber direction is 20° from the x-axis. This is presumably the direction of the true anatomical circumferential direction. Figure 5-11 indicates that the preferential alignment of the collagen fibers are along the longitudinal direction. In this image, regardless of the intervening blood vessel, the rose plot shows a strong fiber alignment to the x-direction which is the anatomical logindituanl direction.

2-dimensional ellipses were fit to the rose plots in Figures 5-10D and 5-11D, and normalized principal axes of a fitting 3-D ellipsoid were obtained: A =1.47, B =1.07, and C =0.51. The normalization condition was $A^2 + B^2 + C^2 = 3$. The directions corresponding to A, B, and C were the anatomical longintudinal, circumferential, and radial directions, respectively. The fiber analysis indicated that there was a fiber direction bias in the longitudinal direction. These numbers are similar to the model fit structure parameters reported in Table 5.2. However, there was not a one-to-one correspondance between model fit parameters and the measured structural parameters because the tissue sample was not tested along its principals axes.

5.2 Future Work

The brief study presented in this Chapter is a good example of the future research directions for the research effort initiated by this doctoral work. A need for further model development is evident when investigating the model fit presented here. The model performed well in capturing the peak stresses related to the anisotropic compression and tension specimen from a single cervical slice. However, the model could not capture the stress-relaxation behavior. It is hypothesized that the bulk moduli chosen for this fit is too high for these cervical specimen. It was not feasible to continue with the model fit procedure because of the lack of an automatic fitting tool for Abaqus. It is recommended that an automatic fitting tool be developed to aid in the fitting process. Further, it was apparent that the tissue specimens were swelling slightly during the mechanical experiments. The model does not account for this swelling behavior, therefore, it was unable to capture the time-dependent volumetric behavior.

In addition to developing the 3-dimensional constitutive model, imaging more tissue spec-

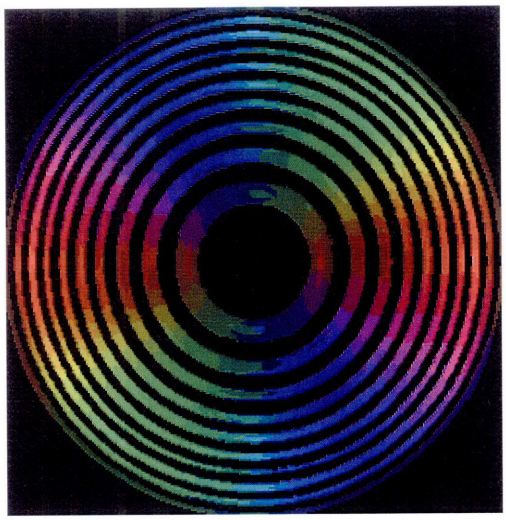

Figure 5-9: Fiber direction key for Figures 5-10B and 5-11B. The color indicates the fiber angle from the x-axis (the horizontal axis.)

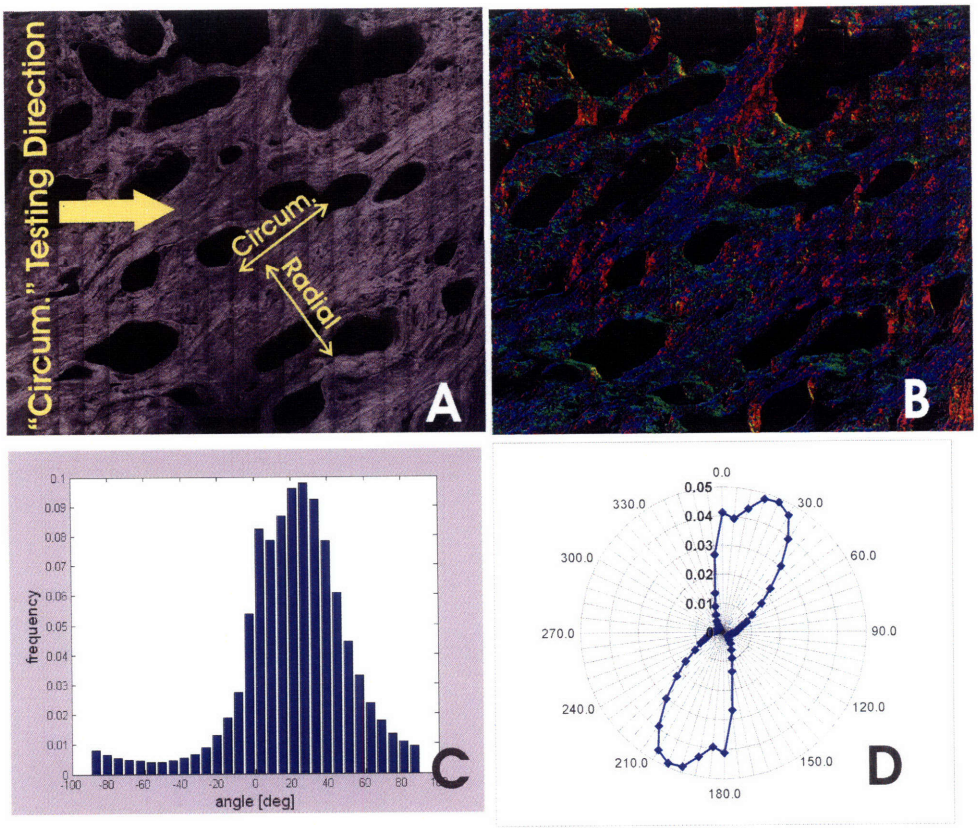

Figure 5-10: Fiber direction analysis of the longitudinal testing direction of the compression specimen investigated in Section 5.1.2 (Image and results courtesy of Dimitrios Tzeranis). A) Second harmonic image. Note that the true anatomical circumferential direction did match the circumferential testing direction. B) Fiber direction measurements. The color key in Figure 5-9 indicates the fiber angle from the x-axis. C) Histogram indicating fiber alignment. D) Rose plot of the 360° distribution of fibers. This plot indicates that the preferential alignment of the fibers is 20° from the horizontal axis.

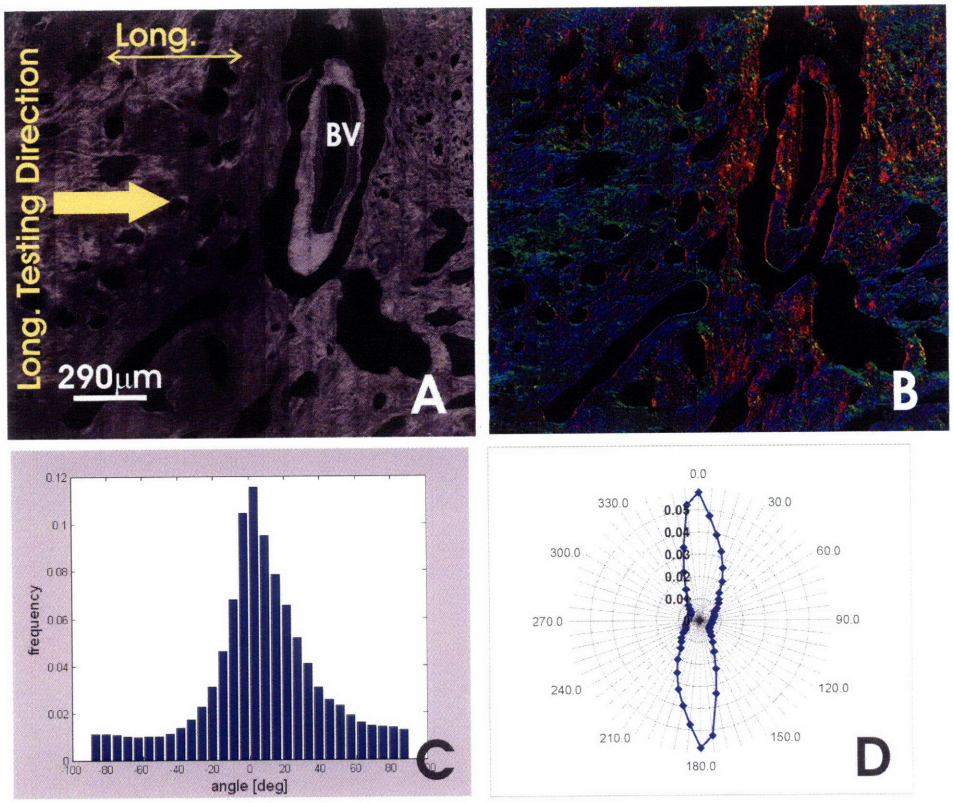

Figure 5-11: Fiber direction analysis of the circumferential testing direction of the compression specimen investigated in Section 5.1.2 (Image and results courtesy of Dimitrios Tzeranis). A) Second harmonic image. BV marks a blood vessel. Note that the longitudinal direction matched the longidutindal testing direction for this specimen. However, the true anatomical circumferential direction did match the circumferential testing direction. B) Fiber direction measurements. The color key in Figure 5-9 indicates the fiber angle from the x-axis C) Histogram indicating fiber alignment. D) Rose plot of the 360° distribution of fibers. This plot indicates that the perferential alignment of the fibers is along the horizontal axis, the logitudinal direction.

imens with the Second Harmonic Generation technique will give further insight into fiber direction and tissue swelling levels. A study that is currently being conducted includes imaging a non-swollen mechanical testing specimen and a swollen specimen using the SHG technique. The mechanical testing specimens in this doctorol work were tested in a "swollen" state after overnight equilbration in PBS. Further imaging should be done to quantify the amount of swelling during this protocol and to compare this testing state to the in-vivo swelling state.

In conclusion, additional work related to this doctoral presentation include the collection of mechanical and biochemical data for more patients to increase the power of the statistical comparison between the different obstetric cases. This Ph.D. study established strong correlations with measured material properties (derived from a 1-D viscoelastic model), biochemical content, and the obstetric history of the patient. However, some relationships lack data points to establish a statistically significant difference (i.e. Student's t-test with p-values ~ 0.1). Once sufficient data is collected, a regression analysis can be performed between the mechanical properties and the corresponding structural properties of the collagen and proteoglycans. This regression analysis would determine the statistical significance of the relationship between model parameters and measured biochemical properties. An example of such a regression analysis would be to quantify the mathematical relationship between the material parameter α (from the 1-D model presented in Chapter 3) and the collage solubility of the tissue by graphing α as a function of the solubility. It is hypothesized that α decreases with the increase in solubility (see discussion in Section 3.2). It was shown that the smaller α measured for pregnant tissue was correlated to increased tissue solubility, or a weaker collagen crosslink density. However, the exact mathematical relationship is unknown because of the low number of specimens. A regression analysis for both the 1-D and 3-D model parameters will be needed to establish the micro-structural basis for these constitutive models.

5.3 Conclusions

The mechanical response of human cervical tissue is non-linear, time-dependent, and anisotropic. The biochemical organization and content of the cervical stroma influence this mechanical behavior with the collagen network organization and proteoglycan struture providing strength

and integrity. The 1-D rheological model provided a good minimal framework to capture the nominal stress response for the different tissue samples, and it was found that tissue samples taken from patients with different obstetric histories have different mechanical properties. Further, the measured changes in mechanical properties correlated well to measured biochemical changes for the different obstetric categories.

This doctoral study, for the first time, presents data to appropriately guide the development of a 3-D constitutive model for human cervical tissue. Overall, this work provides insight into the mechanical behavior of human cervical tissue. An improved knowledge of the structure-function relationship is an important first step in understanding how the microstructure of the extracellular matrix (ECM) relates to its macroscopic mechanical response. In addition, the identification of key biochemical regulators of mechanical properties can constitute the basis for pharmacological intervention to correct pathological abnormalities in tissue response.

Appendix A

Acta Biomaterialia Publication

Available online at www.sciencedirect.com
ScienceDirect
Acta Biomaterialia 4 (2008) 104–116
Acta BIOMATERIALIA
www.elsevier.com/locate/actabiomat

Mechanical and biochemical properties of human cervical tissue

K.M. Myers [a], A.P. Paskaleva [a], M. House [b], S. Socrate [a,*]

[a] Department of Mechanical Engineering, Massachusetts Institute of Technology, Cambridge, MA 02139, USA
[b] Division of Maternal Fetal Medicine, Tufts-New England Medical Center, Boston, MA 02108, USA

Received 19 November 2005; received in revised form 18 April 2007; accepted 23 April 2007
Available online 27 September 2007

Abstract

The mechanical integrity of cervical tissue is crucial for maintaining a healthy gestation. Altered tissue biochemistry can cause drastic changes in the mechanical properties of the cervix and contribute to premature cervical dilation and delivery. We present an investigation of the mechanical and biochemical properties of cervical samples from human hysterectomy specimens. Three clinical cases were investigated: nonpregnant hysterectomy patients with previous vaginal deliveries; nonpregnant hysterectomy patients with no previous vaginal deliveries; and pregnant hysterectomy patients at time of cesarean section. Tissue samples were tested in confined compression, unconfined compression and tension. Cervical tissue samples for the three clinical cases were also subjected to biochemical analysis. Biochemical assays measured cervical tissue hydration, collagen content, collagen extractability and sulfated glycosaminoglycan (GAG) content. Results from the mechanical tests indicate that cervical stroma has a nonlinear, time-dependent stress response with varying degrees of conditioning and hysteresis depending on its obstetric background. It was found that the nonpregnant tissue was significantly stiffer than the pregnant tissue in both tension and compression. Further, collagen extractability, sulfated GAG content and hydration were substantially higher in the pregnant tissue. This study is the first important step towards the attainment of an improved understanding of the complex interplay between the molecular structure of cervical tissue and its macroscopic mechanical properties.

Keywords: Cervix; Cervical maturation; Preterm delivery; Cervical biochemistry; Cervical insufficiency

1. Introduction

The human uterine cervix is a passive organ located at the lower end of the uterus (Fig. 1) whose mechanical response during gestation has a critical influence on the outcome of the pregnancy. It has a dual structural function: prior to term, the cervix must stay closed to allow the fetus normal development (Fig. 1A); and at term, the cervix must dilate under the influence of uterine contractions to allow the fetus passage (Fig. 1B). This dual mechanical functionality is reflected in the changing mechanical properties of the cervical stroma. Firm and rigid at the beginning of pregnancy, the cervix undergoes progressive remodeling during gestation until it is noticeably soft at term. This drastic change in tissue properties is the physical manifestation of a complex biochemical process commonly referred to as cervical maturation (or ripening). The clinical implications of an impaired cervical function are well known to clinicians. For example, cervical insufficiency is a condition in which the cervix softens and dilates prematurely in the absence of apparent uterine contractions. Cervical insufficiency can lead to preterm delivery and in many cases causes extremely premature birth [1]. At the other end of the biomechanical spectrum, a cervix that fails to dilate at term can result in substantial maternal and fetal morbidity [2].

Biochemical mechanisms of cervical softening have interested investigators in the obstetric community for many years [3,4]. The extracellular matrix (ECM) of the cervical stroma is the load-bearing component of the cervical tissue [5]. Smooth muscle constitutes less than 15% of the stroma [6] and does not appear to contribute to cervical strength [7]. The ECM of the stroma is similar to other

* Corresponding author. Tel.: +1 617 452 2689; fax: +1 617 258 8742.
E-mail address: ssocrate@mit.edu (S. Socrate).

1742-7061/$ - see front matter
doi:10.1016/j.actbio.2007.04.009

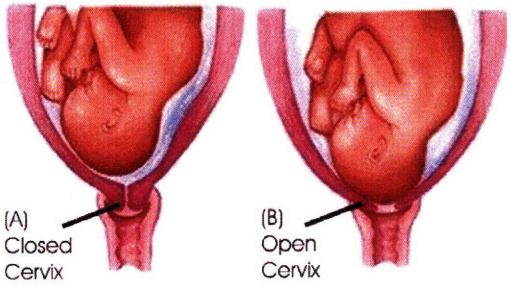

Fig. 1. The cervix uteri during pregnancy (A) and at delivery (B). Published with permission, Copyright Krames/StayWell.

fibrous connective tissues. The primary constituents are type I and type III collagen [8], hyaluronan (HA) and proteoglycans (PGs) [9], elastin [10] and water.

Several lines of evidence implicate disruption of the collagen network as the microstructural mechanism associated with macroscopic cervical softening. Light and electron microscopy studies [11–13] and collagen solubility experiments [8,9,14,15] show that softening of the cervix is associated with collagen fiber disruption and a decrease in collagen crosslinking. HA, matricellular proteins and PGs are also suspected to play an important role in cervical maturation [16] by influencing the collagen and tissue architecture. The observed increase in HA content during pregnancy, in particular nearing delivery, has been directly related to an increase in cervical hydration and disorganization of the collagen network [17]. A number of studies on animal models have used targeted gene disruption to identify ECM components with a prominent effect on collagen morphology and tissue properties. In particular, studies on decorin [18] and thrombospondin 2 [19] substantiate the hypothesis of a direct involvement of these ECM components in the regulation of cervical tissue properties. Recent studies indicate that the biochemical cascade leading to cervical maturation can be activated by mechanical deformation of the cervical fibroblast cells [20,21].

Few studies have been able to correlate biochemical variables to stroma mechanical properties. Rather, investigators have demonstrated correlations between stroma biochemistry and clinical variables. Studies have shown a correlation between tissue hydration, collagen extractability and obstetric history. Pregnant cervical tissue is more hydrated and has higher collagen extractability than nonpregnant tissue [14,15,23]. Furthermore, obstetricians know that prior vaginal birth increases the speed of a subsequent birth, presumably via an effect on the cervical stroma [22]. Hence, it is not surprising that increasing parity (number of previous vaginal deliveries) has been shown to correlate with a weaker collagen network [23,15]. Cervical insufficiency was found to be associated with increased collagen extractability [15]. In contrast, protracted labor has been associated with higher collagen content and lower extractability [24]. Collagen crosslinking has been investigated in vivo with a noninvasive autofluorescence tool [25]. The cervical autofluorescence signature changes with increasing gestational age, presumably because fewer collagen crosslinks are present.

The number of investigations on quantitative measurements of the tissue mechanical properties ("softness") is very limited, especially when compared to the substantial number of studies dedicated to cervical tissue biochemistry. Most studies employed animal models (e.g. [19,26,27]), while a small number of investigations performed on human tissue in tension did confirm that the pregnant cervix is significantly more deformable compared to the nonpregnant cervix [14,28].

In current clinical practice, the biomechanical status of the cervix is assessed in terms of a subjective scoring system introduced by Bishop [29]. Objective methods for measuring cervical softness during pregnancy have not found their way into clinical practice, although tonometric techniques have been proposed [30,31]. These tonometric measurements demonstrated that cervical softening occurs in a gradual fashion throughout gestation. More recently, an aspiration device was developed to measure cervical softness [32]. This study on nonpregnant human cervical tissue concluded that variations in the mechanical properties of the cervix measured in vivo and in vitro were negligible.

The long-term objective of our study is to investigate cervical mechanical function during pregnancy. A crucial component of this study is an investigation of the structure–property relations for the constitutive behavior of cervical tissue, connecting changes in biochemical composition of the tissue to the observed variations in its mechanical properties. The role of different tissue components can be more prevalent in specific modes of deformation (e.g. collagen in tension, glycosaminoglycans (GAGs) in compression). In order to elucidate these effects, we needed to develop a stringent experimental protocol to collect comprehensive data on the biochemical composition and mechanical properties of ex vivo tissue samples under different loading modes (e.g. tension, confined compression, unconfined compression) and loading histories (e.g. constant strain rate, ramp-relaxation).

Notwithstanding the abundant number of studies on cervical tissue biochemistry, the disparity of methods and protocols yields large discrepancies in the results reported in the literature. In this study, we aimed at identifying appropriate biochemical assays to determine collagen content and collagen extractability in human cervical specimens. Total sulfated GAG concentrations were also determined, while protocols to determine the specific concentrations of individual GAG types are the subject of current investigation.

Here we present preliminary results of our experimental studies and discuss relevant issues pertaining to the established protocols. We obtained tissue samples from hysterectomy specimens from both cesarean deliveries and from premenopausal surgery. Although this preliminary study involved a limited number of specimens, the results of our investigation qualitatively confirm the expected trends concerning the influence of gestational age and obstetric

history on mechanical and biochemical measurements. Further, the results presented here provide the first quantitative mechanical measurements of cervical stroma in confined and unconfined compression. These results are the foundation for the development of an appropriate constitutive model for cervical stroma and will guide future studies to further explore the tissue's anisotropic response in compression and tension.

2. Methods

2.1. Tissue harvesting and specimen preparation

Hysterectomy specimens from pre-menopausal women with benign gynecological conditions were obtained from the Tufts–New England Medical Center. Two cervices were obtained from cesarean hysterectomy patients. Both patients underwent cesarean hysterectomy because of suspected placenta accreta and did not labor. Nonpregnant cervices were categorized according to parity and labeled NPND for women with no previous vaginal deliveries and NPPD for women with previous vaginal deliveries. The pregnant specimens were labeled PCS. Please refer to Table 1 for abbreviation definitions and to Table 2 for specific patient obstetric history. Approval from the Institutional Review Board was obtained from both the Tufts–New England Medical Center and the Massachusetts Institute of Technology prior to initiating the study.

Table 1
Sample labels

Obstetric history	Abbreviation
Non-pregnant: no previous vaginal deliveries	NPND
Non-pregnant: previous vaginal deliveries	NPPD
Pregnant: taken at time of cesarean section	PCS

The uterus and cervix were excised from the patients and placed on ice. A custom-designed stainless steel sectioning tool (Fig. 2A) was used to obtain from each cervix four 4 mm parallel disks perpendicular to the inner canal. Each cervical slice was labeled to distinguish its position relative to the internal and external os (Fig. 2B). Note that the 2 cm of cervix closest to the external os was not tested because this portion was reserved for pathological examination. The cervical tissue slices were stored flat at −80 °C. Preliminary tests performed on fresh and previously frozen tissue from the same cervical slice [37] confirmed that freezing does not alter the mechanical properties, a result consistent with similar findings for cartilage (e.g. [33]). Prior to testing, each 4 mm slice was thawed for approximately 3 min in phosphate-buffered saline (PBS) at an ionic concentration of 0.15 M.

Mechanical and biochemical specimens were cut exclusively from the cervical stroma. The location of the cervical stroma in relation to the cervical mucosa and fascia is illustrated in Fig. 2C. For compressive mechanical tests, cylindrical specimens were cut with an 8 mm biopsy punch at the same radial location for each slice, with the cylinder axis parallel to the inner canal. Care was taken in labeling the samples according to their anatomical site, as data in the literature [28] indicate some variation in mechanical properties with longitudinal position along the axis of the cervix, and radial distance from the cervical canal. For tension mechanical experiments, two concentric circular

Table 2
Patient-specific obstetric history

Patient	Age	G	P	Hysterectomy indication	Obstetric history	Labor?	Endometrial pathology
NPND Patient 1	37	0	0	Fibroid uterus		No	Proliferative
NPND Patient 2	38	4	4	DUB	C/Sx4	No	Secretory
NPND Patient 3	43	4	3	Fibroid uterus	C/Sx3	Dilated to 4 cm in first pregnancy. Did not labor in second and third pregnancies	Secretory
NPND Patient 4	37	0	0	Fibroid uterus		No	Proliferative
NPND Patient 5	35	0	0	Fibroid uterus		No	Secretory
NPPD Patient 1	53	2	2	Fibroid uterus	NSVDx2	Yes	Proliferative
NPPD Patient 2	43	2	2	DUB	NSVDx2	Yes	
NPPD Patient 3	46	1	1	Dysynchronous Fibroid uterus	NSVDx1	Yes	Proliferative
PCS Patient 1	33	4	2	34 weeks gestation; suspected placenta increta	C/Sx2	No, C/S performed prior to labor	Increta confirmed
PCS Patient 2	32	5	5	37 weeks gestation; suspected placenta accreta	C/Sx5	No, C/S performed prior to labor	Accreta confirmed

G = gravida, P = para, DUB = dysfunctional uterine bleeding, NSVD = normal spontaneous vaginal delivery, C/S = cesarean section.

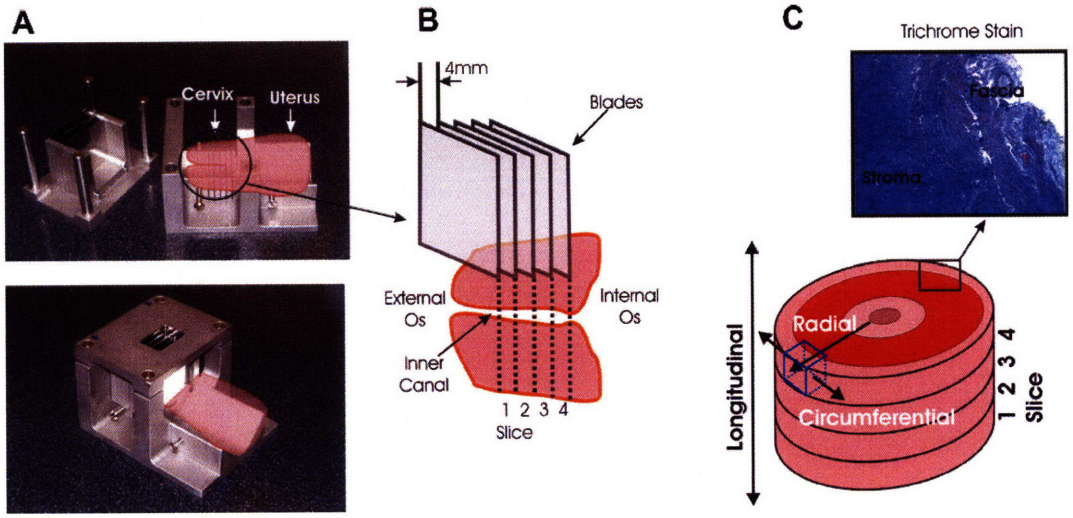

Fig. 2. Specimen preparation. (A) Stainless steel sectioning tool. (B) Cervical slice labeling convention and blade orientation. (C) Cervical tissue. The mucosa is the soft cellular layer lining the cervical canal, and the fascia is the soft cellular layer surrounding the stroma. The stroma is the firm fibrous inner core. Conventions for anatomical orientation within the cervix are indicated.

blades were used to obtain from each slice a singular ring of stroma of ~6–8 mm inner diameter and ~16–18 mm outer diameter. For biochemical specimens, ~20 mg of tissue adjacent to the location of the mechanical specimens were excised from the stroma.

Each cervical slice yielded compression specimens (1–3 specimens, depending on the visual homogeneity of individual slices) or a single tension specimen, as well as several biochemical specimens. The mechanical specimens were weighed and equilibrated overnight in PBS at 4 °C, and the biochemical specimens were stored at −80 °C until time of pulverization.

2.2. Mechanical testing

All tests were conducted on a universal material testing machine (Zwick Z2.5/TS1S, Ulm, Germany) with the specimens immersed in a PBS bath in custom-designed acrylic fixtures (Fig. 3B). A 20 N load cell was used to collect compression data, and a 500 N load cell was used to collect tension data. Video extensometer data were collected with a Qimaging Retiga 1300 CCD camera equipped with a 200 mm f/4 Nikkor lens. Strain data were obtained with digital image correlation (DIC) techniques using Correlated Solutions VIC-2D (v. 4.4.0) software.

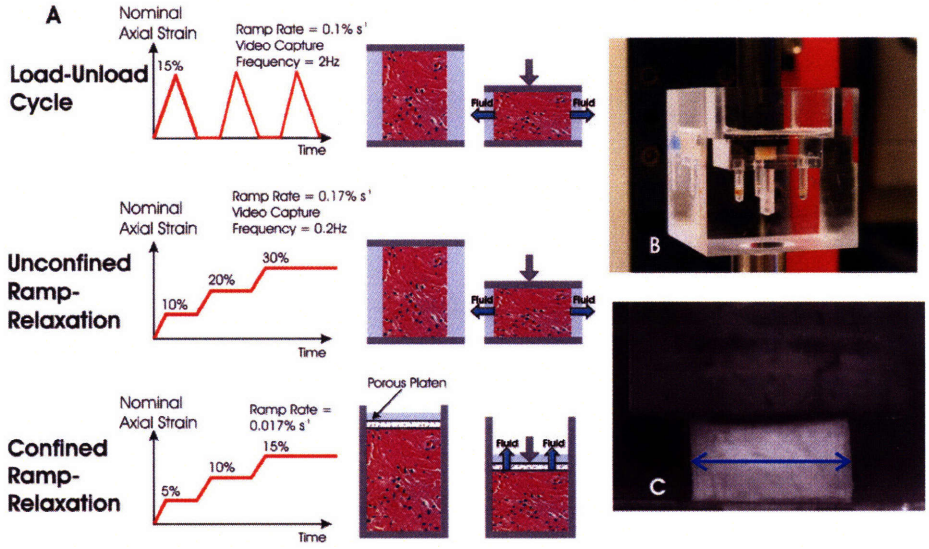

Fig. 3. Compression test protocol. (A) Imposed deformation history for each testing mode. (B) Cervical specimen in compression fixture. (C) Cervical specimen in unconfined compression. Radial stretch history is recorded by a video extensometer.

Measurement variability is inherent in the Zwick load cell and video extensometer analysis. The resolution of the 20 N Zwick load cell is ±0.001 N (~0.01 kPa for an 8 mm diameter specimen), and the resolution of the 500 N Zwick load cell is ±0.025 N (~1.0 kPa for a typical ring geometry). The tolerance of the lateral stretch measurements is a function of the resolution and contrast quality of the video extensometer image. A full discussion of error calculations for the video extensometer can be found in Parson [34]. For our unconfined compression tests an estimate of error was obtained by performing a lateral stretch analysis multiple times for the same image data. The variation in strain due to noise in the video extensometer analysis was found to be within ±1% for testing conditions typical of the unconfined compression configuration. For the ring tension tests, a preliminary image-analysis experiment was conducted using rigid body motion to calibrate the strain error for a particular speckle pattern and camera resolution. For the resolution and speckle pattern used in the tension experiments, the strain error was found to be within ±0.1%.

All mechanical specimens were equilibrated overnight in PBS at 4 °C, weighed and measured prior to testing. A discussion of the motivation and implications for this equilibration procedure, which alters the hydration level of the tissue, is presented in Section 4.1.

Each compression specimen was subjected to three different testing modes: load–unload cycle; unconfined ramp-relaxation; and confined ramp-relaxation. A preload of 0.005 N (corresponding to a compressive stress of 100 Pa) was imposed on each sample prior to testing in order to accurately determine the sample thickness and, for the confined compression tests, improve confinement. Fig. 3A illustrates the imposed deformation histories for the three tests. The compression testing protocol for each specimen consisted of the following sequence of tests: (1) load–unload cycle, (2) unconfined ramp-relaxation, (3) load–unload cycle, (4) confined ramp-relaxation. Each specimen was first loaded in unconfined compression to 15% axial-engineering strain and unloaded to 0% strain at a constant engineering strain rate of 0.1% s^{-1}. This load–unload cycle was repeated three times. After re-equilibration in an unloaded state for at least 30 min in PBS at 4 °C, the specimen was subsequently subjected to an unconfined ramp-relaxation test to axial-engineering strain levels of 10%, 20% and 30% with a ramp strain rate of 0.17% s^{-1}. Each strain level was held for 30 min to measure the relaxation response of the tissue. After re-equilibration in an unloaded state for at least 30 min in PBS at 4 °C, the load–unload cycle test was repeated. The measured response was compared to the response recorded in the first load–unload test to verify that the specimen had not undergone any damage or degradation that might alter its mechanical response. The specimen was then allowed to re-equilibrate for 30 min in PBS. After equilibration, the specimen was placed in an 8 mm impermeable rigid well and subjected to a confined ramp-relaxation test to axial strain levels of 5%, 10% and 15% with a ramp strain rate of 0.017% s^{-1}. Each strain level was held for 30 min to measure the relaxation response of the tissue. The history of radial stretch for the unconfined compression tests (both load–unload cycles and ramp-relaxation) was recorded using the video extensometer. The video capture frequencies for the load–unload cycle and the ramp-relaxation test were 2 and 0.2 Hz respectively. Fig. 3C shows a typical video image for an unconfined compression test.

For tensile tests, prior to loading, an airbrush pattern was applied to the ring-shaped tension specimens using India ink. A representative speckle pattern density is illustrated in Fig. 4A. The speckled cervical rings were extended along a diameter using 5 mm wide woven Kevlar strips, which were looped around the specimen and gripped in tensile jaws (Fig. 4). This testing configuration was selected to reduce stress concentration in the gripped region of the specimen, while adding negligible axial compliance to the grip assembly. Specimen and grip assembly were immersed

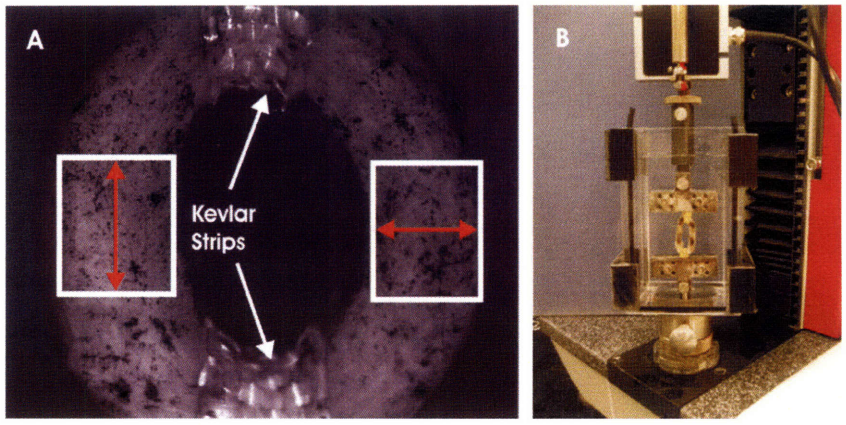

Fig. 4. Tension test configuration. (A) Representative speckle pattern for cervical tension specimens. Axial and lateral stretch histories are recorded for the boxed regions indicated in the figure, where the deformation is sufficiently homogeneous, and the stress state more closely approaches uniaxial tension. (B) Experimental fixture for cervical tension test. Two strips of woven Kevlar are looped around the specimen and gripped in tensile jaws.

in a PBS bath in an acrylic fixture (Fig. 4B). The inner diameter of the cervical ring was elongated at a rate of 0.05 mm s^{-1}. Multiple tension-loading cycles were imposed on each specimen, with 30 min of equilibration time between each cycle. Images of the deforming specimen were recorded at a frequency of 10 Hz. The two-dimensional strain field was obtained for the two central regions of the specimen as indicated in Fig. 3A using the Correlated Solutions Vic 2-D DIC software [34]. Axial and lateral stretch histories were then averaged for these mostly uniform regions of deformation. Based on lateral stretch history and initial specimen dimensions, a (true) axial stress history for the central region of the specimen was estimated.

2.3. Biochemical analysis

Cervical tissue was defatted and homogenized prior to all biochemical assays. Samples were defatted in acetone for 3 days at 4 °C and then homogenized by pulverizing approximately 20 mg of wet tissue in a stainless steel chamber cooled with liquid nitrogen. Collagen content was measured using a standard hydroxyproline assay [35]. The hydroxyproline content was obtained using a colorimetric procedure, and was converted into collagen content using a mass ratio of collagen to hydroxyproline of 7.64:1. Collagen content was normalized by tissue dry weight.

Collagen extractability was measured by extracting approximately 20 mg of wet pulverized tissue in 0.5 M acetic acid containing 1 mg ml^{-1} of pepsin (150 μl mg^{-1} wet tissue) for 3 days at 4 °C. The sample was centrifuged at 15,000*g* for 1 h and the supernatant and tissue pellet were stored at −80 °C. The hydroxyproline content was measured in the tissue pellet and the supernatant. The extractability is defined as the fraction of hydroxyproline in the supernatant compared to the total amount of hydroxyproline.

Sulfated GAG content was measured using a standard dimethylmethylene blue (DMB) assay [36] with chondroitin-6-sulfate (Sigma–Aldrich) as the standard. Approximately 20 mg of wet cervical tissue was pulverized and then freeze-dried overnight. The dry tissue was then incubated overnight in 1 ml of 0.1 mg ml^{-1} solution of proteinase K (Roche Applied Science). After incubation, the tissue was assayed for sulfated GAGs using a 1,9-dimethylmethylene blue dye (Polyscience Inc.).

3. Results

Mechanical and biochemical properties were measured for the NPPD, NPND and PCS (Refer to Table 1 for abbreviation definitions) clinical cases and averaged according to this classification. N_c represents the number of cervices and N_s represents the total number of specimens tested for each clinical case.

The appearance and the texture of cervical tissue were visibly different for the three clinical cases. The pregnant tissue was noticeably softer and the collagen network appeared to be loosely connected, in agreement with observations reported in the literature [4]. The nonpregnant tissue appeared fibrous, with a densely connected collagen network, especially for the NPND clinical cases.

3.1. Mechanical testing

Compression tests were performed, on cylindrical specimens, and Fig. 5 shows the averaged stress responses of the tissue to the load–unload compression cycles for the three clinical cases. The averaged peak stresses in Fig. 5 reflect an order of magnitude difference between the averaged responses for the NPND and PCS cases, and a substantial difference between the NPND and NPPD responses. Standard variations in peak stress (at 15% axial strain) for the three obstetric histories are reported in Table 3.

For constant strain rate load–unload cycles, the material displays a nonlinear response, with marked hysteresis. The first loading cycle is consistently associated with a stiffer response and more substantial hysteresis. The response in subsequent loading ramps becomes more compliant, while the unloading response is not substantially altered between cycles. This softening behavior with subsequent deformation cycles has been observed in other classes of soft tissues and is often referred to as "conditioning".

Fig. 6 shows the averaged stress responses of the tissue to the ramp-relaxation tests in unconfined and confined compression for the three clinical cases. Standard variations in

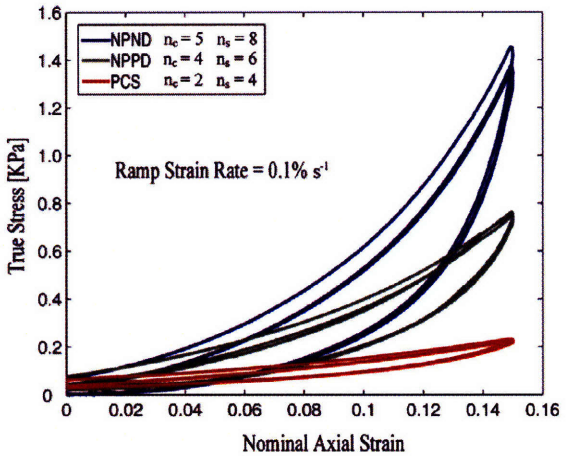

Fig. 5. Cervical stroma response to uniaxial compression cycles. Experimental curves were averaged for each obstetric case.

Table 3
Standard variation in peak stress values (at 15% axial strain) for the load–unload compression tests

Obstetric case	N_c	N_s	Standard variation in peak stress (kPa)
NPND	5	7	±1.2
NPPD	3	9	±0.4
PCS	2	3	±0.1

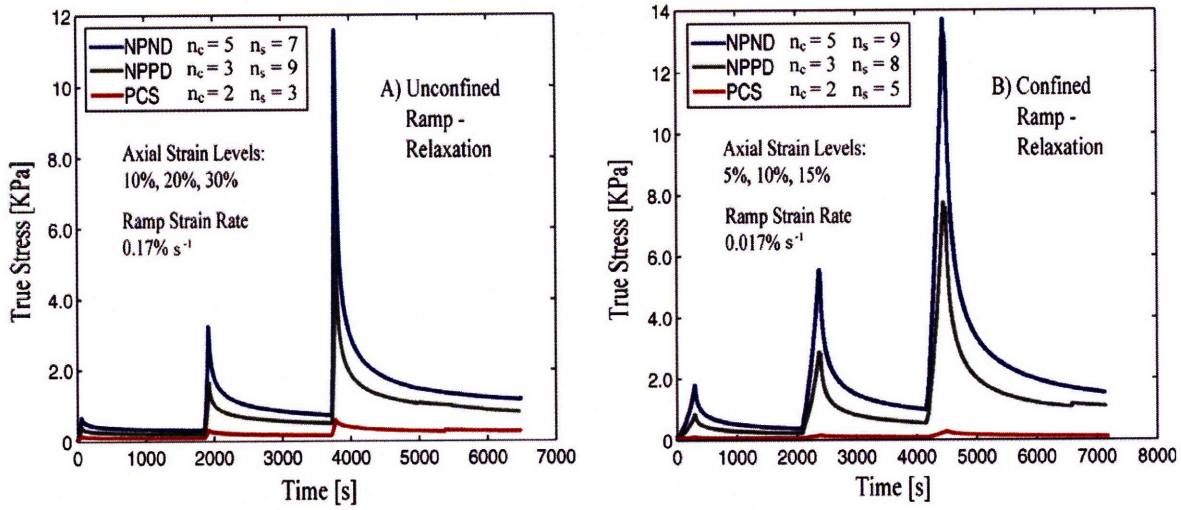

Fig. 6. Cervical stroma response to ramp-relaxation in (A) unconfined compression, and (B) confined compression. Experimental curves were averaged for each obstetric case.

Table 4
Peak and equilibrium stresses for unconfined compression

Obstetric case	N_c	N_s	10% Peak (kPa)	20% Peak (kPa)	30% Peak (kPa)	10% Equilibrium (kPa)	20% Equilibrium (kPa)	30% Equilibrium (kPa)
NPND	5	7	0.66 ± 0.46	3.2 ± 3.2	12 ± 14	0.31 ± 0.24	0.72 ± 0.53	1.2 ± 0.78
NPPD	3	9	0.39 ± 0.38	1.6 ± 2.3	6.0 ± 9.6	0.21 ± 0.17	0.50 ± 0.39	0.82 ± 0.76
PCS	2	3	0.15 ± 0.12	0.30 ± 0.24	0.56 ± 0.64	0.10 ± 0.06	0.17 ± 0.15	0.28 ± 0.23

Table 5
Peak and equilibrium stresses for confined compression

Obstetric case	N_c	N_s	5% Peak (kPa)	10% Peak (kPa)	15% Peak (kPa)	5% Equilibrium (kPa)	10% Equilibrium (kPa)	15% Equilibrium (kPa)
NPND	5	9	1.8 ± 3.7	5.6 ± 9.4	14 ± 17	0.38 ± 0.57	0.99 ± 1.1	1.5 ± 1.4
NPPD	3	8	0.82 ± 2.0	2.9 ± 5.7	7.8 ± 13	0.23 ± 0.40	0.55 ± 0.78	1.1 ± 1.2
PCS	2	5	0.12 ± 0.07	0.17 ± 0.10	0.28 ± 0.18	0.07 ± 0.07	0.10 ± 0.08	0.12 ± 0.08

peak stresses and equilibrium stresses are reported in Tables 4 and 5. There is a trend towards significantly decreased amplitude in the stress response of pregnant tissue when compared to nonpregnant tissue ($p = 0.1$, Student's t-test) and in NPPD tissue when compared to NPND tissue ($p = 0.1$, Student's t-test). These findings are consistent with the clinical observation that pregnant tissue is softer than nonpregnant tissue, and women with previous deliveries tend to have a softer cervix when compared to women who have not delivered vaginally.

Averaged transverse stretch histories for the three clinical cases in unconfined ramp-relaxation tests are reported in Fig. 7. The results indicate that the specimens undergo a substantial volume change in unconfined compression tests. Error bars are not indicated in the figure to avoid cluttering, but typical variations among specimens were of order ± 0.03. This large variation in transverse stretch measurements was probably due to tissue anisotropy and

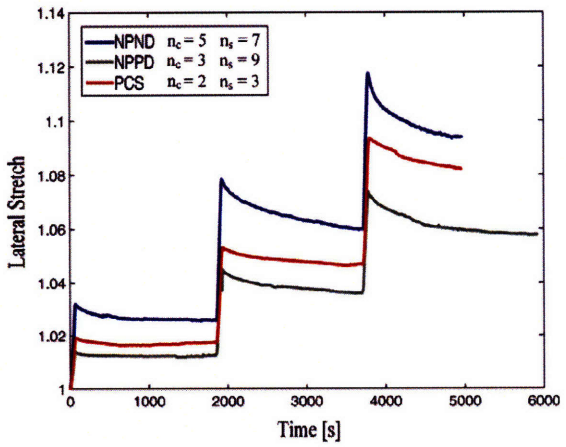

Fig. 7. Radial transverse stretch of specimens subjected to ramp-relaxation unconfined compression. Experimental curves were averaged for each obstetric case.

specimen orientation inconsistencies: the loading direction is "anatomically" consistent for all specimens (longitudinal in the cervix, i.e. parallel to the direction of the inner canal, see Fig. 2). However the orientation of each specimen with respect to radial and circumferential direction in the cervix was not recorded or marked on each specimen, and the transverse direction for which the stretch was recorded was not anatomically consistent among specimens.

Figs. 8 and 9 show the results for preliminary tension experiments conducted on cervical specimens with different obstetric backgrounds and different anatomical locations. Fig. 8. shows results from three specimens taken from cervices with different obstetric backgrounds. Fig. 9 shows results from two specimens taken from the same pregnant cervix, where the specimens were taken from different anatomical sites. Results are presented in terms of averaged true stress vs. averaged axial stretch in the central regions of the specimens, as discussed in Section 2. Fig. 8 shows that pregnant tissue is found to be orders of magnitude more compliant than nonpregnant tissue. This result confirms trends identified in the compression tests. Further, Fig. 8 indicates no significant difference in the stress–stretch response for the two nonpregnant cases. Fig. 9 shows that the stress response of cervical tissue is dependent on anatomical site. The specimen taken closer to the external os has a stiffer stress response when compared to the specimen taken closer to the internal os. This result is consistent with clinically observed progression in cervical ripening.

The tensile response of the tissue is extremely nonlinear, with a degree of hysteresis that increases with the level of applied deformation. Similar to the findings for compressive axial deformation, the response of nonpregnant cervical tissue experienced a degree of conditioning during the first loading cycle, and then stabilized in subsequent cycles. Conversely, the pregnant tissue continued to elongate with each loading cycle.

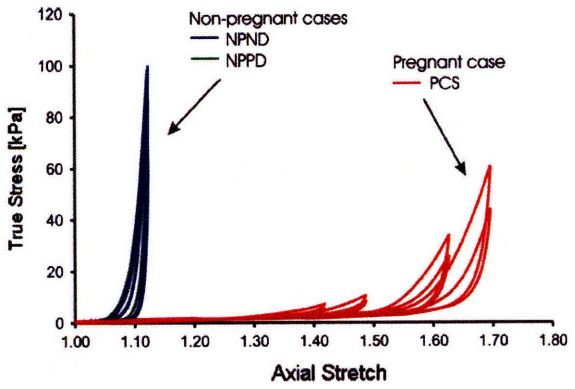

Fig. 8. Cervical stroma response in tension for three specimens from three patients with different obstetric backgrounds. Between each cycle, the unloaded specimen was equilibrated for 30 min in PBS.

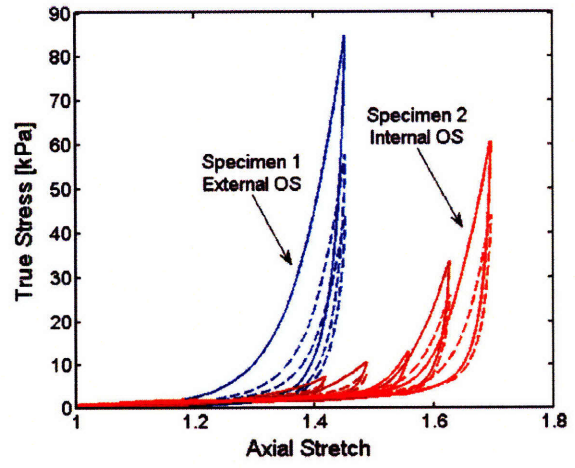

Fig. 9. Cervical stroma response in tension for two specimens from a single pregnant cervix. Specimen 1 was taken close to the external OS, and specimen 2 was taken close to the internal OS. Between each cycle, the unloaded specimen was equilibrated for 30 min in PBS.

3.2. Biochemical analysis

Cervical tissue samples for the three (NPND, NPPD and PCS) clinical cases were subjected to biochemical analysis. Biochemical assays measured cervical tissue hydration, collagen content, collagen extractability and sulfated GAG content. Table 6 reports the biochemical content measured for the three clinical cases. Data were averaged among cervices with the same obstetric history. Table 6 gives both average values and standard deviations over the number of samples (N_s) analyzed for each assay. A significant ($p < 0.05$, Student's t-test) difference in hydration and collagen extractability was established between pregnant and nonpregnant specimens. Pregnant tissue was more hydrated and its collagen network was more soluble in acetic acid when compared to the nonpregnant tissue samples. There was no statistically significant difference in hydration and collagen extractability when comparing the two nonpregnant cases. Further there was no significant difference in collagen content among all clinical cases. Lastly, a limited number of pregnant samples were tested for sulfated GAG content. The results indicate a

Table 6
Results of biochemical assays

Obstetric case	Hydration	Collagen content (% per dry weight)	Collagen extractability	Sulfated GAGs (% per dry weight)
NPND	$73.8 \pm 5.9\%$ $N_c = 5$ $N_s = 40$	$71.0 \pm 8.6\%$ $N_c = 3$ $N_s = 25$	$28.6 \pm 5.9\%$ $N_c = 2$ $N_s = 6$	$1.20 \pm 0.74\%$ $N_c = 5$ $N_s = 21$
NPPD	$76.7 \pm 2.0\%$ $N_c = 8$ $N_s = 80$	$77.5 \pm 8.3\%$ $N_c = 5$ $N_s = 18$	$33.1 \pm 6.1\%$ $N_c = 4$ $N_s = 8$	$1.53 \pm 0.16\%$ $N_c = 4$ $N_s = 20$
PCS	$87.2 \pm 1.6\%$ $N_c = 1$ $N_s = 3$	$77.6 \pm 9.8\%$ $N_c = 2$ $N_s = 8$	$78.5 \pm 1.1\%$ $N_c = 2$ $N_s = 6$	$5.52 \pm 2.29\%$ $N_c = 1$ $N_s = 2$

substantial increase in sulfated GAG content in pregnant tissue when compared to nonpregnant tissue. There was no difference measured in sulfated GAGs when comparing the two nonpregnant cases.

4. Discussion

This study had two complementary objectives: (i) the establishment of a stringent experimental protocol to collect data on the biochemical composition and mechanical properties of cervical tissue under different loading modes; (ii) a preliminary investigation of normal ranges of variation in tissue properties for nonpregnant and pregnant patients. Here we discuss the motivation and implications of our testing protocols, discuss the experimental results, explain the sources of variability in the experimental findings, and suggest changes to the current experimental protocol for future studies.

4.1. Discussion of the testing protocol

The motivation behind the selected modes of deformation, strain levels and strain rates arises from physiological considerations, ranges of operation of the test equipment and mechanical modeling concerns. This extensive experimental characterization of the mechanical tissue response was necessary to guide the development of an appropriate constitutive model for cervical stroma [37]. The experimental protocol was designed so as to provide sufficient data to uniquely determine the constitutive material parameters that describe the mechanical behavior of each cervical specimen [37]. The advantage of testing each cervical specimen in both confined and unconfined compression is that these combined protocols provide sufficient data to characterize the three-dimensional, poroelastic and viscoelastic nature of the tissue response [38–40]. Confined compression tests impose larger volume changes, and the experimental response is typically interpreted in a poroelastic framework to provide estimates for the (strain-dependent) hydraulic permeability of the tissue [41]. Unconfined compression tests typically result in larger levels of shear deformation. The three-dimensional behavior of the tissue is captured by the lateral stretch measurements taken by the video extensometer.

The rationale for testing samples along the longitudinal direction in compression tests, and testing samples along the circumferential direction in tensile tests arises, from physiological considerations [42,28] and from preliminary results of finite element analyses (FEA) of the loading conditions in pregnant patients [43]. Gravity, intrauterine pressure and the weight of the fetus impose a complex three-dimensional stress state on the cervix: the weight of the fetus gives rise to compression loads in the longitudinal direction, and the resistance to cervical dilation gives rise to tensile loads in the circumferential direction [42,43].

Strain levels and strain rates were selected on the basis of preliminary experimental investigations [37]. Strain levels were selected to meet the criteria that they should not cause damage to the specimens, but should be high enough to capture the nonlinearity of the tissue response. Physiologically, the strain rates experienced in vivo by the tissue under time-varying loading conditions (gravity, uterine contractions, etc.) will vary widely among patients. Strain rates for the load–unload cycles and for the ramp loading in relaxation tests reflect the short loading times characteristic of physiological conditions such as uterine contractions and temporary increases in intra-abdominal pressure (e.g. from coughing). The relaxation transient is meant to capture longer-term (and equilibrium) tissue response. The strain rate for the tension test protocol is similar to the rate adopted in the tension tests by Conrad et al. [28]. Also, strain rates were selected so as to meet the following criteria: (i) the load did not exceed the limit of the load cell; (ii) the tissue samples were not damaged during loading; (iii) inertial effects could be neglected; and (iv) the time-dependent nature of the tissue response (hysteresis, relaxation) could be captured. The characteristic relaxation times in confined compression experiments are dominated by the effects of fluid diffusion and are higher than the characteristic relaxation times in unconfined compression. To avoid overloading the specimen and load cell, lower strain levels and strain rates were selected for confined compression tests.

We found that, to obtain repeatable results, a number of precautions were necessary. First, to prevent tissue degradation, the cervical slices were stored at −80 °C at time of excision until the experiments were performed. Second, to eliminate transient effects associated with swelling, mechanical specimens were equilibrated overnight in PBS at 4 °C prior to testing.

The hydration levels of the stroma significantly affect its mechanical response. As mechanical specimens are excised from the surrounding tissue, constraints from the interconnected collagen network are relaxed. Freezing the tissue can also result in partial loss of hydration. When the excised tissue is placed in saline at physiological concentration, the specimen swells to reach a new equilibrium state at a higher hydration level. Typical swelling curves for compression specimens are shown in Fig. 10 where the wet weights of two specimens are plotted as a function of the hydration time in PBS. These curves display a rapid rise in hydration level, immediately following the placement of the specimen in saline, with exponentially decreasing hydration rates over time. Typical characteristic time constants for this hydration transient (~5 h) are comparable with testing time intervals. If a specimen is not allowed to equilibrate properly prior to testing, the testing results will be confounded by the superposition of effects due to the hydration process.

Fig. 11 demonstrates the significant influence of hydration levels on the measured mechanical properties. Two compression samples were excised from the same cervical slice and tested after short hydration intervals (1.5 and 3 h). The sample that was allowed to hydrate for a longer

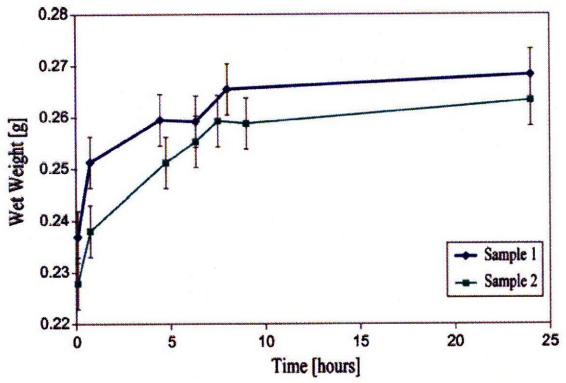

Fig. 10. Swelling curve from two compression specimens obtained from the same cervical slice.

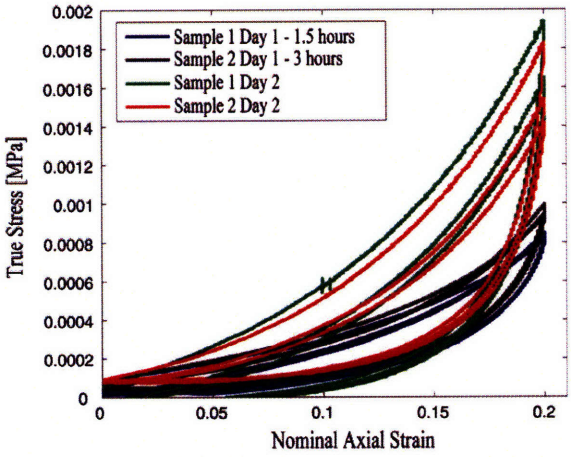

Fig. 11. Uniaxial load–unload compression cycle response for different equilibration times. The two specimens were obtained from the same cervical slice.

interval displayed a stiffer response. The same specimens were then placed in saline, equilibrated overnight and retested. A noticeably stiffer response was obtained for the fully equilibrated specimens. Interestingly, the sample that had originally appeared stiffer proved to be the more compliant of the two when equilibrated. It could be argued that the adopted equilibration protocol alters the tissue properties from their in vivo state. However, the purpose of this investigation was not to obtain absolute values of tissue properties, but rather to identify overall qualitative features of the tissue response and to investigate relative variations in properties between specimens from patients with different obstetric histories. The equilibration protocol is evenly applied to all samples, and the increased hydration level only affects the amplitude of the stress response and not the qualitative feature of the curves. For the purpose of this investigation, the effects of the equilibration step are therefore inconsequential. In future studies, we propose to use a stronger ionic bath, both in the equilibration and in the mechanical testing procedures, to limit the swelling of the tissue and reach equilibrium hydration levels comparable to the in vivo levels.

4.2. Discussion of results

Many observations about the characteristics of the material response can be used to guide the development of an appropriate constitutive model for the mechanical behavior of cervical stroma. The stress–strain behavior is noticeably nonlinear both in tension and compression, with a much stiffer response when the tissue is loaded in tension: in nonpregnant tissue, for strain levels of approximately 10%, there are two orders of magnitude between the corresponding stress levels in tension (~100 kPa) and compression (~1 kPa). The nonlinearity of the stress–strain behavior is also reflected in the relationship between peak stresses and strains for the ramp-relaxation results in confined and unconfined compression. Conversely, for both unconfined and confined compression tests, and for all three clinical cases, the increase in equilibrium stresses with axial strain was nearly linear. While the peak stress levels for the nonpregnant specimens were an order of magnitude higher than the equilibrium levels, the peak stress levels for the pregnant specimens were not substantially higher than the equilibrium levels. Since fluid diffusion controls the transient peak response, this result is consistent with qualitative observations of the tissue morphology: much higher hydraulic permeability coefficients are probably associated with the loosely connected pregnant tissue.

The data suggest that the relaxation behavior is associated with at least two separate mechanisms. The first mechanism occurs in a very short time interval (~10 s) with substantial relaxation immediately following the loading ramp. After this sharp stress drop, the stress continues to decrease at a much lower rate, suggesting the presence of a second relaxation mechanism with a much larger characteristic decay time. A relaxed state is only partially attained at the end of the 30 min relaxation interval. Also, relaxation times are slightly reduced for the unconfined compression cases, possibly due to differences associated with the transient diffusion of interstitial fluid. This difference arises because the surface of the unconfined specimens in contact with the bathing solution is nearly doubled. Furthermore, the confined compression configuration imposes a volumetric strain on the tissue equal to the axial strain, while in the unconfined compression configuration the specimen is free to expand radially (friction effects between specimen and compression platens are negligible). In the unconfined compression configuration the volumetric strains (and thus interstitial fluid outflow) are therefore controlled by the balance between the bulk and shear stiffness of the specimen.

Although the unconfined compression test subjects the specimens to 2-fold levels of axial strain, and a 10-fold ramp strain rate, as compared to the confined compression tests, the recorded peak stresses and equilibrium stresses are comparable for the two testing modes.

4.3. Variability in mechanical measurements

In agreement with the findings of Conrad et al. [28], we noted some degree of variability in stroma properties for samples excised from the same cervix but at different anatomical sites. On average, the maximum variability for samples taken from the same cervix was ±0.2 kPa for equilibrium and ±2.4 kPa for peak stress at 30% axial strain in unconfined compression. In general, there is a larger variability in tissue properties between patients (even patients with the same obstetric history) than between specimens from the same cervix. The standard variation in the stress levels reported in Tables 3–5 is due to the combined effects of variability among different patients and different cervical anatomical sites.

Preliminary histological studies were performed on stained stroma samples from human cervices obtained from hysterectomy specimens [37]. We were not able to identify a substantial degree of anisotropy in the arrangement of the collagen bundles; therefore, effects of specimen orientation were not expected to be significant, and during unconfined compression experiments no particular care was taken to align the transverse direction consistently among specimens. In other words, it was unknown if the lateral stretch measured from the video extensometer was associated with the circumferential, radial or any intermediate direction within the cervix. A large variability was noted in the lateral stretch measurements. If the tissue is anisotropic, then the lateral stretch will be dependent on tissue orientation and the variability in the findings can be easily explained. Possible effects of anisotropy on the tissue response are currently under investigation. For future experiments, we propose to cut the tissue into rectangular blocks and mark the orientation of the orthogonal anatomical planes. We believe that, by marking the cervix orientation on the testing specimens, variability will be reduced for the lateral stretch measurements.

4.4. Comparison between biochemistry analysis results and literature data

The biochemical measurements reported herein are in good agreement with previously reported biochemical results for human cervical tissue. Previous studies by Danforth et al. [23], Petersen et al. [15] and Rechberger et al. [14] reported significant differences in hydration and collagen extractability between nonpregnant and pregnant tissue samples. Table 7 summarizes these previous findings. All three investigations report that pregnant tissue is more hydrated than nonpregnant tissue. Furthermore, Petersen et al. concluded that collagen extractability is higher in NPPD tissue as compared to NPND tissue [15]. Rechberger et al. measured higher collagen extractability in pregnant tissue as compared to nonpregnant tissue [14]. Total collagen content and sulfated GAG measurements also fall within the range of data in the literature. Shimuzu et al. [44] measured 0.75% and 0.97% sulfated GAGs per dry weight of tissue for nonpregnant and pregnant tissue, respectively. Petersen et al. [15] measured 94.4% and 73.6% collagen content per dry weight of tissue for NPND and NPPD cervical tissue, respectively.

5. Conclusions and future work

The mechanical properties of biological tissue can be drastically altered by relatively small modifications in its biochemistry. Nature modulates the mechanical properties of cervical tissue by subtle readjustments of its composition. The compliance of cervical stroma changes by orders of magnitude when the pregnancy nears term. A remarkable change in macroscopic properties is accomplished through subtle shifts in biochemical constituents. The total collagen content remains almost unchanged, while more significant changes are seen in collagen crosslinking and the relative quantities of sulfated GAGs and hyaluronic acid. The experimental results presented in Section 3 indicate that there is a correlation between obstetric history and biochemical and mechanical properties of the tissue. The results of this study also confirm that higher collagen extractability and hydration levels are associated with more compliant tissue behavior.

Future work will focus on improving the statistical power of this study, investigating the anisotropy of the tissue, exploring the electrical properties of individual classes of GAGs, improving the configuration of the tension specimens, and investigating the tissue's swelling properties. As stated in Section 4.3, we plan to investigate tissue anisotropy by loading marked tissue samples in different directions and measuring the lateral strain in both transverse directions. Studies by Petersen found that the mechanical properties were dependent on the direction of loading, where tissue cut in the longitudinal direction had a higher creep rate when compared to tissue cut in the circumferential direction [7]. We are also developing protocols to quantify the concentrations of distinct GAGs by fluorophore-assisted carbohydrate electrophoresis (FACE) [45]. Studies by Osmer et al. [16] and von Maillot et al. [9] investigated the importance of the relative concentrations of

Table 7
Summary of hydration and collagen extractability data available in the literature

Study	Hydration non-pregnant	Hydration pregnant	Extractability NPND	Extractability NPPD	Extractability pregnant
Danforth [23]	74.4%	78.4%	N/A	N/A	N/A
Petersen [15]	76.7%	79.5%	42.6%	49.5%	N/A
Rechberger [14]	81.1%	83.7%	Average: 68.8%		90.8%

different GAGs during pregnancy and labor. It has been shown that the shift in GAG concentration among hyaluronic acid, dermatan sulfate and the chondroitin sulfates facilitates cervical softening during labor. It has also been shown that the finer structure of the GAG relating to the length of the GAG disaccharide chain and the degree of sulfation is important in the biomechanics of hydrated tissue (e.g. in cornea tissue [46] and osteoarthritic cartilage [47]). Our current DMB assay only measures total sulfated GAG content. The DMB assay does not characterize the electrostatic properties of the distinct GAG chains and cannot measure the hyaluronic acid content. The new FACE assay will allow us to overcome these limitations and will provide another means to differentiate the biomechanical properties of cervical specimens. Further, we will investigate the swelling properties of cervical stroma samples by exposing samples to different ionic bath concentrations and measuring their hydration. Currently, no studies in the literature have explored the electrical properties of cervical stroma. Therefore, the FACE analysis and swelling studies will explore the role of the GAG electrical interactions in the mechanical integrity of the cervical stroma.

This study represents a first important step towards the attainment of an improved understanding of the complex interplay between the molecular structure of the tissue and its macroscopic mechanical properties. This study established mechanical testing and biochemical analysis protocols that will provide the foundation for our investigation of structure–property relations in cervical tissue.

Acknowledgements

We acknowledge the support of the Whitaker Foundation Biomedical Engineering Research Grant RG-02-0803, the National Science Foundation Graduate Research Fellowship, and the Society for Maternal Fetal Medicine – American Association of Obstetrician Gynecologists Foundation Scholarship. The authors thank Dr. Robert Kokenyesi and Dr. Phyllis Leppert for their kind help and guidance on the biochemistry analysis, Professor Alan Grodzinsky and Dr. Han-Hwa Hung for advice and guidance on the testing protocols. We also appreciate the support of the Departments of Gynecology and Pathology at the Tufts – New England Medical Center for providing hysterectomy specimens.

References

[1] Owen J, Iams JD, Hauth JC. Vaginal sonography and cervical incompetence. Am J Obstet Gynecol 2003;188(2):586–96.
[2] Hofmeyr GJ. Obstructed labor: using better technologies to reduce mortality. Int J Gynaecol Obstet 2004;85(Suppl. 1):S62–72.
[3] Winkler M, Rath W. Changes in the cervical extracellular matrix during pregnancy and parturition. J Perinat Med 1999;27:45–61.
[4] Leppert PC. Anatomy and physiology of cervical ripening. Clin Obstet Gynecol 1995;38(2):267–79.
[5] Uldbjerg N, Ekman G, Malmstrom A, Olsson K, Ulmsten U. Ripening of the human uterine cervix related to changes in collagen, glycosaminoglycans, and collagenolytic activity. Am J Obstet Gynecol 1983;147(6):662–6, November 15.
[6] Danforth DN. The fibrous nature of the human cervix, and its relation to the isthmic segment in gravid and nongravid uteri. Am J Obstet Gynecol 1947;53(4):541–60.
[7] Petersen LK, Oxlund H, Uldbjerg N, Forman A. In vitro analysis of muscular contractile ability and passive biomechanical properties of uterine cervical samples from nonpregnant women. Obstet Gynecol 1991;77(5):772–6.
[8] Kleissl HP, Van Der Rest M, Naftolin F, Glorieux FH, De Leon A. Collagen changes in the human uterine cervix at parturition. Am J Obstet Gynecol 1978;130:748–53.
[9] von Maillot K, Stuhlsatz HW, Gentsch HH. Connective tissue changes in the human cervix in pregnancy and labour. In: Ellwood DA, Anderson ABM, editors. The cervix in pregnancy and labour: clinical and biochemical investigations. New York: Churchill Livingston Inc.; 1981 [chapter 9].
[10] Leppert P, Yu S. Elastin and collagen in the human uterus and cervix: biochemical and histological correlation. In: Leppert PC, Woessner JF, editors. The extracellular matrix of the uterus, cervix and fetal membranes: synthesis, degradation and hormonal regulation. Perinatology Press; 1991 [chapter 5].
[11] Danforth DN. The morphology of the human cervix. Clin Obstet Gynecol 1983;26(1):7–13.
[12] Theobald PW, Rath W, Kühnle H, Kuhn W. Histological and electron-microscopic examinations of collageneous connective tissue of the non-pregnant cervix, the pregnant cervix, and the pregnant prostaglandin-treated cervix. Arch Gynecol 1982;231:241–5.
[13] Uldbjerg N, Ekman G, Malmström A, Sporrong B, Ulmsten U, Wingerup L. Biochemical and morphological changes of human cervix after local application of prostaglandin E2 in pregnancy. The Lancet 1981;31:267–8.
[14] Rechenberger T, Uldbjerg N, Oxlund H. Connective tissue changes in the cervix during normal pregnancy and pregnancy complicated by cervical incompetence. Obstet Gynecol 1988;71:563–7.
[15] Petersen LK, Uldbjerg N. Cervical collagen in non-pregnant women with previous cervical incompetence. Eur J Obstet Gynecol Reprod Biol 1996;67:41–5.
[16] Osmers R, Rath W, Pflanz MA, Kuhn W, Stuhlsatz HW, Szeverényi M. Glycosaminoglycans in cervical connective tissue during pregnancy and parturition. Obstet Gynecol 1993;81:88–92.
[17] Rath W, Osmers R, Szeverényi M, Stuhlsatz HW, Kuhn W. Changes of glycosaminoglycans in cervical connective tissue. In: Leppert PC, Woessner JF, editors. The extracellular matrix of the uterus, cervix and fetal membranes: synthesis, degradation and hormonal regulation. Perinatology Press; 1991 [chapter 18].
[18] Danielson KG, Baribault H, Holmes DF, Graham H, Kadler KE, Iozzo V. Targeted disruption of decorin leads to abnormal collagen fibril morphology and skin fragility. J Cell Biol 1997;136(3):729–43, February 10.
[19] Kokenyesi R, Armstrong LC, Agah A, Artal R, Bornstein P. Thrombospondin 2 deficiency in pregnant mice results in premature softening of the uterine cervix. Biol Reprod 2004;70:385–90.
[20] Takemura M, Itoh H, Sagawa N, Yura S, Korita D, Kakui K, et al. Cyclic mechanical stretch augments hyaluronan production in cultured human uterine cervical fibroblasts cells. Mol Hum Reprod 2005;11(9):659–65.
[21] Yoshida M, Sagawa N, Itoh H, Yura S, Takemura M, Wada Y, et al. Prostaglandin F2a, cytokines and cyclic mechanical stretch augment matrix metalloproteinase-1 secretion from cultured human uterine cervical fibroblast cells. Mol Hum Reprod 2002;8(7):681–7.
[22] Friedman EA, Kroll BH. Computer analysis of labor progression III. Pattern variations by parity. J Reprod Med 1971;6(4):63–7.
[23] Danforth DN, Veis A, Breen M, Weinstein HG, Buckingham JC, Manalo P. The effect of pregnancy and labor on the human cervix: changes in collagen, glycoproteins, and glycosaminoglycans. Am J Obstet Gynecol 1974;120(3):641–51.

[24] Granstrom L, Ekman G, Malmstrom A. Insufficient remodeling of the uterine connective tissue in women with protracted labour. Br J Obstet Gynaecol 1994;116:502–13.
[25] Garfield RE, Maul H, Maner W, Fittkow C, Olson G, Shi L, et al. Uterine electromyography and light-induced fluorescence in the management of term and preterm labor. J Soc Gynecol Investig 2002;9:265–75.
[26] Harkness MLR, Harkness RD. Changes in the physical properties of the uterine cervix of the rat during pregnancy. J Physiol 1959;148:524–47.
[27] Stys SJ, Clewell WH, Meschia G. Changes in cervical compliance at parturition independent of uterine activity. Am J Obstet Gynecol 1978;130(4):414–8.
[28] Conrad JT, Tokarz RD, Williford JF. Anatomic site and stretch modulus in the human cervix. In: Naftolin F, Stubblefield PG, editors. Dilatation of the uterine cervix: connective tissue biology and clinical management. New York: Raven Press; 1980. p. 255–64.
[29] Bishop EH. Pelvic scoring for elective induction. Obstet Gynecol 1964;24(2):266–8.
[30] Bakke T. Cervical consistency in women of fertile age measured with a new mechanical instrument. Acta Obstet Gynec Scand 1974;53: 293–302.
[31] Cabrol D. Cervical distensibility changes in pregnancy, term, and preterm labor. Semin Perinatol 1991;15(2):133–9.
[32] Mazza E, Nava A, Bauer M, Winter R, Bajka M, Holzapfel GA. Mechanical properties of the human uterine cervix: An in vivo study. Med Image Anal 2006;10(2):125–36.
[33] Kiefer GN, Sundby K, McAllister D, Shrive NG, Frank CB, Lam T, et al. The effect of cryopreservation on the biomechanical behavior of bovine articular cartilage. J Orthop Res 1989;7(4):494–501.
[34] Parsons EM, Boyce MC, Parks DM, Weinberg M. Three-dimensional large-strain tensile deformation of neat and calcium carbonate-filled high-density polyethylene. Polymer 2005;46:2257–65.
[35] Woessner JF. Determination of hydroxyproline in connective tissues. In: Hall DA, editor. Methodology of connective tissue research. Oxford: Joynson–Bruvvers Ltd.; 1976. p. 976.
[36] Farndale RW, Sayers CA, Barett AJ. A direct spectrophotometric microassay for sulfated glycosaminoglycans in cartilage cultures. Connect Tissue Res 1982;9:247–8.
[37] Febvay S. A three-dimensional constitutive model for the mechanical behavior of cervical tissue. Master's thesis, Massachusetts Institute of Technology, Cambridge, MA; 2003.
[38] Eisenberg SR, Grodzinsky AJ. Swelling of articular cartilage and other connective tissue: electromechanochemical forces. J Orthop Res 1985;3(2):148–59.
[39] Bursac PM, Obitz TW, Eisenberg SR, Stamenovic D. Confined and unconfined stress relaxation of cartilage: appropriateness of a transversely isotropic analysis. J Biomech 1999;32:1125–30.
[40] Chen AC, Bae WC, Schinagl RM, Sah RL. Depth- and strain-dependent mechanical and electromechanical properties of full-thickness bovine articular cartilage in confined compression. J Biomech 2001;34:1–12.
[41] Ateshian GA, Warden WH, Kim JJ, Grelsamer RP, Mow VC. Finite deformation biphasic material properties of bovine articular cartilage from confined compression experiments. J Biomech 1997;30:1157–64.
[42] Aspden RM. Collagen organisation in the cervix and its relation to mechanical function. Collagen Rel Res 1988;8:103–12.
[43] House M, Paskaleva A, Myers K, Febvay S, Socrate S. The biomechanics of cervical funneling: the effect of stroma properties, anatomic geometry and pelvic forces on funnel formation. Am J Obstet Gynecol 2004;191(6):S17.
[44] Shimizu T, Endo M, Yosizawa Z. Glycoconjugates (glycosaminoglycans and glycoproteins) and glycogen in the human cervix uteri. Tohoku J Exp Med 1980;131:289–99.
[45] Calabro A, Hascall VC, Midura RJ. Adaptation of FACE methodology for microanalysis of total hyaluronan and chondroitin sulfate composition from cartilage. Glycobiology 2000;10(3):283–93.
[46] Plaas AH, West LA, Thonar EJA, Karcioglu AZ, Smith CJ, Klintworth GK, et al. Altered fine structures of corneal and skeletal keratin sulfate and chondroitin/dermatan sulfate in macular corneal dystrophy. J Biol Chem 2001;276(43):39788–96, October 26.
[47] Plaas AH, West LA, Wong-Palms S, Nelson FR. Glycosaminoglycan sulfation in human osteoarthritis. J Biol Chem 1998;273(20):12642–9, May 15.

Appendix B

Additional Data and Model Fits from Anisotropy Study

SAMPLE		c = compression t = tension	Direction of Loading	E [Pa]		fv	So [Pa]	n	eta	Eback [Pa]	E (hand fit) [Pa]
	3-Mar-06	NPND									
	NPND	cx3C1	circum	478.56	31.84	1.00	45930.39	1.34	0.000600	6181.86	3400.00
	Patient 1	cx3C1	long	272.68	34.60	1.00	43005.53	1.21	0.000540	4991.84	1800.00
		cx3T1	circum	2355.88	45.64	0.93	12251.24	1.23	0.000023	22133.81	8100.00
	16-Feb-06										
	NPND	cx4T1	circum	1860.36	49.61	0.88	124351.41	1.65	0.000108	148505.84	14300.00
	Patient 2										
	15-May-06										
	NPND	cx4C1	circum	41.25	40.62	1.00	19300.63	1.17	0.000106	8789.91	4700.00
	Patient 3	cx4C1	long	41.66	41.66	1.00	39724.30	1.00	0.000150	9531.44	2600.00
		cx4C2	circum	43.78	43.74	1.00	27215.27	1.14	0.000130	9424.43	6300.00
		cx4C2	long	33.37	33.27	1.00	4160.01	1.08	0.000010	11659.70	2500.00
	22-Jan-07										
	NPPD	cx4C2	circum	45.14	38.09	1.00	19763.82	1.15	0.000144	8220.05	4300.00
	Patient 1	cx4C2	long	44.01	42.11	1.00	27879.89	1.11	0.000156	8319.11	2700.00
		cx4T1	circum	4690.10	42.91	1.00	71031.23	2.38	0.000017	809132.21	24700.00
		cx4T2	circum	7198.88	46.07	1.00	122554.09	2.21	0.000028	854773.96	31400.00
	21-Feb-07										
	NPPD	cx4C1	circum	940.96	11.92	1.00	5490.83	1.57	0.000467	3397.51	2600.00
	Patient 2	cx4C1	long	160.70	26.64	1.00	6803.18	1.17	0.000255	1434.26	1700.00
		cx4C2	circum	346.29	28.79	1.00	11238.80	1.21	0.000111	5902.97	4000.00
		cx4C2	long	233.57	29.49	1.00	2539.89	1.22	0.000021	4878.29	3100.00
		cx3C1	circum	667.59	11.19	1.00	4708.86	1.19	0.000169	2184.46	1500.00
		cx3C1	long	236.14	21.89	1.00	12939.37	1.19	0.000845	1114.50	900.00
		cx3C2	circum	101.24	25.31	1.00	8732.99	1.35	0.000440	2800.00	1800.00
		cx3C2	long	119.66	34.87	1.00	9730.19	1.29	0.000261	2414.16	1900.00
		cx3C3	circum	602.73	6.83	1.00	6611.41	1.68	0.003198	908.37	1000.00
		cx3C3	long	136.90	19.96	1.00	4318.66	1.75	0.003181	1037.90	600.00
		cx3C4	circum	663.64	6.77	1.00	113758.28	1.08	0.010000	1567.69	1000.00
		cx3C4	long	186.07	13.21	1.00	120210.67	1.00	0.009678	864.87	500.00
		cx3T2	circum	3887.01	35.47	0.91	31156.06	1.92	0.000265	56318.70	19600.00
	22-Feb-07										
	PCS	cx2C1	circum	364.18	4.69	1.00	259.27	2.00	0.000071	484.71	300.00
	Patient 1	cx2C1	long		DAMAGED						
		cx2C2	circum	317.82	6.36	1.00	2579.69	1.79	0.004098	536.59	500.00
		cx2C2	long		DAMAGED						
		cx2T3	circum	1912.32	18.96	0.99	23203.45	1.68	0.001316	17046.07	5300.00
	2-May-07										
	PCS	cx4C1	circum	493.56	8.89	1.00	16063.04	1.24	0.002542	1173.17	700.00
	Patient 2	cx4C1	long		DAMAGED						
		cx4C2	circum	510.48	8.98	1.00	6009.62	1.78	0.006888	1408.04	1000.00
		cx4C2	long		DAMAGED						
		cx4T1	circum	3388.43	3.38	1.00	14445.79	1.11	0.000011	16487.67	4300.00
	24-May-07										
	NPPD	cx3C1	circum	274.29	19.86	1.00	6021.93	1.23	0.000110	4078.96	1000.00
	Patient 3	cx3C1	long	329.09	15.39	1.00	11185.25	1.42	0.000414	3426.37	900.00
		cx3C2	circum	272.99	21.18	1.00	6150.27	1.29	0.000065	6483.55	1000.00
		cx3C2	long	64.75	27.35	1.00	3081.61	1.22	0.000024	6168.16	500.00
		cx2c1	circum	237.70	26.78	1.00	29982.29	1.21	0.000299	6497.53	2300.00

Figure B-1: Best-fit material properties for cervical samples in Chapter 3.

Appendix C

Second Harmonic Generation Images

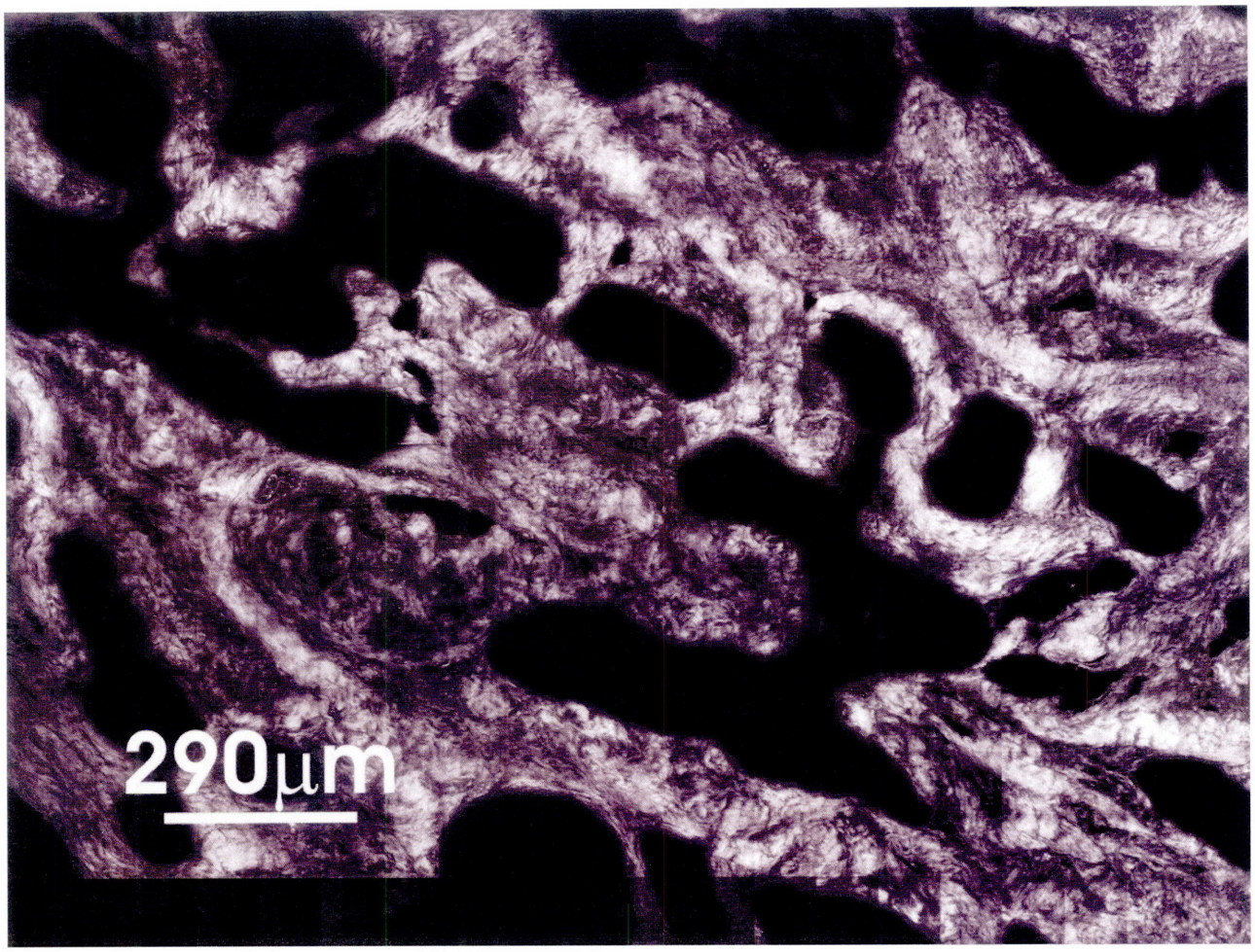

Figure C-1: A second harmonic image of nonpregnant cervical tissue. The plane of this image is perpendicular to the longitudinal direction of the cervix. This specimen was taken from NPPD patient 2 (refer to Table 3.1). Images taken by Dimitrios Tzeranis from the So Lab - Bioinstrumentation Engineering Analysis and Microscopy at MIT.

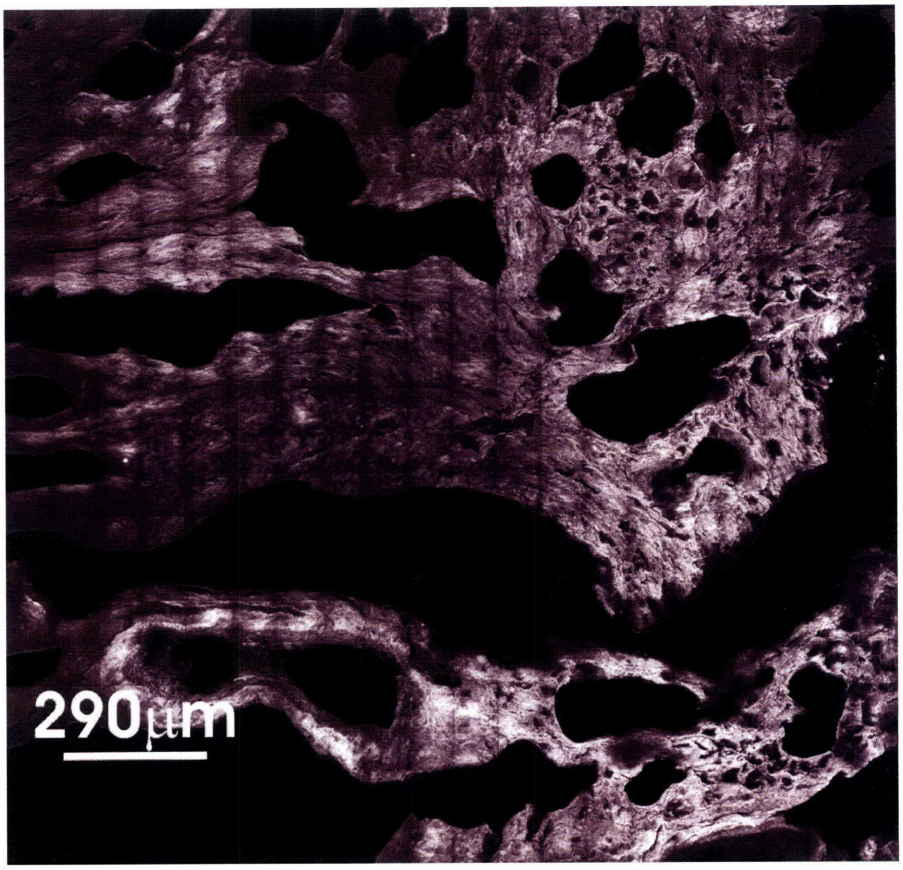

Figure C-2: A second harmonic image of pregnant cervical tissue. The plane of this image is perpendicular to the circumferential direction of the cervix. This specimen was taken from PCS patient 2 (refer to Table 3.1). Images taken by Dimitrios Tzeranis from the So Lab - Bioinstrumentation Engineering Analysis and Microscopy at MIT.

Bibliography

[1] SM Althuisius, GA Dekker, P Hummel, DJ Bekedam, and HP van Geijn. Final results of the cervical incompetence prevention randomized cerclage trial (cipract): Therapeutic cerclage with bed rest versus bed rest alone. *Am J Obstet Gynecol*, 185(5):1106–1112, November 2001.

[2] GS Anthony, AA Calder, and MC Macnaughton. Cervical resistance in patients with previous spontaneous mid-trimester abortion. *Br J Obstet Gynaecol*, 89(12):1046–1049, 1982.

[3] EM Arruda and MC Boyce. A three-dimensional consitutive model fot the large stretch behavior of rubber elastic materials. *J. Mech. Phys. Solids*, 41(2):389–412, 1993.

[4] RM Aspden. Collagen organization in the cervix and its relation to mechanical function. *Collagen Rel. Res.*, 8:103–112, 1988.

[5] RM Aspden. The theory of fibre-reinforced composite materials applied to changes in the mechanical properties of the cervix during pregnancy. *J. Theor. Biol.*, 130:213–221, 1988.

[6] GA Ateshian, WH Warden, JJ Kim, RP Grelsamer RP, and VC Mow. Finite deformation biphasic material properties of bovine articular cartilage from confined compression experiments. *Journal of Biomechanics*, 30(11-12):1157–1164, 1997.

[7] AJ Bank, H Wang, JE Holte, K Mullen, R Shammas, and SH Kubo. Contribution of collagen, elastin, and smooth muscle to in vivo human brachial artery wall stress and elastic modulus. *Circulation*, 94(12):3263–3270, 1996.

[8] PJ Basser, R Schneiderman, RA Bank, E Wachtel, and A Maroudas. Mechanical properties of the collagen network in human articluar cartilage as measured by osmotic stress technique. *Archives of Biochemistry and Biophysics*, 351(2):207–219, March 1998.

[9] PJ Basser, R Schneiderman, RA Bank, E Watchel, and A Maroudas. Mechanical properties of the collagen network in human articular cartilage as measured by osmotic stress technique. *Archives of Biochemistry and Biophysics*, 351(2):207–219, March 1998.

[10] JF Bateman, SR Lamande, and JAM Ramshaw. *Extracellular matrix: molecular components and interactions*, chapter 3: The elastic fiber. Overseas Publishers Association, 1996.

[11] M BAUER, E MAZZA, A NAVA, W ZECK, M EDER, M BAJKA, F CACHO, UWE LANG, and GA HOLZAPFEL. In Vivo Characterization of the Mechanics of Human Uterine Cervices. *Annals of the New York Academy of Sciences*, 1101(1):186, 2007.

[12] RE Behrman, AS Butler, Institute of Medicine (US), Committee on Understanding Premature Birth, and Assuring Healthy Outcomes. *Preterm Birth: Causes, Consequences, and Prevention.* National Academies Press, 2007.

[13] V Berghella, SF Daly, JE Tolosa, MM Divito, R Chalmers, and N Garg. Prediction of preterm delivery with transvaginal ultrasonography of the cervix in patients with high-risk pregnancies: does cerclage prevent prematurity? *Am J Obstet Gynecol*, 181:809–815, 1999.

[14] JE Bischoff, EM Arruda, and K Grosh. A microstructurally based orthotropic hyperelastic constitutive law. *Journal of Applied Mechanics*, 69:570, 2002.

[15] GC Blobe, WP Schiemann, and HF Lodish. Role of Transforming Growth Factor {beta} in Human Disease. *New England Journal of Medicine*, 342(18):1350, 2000.

[16] DW Branch. Operations for cervical incompetence. *Clin Obstet Gynecol*, 29(2):240–54, 1986.

[17] ND Broom and A Poole. Articular cartilage collagen and proteoglycans: Their functional interdependency. *Arthritis and Rheumatism*, 26(9), September 1983.

[18] ND Broom and H Silyn-Roberts. The three-dimensional 'knit' of collagen fibrils in articular cartilage. *Connective Tissue Research*, 23:261–277, 1989.

[19] WM Bryant, JE Greenwell, and PM Weeks. Alterations in collagen organization during dilatation of the cervix uteri. *Surg Gynecol Obstet*, 126(1):27–39, 1968.

[20] C Buehler, KH Kim, U Greuter, N Schlumpf, and PTC So. Single-Photon Counting Multicolor Multiphoton Fluorescence Microscope. *Journal of Fluorescence*, 15(1):41–51, 2005.

[21] PM Bursać, TW Obitz, SR Eisenberg, and D Stamenović. Confined and unconfined stress relaxation of cartilage: appropriateness of a transversely isotropic analysis. *Journal of Biomechanics*, 32(10):1125–1130, 1999.

[22] D Cabrol, D Jannet, R Le Houezec, W Dudzik, E Bonoris, and L Cedard. Mechanical properties of the pregnant human uterine cervix use of an instrument to measure the index of cervical distensibility. *Gynecol Obstet Invest*, 29(1):32–6, 1990.

[23] A Calabro, R Midura, A Wang, L West, A Plaas, and VC Hascall. Fluorophore-assisted carbohydrate electrophoresis (FACE) of glycosaminoglycans. *Osteoarthritis and Cartilage*, 9:16–22, 2001.

[24] NO Chahine, CCB Wang, CT Hung, and GA Ateshian. Anisotropic strain-dependent material properties of bovine articular cartilage in the transitional range from tension to compression. *Journal of Biomechanics*, 37(8):1251–1261, 2004.

[25] AC Chen, WC Bae, RM Schinagl, and RL Sah. Depth-and strain-dependent mechanical and electromechanical properties of full-thickness bovine articular cartilage in confined compression. *Journal of Biomechanics*, 34(1):1–12, 2001.

[26] DL Christiansen, DJ Riley, CA Tozzi, and FH Silver. *The Extracellular Matrix of the Uterus, Cervix and Fetal Membranes: Synthesis, Degradation and Hormonal Regulation*, chapter Chapter 4: The mechanical properties of the extracellular matrix. Perinatology Press, 1991.

[27] K Clark, H Ji, H Feltovich, J Janowski, C Carroll, and EK Chien. Mifepristone-induced cervical ripening: Structural, biomechanical, and molecular events. *American Journal of Obstetrics and Gynecology*, 194(5):1391–1398, 2006.

[28] HJ Conn and MA Darrow. *Staining Procedures Used by the Biological Stain Commission.* Williams & Wilkins Baltimore, 1960.

[29] J Conrad, R Tokarz, and J Williford. *Dilation of the Uterine Cervix: Connective Tissue Biology and Clinical Management*, chapter 18, pages 255–264. Raven Press, New York, 1980.

[30] John T. Conrad, Richard D. Tokarz, and John F. Williford. *Dilatation of thet Uterine Cervix: Connective Tissue Biology and Clincial Managemen*, chapter Chapter 18: Anatomic Site and Stretch Modulus in the Human Cervix, pages 255–264. Raven Press, 1980.

[31] G Cox, E Kable, A Jones, I Fraser, F Manconi, and MD Gorrell. 3-Dimensional imaging of collagen using second harmonic generation. *Journal of Structural Biology*, 141(1):53–62, 2003.

[32] RK Creasy and R Resnik. *Maternal-Fetal Medicine*, chapter 29. W.B. Saunders Company, 4 edition.

[33] DN Danforth. The effect of pregnancy and labor on the human cervix: Changes in collagen, glycoproteins, and glycosaminoglycans. *Am J Obstet Gynecol*, 120(3):641–651, November 1974.

[34] DN Danforth. The morphology of the human cervix. *Clinical Obstetrics and Gynecology*, 26(1):7–14, March 1983.

[35] KG Danielson, H Baribault, DF Holmes, H Graham, KE Kadler, and V Iozzo. Targeted disruption of deorin leads to abnormal collagen fibril morphology and skin fragility. *J of Cell Bio*, 136(3):729–743, February 1997.

[36] J Darnel, H Lodish, and D Baltimore. *Molecular Cell Biology*, chapter 23. Scientific American Books, 2 edition, 1990.

[37] SR Eisenberg and AJ Grodzinsky. Swelling of Articular Cartilage and Other Connective Tissues: Electrornechanochemical Forces. *J Orthop Res*, 3(2), 1985.

[38] G Ekman, H Almstrom, L Granstrom, A Malmstrom, M Norman, and JF Woessner Jr. *The Extracellular Matrix of the Uterus, Cervix and Fetal Membranes: Synthesis, Degradation and Hormonal Regulation*, chapter Chapter 8: Connective tissue in human cervical ripening. Perinatology Press, 1991.

[39] RW Farndale, CA Sayers, and AJ Barrett. A direct spectrophotometric microassay for sulfated glycosaminoglycans in cartilage cultures. *Connective Tissue Research*, 9:247–248, 1982.

[40] S Febvay and Massachusetts Institute of Technology. *A Three-dimensional Constitutive Model for the Mechanical Behavior of Cervical Tissue.* PhD thesis, Massachusetts Institute of Technology, Dept. of Mechanical Engineering, 2003.

[41] S Febvay, S Socrate, and MD House. Biomechanical modeling of cervical tissue. a quantitative investigation of cervical funneling. *Proceedings of the ASME 2003 International Mechanical Engineering Congress and Exposition, Washington, D.C.*, November 2003.

[42] L Frederik. Clinical aspects of cervical insufficiency. *BMC Pregnancy and Childbirth.*

[43] I Freund, M Deutsch, and A Sprecher. Connective tissue polarity. Optical second-harmonic microscopy, crossed-beam summation, and small-angle scattering in rat-tail tendon. *Biophysical Journal*, 50(4):693–712, 1986.

[44] YC Fung. *Biomechanics: Mechanical Properties of Living Tissues.* Springer-Verlag, 2 edition, 1993.

[45] RE Garfield, G Saade, C Buhimschi, I Buhimschi, L Shi, SQ Shi, and K Chwalisz. Control and assessment of the uterus and cervix during pregnancy and labour. *Human Reproduction Update*, 4(5):673–695, 1998.

[46] K Gelse, E Pöschl, and T Aigner. CollagensÛstructure, function, and biosynthesis. *Advanced Drug Delivery Reviews*, 55(12):1531–1546, 2003.

[47] RL Goldenberg, BM Mercer, JD Iams, AH Moawad, PJ Meis, A Das, D McNellis, M Miodovnik, MK Menard, and SN Caritis. The preterm prediction study: Patterns of cervicovaginal fetal fibronectin as predictors of spontaneous preterm delivery. *Am J Obstet Gynecol*, 177:8–12, 1997.

[48] L Granstrom, G Ekman, and A Malmstrom. Insufficient remodelling of the uterine connective tissue in women with protracted labour. *BJOG: An International Journal of Obstetrics & Gynaecology*, 98(12):1212–1216, 1991.

[49] SFA Grant, DM Reid, G Blake, R Herd, I Fogelman, and SH Ralston. Reduced bone density and osteoporosis associated with a polymorphic Sp 1 binding site in the collagen type I α 1 gene. *Nature Genetics*, 14(2):203–205, 1996.

[50] ER Guzman, R Mellon, AM Vintzileos, CV Ananth, C Walters, and K Gipson. Relationship between endocervical canal length between 15-24 weeks gestation and obsteric history. *J of Maternal-Fetal Med*, 7:269–272, 1998.

[51] ER Guzman, C Walters, CV Ananth, C O'Reilly-Green, CW Benito, A Palermo, and AM Vintzileos. A comparison of sonogrpahic cervical parameters in predicting spontaneous preterm birth in high-risk singleton gestations. *Ultrasound Obstet Gynecol*, 18:204–210, 2001.

[52] VC Heath, AP Souka, I Erasmus, DM Gibb, and KH Nicolaides. Cervical length at 23 weeks of gestation: the value of shirodkar suture for the short cervix. *Ultrasound Obstet Gynecol*, 12:318–322, 1998.

[53] B Herman. *Fluorescence microscopy.* Springer New York, 1998.

[54] JU Hibbard, J Snow, and AH Moawad. Short cervical length by ultrasound and cerclage. *J Perinatol*, 20:161–165, 2000.

[55] AM Hocking, T Shinomura, and D McQuillan. Leucine-rich glcyoproteins of the extracellular matrix. *Matrix Biology*, 17:1–19, 1998.

[56] MD House, A Paskaleva, KM Myers, S Febvay, S Craigo, and S Socrate. The Biomechanics of Cervical Funneling: The Effect of Stroma Properties, Anatomic Geometry and Pelvic

Forces on Funnel Formation. *American Journal of Obstetrics and Gynecology*, 191(6):S17, 2004.

[57] MD House and S Socrate. The cervix as a biomechanical structure. *Ultrasound Obstet. Gynecol*, 28:745–749, 2006.

[58] JD Iams, FF Johnson, J Sonek, L Sachs, C Gebauer, and P Samuels. Cervical competence as a continuum: A study of ultrasonographic cervical length and obstetric performance. *A J of Obstet Gyn*, 172(4):1097–1106, April 1995.

[59] A Ito, K Kitamura, Y Mori, and S Hirakawa. The change in solubility of type I collagen in human uterine cervix in pregnancy at term. *Biochem Med*, 21(3):262–70, 1979.

[60] A ITO, YO MORI, and S HIRAKAWA. Purification and Characterization of an Acid Proteinase from Human Uterine Cervix. *Chemical & Pharmaceutical Bulletin*, 27(4):969–973, 1979.

[61] B Jähne. *Digital Image Processing*. Springer, 2005.

[62] P Jordan, AE Kerdok, S Socrate, and RD Howe. Identifying a Minimal Rheological Configuration: Preliminary Steps for Effective Constitutive Modeling of Soft Tissues. *in prepration*, 2008.

[63] A Jorgensen, Z Alfirevic, C Tudur Smith, and P Williamson. Cervical stitch (cerclage) for preventing pregnancy loss: individual patient data meta-analysis. *BJOG*, 2007.

[64] JF Woessner Jr. *Methodology of Connective Tissue Research*, chapter 23 Determination of Hydroxyproline in Connective Tissues. Joynson-Bruvvers Ltd., Oxford, 1976.

[65] DR Keene, JD San Antonia, R Mayne, DJ McQuillan, G Sarris, SA Santoro, and RV Iozzo. Decorin binds near the c terminus of type i collagen. *J of Bio Chem*, 257(29):21801–21804, 2000.

[66] GN Kiefer, K Sundby, D McAllister, NG Shrive, CB Frank, T Lam, and NS Schachar. The effect of cryopreservation on the biomechanical behavior of bovine articular cartilage. *Journal of Orthopaedic Research*, 7(4):494–501, 1989.

[67] BM Kim, J Eichler, KM Reiser, AM Rubenchik, and LB Da Silva. Collagen structure and nonlinear susceptibility: effects of heat, glycation, and enzymatic cleavage on second harmonic signal intensity. *Lasers Surg Med*, 27(4):329–35, 2000.

[68] R Kiwi, MR Neuman, IR Merkatz, MA Selim, and A Lysikiewicz. Determination of the elastic properties of the cervix. *Obstet. Gynecol.*, 71(4):568–574, 1988.

[69] DA Kleinman. Theory of Second Harmonic Generation of Light. *Physical Review*, 128(4):1761–1775, 1962.

[70] HP Kleissl, M van der Rest, F Naftolin, FH Glorieux, and A de Leon. Collagen changes in the human uterine cervix at parturition. *Am J Obstet Gynecol*, 130(7):748–53, 1978.

[71] R Kokenyesi. *The Extracellular Matrix of the Uterus, Cervix and Fetal Membranes: Synehesis, Degradation and Hormonal Regulation*, chapter Chapter 2: Collagen and proteoglycans. Perinatology Press, 1991.

[72] R Kokenyesi, LC Armstrong, A Agah, R Artal, and P Bornstein. Thrombospondin 2 deficiency in pregnant mice results in premature softening of the uterine cervix. *Biology of Reproduction*, 70:385–390, 2004.

[73] R Kokenyesi and JF Woessner Jr. Relationship between dilatation of the rat uterine cervix and a small dermatan sulfate proteoglycan. *Biology of Reproduction*, 1990.

[74] W Kuhn and F Gruehn. Beziehungen zwischen elastischen konstanten und dehnungsdoppelelbrechung hochelastischer stoffe. *Kolloid-Z.*, 101:248–271, 1942.

[75] R LaComb, O Nadiarnykh, SS Townsend, and PJ Campagnola. Phase matching considerations in second harmonic generation from tissues: Effects on emission directionality, conversion efficiency and observed morphology. *Optics Communications*, 2007.

[76] PC Leppert. Cervical softening, effacement, and dilatation: A complex biochemical cascade. *The Journal of Maternal-Fetal Medicine*, 1:213–223, 1992.

[77] PC Leppert. Anatomy and physiology of cervical ripening. *Clinical Obstetrics and Gynecology*, 38(2):267–279, June 1995.

[78] PC Leppert. The biochemistry and physiology of the uterine cervix during gestation and parturition. *Prenat Neonat Med*, 3:103–105, 1998.

[79] PC Leppert, R Kokenyesi, CA Lemenich, and J Fisher. Further evidence of a decorin-collagen interaction in the disruption of cervical collagen fibers during rat gestation. *Am J Obstet Gyncol*, 182(4):805–812, April 2000.

[80] PC Leppert and SY yu. *The Extracellular Matrix of the Uterus, Cervix and Fetal Membranes: Synthesis, Degradation and Hormonal Regulation*, chapter Chapter 5: Elastin and collagen in the human uterus and cervix. Perinatology Press, 1991.

[81] PC Leppert and SY yu. *The Extracellular Matrix of the Uterus, Cervix and Fetal Membranes: Synthesis, Degradation and Hormonal Regulation*, chapter Chapter 6: The collagenous tissue of the cervix during pregnancy and delivery. Perinatology Press, 1991.

[82] K Maillot and BK Zimmermann. The solubility of collagen of the uterine cervix during pregnancy and labour. *Archives of Gynecology and Obstetrics*, 220(4):275–280, 1976.

[83] E El Maradny, N Kanayama, H Kobayashi, B Hossain, S Khatun, S Liping, T Kobayashi, and T Terao. The role of hyaluronic acid as a mediator and regulator of cervical ripening. *Human Reproduction*, 2(5):1080–1088, 1997.

[84] A Maroudas and J Urban. Articular cartilage and the intervertebral disc. *Encyclopedia of Human Biology*, 1:365–370, 1991.

[85] A Maroudas and J Urban. Articular catilage and the intervertebral disc. *Encyclopedia of Human Biology*, 1:365–370, 1991.

[86] PD Marx. Transabdominal cervicoisthmic cerclage: a review. *Obstet Gynecol Surv*, 44(7):518–22, 1989.

[87] E Mazza, A Nava, M Bauer, R Winter, M Bajka, and GA Holzapfel. Mechanical properties of the human uterine cervix: an in vivo study. *Med. Image Anal*, 10:125–136, 2006.

[88] AC Millard, PJ Campagnola, W Mohler, A Lewis, and LM Loew. Second harmonic imaging microscopy. *Methods Enzymol*, 361:47–69, 2003.

[89] W Mohler, AC Millard, and PJ Campagnola. Second harmonic generation imaging of endogenous structural proteins. *Methods*, 29(1):97–109, 2003.

[90] KM Myers. Mechanical and biochemical properties of human cervical tissue, ms thesis. *Acta Biomaterialia*, 2005.

[91] KM Myers, A Paskaleva, MD House, and S Socrate. Mechanical and biochemical properties of human cervical tissue. *Acta Biomaterialia*, 4:104–116, 2008.

[92] H Nagase. *The Extracellular Matrix of the Uterus, Cervix and Fetal Membranes: Synthesis, Degradation and Hormonal Regulation*, chapter Chapter 3: Matrix metalloproteinases 1, 2, and 3: substrate specificities. Perinatology Press, 1991.

[93] EM Parsons, MC Boyce, DM Parks, and M Weinberg. Three-dimensional large-strain tensile deformation of neat and calcium carbonate-filled high-density polyethylene. *Polymer*, 46(7):2257–2265, 2005.

[94] A Paskaleva. *Biomechanics of Cervical Function in Pregnancy Case of Cervical Insufficiency.* PhD thesis, Massachusetts Institute of Technology, Dept. of Mechanical Engineering, 2007.

[95] A Paskaleva, KM Myers, S Socrate, and MD House. Biomechanics of cervical insufficiency. *Proceedings of the First International Conference on Mechanics of Biomaterials and Tissues, Waikoloa, HI*, December 2005.

[96] LK Petersen, H Oxlund, N Uldbjerg, and A Forman. In vitro analysis of muscular contractile ability and passive biomehcanical properties of uterine cervical samples from nonpregnant women. *Obstetrics and Gynecology*, 77(5):772–776, May 1991.

[97] LK Petersen and N Uldbjerg. Cervical collagen in non-grenant women with previous cervical incompetence. *Europ J Obstet Gynec Repr Bio*, 67:41–45, 1996.

[98] AH Plaas, LA West, EJA Thonar, ZA Karcioglu, CJ Smith, GK Klintworth, and VC Hascall. Altered Fine Structures of Corneal and Skeletal Keratan Sulfate and Chondroitin/Dermatan Sulfate in Macular Corneal Dystrophy. *Journal of Biological Chemistry*, 276(43):39788–39796, 2001.

[99] W Rath, R Osmers, M Severenyi, HW Stuhlsatz, and W Kuhn. *The Extracellular Matrix of the Uterus, Cervix and Fetal Membranes: Synthesis, Degradation and Hormonal Regulation*, chapter Chapter 10: Changes of glycosaminoglycans in cervical connective tissue. Perinatology Press, 1991.

[100] CP Read, RA Word, MA Ruscheinsky, BC Timmons, and MS Mahendroo. Cervical remodeling during pregnancy and parturition: molecular characterization of the softening phase in mice. *Reproduction*, 134(2):327–340, 2007.

[101] T Rechberger, N Uldbjerg, and H Oxlund. Connective tissue changes in the cervix during normal pregnancy and pregnancy complicated by cervical incompetence. *acogjnl*, 71(4):563–567, 1988.

[102] JM Rennie. Perinatal management at the lower margin of viability. *Arch Dis Child*, 74:F214–18, 1996.

[103] BA Roeder, K Kokini, JE Sturgis, JP Robinson, and SL Voytik-Harbin. Micromechanics of extracellular matrix: three-dimensional microstructure under load. *ASME-PUBLICATIONS-BED*, 51:331–332, 2001.

[104] R Romero, J Espinoza, O Erez, and S Hassan. The role of cervical cerclage in obstetric practice: Can the patient who could benefit from this procedure be identified? *American Journal of Obstetrics and Gynecology*, 194(1):1–9, 2006.

[105] R Romero, J Espinoza, J Kusanovic, F Gotsch, S Hassan, O Erez, T Chaiworapongsa, and M Mazor. The preterm parturition syndrome. *BJOG*, 113(3):17–42, 2006.

[106] OA Rust, RO Atlas, J Reed, J van Gaalen, and J Balducci. Revisiting the short cervix detected by transvaginal ultrasound in the second trimester: Why cerclage therapy may not help. *Am J Obstet Gynecol*, 185(5):1098–1105, November 2001.

[107] MB Sennström, A Brauner, B Byström, A Malmström, and G Ekman. Matrix metalloproteinase-8 correlates with the cervical ripening process in humans. *Acta Obstetricia et Gynecologica Scandinavica*, 82(10):904–911, 2003.

[108] T Shimizu, M Endo, and Z Yosizawa. Glycoconjugates (glycosaminoglycans and glycoproteins) and glycogen in the human cervix uteri. *Tohoku J. exp. Med.*, 131:289–299, 1980.

[109] H Stegeman and K Stalder. Determination of hydroxyproline. *Clin Chem Acta*, 18:267–273, 1967.

[110] A Stevens and JS Lowe. *Human histology.* Mosby, 1997.

[111] W Tin, U Wariyar, and E Hey. Changing prognosis for babies of less than 28 weeks' gestation in the north of england between 1983 and 1994. *BR med J*, 314, 1997.

[112] N Uldbjerg, G Ekman, A Malmstrom, K Olsson, and U Ulmsten. Ripening of the human uterine cervix related to changes in collagen, glycosaminoglycans, and collagenolytic activity. *Am J Obstet Gynecol*, 147(6):662–6, 1983.

[113] D Voet and JG Voet. *Biochemistry: Biomolecules, Mechanisms of Enzyme Action, and Metabolism*, volume 1, chapter 8. John Wiley & Sons, Inc., 2004.

[114] JE Warren, RM Silver, J Dalton, LT Nelson, D Branch, and TF Porter. Collagen 1a1 and transforming growth factor-{beta} polymorphisms in women with cervical insufficiency. *Obstetrics & Gynecology*, 110(3):619, 2007.

[115] IT Weber, RW Harrison, and RV Iozzo. Model structure of decorin and implication for collagen fibrillogenesis. *J Of Bio Chem*, 271(50):31767–31770, 1996.

[116] S Weiss, T Jaermann, P Schmid, P Staempfli, P Boesiger, P Niederer, R Caduff, and M Bajka. Three-Dimensional Fiber Architecture of the Nonpregnant Human Uterus Determined Ex Vivo Using Magnetic Resonance Diffusion Tensor Imaging. *Anat. Rec. A. Discov. Mol. Cell Evol. Biol*, 288:84–90, 2006.

[117] T Wight, DK Heinegard, and VC Hascall. *Cell Biology of Extracelluar Matrix*, chapter 2: Proteoglycans Structure and Function. Plenum Press, 2 edition, 1991.

[118] SY Yu. Collagen changes in rat cervix in pregnancy–polarized light microscopic and electron microscopic studies. *Experimental Biology and Medicine*, 209(4):360–368, 1995.

[119] FJ Zlatnik and LF Burmeister. Interval evaluation of the cervix for predicting pregnancy outcome and diagnosing cervical incompetence. *J Reprod Med*, 38(5):365–9, 1993.